AN ABSTRACT OF THE THESIS OF

Jacob Hans Goebel for the degree of Master of Science in Civil Engineering presented on June 10, 2011.

Title: Design and Environmental Performance of Near-Surface Mounted Carbon Fiber Reinforced Polymer Strips for Shear Strengthening Reinforced Concrete Bridge Girders.

Abstract approved:

Christopher C. Higgins

During the interstate expansion of the 1950s, many conventionally reinforced concrete deck girder bridges were built throughout the country. These now vintage bridges commonly exhibit diagonal cracking and rate inadequately for shear, thus they are candidates for shear strengthening to extend their useful life. Near-surface mounted (NSM) retrofitting is a promising new strengthening technique, but limited test data are available for carbon fiber reinforced polymer (CFRP) in shear strengthening making the long-term durability of NSM-CFRP unknown. This paper provides experimental results from realistic full-scale specimens strengthened with NSM-CFRP. Specimens were tested for shear strength and subjected to environmental exposures to assess long-term durability.

Small cylinder specimens were tested to investigate relative performance of different adhesives on bond strength under different environmental exposures. Test results provide a better understanding of the NSM-CFRP shear behavior and strength. Recommendations for shear strength design with NSM-CFRP are made.

Design and Environmental Performance of Near-Surface Mounted Carbon Fiber Reinforced Polymer Strips for Shear Strengthening Reinforced Concrete Bridge Girders

by
Jacob Hans Goebel

A THESIS

submitted to

Oregon State University

in partial fulfillment of
the requirements for the
degree of

Master of Science

Presented June 10, 2011
Commencement June 2012

Master of Science thesis of Jacob Hans Goebel presented on June 10, 2011.

APPROVED:

_____

Major Professor, representing Civil Engineering

_____

Head of the School of Civil and Construction Engineering

_____

Dean of the Graduate School

I understand that my thesis will become part of the permanent collection of Oregon State University libraries. My signature below authorizes release of my thesis to any reader upon request.

_____

Jacob Hans Goebel, Author

ACKNOWLEDGEMENTS

I wish to extend sincere thanks to Dr. Chris Higgins for his guidance and the opportunity to work on this project. His direction and continual patience brought this research to life and made it possible to complete.

I would like to thank the Oregon Department of Transportation for taking interest and funding this project.

This was a huge undertaking that would not have happened without the work and input of many friends and co-workers, including: Brandon Johnson, Mary Ann Triska, Tugrul Turan, Michael Dyson, Thomas Schumacher, Jora Lehrman, Josh Goodall, Scott Mersereau, Brandon Mahon, Anthony Peressini, Nick Atanasov, and Matthew Brand.

Thank you to my committee members for their comments and feedback: Dr. Michael Scott, Dr. Jason Ideker, and Dr. Harold Parks.

Lastly, I would like to thank my future wife Holly and my family for their support.

CONTRIBUTION OF AUTHORS

Brandon Johnson was involved with the writing of Chapter 2.

TABLE OF CONTENTS

Page

TABLE OF CONTENTS (Continued)

Page

TABLE OF CONTENTS (Continued)

Page

TABLE OF CONTENTS (Continued)

Page

LIST OF FIGURES

Figure Page

LIST OF FIGURES (Continued)

Figure Page

LIST OF FIGURES (Continued)

Figure Page

LIST OF FIGURES (Continued)

Figure Page

LIST OF TABLES

LIST OF TABLES (Continued)

Table Page

LIST OF APPENDIX FIGURES

Figure Page

LIST OF APPENDIX FIGURES (Continued)

Figure Page

LIST OF APPENDIX FIGURES (Continued)

Figure Page

LIST OF APPENDIX FIGURES (Continued)

Figure Page

LIST OF APPENDIX FIGURES (Continued)

Figure Page

LIST OF APPENDIX FIGURES (Continued)

Figure Page

DESIGN AND ENVIRONMENTAL PERFORMANCE OF NEAR-SURFACE MOUNTED CARBON FIBER REINFORCED POLYMER STRIPS FOR SHEAR STRENGTHENING REINFORCED CONCRETE BRIDGE GIRDERS

1. INTRODUCTION

Many reinforced concrete deck girder (RCDG) bridges were constructed in the 1950's and 1960's during expansion of the highway infrastructure in the United States. These now old bridges were designed with light shear reinforcement and are reaching the end of their intended design life. Since the bridges were built, the magnitude of traffic loading and traffic frequency has increased. The specifications used for their design are now considered deficient. Recently, the Oregon Department of Transportation inspected approximately 1,800 of these vintage RCDG bridges and identified over 500 with varying levels of diagonal cracking [Williams and Higgins, 2008]. The diagonal cracks in RCDG bridges indicate overestimation of the concrete contribution to shear during original design. Upon performing more detailed evaluations, some bridges have been identified as deficient. Replacing all shear-deficient RCDG bridges in Oregon exceeds the available resources. Therefore efforts to repair bridges and extend their useful service life are of interest. One potential strengthening method is near-surface-mount (NSM) retrofit using carbon fiber reinforced polymer (CFRP) strips (NSM-CFRP). This is a relatively new technique and it is uncertain how long these materials will withstand field conditions including environmental exposure. This research examines shear repair with NSM-CFRP strips and its potential service life under environmental exposure.

2. BACKGROUND

There are several methods and materials that can be used to retrofit a RCDG bridge. Carbon fiber has some particularly beneficial attributes as a retrofit material because it resists corrosion and has a high strength-to-weight ratio. One retrofitting technique that has gained recent popularity is externally bonded repair (EBR) with CFRP sheets. This method uses wet layup construction and bonds CFRP sheets to the surface of the concrete member typically in a u-wrap configuration. The CFRP sheet is exposed on the outer surface, which can make it susceptible to both environmental deterioration and vandalism. Research has identified that environmental exposure causes the CFRP sheets to debond from the concrete, resulting in lower shear capacities [Mitchell, 2008].

The emerging NSM technique places reinforcement into grooves that are saw-cut into the concrete surface. The NSM reinforcement technique is not a new idea. Literature references date back to Asplund in 1949 who discusses a reinforced concrete bridge in Sweden strengthened with steel rods embedded into grooves on the concrete surface [De Lorenzis, *et al*. 2001]. Using CFRP reinforcing with the NSM technique has potential benefits which should alleviate several of the EBR retrofitting issues. By placing the CFRP strip in a groove it is expected to be less susceptible to environmental deterioration. The strip is surrounded by epoxy and bonded to the groove on three sides. This could produce a stronger bond compared to the EBR technique and prevent peeling. Another advantage is that the NSM technique requires less surface preparation of the concrete and less adhesive than the EBR technique. This should make it less expensive and quicker to install.

2.1 Literature Review

2.1.1 Shear Strength

The idea of NSM retrofitting with CFRP bars is still relatively new. Only a few studies have examined this technique for shear reinforcing.

The first experiments to examine NSM retrofitting with CFRP rods as shear reinforcement were performed by De Lorenzis, *et al.* [2001]. Eight small-scale specimens were tested. The T-shaped specimens were 3 m (10 ft.) long and 406 mm (16 in.) tall. The specimen's flanges were 381 mm (15 in.) wide and 102 mm (4 in.) thick and the web was 152 mm (6 in.) thick. The specimens were tested under four-point bending with a shear span of 1.07 m (42 in.). This corresponds to an a/d radio of 3. To ensure a shear failure, the specimens were constructed with two 28.7 mm (#9) bars as flexural reinforcement. Deformed 9.5 mm (#3) round CFRP rods were used as NSM reinforcing. The NSM grooves were a square measuring 19 mm (0.75 in.). The adhesive was BASF's Concresive paste. The specified epoxy tensile strength is 13.8 MPa (2000 psi). Six of the specimens had no internal steel stirrups for shear reinforcing and two of the specimens had 9.5 mm (#3) stirrups spaced at 356 mm (14 in.) . Five of the specimens without stirrups were reinforced with NSM-CFRP rods and one was used as a control. The five reinforced beams varied the CFRP rod spacing between 127 and 178 mm (5 and 7 in.). They also examined inclination angles of the NSM from 45˚ to 90˚, and anchoring of the CFRP rods into the specimen flange. They reported large gains in shear capacity for the NSM reinforced specimens compared to the control specimen. The largest gains were exhibited in the specimens with bars inclined at 45˚ or specimens with rods anchored into the flange. Of the two specimens with internal steel, one was used as a control and one was reinforced with NSM-CFRP rods at 178 mm

(7 in.). A gain in shear strength was reported for the specimen with NSM reinforcing compared to the control specimen. However, the strength gain was not as large as the increases in the similar specimens without internal steel stirrups.

The first tests performed on prestressed girders that incorporated NSM-CFRP shear strengthening were done by Nanni, *et al*. [2004]. The test specimens were full-scale prestressed bridge girders. Two damaged prestressed double-T girders were retrieved from a bridge in Kansas and cut longitudinally. This created four single-T test specimens that were 12.2 m (40 ft.) long and 584 mm (23 in.) deep. The specimen flange was 125 mm (5 in.) thick and 914 m (36 in.) wide, and the web was 115 mm (4.5 in.) thick. The specimens were tested using four-point loading with a shear span of 3.6 m (12 ft.). Of the four specimens one was tested as a control and two were strengthened with EBR-CFRP sheets for flexure. These are not applicable to this study, but the fourth specimen was retrofit with EBR-CFRP sheets for flexure and with NSM-CFRP strips for shear. The research used Hughes Brothers Aslan 500 tape with dimensions of 2 mm by 16 mm (0.08 in. by 0.63 in.) for the CFRP strip material. The NSM grooves were spaced every 203 mm (8 in.) along the girder. The grooves measured 6 mm (0.24 in.) wide and 19 mm (0.75 in.) deep and were cut at a 60˚ inclination. The report showed that the specimen strengthened with both EBR and NSM actually failed in flexure. This does not allow the shear capacity to be determined. However, the specimen still had a significantly higher ultimate capacity than the beams strengthened only for flexure, which demonstrates the NSM-CFRP strips did contribute to the girder's strength.

Barros, *et al.* [2006] conducted NSM-CFRP experiments on rectangular beam specimens. A total of 20 specimens were tested which included two different sized specimens to

investigate beam depth effects. The larger specimens spanned 1500 mm (59 in.) and measured 150 mm by 300 mm (5.9 in. by 11.8 in.). The smaller specimens spanned 900 mm (35.4 in.) and measured 150 mm by 150 mm (5.9 in. by 5.9 in.). The specimens were constructed with various shear reinforcing. One group of specimens was made with no shear reinforcing as controls. One group was built with various spacing of standard steel stirrups that were 6 mm (0.24 in.) diameter. Another set was reinforced with the U-shaped EBR technique using S&P C-Sheet 530 as the material. The final set of specimens was reinforced with the NSM technique using S&P laminate CFK 150/2000 strips which have dimensions of 10 mm by 1.4 mm (0.39 in. by 0.55 in.). Various NSM groove spacings were investigated along with 45° and 90° groove orientations. The NSM groove measured 5 mm (0.3 in.) wide and 12 mm (0.4 in.) deep. To evaluate the influence of the longitudinal steel, the longitudinal reinforcing ratio was also varied. The maximum capacity, deflection, and strengthening contributions per unit length were assessed in the report. Different failure modes were reported for the NSM retrofit specimens including flexural failures and the end of CFRP strips slipping. Another reported failure mode was two concrete lateral walls separating from the interior concrete and the interior core rupturing in shear. The NSM technique, especially the 45° orientation, was the most effective strengthening method in terms of increasing beam load carrying capacity and deformation at failure. Barros *et al.* did not specifically study the relationship between the amounts of flexural reinforcing steel and shear strength. However, they did note that an increase in the flexural reinforcing ratio leads to an increase in the shear strength of the beam.

Further investigation using NSM-CFRP retrofitting was performed by Dias, *et al.* [2007] on T-beams that had a low concrete compressive strength. The specimens test day

compressive strength was 18.6 MPa (2,700 psi). The specimens spanned 2450 mm (96.5 in.), had a depth of 356 mm (14.0 in.), a flange width of 450 mm (17.7 in.), a flange thickness of 100 mm (3.94 in.), and a web width of 180 mm (7.09 in.) A total of 13 specimens were constructed including controls. Two series of specimens were constructed with different internal steel stirrup spacings of 300 mm (11.8 in.) and 180 mm (7.09 in.). These specimens were retrofit with various quantities of NSM-CFRP strips oriented at 90°, 60°, and 45°. The CFRP strips used were S&P CFK 150/2000 which have a width of 10 mm (0.39 in.) and a thickness of 1.4 mm (0.55 in.). The NSM grooves were 5 mm (0.2 in.) wide and 12-15 mm (0.5-0.6 in.) deep. Based on the percent of capacity increase, it was reported that the contribution of the NSM reinforcing was negatively affected by the proportion of internal steel stirrups. Reducing the internal stirrup spacing from 300 mm (11.8 in.) to 180 mm (7.09 in.) reduced the average shear strength increase from 27.4% to 16.2%. The specimens exhibited diagonal shear failures and it was noted that by reducing the concrete strength, the concrete around the strips was more likely to detach during failure. As a result, the added shear strength contributed to NSM reinforcement decreased as the concrete strength decreased.

Dias, *et al.* [2008] performed tests on more T-beam specimens retrofit with NSM-CFRP. Twelve specimens were constructed and nine were retrofit with NSM-CFRP strips. The specimens' spans, dimensions, CFRP type, and NSM groove size were the same as the reported factors in Dias *et al.* [2007]. The experimental program included control specimens with no shear reinforcing and internal steel stirrups with a 6 mm (0.24 in.) diameter spaced at 130 mm (5.12 in.) and 300 mm (11.8 in.). The retrofit specimens all had the wider internal steel stirrup spacing and consisted of three different NSM groove spacings and three orientations of 90°, 60°, and 45°. Results were reported for both service

level loads at a deflection of L/400 and a maximum capacity. It was determined that the CFRP strips at 60° was the most effective, 45° the second best, and 90° the least effective. The specimens retrofit with the highest percentage of CFRP strips and wide steel stirrup spacing exhibited almost the same maximum load as the control with the tighter steel stirrup spacing. It was noted that the NSM-CFRP strips contributed significantly to the stiffness of the beam after formation of diagonal cracks.

The effectiveness of shear strengthening with NSM-CFRP bars was also examined by Rizzo *et al*. [2009]. Nine rectangular reinforced concrete specimens were tested. The specimens were 200 mm (79 in.) long with a 200 mm (7.9 in.) by 210 mm (8.3 in.) cross section. The specimens were tested under four-point loading with a shear span of 519 mm (20.4 in.). The specimens were reinforced with 6 mm (0.24 in.) internal steel stirrups spaced at 160 mm (6.3 in.). All the specimens had four 22 mm diameter (# 7) bars in the bottom and two similar bars in the top to prevent flexural failures. One of the specimens was used as a control and one was retrofit with EBR-CFRP sheets in a U-wrap configuration. The other seven specimens were strengthened with NSM-CFRP bars. These specimens looked at two different epoxy types, two inclinations of 90˚ and 45˚, three groove spacings of 45, 73, and 146 mm (1.8, 2.9, 5.7 in.), and round CFRP rods versus rectangular CFRP strips. The CFRP rods had an 8 mm (0.3 in.) diameter and were epoxied in square 12 mm (0.47 in.) saw-cut grooves. The CFRP strips were 2 mm by 16 mm (0.08 in. by 0.63 in) and had a manufacturer's tensile strength of 2.07 GPa (300 ksi.), which is the same as Hughes Brothers Aslan 500 tape. The CFRP strips were epoxied into grooves that were 5 mm (0.2 in.) wide and 18 mm (0.7 in.) deep. The primary failure mode of the retrofit specimens was diagonal cracking and then the concrete cover on each side separating from the core of the specimen. The results showed that the NSM-CFRP

reinforcing technique provided more shear strength than the EBR-CFRP sheets. The epoxy with the lower tensile strength and lower tensile elastic modulus provided higher strength gains. This was reported to be a potential result of the stiffer epoxy accelerating the cracking of the concrete. The specimens with a narrower groove spacing failed at a higher shear capacity. Similarly, specimens with the steeper 45˚ bar inclination failed at a higher shear capacity. They report that the capacity of the specimens retrofit with rectangular strips was slightly less than the capacity of specimens retrofit with round rods. This was attributed to the increased stiffness from the NSM-CFRP strips accelerating the particular failure mode for those specimens. The researchers acknowledge that further experimental research of beams strengthened with NSM-CFRP bars for shear is needed.

Anwarul Islam, [2009] performed experiments on specimens with internal steel and NSM-CFRP shear reinforcing. Four rectangular specimens were tested that measured 2134 mm (7.0 ft.) long, 305 mm (1.0 ft.) tall, and 254 (10 in.) wide. One specimen was a control with steel stirrups spaced at 152 mm (6.0 in.) Two specimens had NSM-CFRP reinforcing and steel stirrups at different spacings and the last specimen just had NSM-CFRP reinforcing spaced at 190 mm (7.5 in.) The internal steel stirrups were 10 mm (#3) bars. The NSM material was Hughes Brothers Aslan 200 bars which have a 10 mm (#3) diameter. The epoxy used was BASF Concresive 1420. The NSM grooves measured 13 mm (0.5 in.) square. The specimens failed in shear, but no debonding or fracture of the NSM was observed. The paper reports that the NSM-CFRP provided shear strength gains of approximately 20% the base capacity and that the measured strain in the CFRP bars only reached approximately 33% of the ultimate tensile strain.

Howell, [2009] investigated NSM-CFRP retrofitting on a full-scale reinforced concrete bridge girder. One inverted T-beam specimen was constructed with a total length of 7925 mm (312 in.). It was tested under four-point loading with a shear span of 2997 mm (115 in.). The cross section height was 1219 mm (48 in.), the flange width was 914 mm (36 in.), the flange thickness was 152 mm (6 in.), and the web width was 356 mm (14 in.). The specimen was reinforced with 12.7 mm (#4) internal steel stirrups at 457 mm (18 in.). It was retrofit with an NSM groove spacing of 749 mm (29.5 in.). The groove measured 6.4 mm (0.25 in.) wide and 19 mm (0.75 in.) deep. The CFRP used was Hughes Brother's Aslan 500 tape and the epoxy used was 3M DP460NS. The specimen was subjected to initial loading to produce diagonal cracking before retrofitting to represent a bridge girder in the field that would be repaired. The failure method was a diagonal shear crack which crossed only one CFRP strip. At failure, the concrete around one end of this strip broke and the strip burst off of the specimen. Compared to the control shear capacity, the retrofit specimen showed an insignificant increase in shear strength and no definitive conclusions could be stated about the NSM-CFRP contribution. This was attributed to the specimen's large NSM-CFRP strip spacing.

More T-beam specimens retrofit for shear strength with NSM-CFRP strips were tested by Dias, *et al.* [2010]. The specimens' dimensions and materials are the same as those used in Dias, *et al.* [2007]. A total of 15 specimens were constructed for this research. They were reinforced with 6 mm (0.24 in.) internal steel stirrups spaced at 300 mm (11.8 in.). Three specimens were controls, three were retrofit with EBR-CFRP sheets, and nine were retrofit with NSM-CFRP strips. The NSM retrofit specimens had various CFRP strip spacing and inclinations of 90°, 60°, and 45°. The failure mode for the wider spaced NSM was debonding of the CFRP strip, which included breaking of the concrete around the strip.

The specimens with narrower CFRP strip spacings failed by separation of the outside walls of concrete from the internal concrete core. The results showed the steeper inclined NSM reinforcing was more efficient. The specimens retrofit with the NSM technique provided larger shear capacities compared to the EBR strengthened specimens. The report compares the experimental CFRP shear contribution to expected values based on a formulation provided in Nanni, *et al*. [2004]. The prediction method provided a CFRP shear contribution that was approximately 61% of the experimentally determined values.

2.1.2 Predictive Models

Nanni, *et al*. [2004] developed a method to predict the shear capacity of NSM-CFRP retrofit specimens. The report provides an equation for the shear contribution of the CFRP. This contribution is added to the concrete and steel shear strength to get a total shear capacity. The CFRP contribution is based on debonding of the strip and uses an effective length based on specimen geometry and a shear crack angle of 45˚.

Bianco, *et al.* [2007] discusses modeling the shear strength contribution of a NSM-CFRP retrofit system. The research acknowledges that the formulation provided by Nanni, *el al.* [2004] is based on debonding as the only failure mode. More current studies have shown another dominate failure mode is the separation of the two concrete side walls holding the CFRP from the internal concrete core. Bianco *et al.* [2007] proposes a formula for calculating the CFRP shear contribution according to concrete tensile strength and specimen geometry. This method is based on a conical failure of concrete around the NSM-CFRP strips. The method accounts for the interaction of adjacent CFRP strips by subtracting when the failure cones overlap. This paper compares experimental shear

values from previous research to predicted range and finds that most of the values fall within the range. It is mentioned that the method does not account for the interaction with internal steel reinforcing stirrups.

Bianco, *et al.* [2009] did further research into the bond and modeling of NSM-CFRP strips in shear strengthened beams. They looked at describing and predicting the bond failure. Equations were developed for the bond stresses of finite and infinite bond lengths. Four bond phases were identified, each with its own analytical procedure: elastic, softening, softening friction, and slipping. Some observations they made were that the elastic modulus of the CFRP strip and the concrete only provided marginal increases in the peak load. More significant increases in bond came from increasing the CFRP strip cross section, particularly increasing its depth into the beam because this provides more confinement for the strip.

Anwarul Islam, [2009] used the approach from the American Concrete Institute (ACI) to predict the shear strength contribution of the retrofit specimens. Based on the strains measured in the CFRP bars at failure, this paper proposes a formula using 0.33% of the CFRP ultimate stress replacing the effective stress in the ACI approach (the ACI approach is discussed later in this paper).

Rizzo, *et al.* [2009b] examines modeling the shear strength of NSM-CFRP systems. The researcher discusses two methods of predicting shear strength based on debonding of the CFRP strips. The first method is a simple method that is a generalized approach to the formula provided by [Nanni, *et al*. 2004]. The second method is a local bond-slip model that is based on an approach used on externally bonded CFRP sheets. The paper compares predictions from the two methods and concludes that the simpler method can offer the

same accuracy as the second method, but it does not consider the failure mode of the outer concrete separating from the inner concrete core.

2.1.3 Bond

To fully describe NSM-CFRP strengthening, it is important to examine the bond performance of the system. The bonding of the adhesive allows stress to be transferred from the CFRP strip through the epoxy and into the concrete substrate. Failure of bond in a NSM system can refer to the epoxy bond to the CFRP failing and causing slippage. Failure of the epoxy and concrete interface, including breaking the concrete around the epoxy is also referred to as bond failure. This latter failure mode is one of the primary modes discussed for a NSM-CFRP reinforced beam.

De Lorenzis, *et al.* [2002] experimentally investigated the bond between NSM-CFRP rods and concrete. A total of 22 T-shaped specimens were tested. The specimens were 1.2 m (4 ft.) long and 254 mm (10 in.) tall. The flange was 254 mm (10 in.) wide and 102 mm (4 in.) thick. The web was 152 mm (6 in.) wide. The concrete compressive strength was 27.6 MPa (4000 psi). The specimens were retrofit and tested in a manner that put tension in the CFRP strip. On the bottom side of the beam a longitudinal groove was cut and an NSM-CFRP rod was embedded with epoxy. The specimen was simply supported when tested and a point load was applied at midspan causing tension in the CFRP rod until failure. Variables included bond length, rod diameter, CFRP material type, CFRP surface configuration, and size of the NSM groove. The bond lengths examined were 6, 12, 18, and 24 bar diameters. As expected the ultimate load increased with bonded length of the rod. The surface configurations looked at was deformed bars and sandblasted bars. The deformed bars produced higher average bond strengths than the sandblasted bars. This

demonstrates that surface texture is important for the bond performance of NSM-CFRP. The various groove dimensions tested were square grooves of 16 mm (0.625 in.), 19 mm (0.75 in.), and 25.4 mm (1 in.). From the results, when failure occurred by the epoxy cover splitting, the larger groove sizes provided higher bond strengths.

Hassan, *et al.* [2003] performed similar tests to that of De Lorenzis, *et al*. [2002] to evaluate bond length of NSM-CFRP strips. A total of Nine T-beam specimens were tested. The beams were 2.5 m (8.2 ft.) long and 300 mm (11.8 in.) tall. The flange was 50 mm (2 in.) thick and 300 mm (11.8 in.) wide, and the web was 150 mm (5.9 in.) thick. One CFRP strip was retrofit in a groove on the bottom of each specimen. A point load was applied at midspan until failure to cause tension in the CFRP strip. The CFRP material was S&P CFK 150/2000 with dimensions of 1.2 mm (0.05 in.) by 25 mm (1 in.). Eight different embedment lengths were considered ranging from 150 mm (5.9 in.) to 1,200 mm (47 in.). The results showed that failure occurred from debonding of the shorter embedment lengths. The longer embedment lengths of 850 mm (33.5 in.) to 1200 mm (47 in.) failed by rupture of the CFRP strips. This study demonstrated a minimum embedment length needed to get full use of the CFRP strips and cause it to fail in rupture for flexural stress conditions.

Sena Cruz, et al. [2004] modeled the bond of NSM-CFRP strips to concrete based on pull-out tests. The researchers developed a bond stress-slip relationship for the bond between concrete and CFRP laminates. It is reported that to use the relationship research is needed to assess the influence of bond length and epoxy thickness.

Shield, *et al.* [2005] examined the effects of adhesive type on the bond of NSM-CFRP strips. Pull-out tests were performed on six small-scale specimens for seven different adhesives. The specimens were 152 mm (6 in.) by 152 mm (6 in.) by 203 mm (8 in.)

blocks. Additionally, six larger specimens were tested. These tests used two 610 mm (2 ft.) by 305 mm (1 ft.) by 305 mm (1 ft.) blocks connected with four strips of NSM-CFRP, one on each side. The blocks were then pulled apart until failure. The CFRP material was Hughes Brothers Aslan 500 tape. The NSM groove size was 6.4 mm wide (0.25 in.) and 19 mm (0.75 in.) deep. The small-scale pull outs investigated the following epoxies: Sikadur Anchorfix-3, Master Builders/Chemrex Concresive 1420, 3M DP600NS, 3M DP460NS, Sonneborn Epofil, Sikadur 35 Hi-Mod LV, and Sikadur 32 Hi-Mod. The strongest ultimate strengths came from 3M DP460NS adhesive. Two adhesives were used on the larger specimens. The 3M adhesive was used based on its small-scale performance and Sika Anchorfix-3 was used because it is a more commonly used adhesive. The results showed the 3M adhesive provided higher ultimate strengths. It is reported the 3M adhesive appeared more ductile at failure, which could provide the higher capacities. Shield et al. also looked at the effect of vibration during the curing of the adhesive. This was done by cyclically loading a specimen while the adhesive in the NSM grooves cured. The point of this was to examine if traffic vibrating a bridge girder would affect the NSM retrofit. The test showed no significant change in strength from this cyclical load during the curing process.

2.1.4 Environmental Exposure

Up to this point no studies have investigated environmental exposure on beams reinforced with NSM-CFRP strips for shear. However, studies as discussed below have investigated the environmental effects of beams externally reinforced with CFRP sheets.

Green, *et al.* [2000] and Green, *et al.* [2003] investigated the effects of freeze-thaw on procured CFRP sheets surface bonded for flexure to concrete. Specimens that were 150

mm by 150 mm by 400 mm (6 in. by 6 in. by 16 in.) and 100 mm by 150 mm by 1220 mm (4 in. by 6 in. by 48 in.) were used. The specimens were flexurally strengthened and then subject to various ranges of freeze-thaw cycles. 0-300 cycles were induced by freezing in air and thawing in water. The research reports no adverse affects from freeze-thaw exposure on the CFRP bond.

Malvar, *et al.* [2003] examined the effects of temperature and moisture on epoxy. They used pull-off tests which consisted of bonding small aluminum dollies to concrete blocks, exposing them to various environmental conditions, and then pulling the dollies off in direct tension. They investigated three different adhesives, three temperatures, and four different relative humidities. Test results indicated that high temperature and high humidity produced significant decreases in measured adhesive bond strength.

Grace, [2004] conducted tests on specimens strengthened for flexure with EBR-CFRP sheets subjected to freeze-thaw cycles. The experiment used 2.5 m (8.2 ft.) long concrete beams with a rectangular cross section that was 152 mm (6 in.) wide and 254 mm (10 in.) tall. The beams were reinforced with CFRP plates and fabrics. The beams were exposed to 350 or 700 freeze-thaw cycles. Freezing occurred in air while water was used for thawing. The specimens were tested under four-point loading after environmental conditioning. Strength was reduced by 3.3% and 9.5% for the respective freeze-thaw cycles.

Myers, *et al.* [2005] investigated the effects of environmental exposure including surface moisture, relative humidity, and temperature on the bond strength of EBR-CFRP sheets to concrete. They performed pull-off tests by attaching small adhesive fixtures to CFRP with epoxy adhesive and then pulling the fixture until failure. The results of the tests showed

that high humidity, high surface moisture content, and low temperature can reduce bond strength.

Further research on full-scale RC girders strengthened with EBR-CFRP sheets has been done at Oregon State University. Higgins, *et al*. [2008] tested reinforced beams for accelerated environmental conditions including freeze-thaw, freeze-thaw combined with high-cycle fatigue, and water immersion. T and IT-specimens were tested that had an overall height of 1219 mm (48 in.), a web thickness of 356 mm (14 in.), a flange thickness of 152 mm (6 in.), a flange width of 914 mm (36 in.) and a length of 7925 mm (26 ft.). The materials were based on vintage RCDG bridges in the field. The experiment tested ten specimens including two control beams, five beams subject to freeze-thaw (300 cycles), two beams subject to moisture exposure, and one beam subject to both freeze-thaw and fatigue loading. The results showed that moisture infiltration behind the CFRP combined with freeze-thaw caused a reduction in shear panel stiffness and shear capacity. Long-term moisture exposure alone produced no significant decrease in shear capacity. Freeze-thaw combined with fatigue had little effect on shear capacity if water infiltration was minimized. Fatigue caused some debonding, but the debonding was not significant enough to affect capacity.

2.1.5 Design Provisions

The emergence of CFRP as an increasingly more common strengthening material for RC has led to the development of a design guide. The current code for the design of NSM-CFRP bar retrofitting systems is ACI 440.2R-08. The ACI guidelines for design are based on limit state design principles. Using much of the research referenced in this paper, minimum groove dimensions, epoxy covering, and development lengths are specified for NSM retrofitting. This guide also has provisions for calculating the shear strength provided by FRP retrofitting systems in general. However, this calculation is primarily based on EBR retrofit systems, and there are no specific design calculations for NSM-CFRP shear strengthening. Recommendations on materials, construction requirements, installation, inspection, maintenance, and guidance on which FRP retrofitting system to choose are also included in the guide.

ACI 440 acknowledges that environmental conditions can have adverse affects on FRP systems. Possible environmental impacts are listed as alkalinity, salt water, high humidity, high temperature, and freezing-and-thawing cycles. The current approach accounts for environmental degradation by using a reduction factor based on the exposure condition and type of FRP material. This table is shown below as Table 2.1.

Table 2.1 – ACI 440: Table 9.1 Environmental reduction factors

Exposure conditions	Fiber type	Environmental reduction factor C_E
Interior exposure	Carbon	0.95
	Glass	0.75
	Aramid	0.85
Exterior exposure (bridges, piers, and unenclosed parking garages)	Carbon	0.85
	Glass	0.65
	Aramid	0.75
Aggressive environment (chemical plants and wastewater treatment plants)	Carbon	0.85
	Glass	0.50
	Aramid	0.70

These modification factors are applied to the design ultimate tensile strength and the design rupture strain of the FRP. They are the only means ACI 440 uses to account for environmental exposure. The reduction factors are conservative estimates based on the relative durability of the fiber type. No research is referenced for the bases of these factors. They do not consider different adhesives or any bond strength reductions. These reductions also do not take into consideration if the FRP system is EBR or NSM.

ACI 440 section 9.3.1 also accounts for the response of FRP and concrete to thermal conditions. It states that strains are induced do to the different thermal expansion coefficients of concrete and FRP. It determines that based on research, for small ranges of temperature change, ±50°F (±28°C), the thermal induced strains do not affect bond.

ASTM D 3039 states testing procedures for testing the strength of CFRP. Similar to other materials, a strip of CFRP is mounted in grips and loaded in tension until failure. This standard gives provisions on the testing apparatus, samples, calibration, and conditioning. Testing procedures are prescribed including the test speed, testing environment, data recording, and possible failures.

3. RESEARCH SIGNIFICANCE

The current state of knowledge on NSM-CFRP shear strengthening has several gaps. Most specimens tested for shear strength with NSM-CFRP strips have not been reinforced with internal steel stirrups. The studies show large gains in shear strength due to the NSM-CFRP strips, but these specimens are not characteristic of in-situ member details or proportions. Similarly, most of the test specimens have been over reinforced in flexure to insure shear failure. Flexural reinforcing contributes to shear strength and influences shear performance. These flexurally over-reinforced specimens with NSM-CFRP may not perform the same as those in service with conventional detailing and proportions. Experimental data are needed on realistically reinforced specimens to characterize likely performance with NSM-CFRP for shear strengthening in bridge applications. Furthermore, very few tests have been performed on full-scale bridge girders. Realistic specimens have not been used to investigate environmental effects on NSM-CFRP strips. Based on this, full-scale tests using common reinforcement details and proportions are needed to quantify shear performance and establish or validate design methods for shear strengthening with NSM-CFRP strips. Environmental exposure tests must be conducted on similar full-scale specimens to quantify performance and identify issues that may affect long-term durability.

Figure 3.1 shows the cross-sections and flexural reinforcing ratios of specimens identified in the literature review for a visual comparison of scale. The specimens in this research will have similar dimensions and flexural reinforcing ratio as the specimen in Howell, [2009].

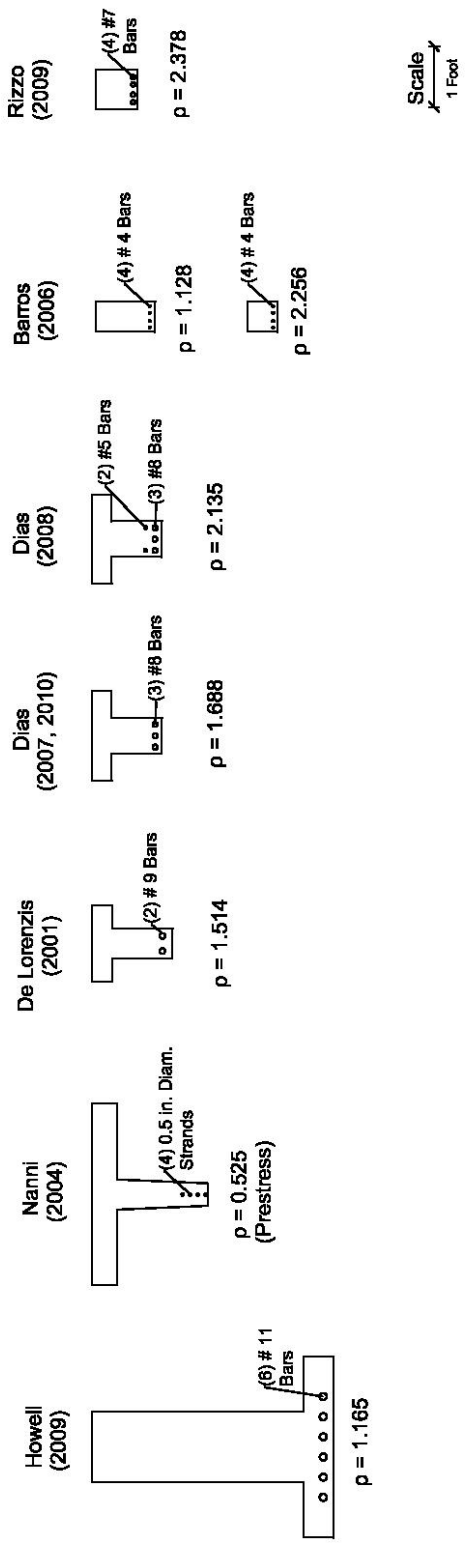

Fig. 3.1 – Scaled cross-sections and flexural reinforcing ratios for literature specimens

4. EXPERIMENTAL PROGRAM (FULL-SCALE SPECIMENS)

To investigate the effectiveness of shear strengthening with NSM-CFRP strips, eight full-scale girder specimens were constructed and tested for this research. Specimens were designed to model the characteristics of full-scale vintage RCDG bridge girders similar to specimens from Higgins, *et al.* [2004]. All of the specimens had consistent dimensions. The overall length was 7920 mm (312 in.) and the depth measured 1220 mm (48 in.). The web width was 356 mm (14 in.) and the flange was 914 mm (36 in.) wide and 152 mm (6 in.) thick. These dimensions are characteristic of those found in typical RCDG bridges designed and constructed in the middle of the last century.

The flexural bars used in all the specimens were 36 mm (#11) bars. To insure anchorage, the flexural bars extended the full length of the specimens and three of the bars located in the stem had hooked ends. This anchorage enabled full development of the flexural steel at critical diagonal crack locations. As discussed later, one of the IT specimens had five flexural bars while the rest had seven. The flexural bars in the IT specimens were located in one layer within the deck, but the T-beam specimens were both constructed with flexural reinforcing bars in two layers of three bars in each layer (6 total) in the stem. The dimensions and flexural reinforcing bars can be seen in typical cross-sections in Figure 4.1.

Typical 7 Bar IT Section

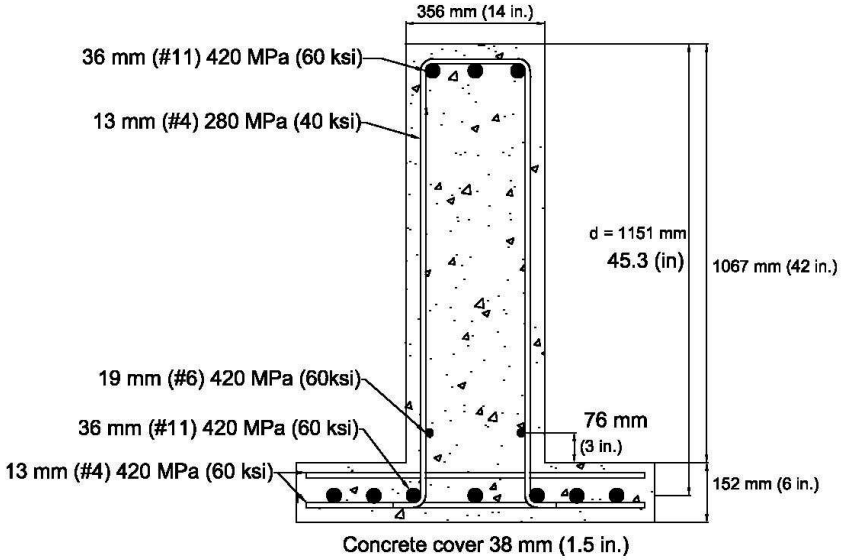

Typical 5 Bar IT Section

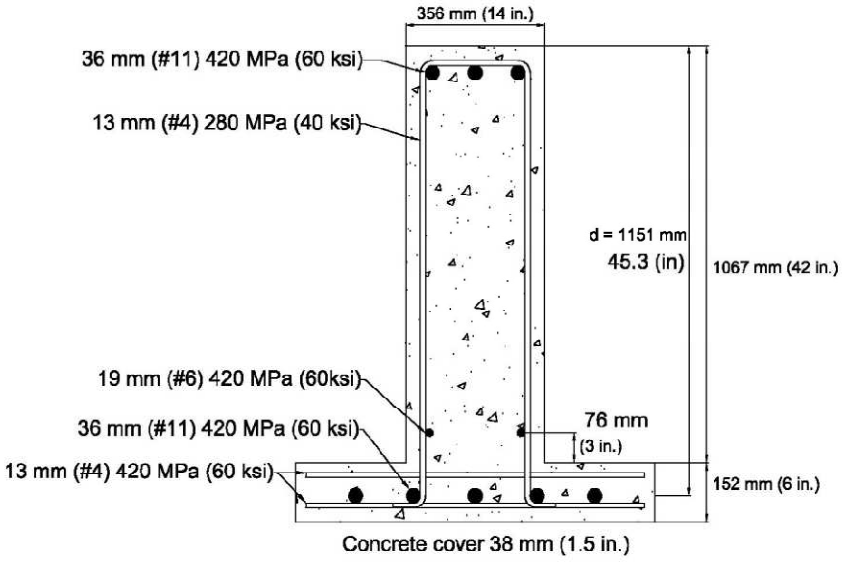

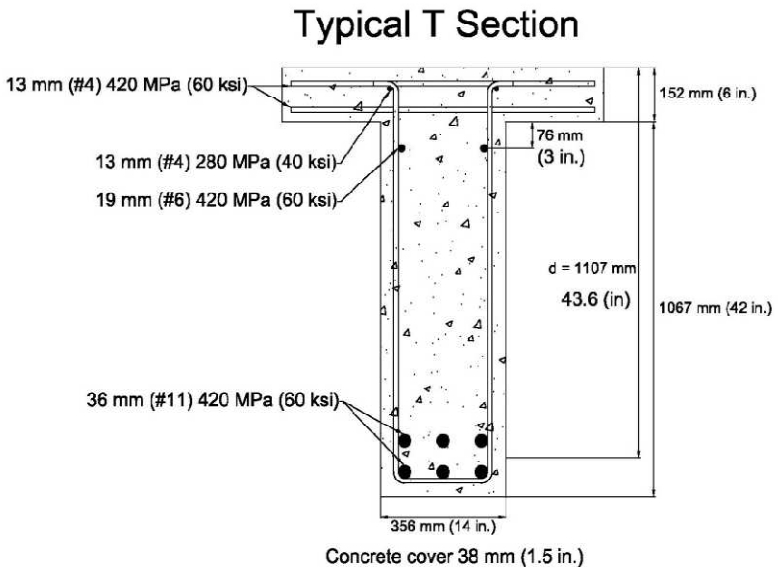

Fig. 4.1 – Typical specimen cross-sections

This research considered several important variables when considering application of NSM-CFRP strengthening of RCDG bridges. Two of the specimens were T-beams which represent shear in the positive moment region of a bridge. These two specimens had different NSM-CFRP strip spacing and were tested to establish shear strength. The other six specimens were IT-beams which represent shear in the negative moment region of a continuous bridge. Four of the IT specimens were tested to establish shear strength and had various amounts of flexural steel, internal steel stirrups, and CFRP strip spacing. One of the IT specimens was tested to investigate the effects of long-term moisture exposure, and one of the IT specimens was tested to identify any deleterious effects from freeze-thaw exposure. Figure 4.2 demonstrates the naming convention used to identify the specimens

and Table 4.1 is the test matrix for the full-scale girder specimens. The method used to determine the stirrup and CFRP strip spacing is explained below.

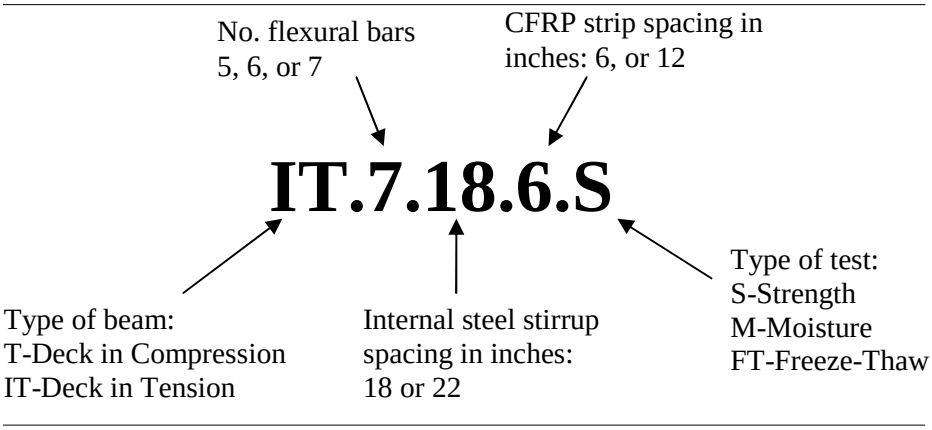

Fig. 4.2 –Full-scale girder specimen identification

Table 4.1 - Full-scale girder test matrix

Specimen	Specimen Type	No. of Flexural Bars	Stirrup Spacing (mm) [in.]	CFRP Spacing (mm) [in.]	Test Type
T.6.18.6.S	T	6	357 [18]	152 [6]	Strength
T.6.18.12.S	T	6	357 [18]	304 [12]	Strength
IT.7.18.6.S	IT	7	357 [18]	152 [6]	Strength
IT.7.18.12.S	IT	7	357 [18]	304 [12]	Strength
IT. 7.22.6.S	IT	7	559 [22]	152 [6]	Strength
IT.5.22.12.S	IT	5	559 [22]	152 [12]	Strength
IT.7.18.6.M	IT	7	357 [18]	152 [6]	Moisture Exposure
IT.7.22.6.FT	IT	7	559 [22]	152 [6]	Freeze-thaw Effects

4.1 Design Method

Before constructing the full-scale girder specimens for this investigation, a prediction of the NSM-CFRP strengthened shear capacity was needed. Due to the lack of available full-scale NSM-CFRP test data, it was uncertain as to the NSM-CFRP contribution to shear strength. The approach used in this research to predict the shear capacities consisted of finding the base shear capacity of test specimens (no NSM-CFRP) and then estimating the additional capacity provided by the NSM-CFRP strips.

The shear strength of the base specimens without NSM-CFRP was calculated using the program Response 2000 (R2K). This computer program was developed at the University of Toronto by Bentz, [2000] for analyzing reinforced concrete sections. R2K performs sectional analysis to determine the member strength based on Modified Compression Field Theory (MCFT). This predicted base shear capacity, $V_{R2K\text{-}base}$, is multiplied by a 0.98 bias for large beams based on experiments done on full-scale RC specimens similar to those considered in this research [Higgins, *et al*. 2004]. Throughout this paper, this bias is applied to adjust the nominal R2K strength to the expected strength when full-scale specimens are being modeled.

The next step was to calculate how much additional shear capacity the NSM-CFRP strips would contribute. From previous research, the full tensile strength of the CFRP strips was not reached when specimens failed because the failure mode usually consisted of concrete cracking around the strip instead of rupturing the CFRP. For that reason, an estimated effective stress for the NSM-CFRP strips was needed to estimate capacity gains. An estimated NSM-CFRP stress was found by review of experiments in previous research and extracting the average NSM-CFRP stresses from these archival specimens. A list of the

previous experimental specimens is shown in Table 4.2. Because the specimens in this research and actual bridges have internal transverse steel reinforcing, only previous research which contained internal steel stirrups and a control specimen with internal steel stirrups was examined.

Table 4.2 – Previous research specimens used for predictions

Researcher	Control Specimen	Strengthened Specimen
De Lorenzis 2001	BSV	BS90-7A
Dias 2007	2S-R	2S-7LV
	4S-R	4S-7LV
Dias 2008	2S-R	2S-3LV
		2S-5LV
		2S-8LV
Rizzo 2009	C	NB90-73-a
		NB90-73-b
		NB90-45-b
		NS90-73-a
Howell 2009	Control	B.IT.NC.NS
Dias 2010	2S-R	2S-4LV
		2S-7LV
		2S-10LV

Using these reported values, the base strength of the specimens for each experiment was computed using R2K. The cross-sections were modeled for every specimen and a graph of Transverse Reinforcing Pressure vs. Average Web Shear Stress was created. In this graph, transverse reinforcing pressure represents the average shear force from the transverse reinforcing relative to the web area. A curve was plotted by varying the amount of transverse reinforcing in the R2K models and recording the corresponding shear capacities for the reported shear-moment ratio in the experimental specimens. The values from R2K were multiplied by a 1.05 bias [Bentz, 2000] based on past experimental calibration of

R2K to smaller beam specimens. The nonlinear characteristic of these curves comes from MCFT and is not linear like ACI 318 would assume. An example graph showing this base curve is shown below in Figure 4.3.

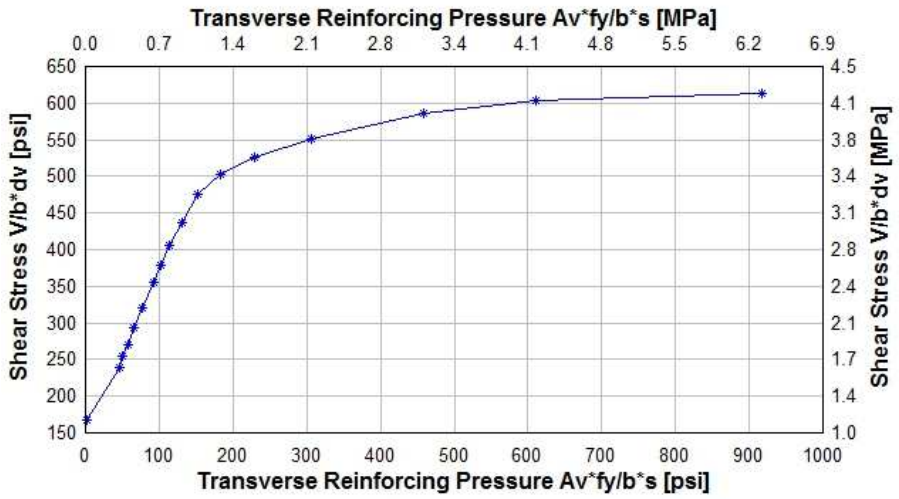

Fig. 4.3 – Example of base shear curve created using R2K

Using these graphs, the shear capacity of each archival specimen was converted to stress and plotted. Then the shear capacity of each retrofitted specimen was converted to a stress and plotted on the y-axis. By finding the corresponding points on the R2K curve, transverse reinforcing pressures were extracted from the x-axis. The difference between these values shows the increase in transverse reinforcing pressure that was attributed to the addition of the NSM-CFRP strips based on MCFT. This is illustrated in Figure 4.4. The R2K curves for all the specimens examined along with their control points and retrofit values are shown in the appendix.

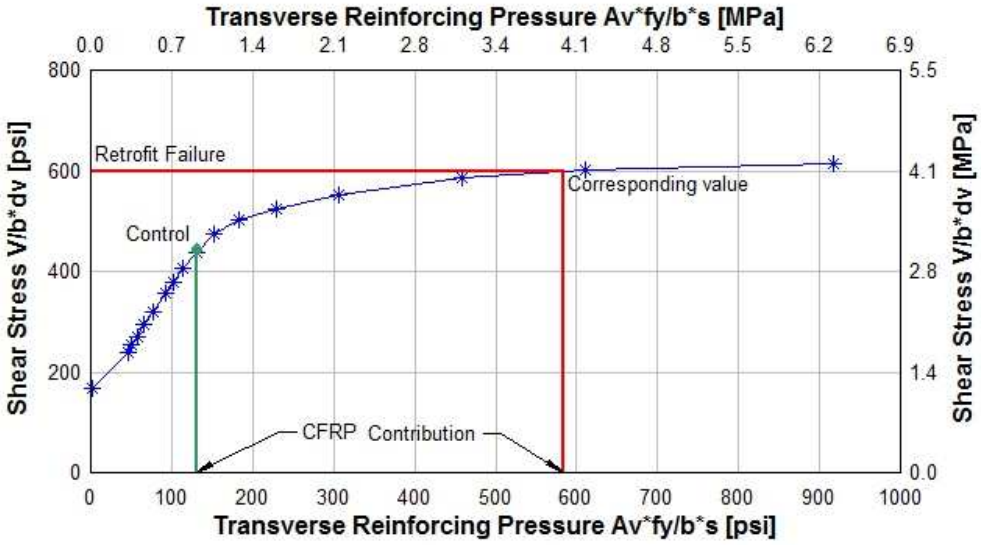

Fig. 4.4 – Example gain in transverse reinforcing pressure due to NSM reinforcing

The internal steel stirrups can support the shear stress up to the control point. The NSM-CFRP strips must provide the additional transverse pressure to be able to achieve the reported shear capacity of the specimens. With the gain in transverse pressure attributed to the NSM-CFRP strips, the stress in the NSM-CFRP strips was then determined as:

$$Gain_{FRP} = \frac{A_{fv} * f_{fe}}{b * s_f} \qquad \text{Equation 4.1}$$

where,

$$f_{fe} = \frac{Gain_{FRP} * b * s_f}{A_{fv}} \qquad \text{Equation 4.2}$$

The effective stress in the CFRP strips (f_{fe}) was found for each specimen in the archival research. The f_{fe} values determined using the above approach are shown below in Table 4.3. The values were tested to see if they fit a normal distribution. As shown in Figure 4.5, the f_{fe} values appear to have a normal distribution because they reasonably fit an ideal Hazen plotting function. The mean f_{fe} value of 441 MPa (64 ksi) from all the previous experiments was then used to predict the strength of the specimens in this research.

Table 4.3 – f_{fe} from specimens in previous research and shear capacities

Strengthened Specimen	V_{exp}		$V_{R2K\text{-}base}$		V_{exp} - $V_{R2K\text{-}base}$		f_{fe}	
	[kN]	[kips]	[kN]	[kips]	[kN]	[kips]	[MPa]	[ksi]
BS90-7A	207	46.5	157	35.4	49.4	11.1	596	86.5
2S-7LV	164	36.9	116	26.0	48.5	10.9	378	54.9
4S-7LV	189	42.5	158	35.5	31.1	7.0	333	48.3
2S-3LV	189	42.6	158	35.5	31.6	7.1	803	116.5
2S-5LV	214	48.2	158	35.5	56.5	12.7	719	104.3
2S-8LV	238	53.4	158	35.5	79.6	17.9	595	86.2
NB90-73-a	176	39.6	105	23.7	70.7	15.9	NA	NA
NB90-73-b	149	33.5	105	23.7	43.6	9.8	228	33.1
NB90-45-b	151	33.9	105	23.7	45.4	10.2	151	21.8
NS90-73-a	173	38.9	105	23.7	67.6	15.2	NA	NA
B.IT.NC.NS	740	166.0	734	165.0	4.4	1.0	13	1.9
2S-4LV	202	45.5	141	31.8	60.9	13.7	558	81.0
2S-7LV	225	50.5	141	31.8	83.2	18.7	500	72.5
2S-10LV	239	53.6	141	31.8	97.0	21.8	417	60.5

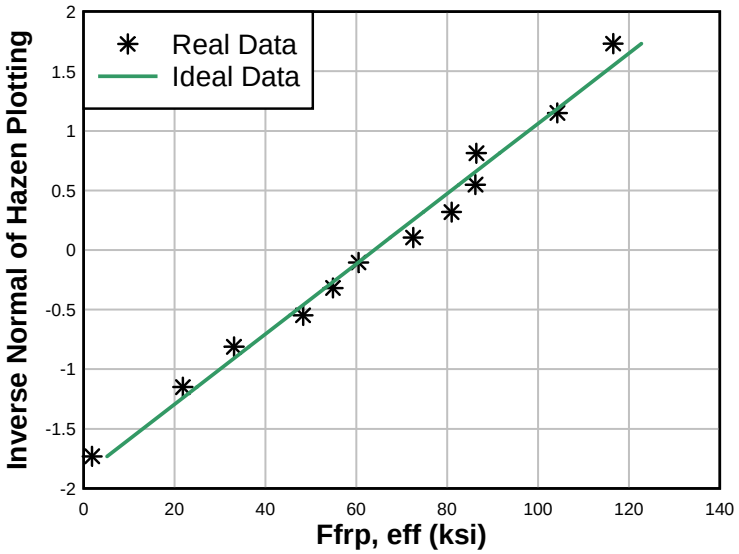

Fig. 4.5 – Distribution of f_{fe} from previous research

4.2 Specimen Shear Design

The estimate for the stress contribution of the NSM-CFRP strips allowed the shear reinforcing for the test specimens to be designed. The first step was to create transverse reinforcing versus average shear stress relationships for the IT and T specimen cross-sections. This was done using the same method as described above by varying the amount of transverse reinforcement and using R2K to solve each typical cross-section for the shear-moment ratio used in the experimental setup. The graphs for the typical IT and T sections are shown in Figure 4.6. For design, these graphs were based on an estimated concrete compressive strength of 27.6 MPa (4000 psi) and manufacturer reported reinforcing steel strengths of 467 MPa (68 ksi) for the flexural steel and 352 MPa (51 ksi) for stirrups. For more accurate strength predictions after construction, a separate graph was made for each specimen taking into account actual day-of-test concrete strengths and steel strengths from material tests.

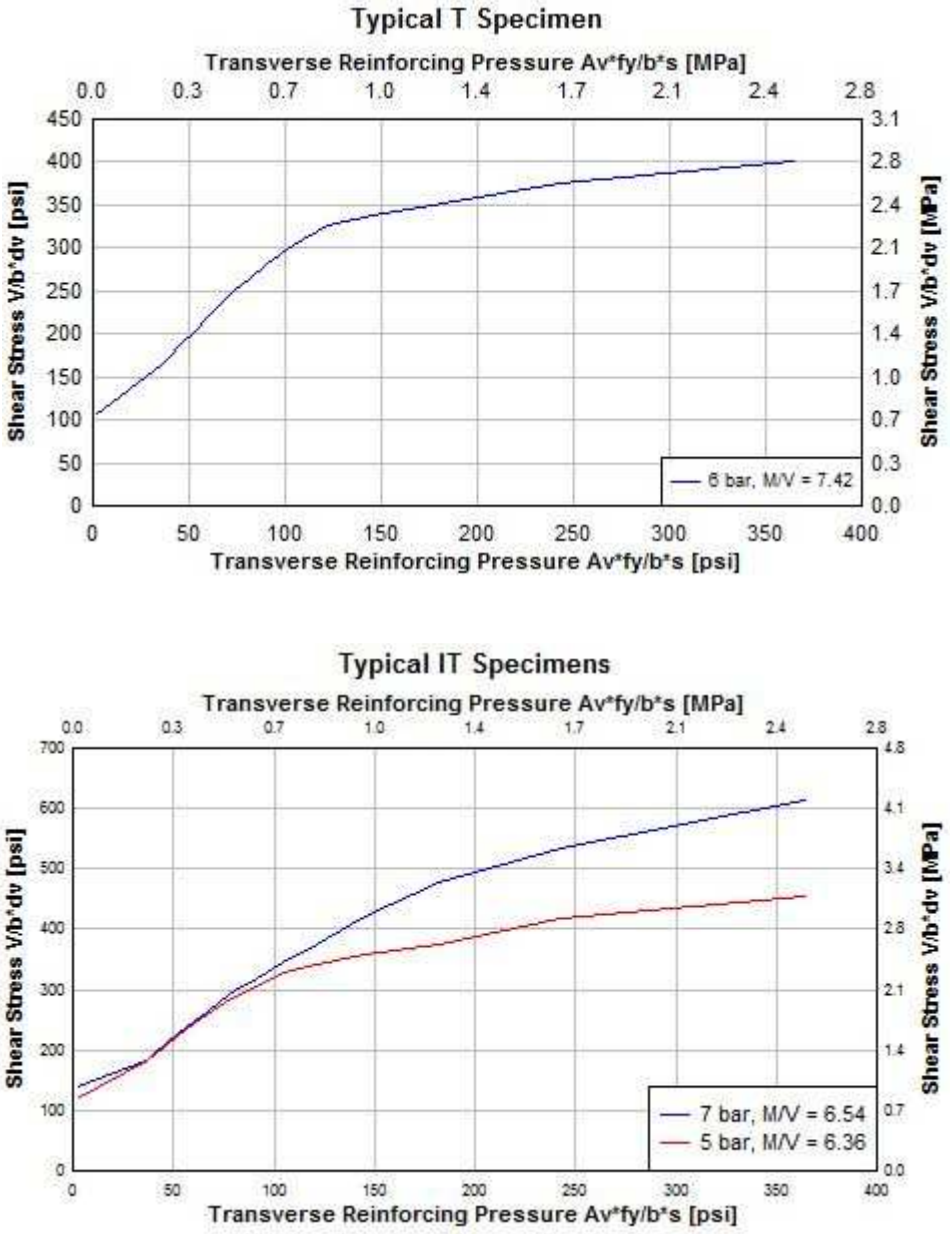

Fig. 4.6 – Shear curves created using R2K for typical cross-sections

It should be noted that the graph for the IT section has curves for specimens with five (5) 36 mm (#11) flexural reinforcing bars and for seven (7) 36 mm (# 11) flexural reinforcing bars. These curves are different because they are based on MCFT which accounts for the

effect of flexural reinforcing on shear strength. A key feature of these curves is that they do not represent a linear increase in shear stress with increasing transverse reinforcing over the range of values. It can be seen in Figure 4.6 that the IT curve with more flexural bars retains the steeper slope over a wider range of transverse reinforcing values. Therefore, by adding the same amount of transverse reinforcing to both cross-sections, the shear capacity of the specimen with seven flexural bars will exhibit a larger increase in shear strength than the specimen with five flexural bars. This interaction is an important practical consideration to ensure that a design can actually achieve the desired strength, especially for girders with low flexural reinforcing ratios. It is also important because in nearly all of the previous research on NSM-CFRP strengthened specimens, heavy flexural reinforcing was used to insure shear failure. Due to this over-reinforcement, the shear strength gains attributed to the NSM-CFRP reinforcing reported in the research are likely larger than what would be observed in realistic field installations. To consider this interaction, specimens were constructed with both five and seven flexural reinforcing bars and the same amount of transverse reinforcing.

In order to observe the shear curves, strength specimens were constructed with two different NSM-CFRP strip spacings of 152 mm (6 in.) and 305 mm (12 in.). These spacings were chosen because they provide substantial strength gains above the control, and were thought to keep the estimated strength below the flexural capacity of the beams. Originally, this research planned for two T specimens, two IT specimens with five flexural bars, and two IT specimens with seven flexural bars to be tested for strength. The two other environmentally subjected beams were IT specimens constructed with the seven flexural bars and 152 mm (6 in.) NSM-CFRP spacing. This provided the largest difference

in shear capacity between the specimen and the non-retrofit control so any degradation due to environmental exposure would be easier to distinguish.

All of the specimens were to be constructed with a 457 mm (18 in.) internal steel stirrup spacing to match previous tests done at Oregon State University and represent a realistic amount of internal steel stirrups above the minimum required by design specifications. The first specimen constructed and tested was an IT with seven 36 mm (#11) bars. This specimen turned out to be stronger than predicted and was at the limits of the hydraulic testing capacity in the laboratory. Therefore, one of the IT specimens with five bars was not constructed; instead an IT with seven flexural bars, 559 mm (22 in.) stirrups, and 152 mm (6 in.) NSM-CFRP spacing was constructed to use as a control in order to lower the final failure load of the remaining unconstructed specimens. The one IT specimen constructed with five bars was also constructed with 559 mm (22 in.) stirrups and strengthened with 152 mm (6 in.) CFRP strip spacing, but this specimen started to fail in flexure. To achieve a shear dominated failure, half the NSM-CFRP was removed by saw-cutting it out of the specimen. This will be discussed further in the results section, but this resulted in the specimen having 305 mm (12 in.) CFRP strip spacing. With all these factors taken into account, the specimens constructed are shown on the curves in Figure 4.7. The baseline points represent the cross-sectional strength without any NSM-CFRP retrofit. The predicted shear strengths of the specimens based on these curves are listed in Table 4.4.

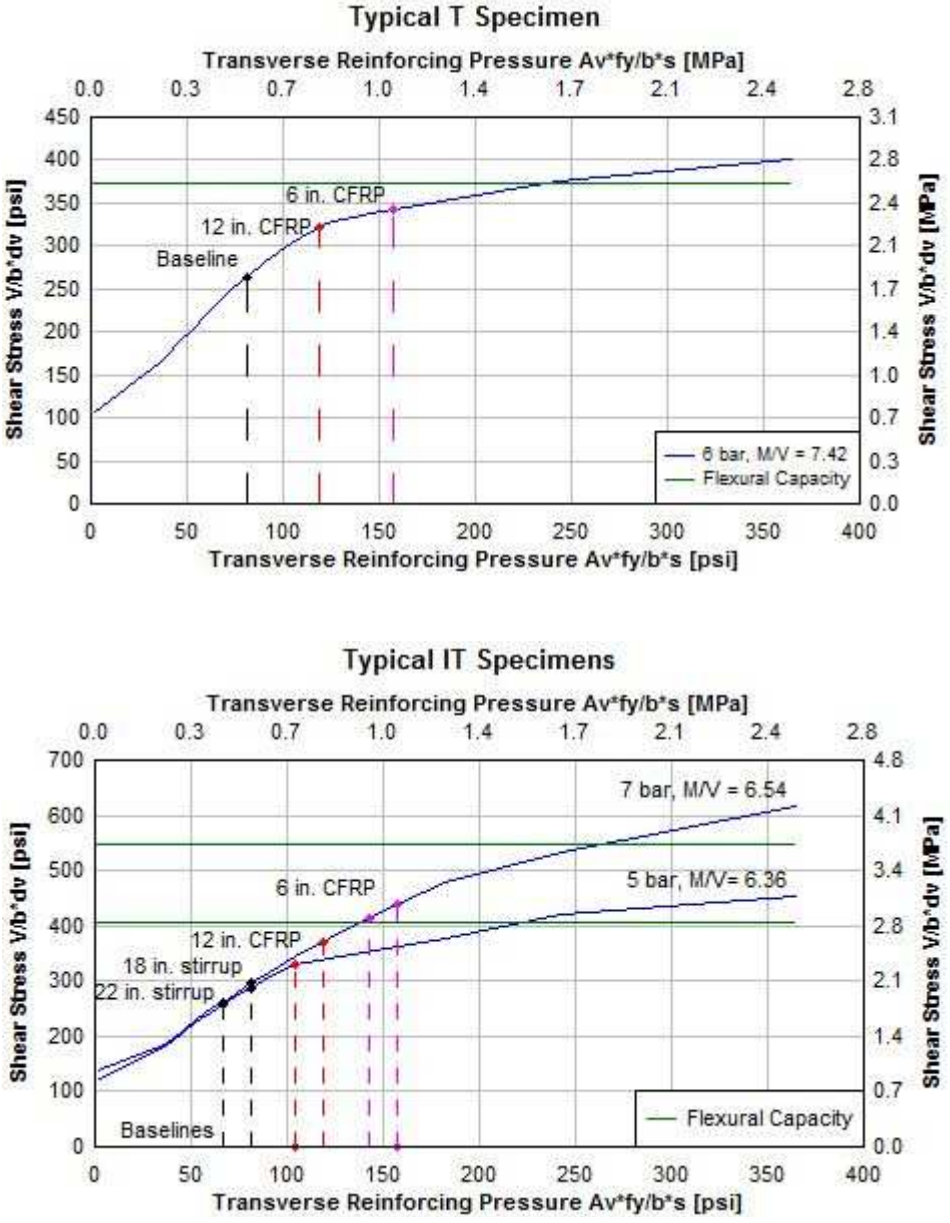

Fig. 4.7 – Typical shear stress vs. transverse reinforcing interactions for constructed specimens

Table 4.4 – Predicted shear strength based on f_{fe} derived from previous experiments and estimated material properties

Specimen	Predicted Shear Strength	
	[kN]	[Kips]
T.6.18.6-S (3)	876	197
T.6.18.12-S (4)	823	185
IT.7.18.6-S (1)	1023	230
IT.7.18.12-S (6)	867	195
IT. 7.22.6-S (7)	965	217
IT.5.22.12-S (5)	814	183
IT.7.18.6-M (2)	1023	230
IT.7.22.6-FT (8)	965	217

A four-point loading scheme was used to test these specimens. This setup applies equal shear stress to both sides of the specimen. Without modifications a specimen would be just as likely to fail on either side. To ensure failure in the NSM-CFRP strengthened half of the specimen, the other half was over-strengthened. This allowed only one side to be instrumented, strengthened, and observed for testing. This was done by placing grade 420 (60 ksi) stirrups at 152 mm (6 in.) on the side opposite the NSM-CFRP. The stirrup layout for the specimens can be seen below in Figure 4.8.

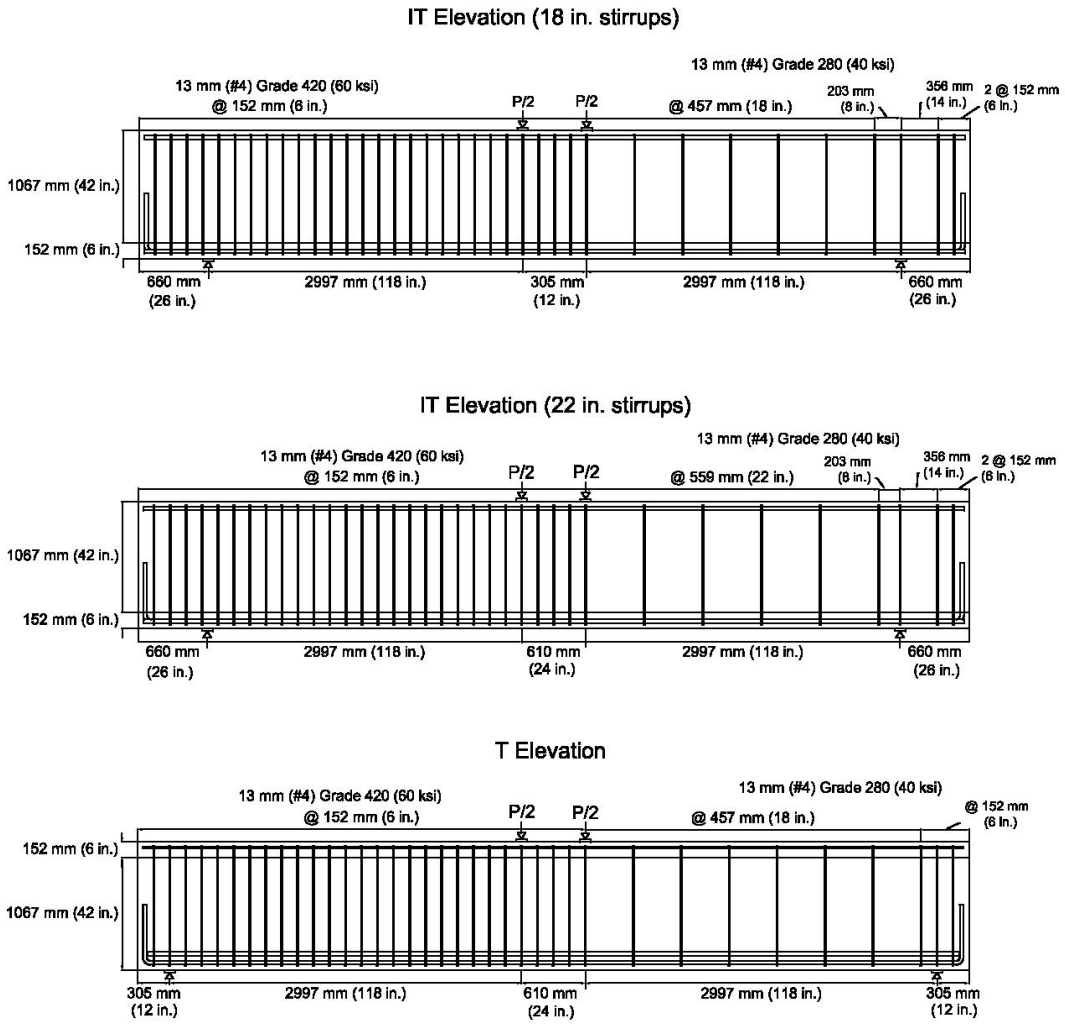

Fig. 4.8 – Specimen elevation view with internal steel reinforcing

4.2 Materials

4.2.1 Concrete

The concrete used to construct the specimens came from a local ready-mix supplier and was the same mix that has been used in previous research at Oregon State University. The mixture design is based on AASHTO “Class A,” with a specified compressive strength of

21 MPa (3000 psi). This is representative of what would have been used in 1950s era bridges [Higgins, *et al*. 2004]. The concrete mixture included admixure agents Daravair at 58 mL/m^3 (1.5 oz/yd^3) and WRDA-64 at 735 mL/m^3 (19 oz/yd^3). Before casting, standard slump tests were performed and water was adjusted to achieve an approximate 127 mm (5 in.) slump. Concrete cylinders that were 305 mm (12 in.) tall and had a 152 mm (6 in.) diameter were cast from the same truck as each specimen. The concrete compressive strength was determined in accordance to ASTM C39M/C 39M-09a and ASTM C617-09a. Cylinders were tested at 28 days, on the day of pre-cracking, and on the day of strength testing. Average concrete strengths for 28 days and the day-of-test are reported in Table 4.5.

Table 4.5 – Concrete compressive strengths

Specimen:	28 Day Compressive Strength		Retrofit		
			Days since cast	Compressive Strength	
	[MPa]	[psi]		[MPa]	[psi]
T.6.18.6.S	24.8	3604	65	25.7	3729
T.6.18.12.S	28.2	4095	76	29.2	4236
IT.7.18.6.S	31.2	4529	56	31.1	4506
IT.7.18.12.S	27.8	4039	98	30.9	4475
IT 7.22.6.S	24.4	3536	56	27.2	3946
IT.5.22.12.S	27.0	3920	59	30.0	4355
IT.7.18.6.M	26.5	3838	267	26.8	3889
IT.7.22.6.FT	29.0	4201	189	30.1	4361

The concrete cylinders were cured at ambient temperatures in the laboratory. The cylinders for specimen IT.7.18.6.M were not cured under the same submerged condition as the specimen. However, this difference is negligible because the full-scale girder specimen cured for approximately 80 days before being submerged in water. Table 4.5 shows that even though all the concrete had the same specified strength, the actual strength had a large

amount of variation and likely contributes to some variation in the test results, but is incorporated in the analysis methods described in later sections.

4.2.2 Steel

Most of the reinforcing steel used in 1950's vintage bridges is 280 MPa (40 ksi) grade steel. This is different than the 420 MPa (60 ksi) standard grade bars commonly used by in construction today. To better represent 1950's bridges, the lower grade steel was desirable. Therefore, the stirrups used for the test section of the specimens were grade 280 (40 ksi) 13 mm (#4) bars. However, Grade 420 (60 ksi) 36 mm (#11 bars) were used as the flexural reinforcing because it is difficult to obtain large diameter Grade 280 (40 ksi) bars. The actual tensile properties of the steel were tested based on ASTM E8/E8M-09a. The coupons for the flexural #11 bars were machined down to 13 mm (0.5 in.) diameter samples to be tested. The reinforcing steel tensile properties are shown in Table 4.6.

Table 4.6 - Reinforcing steel properties from coupon tests

Bars	Grade		Yield Strength, f_y		Ultimate Strength, f_u	
	MPa	ksi	MPa	ksi	MPa	ksi
# 4 Stirrups	280	40	350	50.7	556	80.7
# 11 Flexural bars	420	60	478	69.3	712	103.3

4.2.3 Carbon Fiber Reinforced Polymer

When selecting the NSM-CFRP material it was decided that rectangular strips of CFRP would be better suited for the present NSM application than round bars. The narrow rectangular strips fit into a thinner saw-cut groove than a round bar, which means reduced saw cutting and less exposure to environment. A rectangular strip also provides more surface area for bonding with the epoxy. One of the only commercially available rectangular CFRP strips recommended for NSM strengthening and the most popular one in

the United States is made by Hughes Brothers, in Seward Nebraska. Hughes Brothers carbon fiber has been used in previous research for NSM applications and the carbon fiber strips have a unique roughened surface. Due to this, Hughes Brothers Aslan 500 rectangular carbon fiber tape was chosen as the CFRP material. Coupon tests were performed according to ASTM D 3039 to determine the actual material properties. One issue of testing the CFRP is that the grips of the test machine can damage the CFRP causing it to weaken and break at the grips. This was mitigated by bonding polymer computer board to the ends of the CFRP coupons so the grips would not damage the fibers. Only coupons that failed by rupture/brooming were considered as demonstrated in Figure 4.9.

Table 4.7 – Hughes Brothers CFRP material properties

Property	Manufacture Reported		Measured	
Cross Sectional Area	31.2 mm^2	0.05 in^2	31.2 mm^2	0.05 in^2
Tensile Strength	2068 MPa	300 ksi	2366 MPa	343 ksi
Modulus of Elasticity	124 GPa	18000 ksi	138 GPa	20,081 ksi*
Ultimate Strain	0.017		0.017	

*Modulus of elasticity from experiments done by [Howell, 2009]

Fig. 4.9 – Example of desired CFRP coupon failure

4.2.4 Adhesive

The adhesive used in this project was Concresive 1420 epoxy made by BASF. It was chosen because it is readily available from local distributers, relatively inexpensive, and it is one of the four adhesives Hughes Brothers suggests for NSM installations. Concresive 1420 also performed adequately in the work done by Shield, *et al.* [2005]. It should be noted that 3M DP460NS epoxy performed the best in the experiments from Shield, *et al.* [2005] and has been used in Oregon State University tests before, but this epoxy was not chosen for this research due to its expense. The reported properties for Concresive 1420 are shown in Table 4.8.

Table 4.8 – Concresive 1420 manufacturer material Properties

Manufacturer Reported Property	Concresive 1420	
	[MPa]	[Ksi]
Tensile Strength	34.5	5.03
Compressive Modulus	2900	420
Compressive strength	67.6	9.8
Bond Strength	20.7	3.0
Ensured Full Cure Time	7 days @ 77 °F	

The epoxy was conditioned between 16 and 27 °C (60 and 80 °F) when applied and the concrete specimens were above 4 °C (40 °F) when retrofitted. The epoxy was allowed to cure for at least seven days to ensure a full cure. On colder days a tarp was erected over the specimen with a heater inside to maintain curing temperatures within the manufacturer limits.

5. RESEARCH METHODS

5.1 Construction & Instrumentation

All of the specimens for this research were constructed in the Oregon State University Structural Engineering Research Laboratory. The first step of construction was to attach strain gages to the steel. Strain gages were placed at midheight on one leg of each stirrup on the less reinforced side of the specimen. No strain gages were placed on the over strengthened side of the specimen. Strain gages were also placed at midspan of the 36 mm (#11) flexural bars. To protect the gages a water proof layer of sealant was applied, and a thin neoprene pad and piece of foil was placed over each gage. After strain gaging, the reinforcing cage was assembled while being supported by a steel frame adjacent to the formwork. Standard steel reinforcing ties were used to connect the bars to each other.

Fig. 5.1 – Example of reinforcing cage

After a layer of form oil was applied to the wooden forms, the completed reinforcing cage was lifted into the formwork. Steel chairs and plastic spacers were used to insure the

proper clear cover was achieved. The formwork consisted of two T-shaped forms that allowed two specimens to be poured on each casting day. A separate concrete truck was used for each specimen due to their size. Concrete test cylinders were poured with concrete from the middle of each truck to ensure a representative sample. A concrete vibrator was used to consolidate the concrete and trowels were used to give the specimens a smooth top surface. Wet burlap was placed on top of the specimens to keep them moist while they cured. The specimens were allowed to cure at least seven days before being removed from the forms. The IT-specimens were constructed and cast as a T and then flipped over after curing.

Before testing, the specimens were instrumented with displacement sensors to measure overall deformations. On each side of the specimens a 127 mm (5 in.) string potentiometer was attached at midspan. Support settlements were measured at each corner of the beam over the support with 13 mm (0.5 in.) displacement sensors. These support displacements were subtracted from the midspan displacements to remove the rigid body deformations from the specimens. Diagonal displacements were also measured with six 51 mm (2 in.) string potentiometers that were attached directly to the specimen. The location of all the sensors on the weaker end of a specimen can be seen below in Figure 5.2. When the specimens were tested, data from all sensors were collected along with data from the strain gages and a 2450 kN (550 kip) load cell which was located between the specimen and hydraulic actuator. A more thorough discussion about the sensor labeling along with graphs of all the collected data are reported in the appendix.

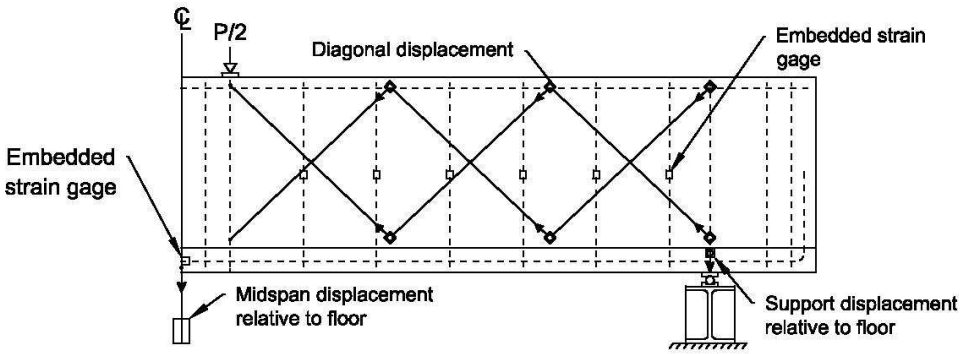

Fig. 5.2 – Typical specimen instrumentation

5.2 Test Setup

The full-scale specimens were all tested under four-point loading. To withstand the high reaction loads, the test frame was located on the strong floor of the Structural Engineering Research Laboratory at Oregon State University. The load was generated with a 2224 kN (500 kip) working load hydraulic actuator which is suspended vertically from the reaction frame. The actuator applied the load to the specimens through a spreader beam. The spreader beam rested on two 51 mm (2 in.) diameter steel rollers which in turn were supported by two 102 mm (4 in.) wide steel plates spaced 610 mm (24 in.) apart at the midspan of the specimens. Hydro-stone was placed between these plates and the concrete specimen to insure the load was applied through a uniform bearing surface. The specimens were supported by 102 mm (4 in.) wide steel plates that rested on 51 mm (2 in.) diameter steel rollers on top of reaction beams. The supports were located 660 cm (260 in.) apart for IT-beam specimens and 731 cm (288 in.) apart for the T-beam specimens. This corresponds to a shear span-to-depth ratio of 2.6 and 3.0 respectively. The T-beam specimens were also braced at the supports laterally by columns with rollers which

prevented the specimens from moving out-of-plane but still allowed them to rotate as they were loaded. The test setup and loading dimensions are shown below in Figure 5.3.

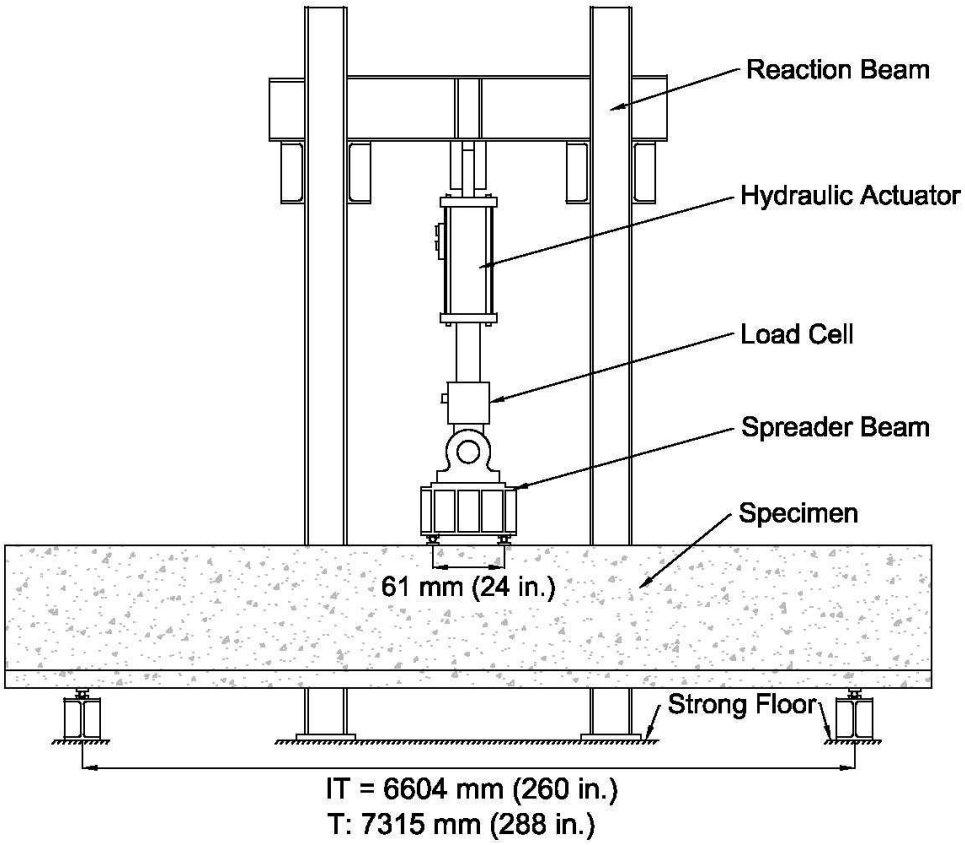

Fig. 5.3 – Full-scale test configuration

5.3 Testing Protocol

All of the specimens were pre-cracked before application of the NSM-CFRP strips. The purpose was to make the specimens a better representation of in-service bridge girders which would have cracking when repaired. The specimens were allowed to cure at least 14 days after the cast date before being instrumented and moved into the test setup for pre-cracking. All of the specimens were placed in the test setup with the weaker reinforced end pointing north. Before testing, a grid was drawn on the east surface of the specimen

with chalk lines. These grid lines were spaced at 25 mm (12 in.) and labeled from the centerline out as N1 through N12. This grid was used to locate cracking in the digital photos. The location of the internal steel stirrups was found using a profometer and marked on the surface. The specimens were incrementally loaded to 890 kN (200 kips) to induce cracking in the member. The 890 kN (200 kip) load was chosen because previous research done at Oregon State University has shown that this load level produces reasonable diagonal cracking and higher loads tend to fail the strain gages. The specimens were tested with a load controlled rate of 4.45 kN/s (1 kip/s). The loading consisted of 111 kN (25 kip) increments up to 445 kN (100 kips) and then 222 kN (50 kip) increments up to 890 kN (200 kips) with unloading between each load step. After each increment, the load was reduced and held at 111 kN (25 kips) below the maximum load so that cracks could be marked on the beam without compromising safety or inducing creep at the peak load. A digital photo was taken at each load step and used to render crack map drawings which are shown in the appendix. At a load of 890 kN (200 kips) the crack widths observed with a hand held crack comparator were at least 0.76 mm (0.03 in.) for each specimen. After pre-cracking, the full load cycle was repeated and data was collected again. This was to retrieve load behavior data for each beam in the cracked condition (baseline condition) which could be compared to the data after retrofitting. The baseline data is different from the pre-crack load data because presence of cracks changes the distribution of internal stresses compared to the uncracked condition.

After application of the NSM-CFRP as discussed below (and for some samples exposure to environmental conditioning), the specimens were ready to be tested for shear strength. The specimens were moved into the test setup and instrumented with the same sensors that were used for pre-cracking. A slaked-lime white wash was applied to the east surface of

the specimen to allow new cracks to be observed, and the chalk gridlines were remarked. The specimens were then incrementally loaded with 111 kN (25 kip) load steps up to 445 kN (100 kips) and then 222 kN (50 kip) load steps up to failure. The specimens were unloaded after each load cycle prior to reloading. Cracks were marked and digital photos were taken after each load step.

5.4 Saw-Cutting

Following the pre-cracking, grooves were cut in the webs of the specimens. The cutting was performed by Columbia Concrete Sawing Company. The groove dimensions were determined to meet ACI 440.2R-08 section 13.3 which states the groove width must be at least three times the CFRP width and the groove depth must be at least 1.5 times the CFRP depth. Therefore, based on the Aslan 500 dimensions of 16 mm (0.63 in.) by 2 mm (0.079 in.) the following must be met.

$$\text{Groove depth} \geq 1.5 * 0.63 \text{ in.} = 0.945 \text{ in.}$$

$$\text{Groove width} \geq 3.0 * 0.079 \text{ in.} = 0.237 \text{ in.}$$

The grooves cut in the specimens had a depth of 25 mm (1.0 in.) and a width of 8 mm (0.31 in.) to meet the requirements. The grooves were cut vertically into the web of the specimens and went as close to the flange as the saw could without cutting into the flange. The cut reached to within 25 mm (1.0 in.) of the flange by using a concrete chain saw with a small point on the end of the saw's bar. After the grooves were cut, a pressure washer was used to clean the grooves, and then they were allowed to dry. Previous research has shown NSM repairs done perpendicular to the crack angle are more effective. Nonetheless, this research chose a vertical orientation because it is more practical to

construct and does not risk cutting any internal steel stirrups if the concrete clear cover is incorrect.

Fig. 5.4 – Sawing NSM grooves in a specimen

5.5 CFRP Retrofitting

After the grooves were dry, the specimens were retrofitted with CFRP. The epoxy used on the full-scale specimens was Concresive 1420. It was applied with a pneumatic gun and the adhesive was warmed before applying to insure proper application procedures. The first step was to fill the groove about 3/4 full with epoxy. Then a CFRP strip was pushed into the center of the groove while making sure epoxy squeezed out on both sides of the CFRP strip. More epoxy was then applied to fill the groove and a putty knife was pulled across the surface to remove the excess adhesive.

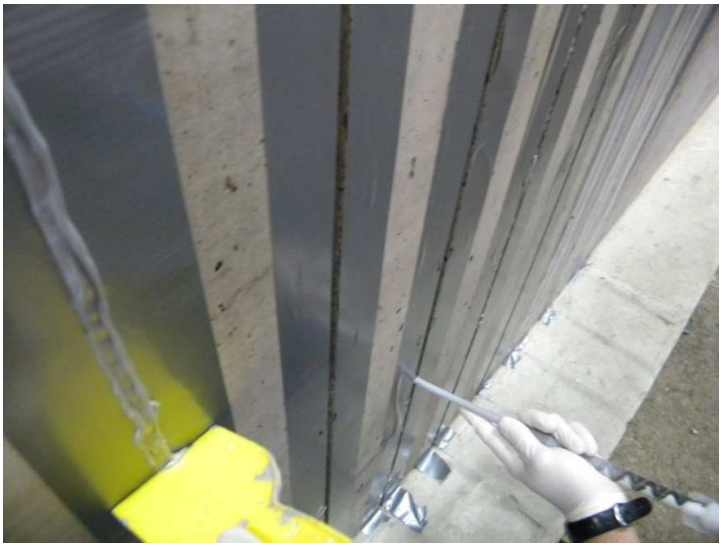

Fig.5.5 – Epoxying CFRP strips into NSM grooves

Some of the CFRP bars were instrumented with strain gages. Gages were placed only on one face of the specimen and were located where major diagonal shear cracks intersected the NSM grooves. A small region was sanded smooth on the CFRP for the strain gage to insure contact but not sanded enough to reduce the cross-sectional area of the bars. A wire was placed on the gage that extended out of the epoxy so strain could be measured in the CFRP at the crack locations. The CFRP strain gage locations are shown in the appendix on the crack maps for each specimen.

After the installation was complete, the specimens were allowed to cure at least seven days. A tent was constructed over the beams with heaters to insure curing temperatures. The beams that cured at a lower temperature were left several days past the seven day minimum to insure full curing.

Table 5.1 – Retrofit curing temperature and relative humidity

Specimen	Avg. cure temp [F]	Avg. cure RH [%]
T.6.18.6.S	71	58
T.6.18.12.S	71	58
IT.7.18.6.S	71	58
IT.7.18.12.S	64	64
IT. 7.22.6.S	56	72
IT.5.22.12.S	65	65
IT.7.18.6.M	71	58
IT.7.22.6.FT	67	61

5.6 Moisture Exposure Process

After installation of the NSM-CFRP, specimen IT.7.18.6.M was subject to moisture exposure. To do this, a tank large enough to hold the full-scale specimen was constructed outside the laboratory. It was built with wooden walls and a wooden floor and had a rubber liner to make it water tight. The specimen was lifted into the tank with a crane and set on two rubber pads to allow water to flow beneath the specimen. Steel rods were placed to hold the walls together and then the tank was filled with fresh water until the specimen was completely submerged. The specimen was allowed to sit in the tank for six months before being removed to test. This time period was chosen to represent a bridge girder during a full wet season in Oregon.

Fig. 5.6 – Specimen IT.7.18.6.M submerged in the dunk tank

5.7 Freeze-Thaw Exposure Process

After installation of the NSM-CFRP, specimen IT.7.22.6.FT was exposed to freeze-thaw cycles. This exposure was intended to reveal any strength deterioration from freezing and thawing typical of Oregon conditions. This was done by placing the specimen in an environmental chamber that could rapidly freeze and thaw the specimen. The chamber monitors the ambient air temperature and has fans to keep the air circulating inside. The freezing and thawing was achieved with a four step cycle. A one hour warm soak at 16°C (61°F), a 30 minute ramp down to -20°C (-4°F), a one hour cold soak at -20°C (-4°F), and then a 30 minute ramp back to 16°C (61°F). The cycle continuously repeated and subjected the specimen to eight freeze-thaw cycles per day. The specimen was subject to a total of 400 freeze-thaw cycles. Type T thermocouples were used to measure the specimen temperature throughout the cycles. Thermocouples were attached to the specimen on both ends and at midspan to monitor surface temperatures. Also, the internal temperature of the

specimen was monitored at depths of 13 mm (0.5 in.), 25 mm (1.0 in.), and 44 mm (1.75 in.) at midspan. This was done by inserting a thermocouple into a drilled whole that was then plugged with insulation. The purpose of this was to ensure that at least the outside 25 mm (1.0 in.) surface was completely frozen and thawed during each cycle because the NSM grooves were 25 mm (1.0 in.) deep. The location of the thermocouples and the typical recorded data are shown below in Figures 5.6 and 5.7. The recorded data show that even the thermocouple embedded 44 mm (1.75 in.) in the concrete was frozen and thawed during each cycle.

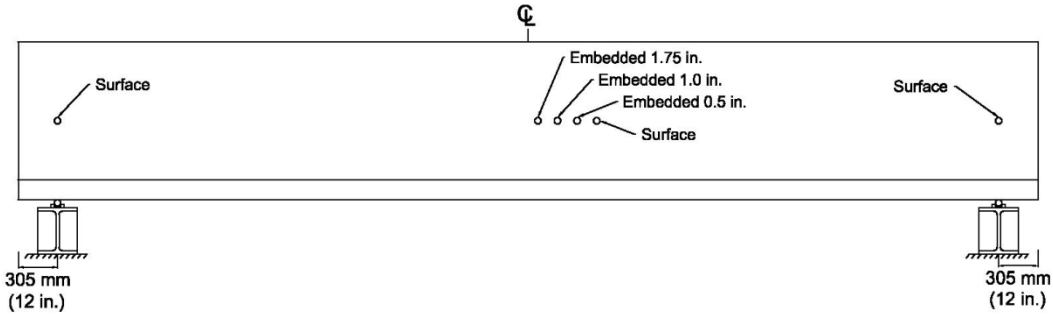

Fig. 5.7 – Thermocouple location on specimen IT.7.22.6.FT

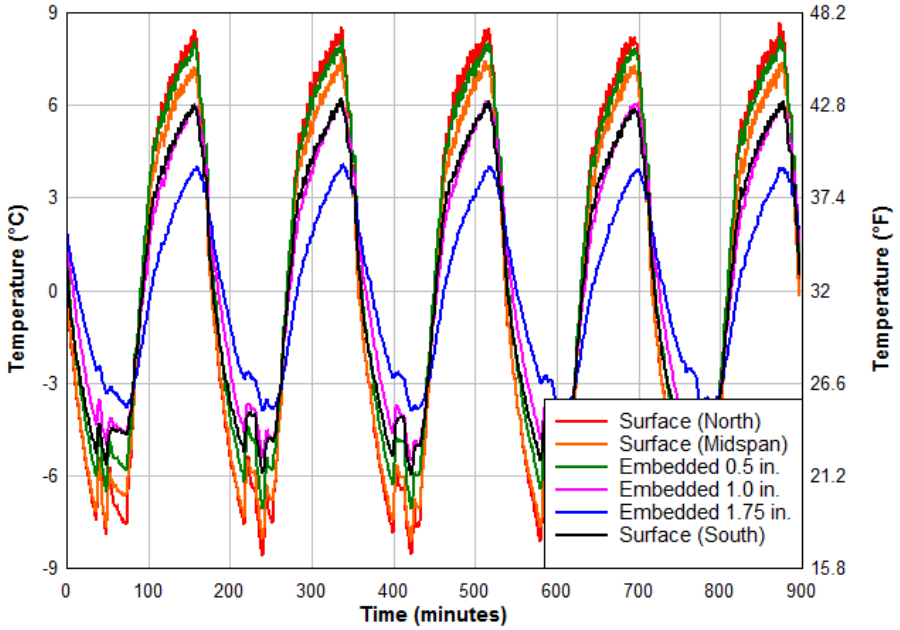

Fig. 5.8 – Typical temperature data from freeze-thaw cycles

When concrete is frozen, water in the concrete pores expands and causes deterioration of the concrete structure [Wight and MacGregor, 2009]. The standard for freeze-thaw testing of concrete, ASTM C 666, indicates that freeze-thaw cycles should be performed under fully wet conditions because the presence of water is what produces concrete deterioration. This is not practical for this research because an in-situ bridge girder is not going to be fully submerged in water. Instead, the surface of the specimen was sprayed with water once a day (every eight cycles). This is the same process that past research at Oregon State University has used, and is representative of the rain and road splash from traffic that an in-situ bridge girder would experience. This process made water available to soak into the concrete and expand during freezing, but also allowed evaporation during the warm cycles. A total cycle count of 400 was chosen to represent severe environmental conditions that an Oregon RCDG bridge could experience. The work of Mitchell, [2008] provides expected freeze-thaw conditions for various regions in Oregon based on data supplied by Remote

Automated Weather Station (RAWS). Representative regions were chosen as the coast region (Tillamook), the Willamette Valley (Stayton), Central Oregon (Tumalo Ridge), and Eastern Oregon (Sage-Hen). The expected number of years to reach 400 freeze-thaw cycles is shown in Table 5.2.

Table 5.2 – Time to achieve 400 freeze-thaw cycle service lives for regions of Oregon

Region (Station)	Freeze-Thaw Frequency (cycles/year)	Years to reach 400 cycles
Coast (Tillamook)	0.73	548
Valley (Stayton)	3.75	107
Central (Tumalo Ridge)	40.5	9.9
Eastern (Sage Hen)	39.5	10.1

The 400 freeze-thaw cycle count clearly represents a different service exposure life for the different regions. The Central and Eastern Oregon sites correspond to an approximate 10 year service exposure. However, it is reasonable to assume that most of these cycles occur with little moisture due to the high desert climate and low precipitation in the regions. Alternatively, the 400 cycle count in the Coastal and Valley sites correspond to a very long service exposure, but most of these cycles would occur with the bridge girder in a wet condition.

6. EXPERIMENTAL RESULTS

After retrofitting and environmental exposure, all of the specimens were tested to failure. Descriptions of each specimen failure along with comparisons between the measured specimen responses are reported in this section. A summary of the salient structural responses are shown below in Tables 6.1 and 6.2. The combination of the force applied by the hydraulic actuator and the dead load of the specimen make up the total experimental shear force (V_{exp}) acting on a specimen at failure. The dead load for each specimen was calculated as the self-weight of the concrete acting on the failure plane assuming the unit weight of reinforced concrete is 23.6 kN/m^3 (150 lb/ft^3).

Table 6.1 – Specimen shear loads at failure

Specimen	Failure Mode	V_{DL}		V_{APP}		V_{exp}	
		[kN]	[kips]	[kN]	[kips]	[kN]	[kips]
T.6.18.6.S	Flexure	17.3	3.9	992	223.0	1011	227.4
T.6.18.12.S	Flexure	17.3	3.9	1026	230.6	1043	234.5
IT.7.18.6.S	Shear	18.2	4.1	1191	267.7	1209	271.8
IT.7.18.12.S	Shear	21.8	4.9	1000	224.8	1022	229.7
IT. 7.22.6.S	Shear	21.4	4.8	1144	257.2	1165	262.0
IT.5.22.12.S	Shear	19.6	4.4	992	222.9	1011	227.3
IT.7.18.6.M	Shear	19.6	4.4	1148	258.1	1168	262.5
IT.7.22.6.FT	Shear	17.8	4.0	1107	248.9	1125	252.9

Table 6.2 – Specimen crack angle and midspan deflection at max shear

Specimen	Failure Angle from Horizontal		Max Midspan Deflection	
	East Side	West Side	[mm]	[in]
T.6.18.6.S	Vertical	Vertical	23.1 yield	0.91 yield
T.6.18.12.S	Vertical	Vertical	19.8 yield	0.78 yield
IT.7.18.6.S	45°	60°	21.8	0.86
IT.7.18.12.S	28°	28°	23.6	0.93
IT. 7.22.6.S	46°	82°	23.4	0.92
IT.5.22.12.S	35°	35°	24.1	0.95
IT.7.18.6.M	60°	54°	24.1	0.95
IT.7.22.6.FT	41°	74°	22.1	0.87

6.1 T.6.18.6.S

This specimen failed in flexure at a load of 1984 kN (446 kips). A vertical crack at midspan grew as the flexural steel yielded and then the concrete in the compression zone failed by crushing. The failure occurred before any attempt was made to force a shear failure. This flexural failure was not desirable because the goal of this research was to test shear capacity. The retrofit specimen was designed to fail in shear, but it failed in flexure because the shear strength contribution of the NSM-CFRP strips was larger than the predicted using small specimens in the archival literature. This result shows the minimum shear contribution from the NSM-CFRP, but the actual shear capacity cannot be determined due to the flexural failure mode.

6.2 T.6.18.12.S

This was the second T-specimen constructed and tested. It was the same as the other T-specimen except it had a 25 mm (12 in.) CFRP strip spacing. This specimen also failed in flexure. At a load of 1895 kN (426 kips) the specimen deflection increased without increasing load. This implied flexural yielding and the test was stopped before the compression zone was compromised. The support locations of the specimen were moved toward the load point to a span of 300 cm (118 in.). This allowed a higher shear force to be applied by decreasing the moment demand. The specimen still began to exhibit flexural yielding so the support was again moved to the base of the largest diagonal crack. This was the final attempt to induce a shear failure, but the specimen still failed in flexure. The compression zone crushed at a load of 2051 kN (461 kips). At failure, the diagonal cracks in this specimen were more pronounced than the other T-specimen. This implies the specimen was close to a shear failure. However, the actual shear capacity cannot be

established as flexural failure occurred. Failure pictures of all of the specimens are shown in Fig. 6.8 through Fig. 6.14

Fig. 6.1 - Specimen T.6.18.12.S was approaching a shear failure (specimen is inverted in photograph prior to loading on a truck for disposal)

6.3 IT.7.18.6.S

This was the first NSM-CFRP strengthened IT specimen for this research, and it achieved a shear dominated failure. The specimen also exhibited higher shear capacity than what was estimated previously. In order to fail the specimen, the hydraulic pressure had to be increased above the working pressure. This allowed the specimen to be loaded to failure, but the hydraulic pump had to be replaced after testing. Since not all the specimens were constructed at this time, some of the specimen' designs were changed to a wider 559 mm (22 in.) steel stirrup spacing. This was done reduce the load needed to achieve shear dominated failure and prevent flexural failures.

Diagonal cracks propagated towards the loading point as the specimen load was increased. The failure was a sudden brittle shear failure that occurred as the concrete separated nearly instantly at a load of 2375 kN (534 kips). No slipping of the NSM repaired CFRP strips

was noticeable. The failure plane of this specimen was not identical on both sides of the specimen, as was the case with many of the specimens. The failure crack on the east side started at the edge of the loading plate and ran diagonally at 59° to the specimen flange. The west side was different because near the loading point the failure crack ran behind the NSM retrofitting for about 81 cm (32 in.) and then it cracks at a steep diagonal slope of 60° down to the base of the stem. The crack on both sides then ran horizontally along the junction of the flange and stem for approximately 76 cm (30 in.) and then cracked diagonally through the flange near the support. In the region where the failure occured horizontally below the CFRP strips, the concrete also cracked behind the NSM retrofit. It appeared that the CFRP strips made a reinforced shell that peeled away from the steel reinforced inner core of the specimen over this short region and at the top of the shear crack on the west side. This peeling behavior is shown in Figure 6.2.

Fig. 6.2 – Specimen IT.7.18.6.S failing around the NSM retrofit and a bent CFRP strip

6.4 IT.7.18.12-S

This specimen was the same as specimen IT.7.18.6.S except it had a 305 mm (12 in.) CFRP strip spacing. The failure surface was a relatively straight diagonal crack extending

from the support to about 305 mm (12 in.) away from the load point. The failure was brittle, but it took place over a time span of about three seconds. The concrete around the top of the third CFRP strip and the bottom of the fourth CFRP strip on the whitewashed side of the beam failed. This occurred just prior to the whole failure crack opening and a still shot from a video shows the concrete exploding around a CFRP strip in Figure 6.3. This failure plane is a typical diagonal shear failure and is a different failure mode than what occurred in the specimens with a six inch CFRP strip spacing. The wider NSM spacing caused the CFRP strips to contribute individually to the strength gain. An outer reinforced shell was not formed and no peeling was observed like occurred in the specimens with a tighter NSM spacing.

Slippage of the CFRP strips occurred in the 3rd and 4th strips from the centerline on the east side of the specimen and on the 2nd, 4th, and 5th strips from the centerline on the west side of the specimen. The CFRP slip can be identified because the top of the strip is no longer visible. It has been pulled down through the epoxy. Additionally, some of the CFRP strips appear to have nearly ruptured in tension; however, it is likely that bending occurs during failure because the strip slips and that contributes to this rupture. An example of a CFRP strip slipping and a strip rupturing due to bending are shown in Figure 6.4.

Fig. 6.3 – Concrete failing around CFRP strip just prior to shear failure

Fig. 6.4 – CFRP bending/rupture combination and slippage at the top of strip

6.5 IT.7.22.6.S

This specimen was the same as IT.7.18.6.S except it had 559 mm (22 in.) steel stirrup spacing. This specimen was constructed because the shear capacity of the 457 mm (18 in.) stirrup spacing was too high. One region of concrete around the bottom of a CFRP strip approximately 152 mm (6 in.) long broke momentarily before the specimen failed. The

specimen failed in shear at a load of 2286 kN (514 kips). The east and west sides of the specimen exhibited slightly different failure paths. The east side failed similarly to other specimens; it broke diagonally from the edge of the load plate to the bottom of the stem, then cracked horizontally along the flange and stem junction, and then cracked diagonally through the flange. The horizontal break ran from approximately 213 cm (84 in.) away from the centerline to 290 cm (114 in.) from the center line. The west side failure crack followed a different path. It cracked along the top of the stem behind the CFRP strips for 86 cm (34 in.). It then cracked vertically down to the top of the flange and horizontally along the stem junction for 107 cm (42 in.). It then cracked diagonally through the flange to near the support location. At the top and bottom of this shear crack it clearly demonstrated the outer shell of NSM reinforcing peeling away from the inner core of the specimen. No CFRP strip slippage was visible in this failure.

6.6 IT.5.22.12.S

This specimen was the only IT beam constructed with five flexural reinforcing bars. The result of this was the specimen had a lower flexural capacity and was difficult to force a shear dominated failure. The specimen was originally designed and constructed with a 152 mm (6 in.) CFRP strip spacing. When the specimen was tested it began to exhibit a flexural failure at a load of 2006 kN (451 kips). This was observable because the deflection began to grow without an increase in load. The testing was halted at this point to avoid a flexural failure. It was decided that making adjustments to force a shear failure would be more insightful than a flexural failure. The first adjustment to force a shear failure was to move the support locations closer to the load point. This changed the shear span and allowed the specimen to be subjected to a higher shear load with the same

moment demand. The support was moved 305 mm (12 in.) and then the specimen was tested again. When the specimen was loaded in this setup it reached a load of 2184 kN (491 kips) and then began to fail in flexure again. It was decided that moving the support any further would start to change the behavior of the specimen. The solution implemented was to saw-cut out every other NSM-CFRP strip. This essentially gave the specimen a 305 mm (12 in.) CFRP strip spacing. The supports were moved back to the original position. The weaker amount of transverse reinforcing allowed the specimen to fail in shear under an applied load of 1979 kN (447 kips).

One side effect of initially loading this specimen until a flexural failure began is the flexural steel experienced strain hardening. Due to this the flexural reinforcing steel would act linear elastic up until the previous applied load levels. Using R2K it was determined that the 476 MPa (69 ksi) steel would begin yielding at a shear of 818 kN (184 kips) and it would take 558 MPa (81 ksi) steel to prevent yielding until the previous shear load of 1001 kN (225 kips). Therefore the flexural reinforcing of this specimen was modeled as 81 ksi steel to represent the actual materiel properties due to strain hardening.

The shear failure of IT.5.22.12.S occurred suddenly across the entire diagonal shear crack. No CFRP strip slippage was visible. Many of the CFRP strips were broken along the crack, but it appeared to be from tension and bending as opposed to pure tensile rupture. The failure crack followed a similar pattern to other specimens. It broke diagonally through the flange and then cracked horizontally along the flange and stem junction. This horizontal failure section is approximately 91 cm (36 in.) long and runs from 259 cm (102 in.) away from the centerline to 168 cm (66 in.) away. From the end of this horizontal section the crack runs diagonally up to the edge of the load plate. There was a region at the

top of the diagonal crack where the outer shell of concrete separated from the inner core which caused pieces of the concrete to fall off in between the grooves from the cut out CFRP.

6.7 IT.7.18.6.M

This specimen was the same as IT.7.18.6.S except it was submerged in water for six months before it was tested for shear capacity. The only visible effect of the moisture exposure was some rust spots on the flange and on the top of the stem where the exposed steel reinforcing chairs had formed rust. As the specimen was tested, damp areas formed on the specimen's surface as water was squeezed out from the induced stress. The specimen failed in shear similar to the other specimens at a load of 2295 kN (516 kips). At the 2224 kN (500 kip) load step, just prior to the specimen's failure, two areas of debonded concrete were visible at the bottom of the stem. An example of this is shown in Figure 6.5. These debonding regions are the beginning of the peeling failure mode observed in most of these specimens. The failure crack ran from the load point behind the CFRP for about 61 cm (24 in.) on both sides of the specimen and then cracked at a steep 60° angle down to the top of the flange. The failure plane then ran along the stem and flange junction to the support. At the top and bottom of the diagonal crack it appears the outer shell of NSM reinforced concrete peeled away from the inner core of concrete. Some of the ends of the CFRP strips had also visibly debonded from the specimen during the failure. The ends of these strips had regions with epoxy still bonded and regions of bare carbon fiber; this implies debonding occurred both by CFRP strips pulling out of the epoxy and from the concrete breaking around the NSM epoxy. The broken concrete was visibly darker than other specimens due to its moisture saturation.

Fig. 6.5 – Specimen IT.7.18.6.M initial peeling and saturated concrete vs. dry concrete

6.8 IT.7.22.6.FT

The specimen was subjected to 400 freeze-thaw cycles before being tested for shear capacity. The most obvious freeze-thaw damage was raveling of concrete on the specimen flange. This was primarily where water was sitting and would not have occurred if the specimen was in the T-orientation. There were also two small areas of debonded surface concrete on the web. Some examples of the freeze-thaw effects are shown below.

Fig. 6.6 – Specimen IT.7.22.6.FT effects from freeze-thaw exposure

This specimen was constructed with the same details as IT.7.22.6.S, which was the control for this specimen. It failed in shear at 2211 kN (497 kips) of load. The east side of the specimen failed diagonally from the edge of the load plate to the top of the flange at an angle of 45°. It then cracked horizontally along the stem junction for 54 cm (25 in.) and diagonally through the flange. The west side broke behind the NSM retrofit for the 51 cm (24 in.) next to the load plate. It then cracked at a steeper 70° angle down to the flange and then horizontally along the flange and stem junction. Slippage of the top of the CFRP strips was observed in the 3rd, 4th, and 5th strips from the load point on the east side of the specimen. On the west side, only the 5th CFRP strip showed signs of slippage. The bottom of one strip on each side exhibited debonding of the concrete around the epoxy. Additionally, one strip on the west side appears to have ruptured in tension. There is a clean break with no signs of slippage on either end of the CFRP to cause bending. This is the only specimen to achieve pure rupture in a CFRP strip.

Fig. 6.7 – Rupture of CFRP strip without slippage

Fig. 6.8 - Specimen T.6.18.6.S and T.6.18.12.S failure

Fig. 6.9 – Specimen IT.7.18.6.S failure

Fig. 6.10 - Specimen IT.7.18.12.S failure

Fig. 6.11 – Specimen IT.7.22.6.S failure

Fig. 6.12 – Specimen IT.5.22.12.S failure

Fig. 6.13 – Specimen IT.7.18.6.M failure

Fig. 6.14 –Specimen IT.7.22.6.FT failure

7. COMPARATIVE ANALYSIS

7.1 Comparison of Pre-Strengthened Capacity to Post-Strengthened Capacity

The increase in shear capacity due to application of NSM-CFRP strips is an important issue for this research. To determine the contribution of the NSM-CFRP to shear capacity it is necessary to have a base shear capacity for each specimen without NSM reinforcing. R2K was used again to estimate the base capacity of each specimen with the measured material properties. Each specimen needed a separate R2K model because of different concrete material properties. Numerical values for the base shear capacity, $V_{R2K\text{-}base}$, and the difference from the actual measured retrofit shear capacity, V_{exp}, are reported in Table 7.1. The difference in these two shear capacity values is attributed to the NSM reinforcing. The results presented in this table include the analysis bias of 0.98 on the work of Higgins *et al*. [2004].

Table 7.1 – R2K base shear capacity vs. experimental shear capacity

Specimen	V_{exp}		$V_{R2K\text{-}base}$		V_{exp} - $V_{R2K\text{-}base}$	
	[kN]	[kips]	[kN]	[kips]	[kN]	[kips]
T.6.18.6.S*	1011	227.4	721.0	162.1	290.5	65.3
T.6.18.12.S*	1043	234.5	752.3	169.1	290.8	65.4
IT.7.18.6.S	1209	271.8	796.3	179.0	412.7	92.8
IT.7.18.12.S	1022	229.7	794.7	178.7	227.0	51.0
IT. 7.22.6.S	1165	262.0	673.5	151.4	491.9	110.6
IT.5.22.12.S	1011	227.3	680.9	153.1	330.1	74.2
IT.7.18.6.M	1168	262.5	749.3	168.5	418.3	94.0
IT.7.22.6.FT	1125	252.9	700.0	157.4	424.9	95.5

*Minimum values due to flexural failure

Another method of determining the base shear capacity is described by the American Concrete Institute (ACI). ACI 318-08 determines the base shear capacity by superimposing the concrete shear capacity and steel shear capacity according to the equations below.

$$V_{318-Base} = V_c + V_s \qquad \text{Eq. 7.1 – ACI 318 (11-2)}$$

$$V_c = 2\lambda\sqrt{f'_c}\,b_w d \qquad \text{Eq. 7.2 – ACI 318 (11-3)}$$

$$V_s = \frac{A_v f_y d}{s} \qquad \text{Eq. 7.3 – ACI 318 (11-15)}$$

The numerical values of the specimen's base shear capacity according to ACI 318, $V_{318\text{-base}}$, and the difference from the measured retrofit shear capacity are reported in Table 7.2. Once again, the difference can be attributed to the NSM-CFRP retrofitting. The ACI values, and all other ACI calculated values in this paper, were multiplied by a 1.05 bias [Turan, *et al*. 2008]. This is to adjust the ACI values to better fit experimental data based on the analysis method.

Table 7.2 – ACI 318 base shear capacity vs. experimental shear capacity

Specimen	V_{exp}		$V_{318\text{-base}}$		V_{exp} - $V_{318\text{-base}}$	
	[kN]	[kips]	[kN]	[kips]	[kN]	[kips]
T.6.18.6.S*	1011	227.4	577.6	129.9	461.4	97.5
T.6.18.12.S*	1043	234.5	600.5	135.0	471.1	99.5
IT.7.18.6.S	1209	271.8	636.0	143.0	603.2	128.8
IT.7.18.12.S	1022	229.7	634.7	142.7	417.3	87.0
IT. 7.22.6.S	1165	262.0	567.2	127.5	625.2	134.5
IT.5.22.12.S	1011	227.3	586.0	131.7	453.0	95.6
IT.7.18.6.M	1168	262.5	607.8	136.6	588.7	125.9
IT.7.22.6.FT	1125	252.9	586.2	131.8	566.6	121.1

*Minimum values due to flexural failure

The graph below visually demonstrates that the base shear capacities calculated with R2K are consistently higher than the base capacities calculated according to ACI. Due to this, if an ACI approach was followed, then higher strength contributions of CFRP would be reported.

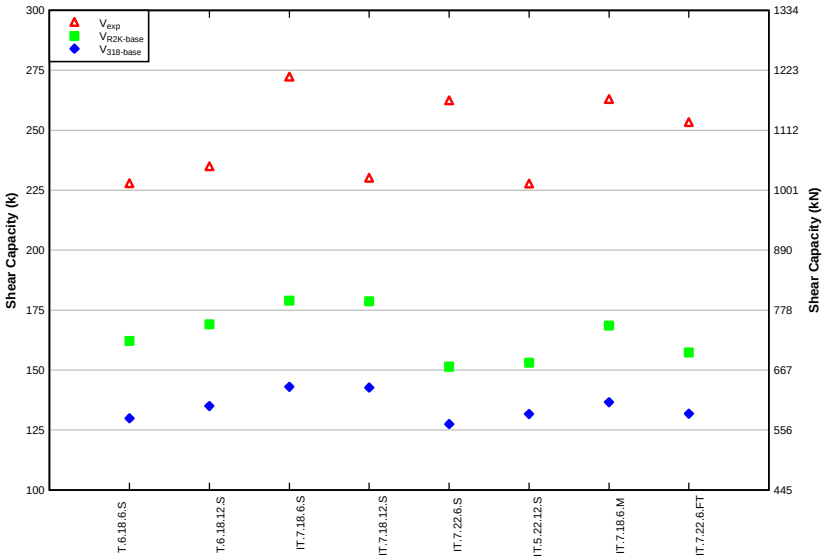

Fig. 7.1 – ACI 318 base shear capacity vs. experimental shear capacity

The individual graphs with unique material properties are shown in Figure 7.3. These graphs show where the R2K and ACI base shear values come from and where the experimental shear capacities correspond with the R2K and ACI curves. The graph for specimen IT.5.22.12.S also shows the difference from strain hardening the flexural steel during the initial loading with 152 mm (6 in.) spaced NSM-CFRP. Due to strain hardening, the curve remained linear until a higher shear value, and thus a smaller effective stress in the NSM-CFRP was determined. Figure 7.2 shows all the specimens plotted on the same graphs, but they have been normalized with respect to the concrete compressive strength. R2K curves for each specimen type have been plotted using an average concrete compressive strength of 29 MPa (4200 psi). These normalized curves allow the strength gains for each specimen to be compared along the R2K curves.

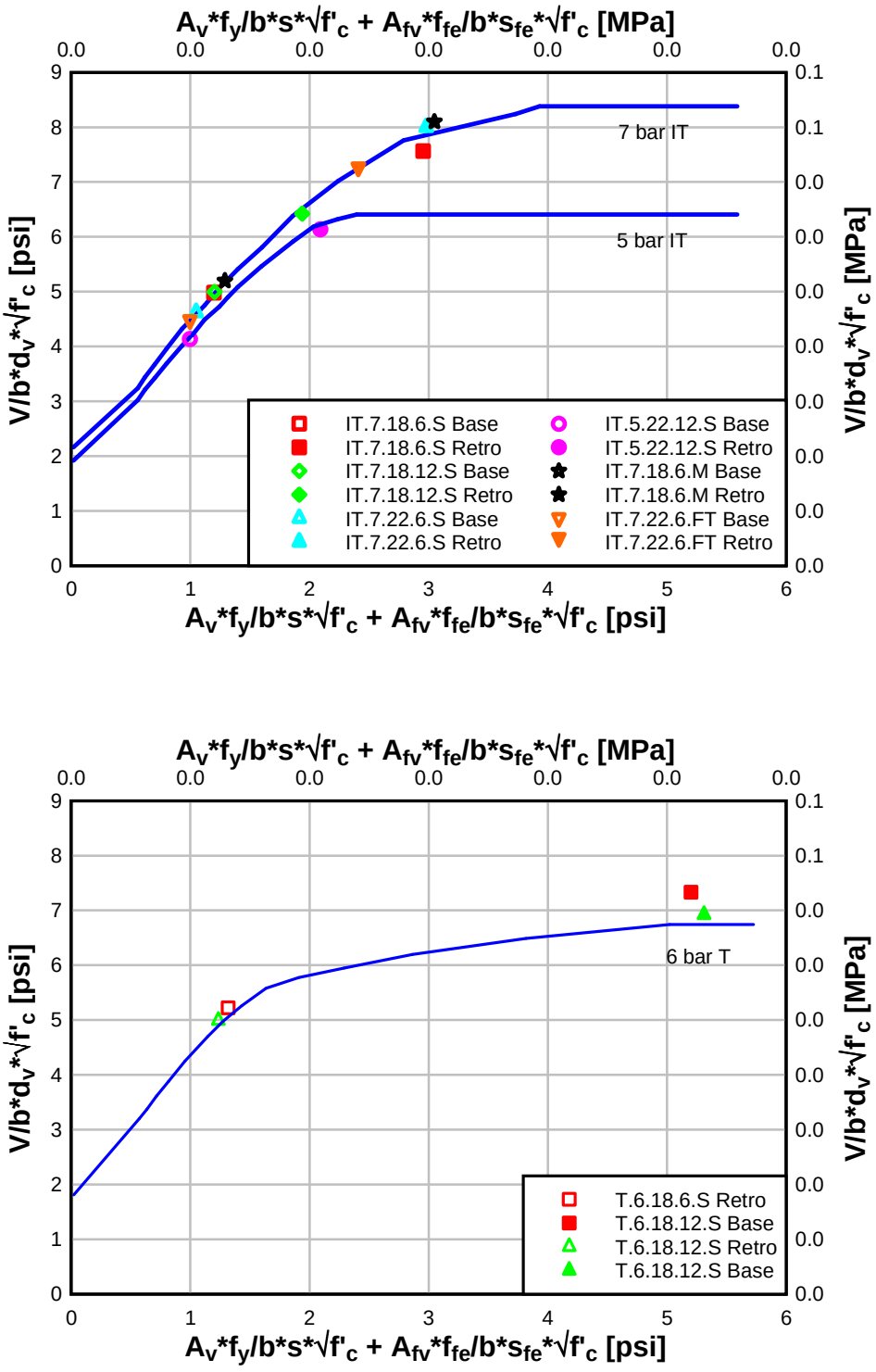

Fig. 7.2 – Normalized specimens plotted on representative specimen-type curves

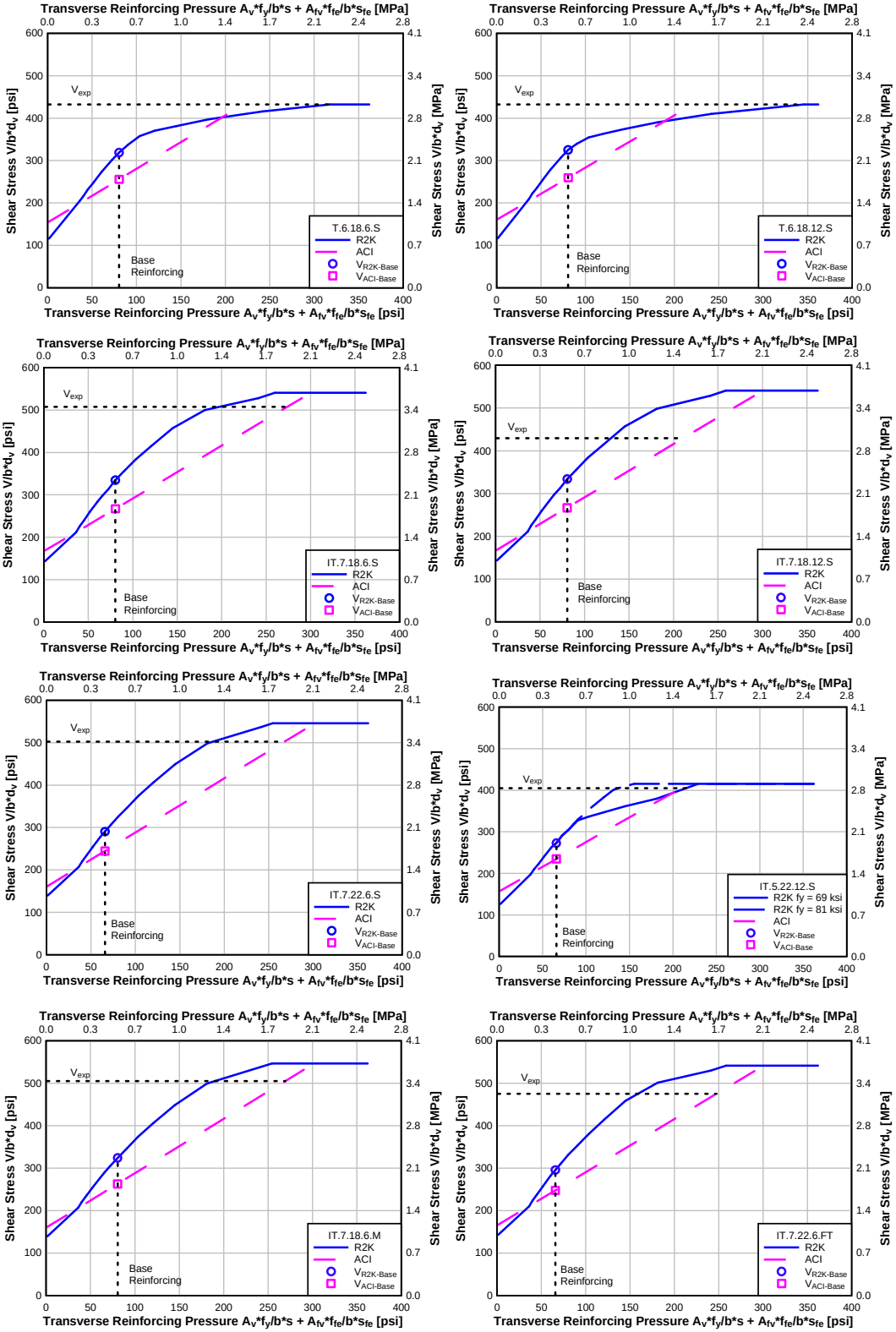

Fig. 7.3 – Specimen R2K and ACI curves showing strength gain

7.2 Determining CFRP Effective Stress

Based on the specimen strength increases over the R2K base value, an effective CFRP stress was calculated. This was done using Equation 4.1 and the same method as described in *Section 4.1*. A curve was created for each test specimen using R2K to establish the relationship between the amount of transverse reinforcing and the average ultimate shear stress in the web. Then a transverse reinforcing pressure associated with the NSM-CFRP was taken from the x-axis based on the experimental shear capacity. This is demonstrated in Figure 7.4.

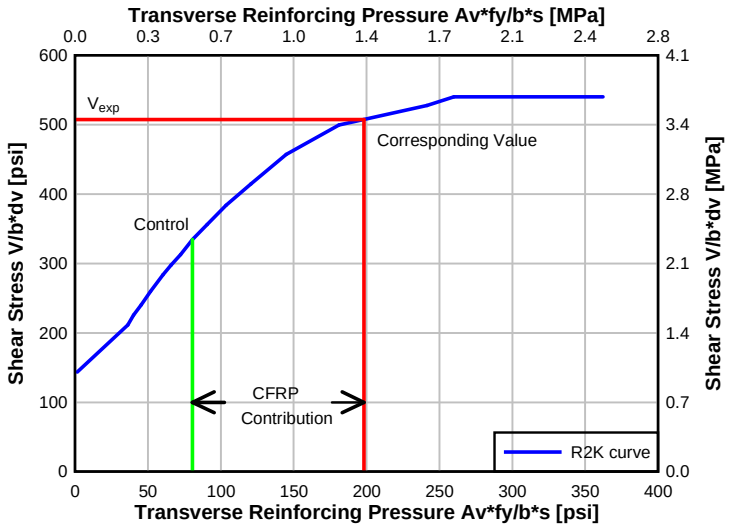

Fig. 7.4 – Example CFRP contribution based on R2K

An effective CFRP stress can also be calculated based on the strength increase compared to the ACI base capacities. This was done similarly to the above R2K method except the ACI 318 base control value and ACI curve were used. A separate curve was created for each specimen using specific material properties. As demonstrated below in Figure 7.5 a transverse reinforcing pressure was taken for each specimen.

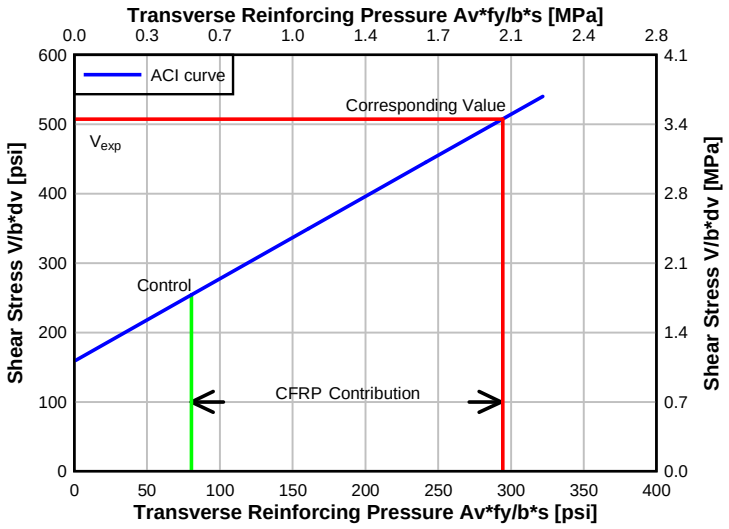

Fig. 7.5 - Example CFRP contribution based on ACI

Using Equations 4.1 and 4.2 the stress in the CFRP strips, f_{fe}, is calculated. The numerical values from R2K, $f_{fe\text{-}R2k}$, and ACI, $f_{fe\text{-}ACI}$, are listed in Table 7.3. The NSM-CFRP stress values of specimens T.6.18.6.S, T.6.18.12.S, and IT.5.22.12.S are much larger than the other stresses from R2K. These specimens either failed in flexure, or nearly failed in flexure. The corresponding points on the R2K curve for these specimens are in the flexurally dominated region near the top. This part of the curve is nearly flat and assigns large increases in transverse stress for small gains in shear strength because the specimens will fail in flexure near that load. For the other specimens that are not flexurally dominated, ACI determines a larger stress. This is because the strength gains occur in the steeper region of the R2K curves, thus R2K does not attribute as much NSM-CFRP stress as ACI to achieve the observed strength gains.

Table 7.3 – Effective CFRP stress based on experimental shear values

Specimen	$f_{fe\text{-}R2k}$		$f_{fe\text{-}ACI}$	
	[Mpa]	[ksi]	[MPa]	[ksi]
T.6.18.6.S	1373.2	199.2	881.4	127.8
T.6.18.12.S	3140.8	455.6	1798.0	260.8
IT.7.18.6.S	681.9	98.9	1120.2	162.5
IT.7.18.12.S	569.4	82.6	1513.6	219.5
IT. 7.22.6.S	702.5	101.9	1169.7	169.7
IT.5.22.12.S	1731.3	121.2	1662.2	241.1
IT.7.18.6.M	634.7	92.1	1094.5	158.8
IT.7.22.6.FT	540.4	78.4	1053.2	152.8

7.3 Comparison of Approaches to Determining Shear Strength

7.3.1 Comparison of Developed Prediction Method to Experimental Capacity:

As discussed in *Section 4.1 Design Method*, an estimated CFRP stress based on previous experiments from the literature review and R2K were used to predict the shear capacity of the specimens before construction. After the specimens were tested these predictions were adjusted to account for the actual concrete and steel material properties. The numerical shear capacity values, $V_{lit\text{-}predicted}$, along with percent difference from V_{exp} are shown in Table 7.4. The method of prediction consistently underestimated the capacity contribution due to the NSM-CFRP strips. The prediction for IT.5.22.12.S did not take into account the effects of strain hardening, which would have made the prediction closer.

Table 7.4 – Predicted capacity based on literature experiments vs. experimental capacity

Specimen	$V_{lit\text{-}predicted}$		V_{exp} - $V_{lit\text{-}predicted}$		$\frac{V_{exp}}{V_{lit-predicted}}$
	[kN]	[kips]	[kN]	[kips]	
T.6.18.6.S	873.6	196.4	137.9	31.0	1.16
T.6.18.12.S	838.4	188.5	204.6	46.0	1.24
IT.7.18.6.S	1121.8	252.2	87.2	19.6	1.08
IT.7.18.12.S	975.0	219.2	46.7	10.5	1.05
IT. 7.22.6.S	1030.2	231.6	135.2	30.4	1.13
IT.5.22.12.S	840.7	189.0	170.4	38.3	1.20
IT.7.18.6.M	1074.6	241.6	93.0	20.9	1.09
IT.7.22.6.FT	1072.4	241.1	52.5	11.8	1.05

7.3.2 Comparison of ACI 440 Predicted Capacity to Experimental Capacity

ACI 440 describes a method to predict the retrofit capacity of a specimen by determining the shear strength contribution of the CFRP. The method is primarily based on the EBR technique, but was adapted here to fit NSM repair. The retrofit shear strength superimposes the contribution from Equation 7.5 with the concrete and steel contribution from ACI 318.

$$V_{440} = V_{318-Base} + V_f \qquad \text{Eq. 7.4}$$

$$V_f = \frac{A_{fv} f_{fe} (\sin\alpha + \cos\alpha) d_{fv}}{s_f} \qquad \text{Eq. 7.5 – ACI 440 (11-3)}$$

In this equation, V_f is the shear contribution of the CFRP, A_{fv} is the area of CFRP, f_{fe} is the effective stress of the CFRP, α is the orientation of the CFRP, d_{fv} is the effective depth of CFRP reinforcement, and s_f is the spacing of the CFRP.

For the specimens in this research, A_{fv} = 65 mm^2 (0.1 in^2), α = 90°, d_{fv} = 1067 mm (42.0 in.) for IT-specimens and 932 mm (37.6 in.) for T-specimens, s_f = 152 or 305 mm (6 or 12 in.). The effective stress f_{fe} is calculated using the following equations.

$$f_{fe} = \varepsilon_{fe} E_f \qquad \text{Eq. 7.6 – ACI 440 (11-5)}$$

$$\varepsilon_{fe} = \kappa_v \varepsilon_{fu} \le 0.004 \qquad \text{Eq. 7.7 – ACI 440 (11-6b)}$$

In this equation, E_f is the CFRP tensile modulus of elasticity. For this research it was taken as 138 GPa (20,082 ksi) based on material tests done by [Howell, 2009]. ε_{fe} is the effective strain of the CFRP. The equation defining the effective strain, Eq. 7.7, is based on an EBR face ply configuration which is not NSM, but it is the closest option. ε_{fu} is the ultimate strain of the CFRP. ε_{fu} was calculated by dividing the average tensile stress from material tests by the modulus of elasticity for a strain value of 0.017. The following equations are used to calculate K_v.

$$\kappa_v = \frac{k_1 k_2 L_e}{468\varepsilon_{fu}} \text{ in US units} \qquad \text{Eq. 7.8 – ACI 440 (11-7)}$$

L_e, k_1, and k_2 are defined as follows:

$$L_e = \frac{2500}{(nt_f E_f)^{0.58}} \text{ in US units} \qquad \text{Eq. 7.9 – ACI (11-8)}$$

$$k_1 = \left(\frac{f'c}{4000}\right)^{2/3} \text{ in US units} \qquad \text{Eq. 7.10 – ACI (11-9)}$$

$$k_2 = \frac{d_{fv} - 2L_e}{d_{fv}} \qquad \text{Eq. 7.11 – ACI (11-10)}$$

For the above equations, L_e is the active bond length, n is the number of plies of CFRP reinforcement, and t_f is the nominal thickness of the CFRP. The NSM technique bonds CFRP strips on three sides in a groove, but this equation is designed for EBR reinforcing that is bonded on only one face. This was approximated by making n = 2 and t_f = half the strip width, to account for the two largest sides of the CFRP bonded surfaces.

Table 7.5 - Predicted capacity based on ACI 440 vs. experimental capacity

Specimen	V_{440}		$V_{exp} - V_{440}$		$\frac{V_{exp}}{V_{440}}$
	[kN]	[kips]	[kN]	[kips]	
T.6.18.6.S	685.4	154.1	326.1	73.3	1.48
T.6.18.12.S	659.2	148.2	383.9	86.3	1.58
IT.7.18.6.S	773.3	173.9	435.6	97.9	1.56
IT.7.18.12.S	703.0	158.0	318.7	71.7	1.45
IT. 7.22.6.S	692.8	155.8	472.5	106.2	1.68
IT.5.22.12.S	653.1	146.8	357.9	80.5	1.55
IT.7.18.6.M	732.3	164.6	435.3	97.9	1.59
IT.7.22.6.FT	720.6	162.0	404.3	90.9	1.56

7.3.3 Comparison of Nanni, *et al*. [2004] Capacity to Experimental Capacity

Nanni, *et. al.* [2004] presents a method of calculating the shear capacity of NSM-CFRP retrofit concrete similar to the ACI 440 method. This method is also suggested on the Hughes Brothers website for design of NSM retrofit structures. The approach is still based on the superposition of the concrete, steel, and CFRP shear contributions. The difference is in the CFRP contribution, V_{fn}, proposed by Nanni, *et. al*. [2004] shown in the equations below.

$$V_{Nanni} = V_c + V_s + V_{fn} \qquad \text{Equation 7.12}$$

$$V_{fn} = 4(a+b)\tau_b L_{tot} \qquad \text{Equation 7.13}$$

The equation is for rectangular bars. The cross sectional dimensions are a and b. The average bond stress, τ_b, is suggested to be taken as 6.9 MPa (1.0 ksi) based on previous research. L_i shown below represents the length of each NSM bar past a shear crack and L_{tot}, is the summation of those attributing lengths.

$$L_i = \begin{cases} \dfrac{s}{\cos\alpha + \sin\alpha} i \le l_{0.004} & \text{for i = 1…n/2} \\ l_{net} - \dfrac{s}{\cos\alpha + \sin\alpha} i \le l_{0.004} & \text{for i = n/2+1…n} \end{cases} \qquad \text{Equation 7.14}$$

The limitation $l_{0.004}$ is based on the integrity of the concrete. In the present calculations, this length was determined as 71 mm (2.8 in.) and controlled for every NSM strip. The value n below must be rounded down to the nearest integer to represent a number of strips.

$$l_{net} = l_b - \frac{2c}{\sin\alpha} \qquad \text{Equation 7.15}$$

$$n = \frac{l_{eff}(1+\cot\alpha)}{s} \qquad \text{Equation 7.16}$$

$$l_{eff} = l_b \sin\alpha - 2c \qquad \text{Equation 7.17}$$

$$l_{0.004} = 0.002\frac{ab}{a+b}\frac{E_f}{\tau_b} \qquad \text{Equation 7.18}$$

$$L_{tot} = \sum L_i \qquad \text{Equation 7.19}$$

Following the prescribed approach, conservative shear strengths were determined for all the specimens. This is expected for a design approach because conservatism is desirable. Table 7.6 below reports the numerical values compared to the experimental values. It

should be mentioned that there are other design approaches discussed in the literature review. Only the Nanni, *et al.* [2004] approach was examined in this paper because it is the method suggested by Hughes Brothers.

Table 7.6 - Predicted capacity based on Nanni, *et al*. [2004] vs. experimental capacity

Specimen	V_{Nanni}		$V_{exp} - V_{Nanni}$		$\frac{V_{exp}}{V_{Nanni}}$
	[kN]	[kips]	[kN]	[kips]	
T.6.18.6.S	791.0	177.8	220.0	49.6	1.28
T.6.18.12.S	707.2	159.0	335.8	75.5	1.47
IT.7.18.6.S	849.4	191.0	359.6	80.8	1.42
IT.7.18.12.S	741.3	166.7	280.7	63.0	1.38
IT. 7.22.6.S	780.5	175.5	384.5	86.5	1.49
IT.5.22.12.S	692.7	155.7	318.3	71.6	1.46
IT.7.18.6.M	821.2	184.6	346.8	77.9	1.42
IT.7.22.6.FT	799.6	179.8	325.4	73.1	1.41

A visual representation of the experimentally measured shear capacities and the various estimated shear capacities can be seen in Figure 7.5. All of the approaches used provided conservative estimates of the actual shear capacity.

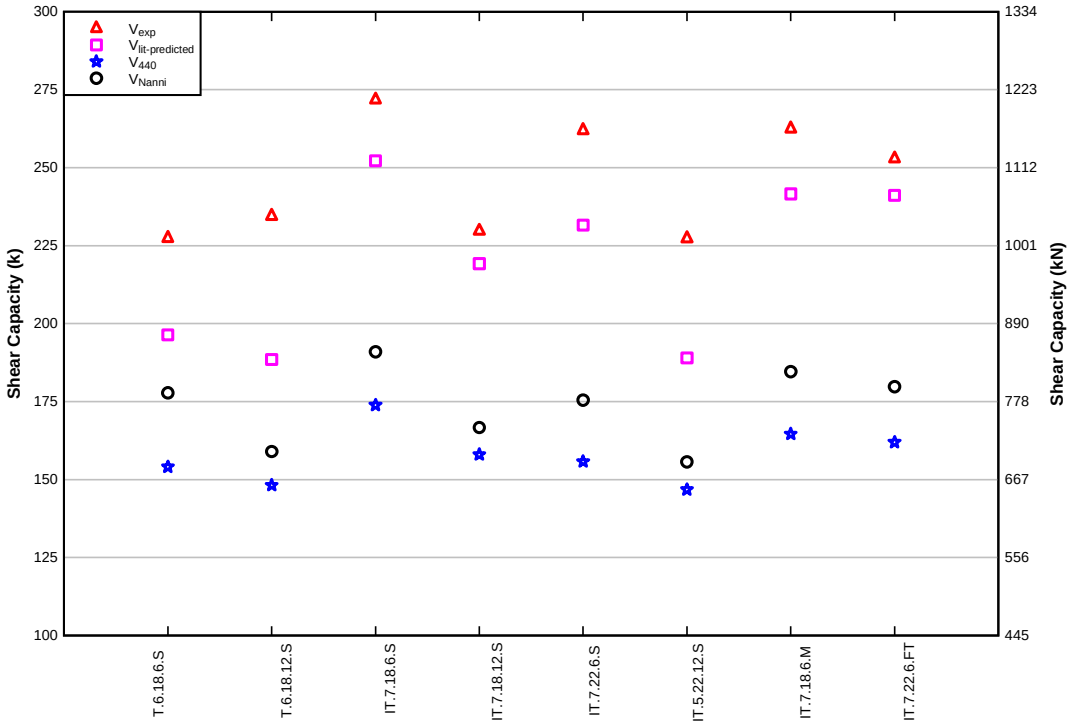

Fig. 7.5 – Comparison of V_{exp} to various estimated shear capacities

7.4 Comparison of Pre-Strengthened vs. Post-Strengthened Stiffness

The effects of NSM-CFRP on stiffness were also investigated. Environmental exposure could have a softening effect on the specimen stiffness. The global member stiffness is indicated by the midspan displacements. More local displacements of three shear panels on the specimen can be measured by the diagonal sensors. The diagonal sensors measure diagonal displacements which can be converted into average vertical strains for a shear panel. This is done using Mohr's circle by a method explained in Dawson, [2008]. The angle of shear cracking effects the measured diagonal displacements, so accounting for this and converting to vertical strains allows for comparison regardless of a different crack angle. Figures 7.6, 7.7, and 7.8 show the midspan displacements and average panel

vertical strains for each specimen. Stiffness effects are examined by comparing the slope of the baseline test before retrofitting with the slope of the retrofit line up to the same shear value. For specimens needing adjustments to fail, the first loading attempt curve was compared because the specimen already has cracking for the failure load step. The slopes of the midspan displacements show no significant changes. This is reasonable because a large portion of the midspan displacements come from flexural strains. Inspecting the panel vertical strain graphs show little or no significant changes. The only apparent stiffness increases are in the shear panels of specimen IT.7.22.6.S.

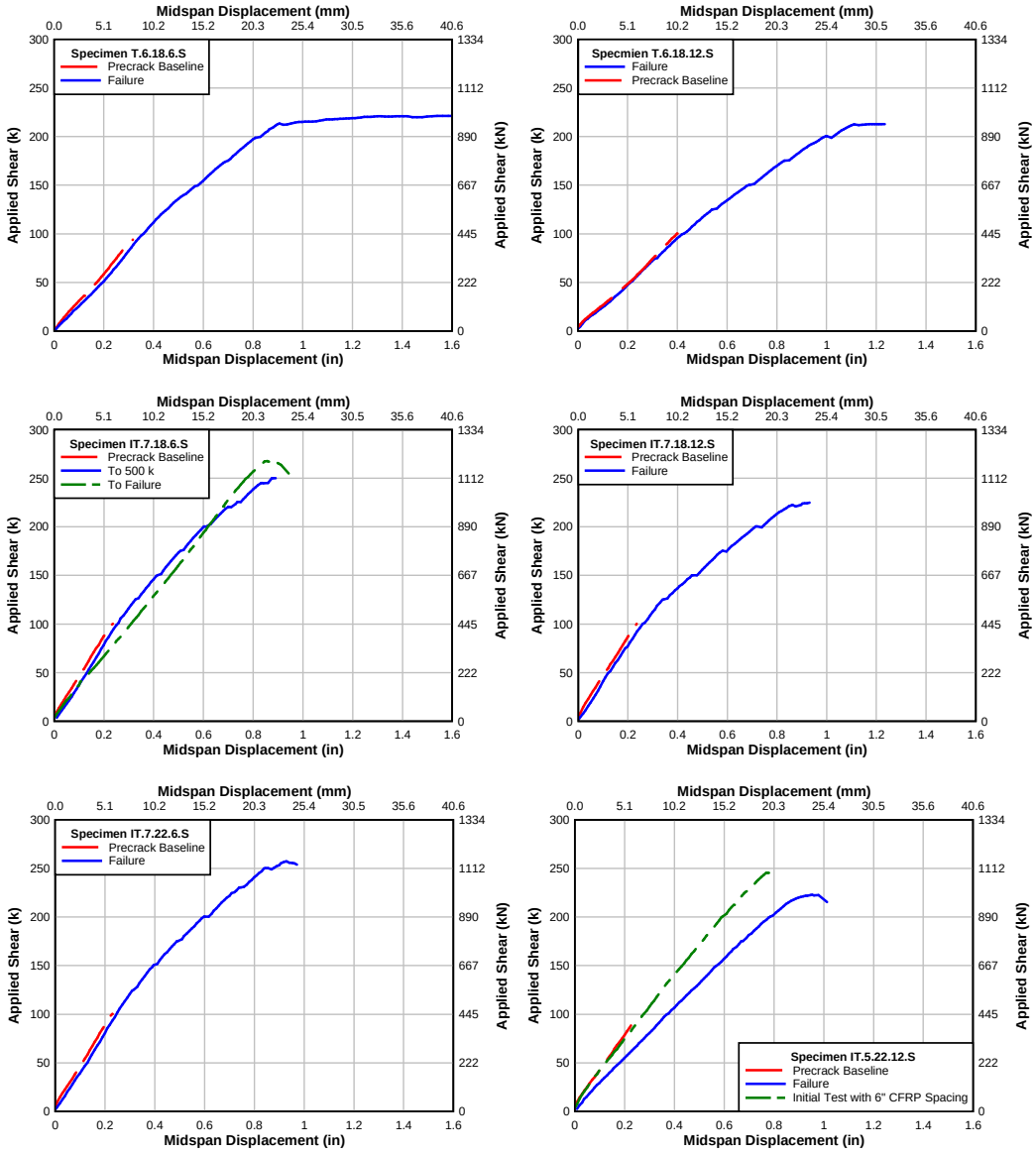

Fig. 7.6 – Overall stiffness comparison for strength specimens

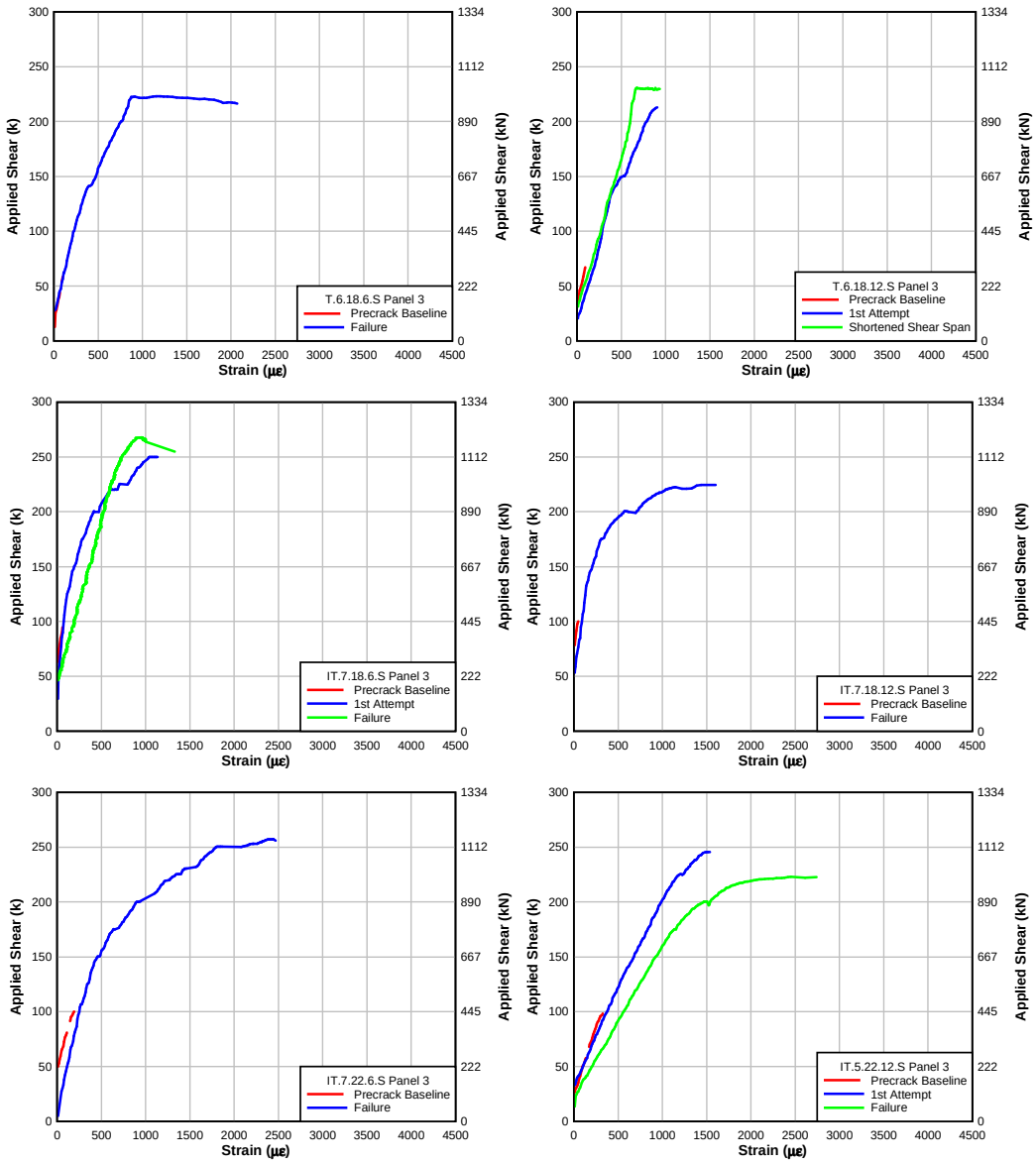

Fig. 7.7 – Shear panel 3 stiffness comparison for strength specimens

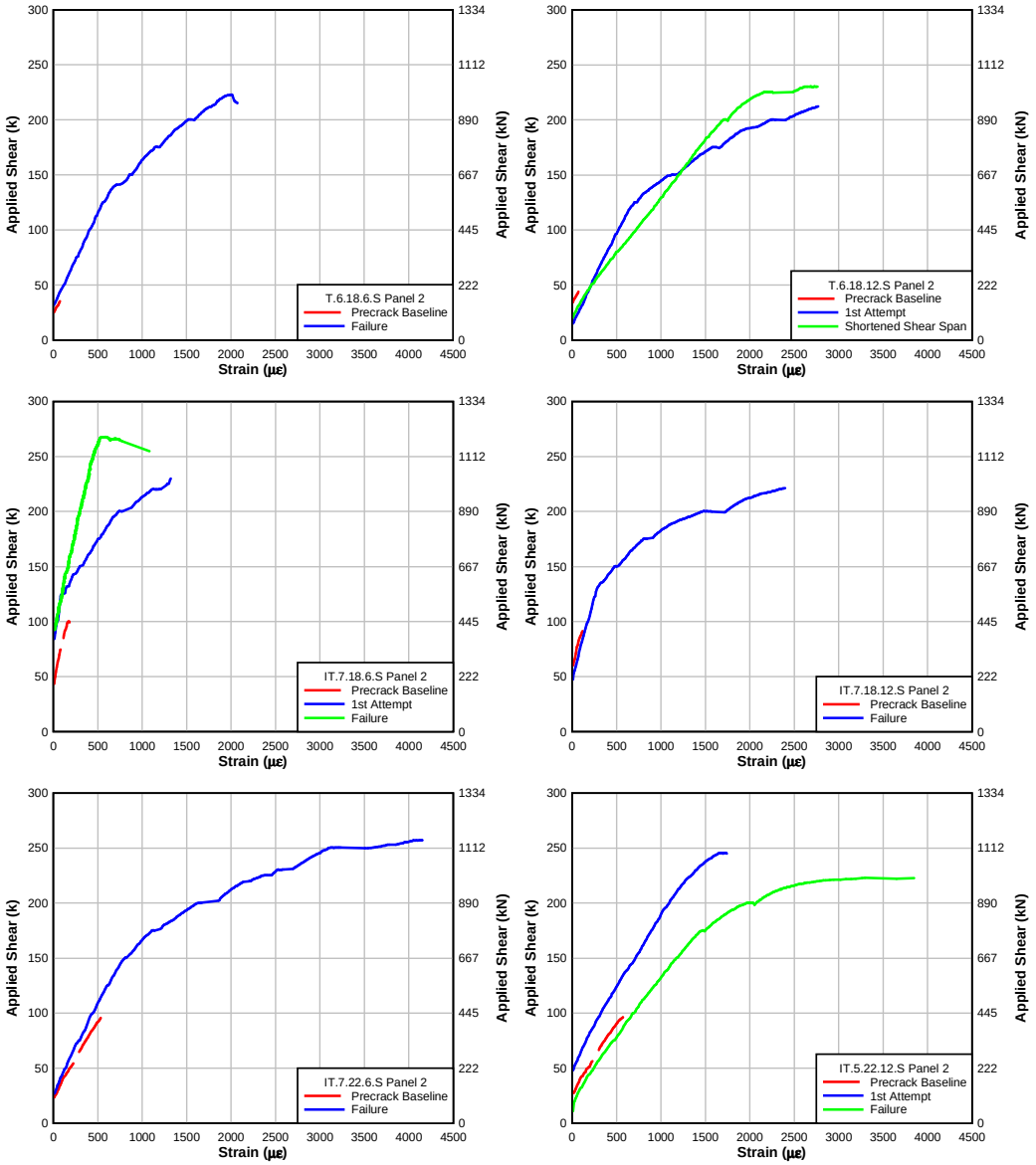

Fig. 7.8 – Shear panel 2 stiffness comparison for strength specimens

The shear panel and sensor locations are shown in the appendix. Panel one is closest to the support, panel two is in the middle of the shear span, and panel three is closest to midspan. For this comparison, the results of panel 1 are not shown because there were very few diagonal cracks near the support which resulted in insignificant data for that panel location. It can be noted in Figure 7.7 and 7.8 that the average vertical strains for the shear panels do not originate at zero loading. The main reason for this behavior is because after initial cracking each specimen had a certain load needed to reopen the diagonal cracks due to internal equilibrium. This load is referred to as a decompression load and remains relatively constant through each load step. An example shear force versus vertical strain curve in Figure 7.9 demonstrates the decompression load remaining equal for each load step. The decompression loads for baseline tests ranged from 18 to 605 kN (4 to 136 k), and for retrofit failure tests ranged from 18 to 739 kN (4 to 166 k).

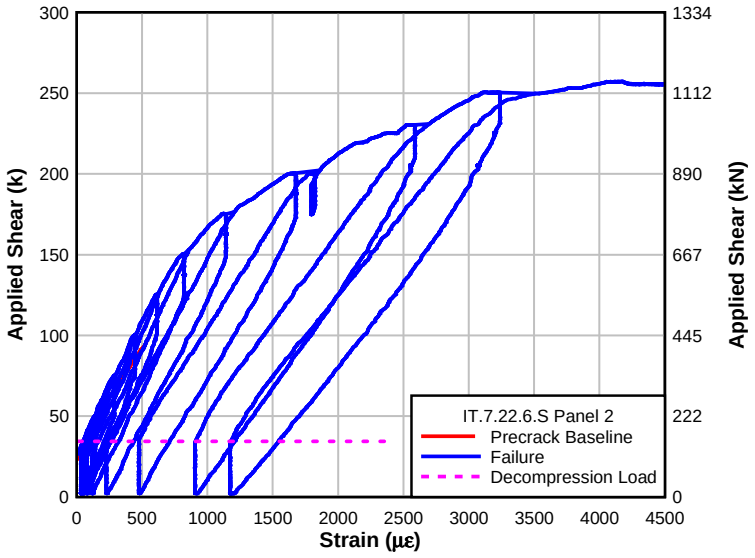

Fig. 7.9 – Example decompression load

7.5 Comparison of Environmental Exposure Specimens to Controls

7.5.1 Shear Strength Gains

Comparing the environmentally exposed specimens to their respective control specimens shows small and insignificant reduction in shear capacity. Both the moisture and freeze-thaw exposed specimens showed a decrease in shear capacity of 3.4%. This is likely in the range of material and construction variability. It is also worth mentioning that the specimen IT.7.22.6.FT-FTG from Johnson, [2011 was exposed to freeze-thaw effects and fatigue loading and failed at a higher load than the control.

Table 7.7 – Environmental shear capacities compared to controls

Specimen	V_{exp}	
	[kN]	[kips]
IT.7.18.6.S	1209	271.8
IT.7.18.6.M	1168	262.5
IT. 7.22.6.S	1165	262.0
IT.7.22.6.FT	1125	252.9

7.5.2 Stiffness Changes

Changes in the stiffness of the environmentally exposed specimens were examined in order to identify impact of freeze-thaw effects on performance. The global stiffness of the member was considered at midspan and at the local shear panels with the average vertical strains. Graphs of the specimen responses are shown below in Figure 7.10. The stiffness of the retrofit failure curves are compared to their baseline curves and to the failure curves of the control specimens. No significant changes in stiffness are noticeable from the comparisons. This is reasonable because there were no apparent increases in stiffness due to the NSM retrofitting and thus any degradation of the NSM reinforcing due to environmental exposure would not impact the stiffness.

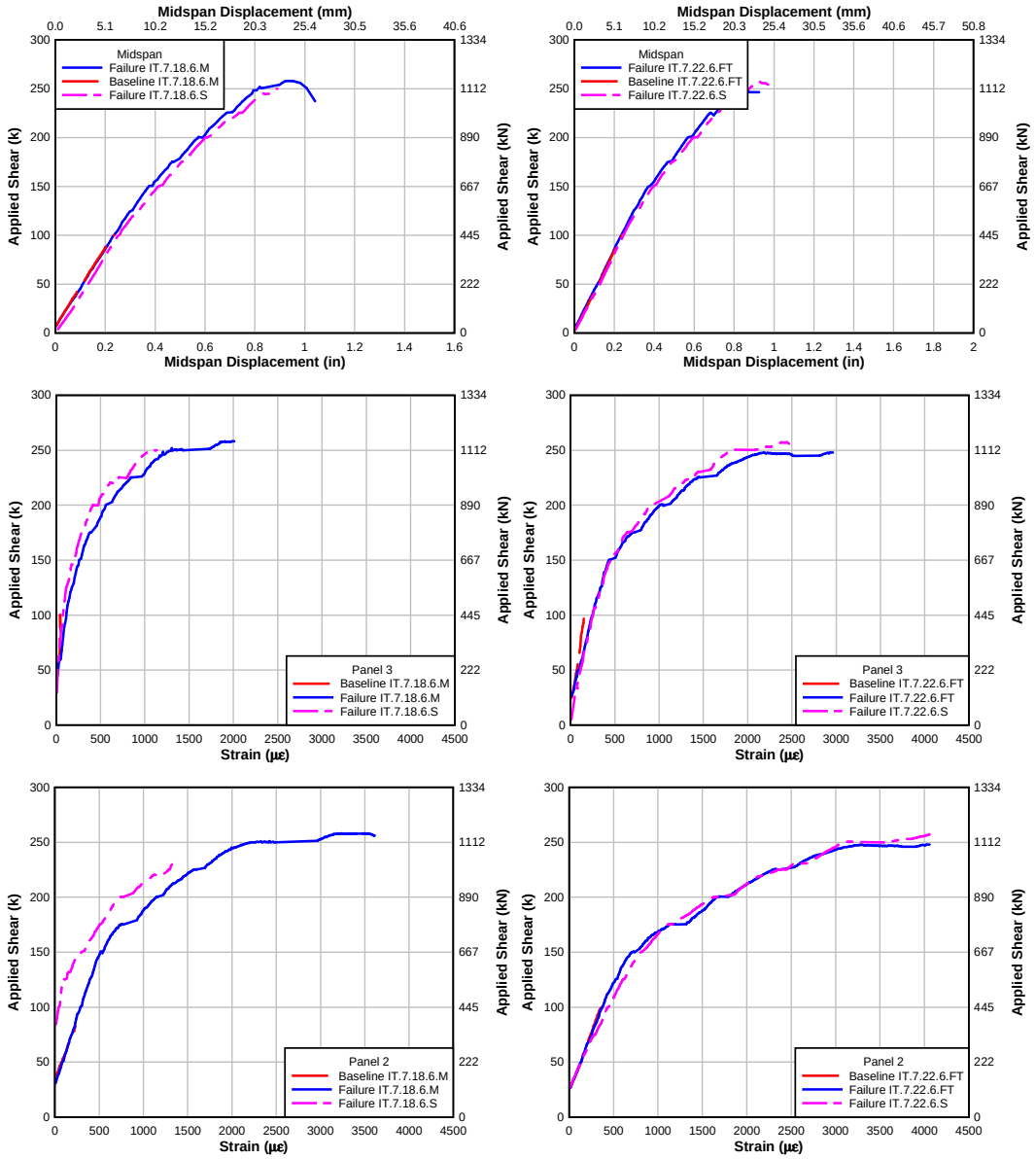

Fig. 7.10 - IT.7.18.6.M and IT.7.22.6.FT stiffnesses vs. control stiffnesses

7.5.3 Thermally Induced Strains

Strains are induced at the NSM bond interface due to temperature changes. This is because normal-weight concrete has a coefficient of thermal expansion (CTE) of approximately 9.9 x 10^{-6}/°C (5.5 x 10^{-6}/°F) [MacGregor and Wight 2005] and the Hughes Brothers' CFRP has a CTE of 0 to -2.2 x 10^{-6}/°C (0 to -4.0 x 10^{-6}/°F). The CTEs are not close and have opposite signs. This implies when the concrete is shrinking the CFRP will be expanding and vice versa, causing stress in the bond. To investigate this, an instrumented concrete cylinder was placed in the environmental chamber during freeze-thaw tests. Two strain gages were placed on the concrete surface, one gage on a strip of CFRP, and one gage on CFRP that was epoxied into an NSM groove on the cylinder. As seen in Figure 5.7, the surface of the specimens underwent a temperature change of approximately 14 °C (25 °F). This caused strains in the materials each freeze-thaw cycle as shown in the graph of measured strains below.

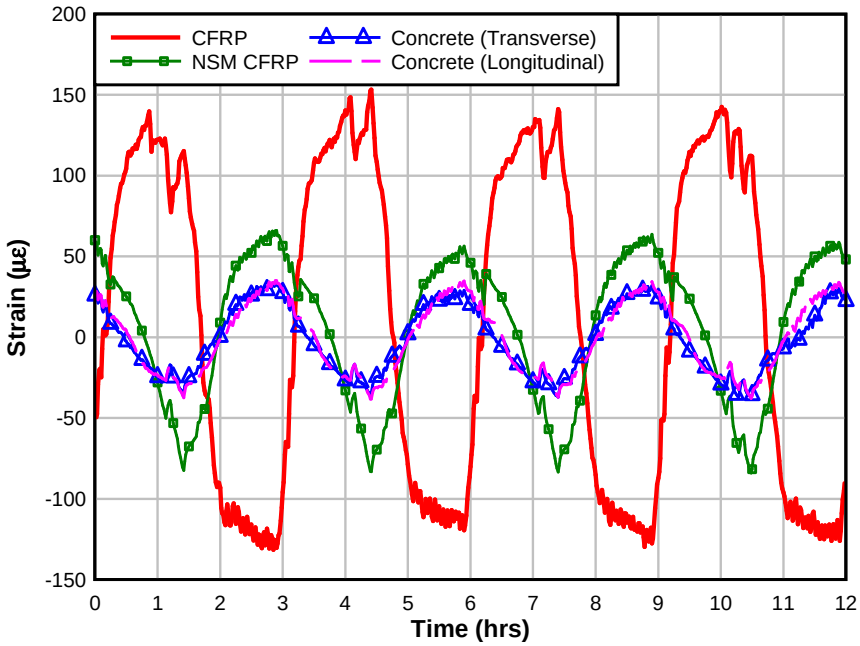

Fig. 7.11 – Thermally induced strains from freeze-thaw cycles

The thermally induced strains from the 400 freeze-thaw cycles did not appear to have any adverse effect on the shear strength or stiffness of the specimens. However, certain locations in Oregon can undergo larger temperature fluctuations from day to night and no conclusions can be made from this research as to how these larger thermal strains would affect NSM retrofitting in the field.

7.6 Comparing Specimen Orientation

One of the goals of this research was to examine the behavior of T-shaped specimens compared to IT-shaped specimens. This represents retrofitting the positive and negative moment regions of a bridge girder, respectively. The obvious difference is that all the IT specimens failed in shear, but the T specimens both failed in flexure. As a result, the strength gains cannot be compared directly because the gains exhibited by the T specimens are not the total gains in shear strength.

The predicted failure in this research placed the shear strength below the flexural capacity, but the achieved shear strength gains were higher than anticipated and caused more demand in the flexural reinforcing. The flexural failure only occurred in the T specimens because the baseline strength of the T specimens are higher up on the R2K curve, which places them closer to the flexurally dominated region. Another idea is that the NSM reinforcing is better anchored in the T specimens because it can extend below the flexural reinforcing and lead to higher shear strength gains. The NSM reinforcing in the IT specimens is blocked from reaching the bottom by the deck.

The results of the T specimen tests demonstrate the importance of the base specimen location on the MCFT curve. If a bridge girder is weak in flexural reinforcing, an

anticipated strength gain may not be achieved and the failure mode may be transferred to flexure, which would be a useful and predictable upper bound response.

7.7 Comparing Effects of Flexural Steel on Transverse Responses

MCFT, which this experimental program used for analytical predictions, includes the influence of the flexural reinforcing on shear capacity. The ACI superposition approach to shear design does not incorporate flexural reinforcing into shear capacity. The actual effects of flexural reinforcing can be investigated by comparing specimen IT.7.22.6.S to IT.5.22.12.S. It is important to remember that specimen IT.5.22.12.S started as IT.5.22.6.S, and the responses of this initial test will be referred to as IT.5.22.6.S. The responses of these two specimens can be directly compared because concrete strength and flexural steel are the only differences.

7.7.1 Diagonal Displacement Comparison

For a similar increase in shear, MCFT would predict higher transverse stress and strain in the specimen with less flexural reinforcing. The diagonal displacements provide a representation for the average strain in a shear panel. It is reasonable to compare the diagonal displacements of the two specimens because the crack patterns are similar. As shown in the diagonal displacements in Figure 7.12, specimen IT.5.22.6.S displays larger strains throughout the loading process, even as the transverse reinforcing details are the same.

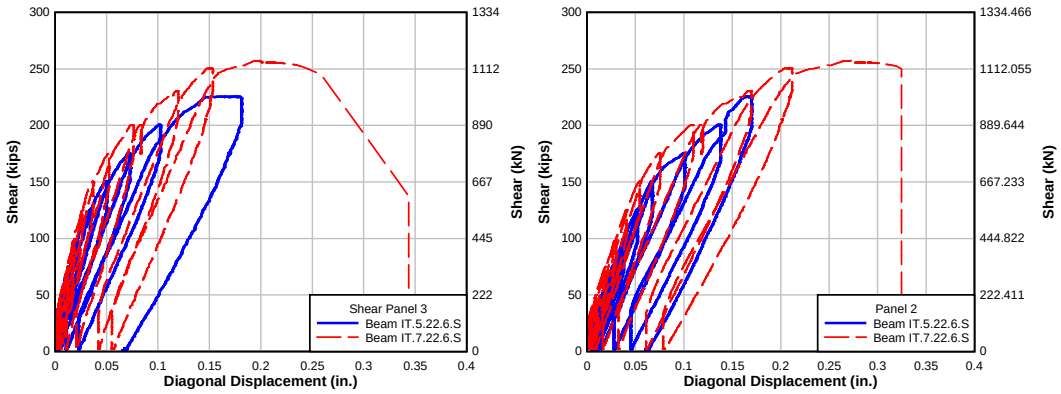

Fig. 7.12 – Diagonal displacements of IT.7.22.6.S vs. IT.5.22.6.S

To examine this further, the ratio of displacement values from these graphs are reported in Table 7.8 for corresponding shear loads. Two R2K models were created to represent the specimens. Additional steel stirrups were added to the models to represent the additional NSM-CFRP. These R2K models were analyzed and the transverse strain was integrated over the cross section at the same shear loads for both specimens. The ratio of the R2K predicted transverse strains are also shown in Table 7.8. It is noticeable that the ratio from R2K is slightly larger than the experimental data. This is reasonable because the specimen with less flexural reinforcing should experience more flexural displacements, and some of these are acquired by the diagonal displacement sensors.

Table 7.8 – R2K estimated vs. diagonal displacements data of IT.7.22.6.S/IT.5.22.6.S

Shear Load		Panel 2 Data	Panel 3 Data	R2K value
[kN]	[kips]	IT.7.22.6.S/ IT.5.22.6.S	IT.7.22.6.S/ IT.5.22.6.S	IT.7.22.6.S/ IT.5.22.6.S
556	125	0.78	0.77	0.84
667	150	0.81	0.74	0.86
778	175	0.74	0.74	0.87

7.7.2 CFRP Strain Comparison

The same phenomenon of higher transverse strains in the specimen with less flexural reinforcing can also be examined in the CFRP strips. This is difficult to do because the sensors on the strips are point specific and sensitive to the proximity and motions of the crossing diagonal cracks. To make a meaningful comparison, the CFRP sensors need to be at the same location in both specimens. By overlaying the specimen crack maps, Figure 7.13 and 7.14, it can be determined that the sensors C4, C6, and C7 in IT.7.22.6.S are close to sensors C4, C8, and C9 in IT.5.22.6.S respectively. Once again strains are reported for corresponding shear loads. Comparing the data in the two specimens shows that the CFRP strains in specimen IT.5.22.6.S are consistently higher in two of the sensor locations and approximately the same in the third.

Table 7.9 – Strain comparison between CFRP strips in similar locations

Shear Load		CFRP Strain		CFRP Strain		CFRP Strain	
[kN]	[kips]	IT.7.22.6.S CFRP (4)	IT.5.22.6.S CFRP (4)	IT.7.22.6.S CFRP (6)	IT.5.22.6.S CFRP (8)	IT.7.22.6.S CFRP (7)	IT.5.22.6.S CFRP (9)
222	50	401	1447	1245	2201	1678	1628
334	75	874	2334	1938	3437	2798	2619
445	100	1457	3381	2957	4459	3764	3525
556	125	1928	4458	3835	*	4528	4674
667	150	2434	*	4583	*	*	*
778	175	3009	*	*	*	*	*

* Out of sensor range

Fig. 7.13 – Specimen IT.5.22.6.S

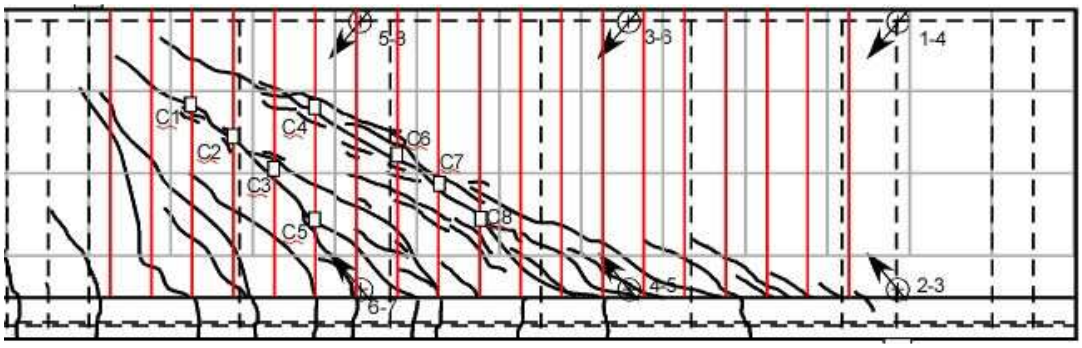

Fig. 7.14 – Specimen IT.7.22.6.S

7.8 Comparison of Pre-Strengthened Steel Stirrup Strains to Post-Strengthened Steel Stirrup Strains

Application of NSM-CFRP should reduce the stresses in the underlying steel stirrups at similar load levels for the base specimen without NSM-CFRP. Stresses can be established from the measured strains, so strain ranges from the steel stirrups were examined to see if a drop was noticeable after retrofitting. The stirrup strain range up to 890 kN (200 kip) load from the baseline data was compared to the same stirrup strain range up to 890 kN (200 kip) load after application of NSM-CFRP. The steel stirrup strain gages were placed at midheight. Consequently, they do not always provide useful data because they may or may not be near a diagonal crack. All the steel stirrups were examined, but only the stirrups reading a strain range of over 500 micro strains during the baseline test were considered. The strain ranges for the stirrups being compared are shown in Figure 7.15. For all of the internal steel stirrups examined, they displayed a reduction in strain after NSM retrofitting.

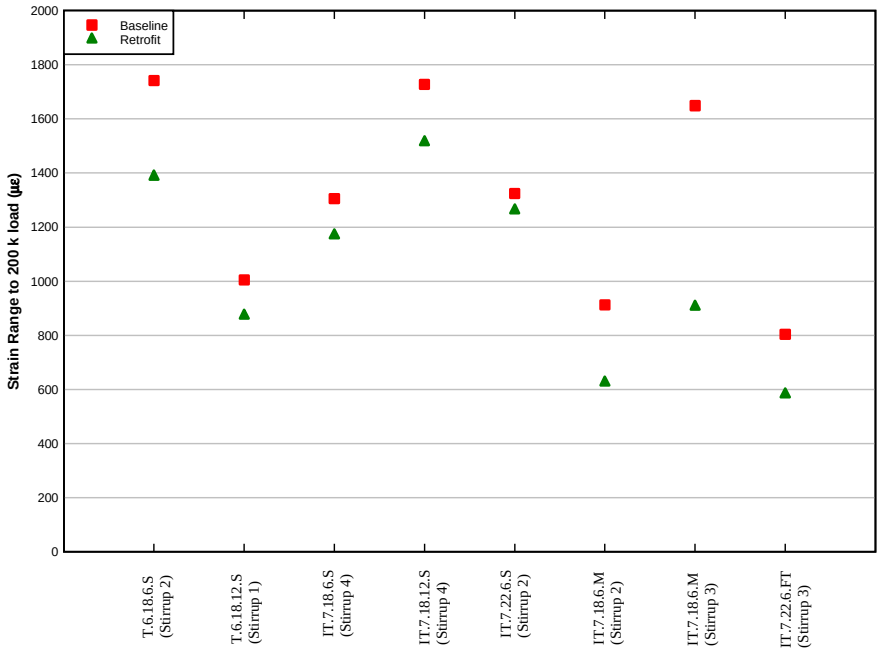

Fig. 7.15 –Pre-strengthened stirrup strain range vs. retrofit stirrup strain range

7.9 Modeling NSM-CFRP with R2K

A topic of interest for this research is investigating analysis methods to predict the strength of NSM-CFRP strengthened girders. In this section, R2K was used to predict shear strength of the reinforced concrete girders strengthened with NSM-CFRP. NSM-CFRP was modeled for the 14 specimens in the archival literature. The material properties of the steel and concrete were set as the reported values for each specimen. The CFRP material properties were modeled using the manufacturer's modulus of elasticity and the average effective CFRP stress based on the literature specimens. This stress was found earlier to be 441 MPa (64 ksi). The CFRP strip was added as a single leg stirrup that extended the length of the actual NSM and was the area of two CFRP strips because there is a strip on each face of the specimen. An example cross section is shown in Figure 7.16.

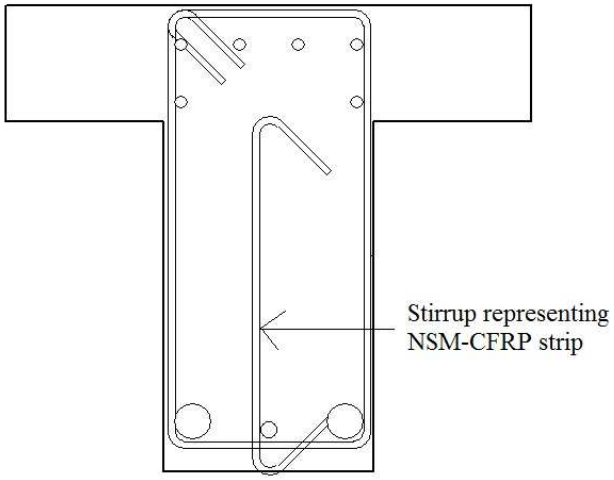

Fig. 7.16– Example R2K specimen with modeled CFRP strip

The resulting R2K shear capacity predictions, V_{R2K-R}, are reported in Table 7.10 and are compared to the reported experimental capacities. The R2K models with the NSM-CFRP over estimated the shear capacity by an average of 10.1% with a coefficient of variation of 12.3%.

Table 7.10 – R2K modeled capacity for literature experiments vs. experimental capacity

Strengthened Specimen	V_{exp}		V_{R2K-R}		V_{R2K-R}/V_{exp}
	[kN]	[kips]	[kN]	[kips]	
BS90-7A	207	46.5	201	45.1	0.97
2S-7LV	164	36.9	192	43.2	1.17
4S-7LV	189	42.5	216	48.5	1.14
2S-3LV	189	42.6	164	36.9	0.87
2S-5LV	214	48.2	200	44.9	0.93
2S-8LV	238	53.4	246	55.2	1.03
NB90-73-a	176	39.6	184	41.4	1.04
NB90-73-b	149	33.5	184	41.1	1.23
NB90-45-b	151	33.9	185	41.6	1.23
NS90-73-a	173	38.9	166	37.4	0.96
B.IT.NC.NS	740	166.0	833	187	1.13
2S-4LV	202	45.5	235	52.8	1.16
2S-7LV	225	50.5	274	61.6	1.22
2S-10LV	239	53.6	316	71.1	1.33

To further investigate modeling NSM-CFRP shear strength with R2K, the specimens from this research were modeled in a similar manner. A representative CFRP strip was added to the base reinforced concrete specimens as a stirrup. The concrete and steel used measured material properties. The CFRP used a modulus of elasticity of 138 GPa (20,082 ksi) based on Howell, [2009]. The CFRP effective stress was taken as 652 MPa (94.5 ksi), which was the average of the effective stresses calculated in *section 7.2* for specimens IT.7.18.6.S, IT.7.18.12.S, and IT.7.22.6.S based on R2K. These three stresses were chosen because the specimens did not have a flexurally dominant failure and were not subjected to any environmental exposure. The resulting R2K shear capacity predictions, $V_{R2K\text{-}R}$, are reported in Table 7.11 and are compared to the experimental capacities. The R2K cross-sections with the modeled NSM-CFRP underestimated the shear capacity by an average of 12% with a coefficient of variation of 5.8%. One method of improving the R2K models would be to refine the value of the CFRP modulus of elasticity and effective stress. The epoxy around the CFRP strips will also deform when stressed, which leads to the modulus of the NSM system being smaller than the modulus of the CFRP material. Pull-out tests could be performed in order to determine a more representative value of the modulus of elasticity for the NSM system.

Table 7.11 – R2K modeled capacity for specimens vs. experimental capacity

Strengthened Specimen	V_{exp}		V_{R2K-R}		V_{R2K-R}/ V_{exp}
	[kN]	[kips]	[kN]	[kips]	
T.6.18.6.S	1011	227.4	925	207.9	0.91
T.6.18.12.S	1043	234.5	826	185.6	0.79
IT.7.18.6.S	1209	271.8	1089	244.8	0.90
IT.7.18.12.S	1022	229.7	911	204.9	0.89
IT. 7.22.6.S	1165	262	1040	233.73	0.89
IT.5.22.12.S	1011	227.3	809	181.9	0.80
IT.7.18.6.M	1168	262.5	1064	239.1	0.91
IT.7.22.6.FT	1125	252.9	1029	231.4	0.91

8. BOND SPECIMENS

8.1 Experimental Program

One of the goals of this research was to make generalized observations about NSM-CFRP performance regardless of what type of CFRP strip or adhesive was used for the NSM repair. To do this, one must test different CFRP strips and adhesives. However, the full-scale specimens are very expensive to construct and time consuming to test. Due to this, the idea of a small "bond specimen" was developed in order to test the bond strength of several specimens with different bonded lengths, CFRP types, epoxy types, and environmental exposures. This paper reports the research and results of different epoxies and environmental exposures. Different CFRP types and bonded lengths are examined in Johnson, [2011].

8.1.1 Specimen Design

A conventional pull-out test could be used to examine the bond specimen variables, but it is difficult to grip the CFRP for a pull-out test without damaging the strip. For that reason it was desired to have a bond specimen made from two pieces of concrete retrofit together with NSM CFRP strips. Then the concrete could be pushed apart (creating direct tension in the NSM-CFRP strips) until failure. One objective of the bond specimens was to make the construction easy and reproducible. To incorporate this, it was decided to construct the bond specimens from standard 305 mm (12 in.) tall concrete cylinders with a 152 mm (6 in.) diameter. These cylinders are cheap, easy to cast, and create a convenient sized specimen to handle. The idea of the specimens was to cut grooves in each cylinder (assuring alignment of the grooves) then cut the cylinders in half and install two 152 mm (6 in.) pieces of NSM-CFRP to attach the halves together, but leave a space between the

two concrete ends. This space allows for a hydraulic jack, load cell, and confinement plates to be placed between the concrete. An example bond specimen can be seen below in Figure 8.1. A steel bolt is tightened in the gap between the concrete to provide stability for handling until testing.

Fig. 8.1 – Example bond specimen

The bond specimens have two strips of CFRP with both ends epoxied in 152 mm (6 in.) long grooves. This leaves four possible failure locations when the concrete is pushed apart. To eliminate this, one of the CFRP strips for each bond specimen was cut shorter so one of the retrofit ends would not extend the full 152 mm (6 in.). This allowed the failure location to be known before testing so it could be recorded. It was decided that 127 mm (5 in.) was a convenient bond length (L) to test. Solving for the bond strength according to equation (13-4) from ACI 440.2R-08 gives a bond stress of 14.5 MPa (2106 psi) which is in the suggested range of 3.5 to 21 MPa (500 to 3000 psi). This is shown in the calculation below.

$$L_{db} = \frac{a_b b_b}{2(a_b + b_b)(\tau_b)} f_{fd}$$ Eq. 8.1 – ACI 440 (13.4)

$$\tau_b = \frac{a_b b_b}{2(a_b + b_b)(L_{db})} f_{fd}$$ Eq. 8.2

$$\tau_b = \frac{0.63in \times 0.079in}{2(0.63in + 0.079in)(5in)} \times 300ksi = 2106\,psi$$

After some testing, it was found that L was long enough that sometimes the 152 mm (6 in.) side failed. To prevent this from occurring, a bond length of L/2, 64 mm (2.5 in.) was used for all the epoxy and environmental tests. Without any modifications there are four primary failure mechanisms the bond specimens could experience. These are failure of the concrete around the NSM groove, failure of the epoxy to concrete bond, failure of the epoxy to CFRP bond, or rupture of the CFRP strip. To see if the bond specimen idea worked some initial trial specimens were constructed and tested until failure. These trial bond specimens all failed by the concrete splitting in a triangular shape around the NSM CFRP strip. An example can be seen below in Figure 8.2.

Fig. 8.2 – Failure of concrete around the NSM repair

These trials showed that the bond specimen idea worked, but the failure mode was only through the concrete. Therefore, the capacity depended only on the strength of the concrete and not on the type of epoxy. It was decided to use confinement plates that were notched to fit around the NSM groove. With these confinement plates between the jack and the concrete it prevented the concrete from cracking and forced a failure to occur in the epoxy or CFRP. By doing this, the strength contribution from different epoxy types and any environmental degradation experienced by the epoxy could be compared. Care was taken to make sure smooth bearing surfaces were located between the confinement plates and concrete. The best way this research found to do this was to use a large concrete saw blade to make one smooth cut and then duct tape the surface during the retrofit process to keep it clean of epoxy. The addition of confinement plates changed the observed failure mode. The concrete around the NSM retrofit could still crack, but it was held in place by the plate and it eventually forced a failure in the epoxy or epoxy concrete interface. The observed failure modes are discussed in the results.

8.1.2 Construction

All the concrete cylinders used for the specimens in this research were cast from the same concrete truck to assure the concrete properties were the same for each specimen. The concrete came from the same truck as the full-scale girder specimen T.6.18.12.S and had a 28 day compressive strength of 28.2 MPa (4095 psi). The first step in construction was to cut two NSM grooves lengthwise on opposite sides of the cylinders. After the grooves were cut, the cylinders were cut in half to make two 152 mm (6 in.) tall cylinders. These were retrofit back together with CFRP strips leaving a 165 mm (6.5 in.) space between the concrete ends. Similar techniques to the full-scale specimens were used to clean the

grooves, clean the CFRP, epoxy the grooves, cure the epoxy, and retrofit the bond specimens.

8.1.3 Test Setup and Instrumentation

In the bond specimen test setup the cylindrical specimens stood vertically on an aluminum plate. This plate held up displacement sensors which pushed against a plate glued to the top of the specimen and measured the overall displacement the specimen underwent during loading. An average displacement was taken from the two sensors. Between the concrete ends sat a steel confinement plate, a 178 kN (40 kip) hydraulic jack, a 222 kN (50 kip) load cell, and a second confinement plate. A hand operated hydraulic pump provided the pressure for the jack to apply load. The setup can be seen below in Figure 8.3.

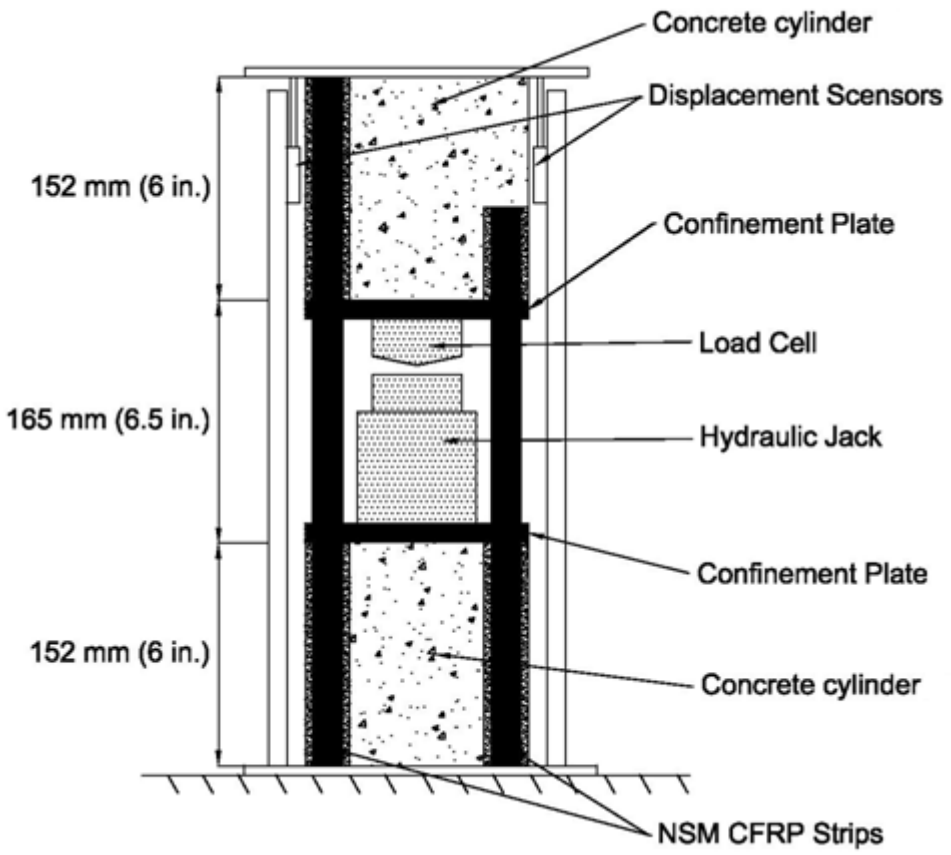

Fig. 8.3 – Bond specimen test setup

8.1.4 Experiment Design

The bond specimens were used to look at several variables. A total of 82 bond specimens were tested for the research in this paper. Three different epoxies were tested including: BASF Concresive 1420 (E1), Hilti Hit-Re 500-SD (E2), and Unitex Pro-Poxy 400 (E3). These are all readily available adhesives and were suggested from the Hughes Brothers' list for NSM repair. Properties for the epoxies are shown in Table 8.1.

Table 8.1 – Adhesive manufacturer material Properties

Manufacturer Reported Property	E1		E2		E3	
	[MPa]	[Ksi]	[MPa]	[Ksi]	[MPa]	[ksi]
Tensile Strength	34.5	5.03	Not reported		43.5	6.31
Compressive Modulus	2900	420	1830	265	1493	220
Compressive strength	67.6	9.8	72.7	10.5	82.7	12.0
Bond Strength	20.7	3.0	19.9	2.89	12.4	1.80
Ensured Full Cure Time	7 days @ 77 DF		3 days		3 days	

Environmental exposure was also tested on bond specimens with each of the three adhesives. It was decided that the CFRP strips would not be as susceptible to environmental degradation; therefore, Hughes Brothers Aslan 500 laminate strips were used as the reinforcing for all of the specimens. Specimens were tested for degradation due to moisture exposure by being submerged in water for six months. Other specimens were exposed to 400 freeze-thaw cycles similar to the full-scale specimen. Some of these specimens were dry while they were frozen and thawed while others experienced a combination of wet and dry exposure. The wet and dry condition was created by placing the cylinder specimens in a trough inside the environmental chamber. Once a day (every eight freeze-thaw cycles) the trough was filled with tap water on a warm cycle. The water was allowed to soak the cylinders for 30 minutes and then pumped out. A similar trough outside the environmental chamber exposed specimens to the same wet and dry conditions without the freezing and thawing. A picture of one of these troughs with the specimens is shown below.

Fig. 8.4 – Bond specimens undergoing freeze-thaw effects and wet-dry conditions

For each type of bond specimen at least three specimens were constructed and tested. This was to account for variance and provide results with average strength values. Due to the long duration of the environmental exposure tests, six specimens for these categories were built and tested to ensure confident average values could be determined. Hughes Brothers CFRP strips and a bond length of L/2 was used for all the epoxy tests, but the specimen names still identify these properties to allow the specimens to be compared to results from Johnson, [2011], which reports different CFRP types and bond lengths. Figure 8.5 below demonstrates the naming convention and Figure 8.6 shows the comparative test diagram for the bond specimens.

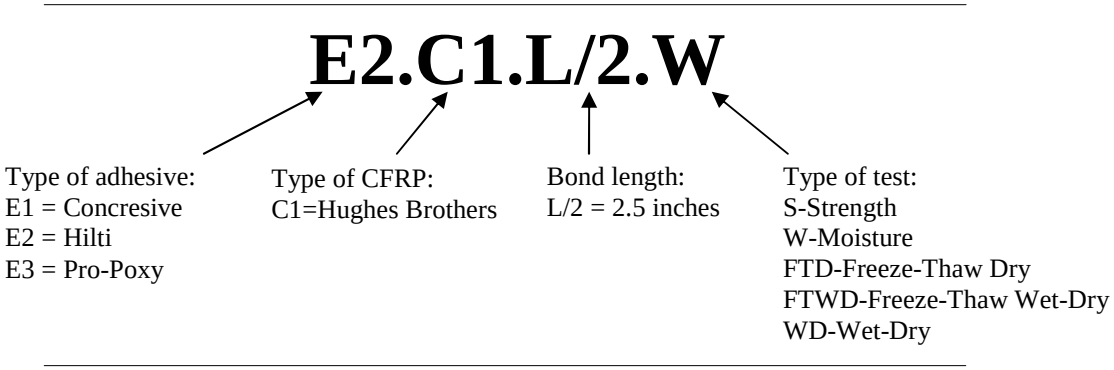

Fig. 8.5 –Bond specimen identification

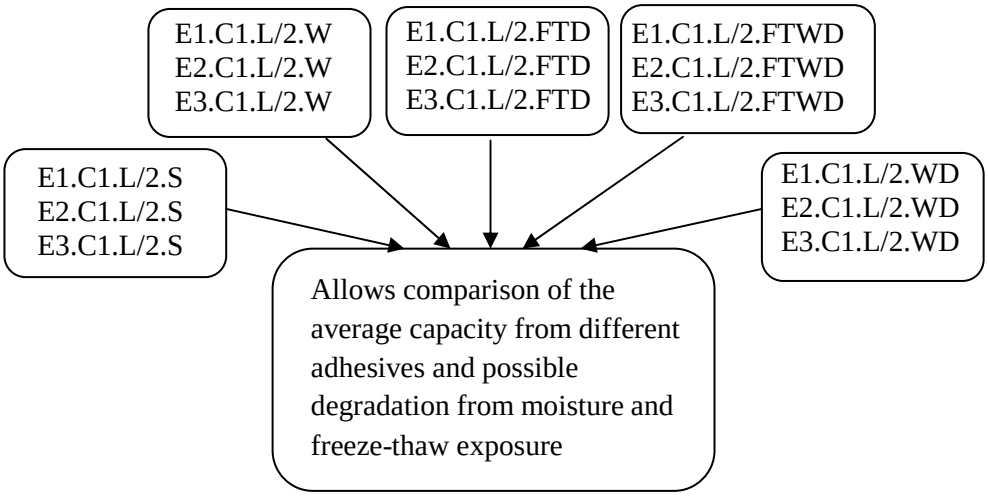

Fig. 8.6 - Bond specimen comparative matrix for adhesive type tests

8.1.5 Test Protocol

For safety purposes a plexiglass box was built to sit around the bond specimens when they were tested. The confinement plates, jack, and load cell were placed in the specimen. Then the jack was pressurized to take the slack out of the system. At this point, the displacement sensors were set in place and zeroed on top of the specimens. The specimens were then loaded with increasing applied force until failure. The moisture specimens were tested while wet before allowing to dry, but the wet-dry specimens were tested in the dry condition.

8.2 Experimental Results

The bond specimens exhibited a variety of failure modes. The concrete around the NSM reinforcement commonly failed in a triangular cone shape. Sometimes only the concrete on one side of the NSM groove failed forming half of a cone. The confinement plates held this concrete in place and forced a failure by either the CFRP pulling out of the epoxy or a column of epoxy pulling out because the interface between the epoxy and concrete failed. Sometimes a combination of epoxy slip and CFRP slip occurred with one side of the CFRP strip clean and the other side still attached to the epoxy. All of the failures fell into eight general failure modes. These modes are listed and described below with pictures to demonstrate them. The numerical results of the bond specimen tests and their respective failure modes are reported in Table 8.2.

Failure Modes:

1) Concrete cone failure and CFRP slip
2) Half concrete cone failure and CFRP slip
3) No concrete cone failure and CFRP slip
4) Concrete cone failure and epoxy concrete interface failed
5) Half concrete cone failure and epoxy concrete interface failed
6) No concrete cone failure and epoxy concrete interface failed
7) Concrete cone failure and CFRP slip/concrete interface combined failure
8) Half concrete cone failure and CFRP slip/concrete interface combined failure

Failure Mode (1)

Failure Mode (2)

Failure Mode (3)

Failure Mode (4)

Failure Mode (5)

Failure Mode (6)

Failure Mode (7)

Failure Mode (8)

Fig. 8.7 – Example failure modes for bonds specimens

Table 8.2 – Bond Specimen failure modes, strengths, and displacements

Specimen	Failure Mode	Load [k]	Disp [in.]
E1.C1.L/2.S (1)	4	4.95	0.042
E1.C1.L/2.S (2)	4	7.27	0.035
E1.C1.L/2.S (3)	1	8.53	0.050
E1.C1.L/2.S (4)	1	7.85	0.036
E2.C1.L/2.S (1)	4	9.30	0.032
E2.C1.L/2.S (2)	1	8.69	0.044
E2.C1.L/2.S (3)	1	7.50	0.032
E3.C1.L/2.S (1)	3	5.12	0.029
E3.C1.L/2.S (2)	5	4.42	0.005
E3.C1.L/2.S (3)	3	6.61	0.041
E1.C1.L/2.FTD (1)	1	5.04	0.027
E1.C1.L/2.FTD (2)	3	8.27	0.053
E1.C1.L/2.FTD (3)	3	9.99	0.071
E1.C1.L/2.FTD (4)	1	6.83	0.035
E1.C1.L/2.FTD (5)	1	10.84	0.069
E1.C1.L/2.FTD (6)	5	8.02	0.043
E2.C1.L/2.FTD (1)	1	9.10	0.049
E2.C1.L/2.FTD (2)	1	8.15	0.042
E2.C1.L/2.FTD (3)	7	6.48	0.037
E2.C1.L/2.FTD (4)	1	9.76	0.051
E2.C1.L/2.FTD (5)	7	7.52	0.037
E2.C1.L/2.FTD (6)	1	6.90	0.072
E3.C1.L/2.FTD (1)	7	4.90	0.023
E3.C1.L/2.FTD (2)	7	5.24	0.032
E3.C1.L/2.FTD (3)	4	3.59	0.021
E3.C1.L/2.FTD (4)	4	3.91	0.021
E3.C1.L/2.FTD (5)	8	3.83	0.015
E3.C1.L/2.FTD (6)	7	4.98	0.027
E1.C1.L/2.WD (1)	4	9.83	0.054
E1.C1.L/2.WD (2)	4	7.12	0.041
E1.C1.L/2.WD (3)	7	8.72	0.045
E1.C1.L/2.WD (4)	4	7.59	0.040
E1.C1.L/2.WD (5)	2	7.91	0.036
E1.C1.L/2.WD (6)	4	7.88	0.029
E2.C1.L/2.WD (1)	3	10.49	0.068
E2.C1.L/2.WD (2)	3	8.41	0.056
E2.C1.L/2.WD (3)	4	7.49	0.035
E2.C1.L/2.WD (4)	1	8.99	0.044
E2.C1.L/2.WD (5)	1	11.71	0.038
E2.C1.L/2.WD (6)	2	12.27	0.068
E3.C1.L/2.WD (1)	1	5.46	0.030
E3.C1.L/2.WD (2)	4	3.94	0.024
E3.C1.L/2.WD (3)	3	7.65	0.048
E3.C1.L/2.WD (4)	7	6.37	0.042
E3.C1.L/2.WD (5)	7	5.69	0.029
E3.C1.L/2.WD (6)	7	5.48	0.033
E1.C1.L/2.FTWD (1)	8	6.79	0.033
E1.C1.L/2.FTWD (2)	4	7.72	0.039
E1.C1.L/2.FTWD (3)	4	6.80	0.031
E1.C1.L/2.FTWD (4)	7	8.74	0.038
E1.C1.L/2.FTWD (5)	7	8.64	0.045
E1.C1.L/2.FTWD (6)	4	5.28	0.019
E2.C1.L/2.FTWD (1)	4	7.57	0.031
E2.C1.L/2.FTWD (2)	3	9.64	0.055
E2.C1.L/2.FTWD (3)	4	8.17	0.059
E2.C1.L/2.FTWD (4)	3	11.02	0.062
E2.C1.L/2.FTWD (5)	3	10.14	0.051
E2.C1.L/2.FTWD (6)	7	5.51	0.029
E3.C1.L/2.FTWD (1)	4	3.94	0.022
E3.C1.L/2.FTWD (2)	2	2.87	0.035
E3.C1.L/2.FTWD (3)	6	3.35	0.022
E3.C1.L/2.FTWD (4)	6	3.90	0.018
E3.C1.L/2.FTWD (5)	4	2.81	0.009
E3.C1.L/2.FTWD (6)	5	4.15	0.024
E1.C1.L/2.W (1)	5	5.71	0.035
E1.C1.L/2.W (2)	4	9.04	0.053
E1.C1.L/2.W (3)	4	5.93	0.032
E1.C1.L/2.W (4)	4	6.85	0.034
E1.C1.L/2.W (5)	8	8.41	0.057
E1.C1.L/2.W (6)	4	7.08	0.034
E2.C1.L/2.W (1)	4	6.02	0.026
E2.C1.L/2.W (2)	1	7.60	0.045
E2.C1.L/2.W (3)	1	9.84	0.060
E2.C1.L/2.W (4)	4	7.28	0.040
E2.C1.L/2.W (5)	2	7.51	0.032
E2.C1.L/2.W (6)	1	9.06	0.047
E3.C1.L/2.W (1)	6	5.43	0.030
E3.C1.L/2.W (2)	3	4.41	0.029
E3.C1.L/2.W (3)	6*	6.11	0.044
E3.C1.L/2.W (4)	6	6.27	0.037
E3.C1.L/2.W (5)	4	4.75	0.029
E3.C1.L/2.W (6)	8	4.40	0.025

*The 152 mm (6 in.) length on the bottom concrete block failed instead of the L/2 length.

8.3 Comparative Analysis

Table 8.3 – Bond Specimen average failure loads with coefficients of variation

Controls		E1	E2	E3
Avg. Load	kN	31.8	37.8	23.9
	[Kip]	[7.15]	[8.50]	[5.38]
COV		21.7 %	10.8 %	20.8 %

WD		E1	E2	E3
Avg. Load	kN	36.4	44.0	25.6
	[Kip]	[8.17]	[9.89]	[5.76]
COV		11.8 %	19.2 %	21.1 %
Difference		14.3%	16.4%	7.1%

W		E1	E2	E3
Avg. Load	kN	31.9	35.1	23.3
	[Kip]	[7.17]	[7.89]	[5.23]
COV		18.5 %	17.3 %	16.0 %
Difference		0.3%	-7.2%	-2.8%

FTD		E1	E2	E3
Avg. Load	kN	36.3	35.5	19.6
	[Kip]	[8.17]	[7.99]	[4.41]
COV		25.7 %	15.9 %	16.1 %
Difference		14.2%	-6.0%	-18.1%

FTWD		E1	E2	E3
Avg. Load	kN	32.6	38.6	15.5
	[Kip]	[7.33]	[8.68]	[3.47]
COV		17.9 %	23.1 %	17.9 %
Difference		2.5%	2.1%	-35.4%

8.3.1 Epoxy Comparison

The bond specimen test results have consistent coefficients of variation. The average COV for all the tests is 18.3%. This is a fairly large COV. However, one clear observation is that epoxy type 3 exhibited consistently weaker strengths than the other two types for the conditions considered in this test series. Table 8.4 reports the percent different for epoxy

type 2 and 3 compared to epoxy type 1. It demonstrates that epoxy type 2 was slightly stronger than type 1, and epoxy type 3 was weaker under all conditions compared to the other adhesives.

Table 8.4 – Difference in strength based on epoxy type

Specimen group	% Difference from E1	
	E2	E3
Controls	18.8%	-24.7%
WD	21.0%	-29.5%
W	10.0%	-27.1%
FTD	-2.2%	-46.0%
FTWD	18.4%	-52.6%

8.3.2 Bond Stress

The average bond stress, $\bar{u}$, of the NSM system can be determined because the CFRP strip dimensions and length are known. The active bond length, L_e, of the shorter length of NSM reinforcing in the test setup was used because this is the length that fails. It was assumed that the bond stress increased linearly along the length of the CFRP strip. The surface area is calculated as the active bond length, L_e, multiplied by the CFRP strip perimeter, p_o. The reported failure load is divided by two because only half of the load is carried by each NSM-CFRP strip due to the test setup. This bond stress is the stress in the CFRP strip at the failure in the setup, and is not necessarily representative of the bond stress in the full-scale specimens because the confinement plate does not allow failure of the concrete to occur and the stress conditions in the cylinder are not representative of an actual girder.

$$\bar{\mu} = \frac{F/2}{L_e * p_o}$$ Equation 8.3 – Bond Stress

F = Failure Load

L_e = 64 mm (2.5 in.)

P_o = 36 mm (1.42 in.)

Table 8.5 – Average bond stress for epoxy type

Epoxy Type:		E1	E2	E3
Control	MPa	6.95	8.26	5.23
Bond Stress	[ksi]	[1.01]	[1.20]	[0.76]
WD	MPa	7.95	9.62	5.60
Bond Stress	[ksi]	[1.15]	[1.40]	[0.81]
W	MPa	6.97	7.67	5.08
Bond Stress	[ksi]	[1.01]	[1.11]	[0.74]
FTD	MPa	7.94	7.76	4.28
Bond Stress	[ksi]	[1.15]	[1.13]	[0.62]
FTWD	MPa	7.13	8.44	3.38
Bond Stress	[ksi]	[1.03]	[1.22]	[0.49]

The calculated CFRP bond stresses range from 3.4 to 9.6 MPa (490 to 1400 psi). These values compare reasonably well to the lower end of the suggested range of 3.5 to 20.7 MPa (500 to 3000 psi) in ACI 440.2R-08 section 13.3.

8.3.3 Environmental Degradation

No environmental degradation was evident for E1 specimens. E1 specimens actually showed 0.3% to 14.3% strength gains when subjected to environmental effects. These results demonstrate the variability of the tests because strength gains are not expected to occur due to environmental exposure. The additional curing of the concrete possible for these cylinders in the environmental exposure may explain the observed increase in

strength. Similarly, E2 showed no degradation. E2 specimens varied from a 7.2% strength loss to a 16.4% strength gain.

E3 did exhibit strength loss due to freeze-thaw exposure. Compared to the controls, the wet and wet-dry E3 specimens gained strength. However, the E3 FTD specimens lost 18.1% strength and the FTWD specimens lost 35.4% strength compared to the control. This was the largest strength change in all of the specimen groups. Based on the mean strength values and the average COV, the mean value for E3 FTWD specimens is 1.94 standard deviations away from the control specimens. Figure 8.8 provides a visual comparison of the measured failure loads for each group of bond specimens.

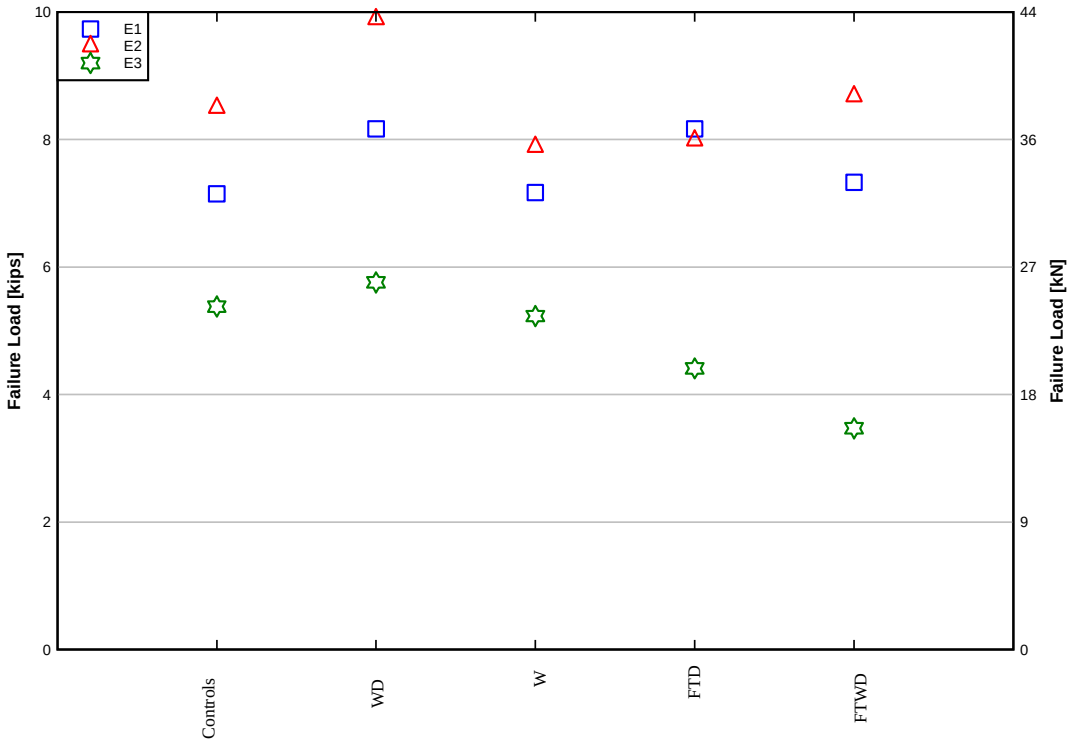

Fig. 8.8 – Comparison of average strengths of bond specimens

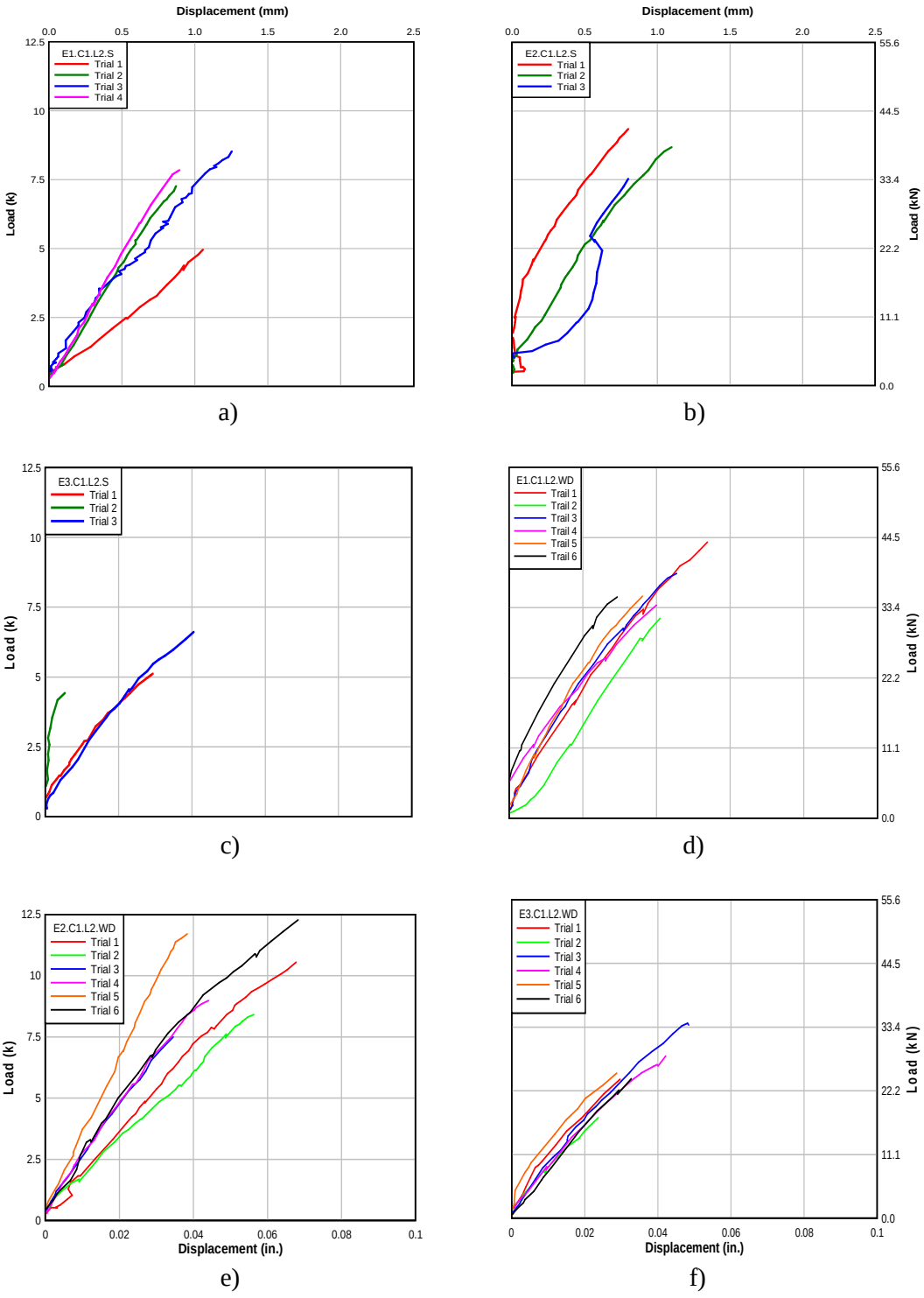

Fig. 8.9 – Load vs. displacement for control and wet-dry bond specimens

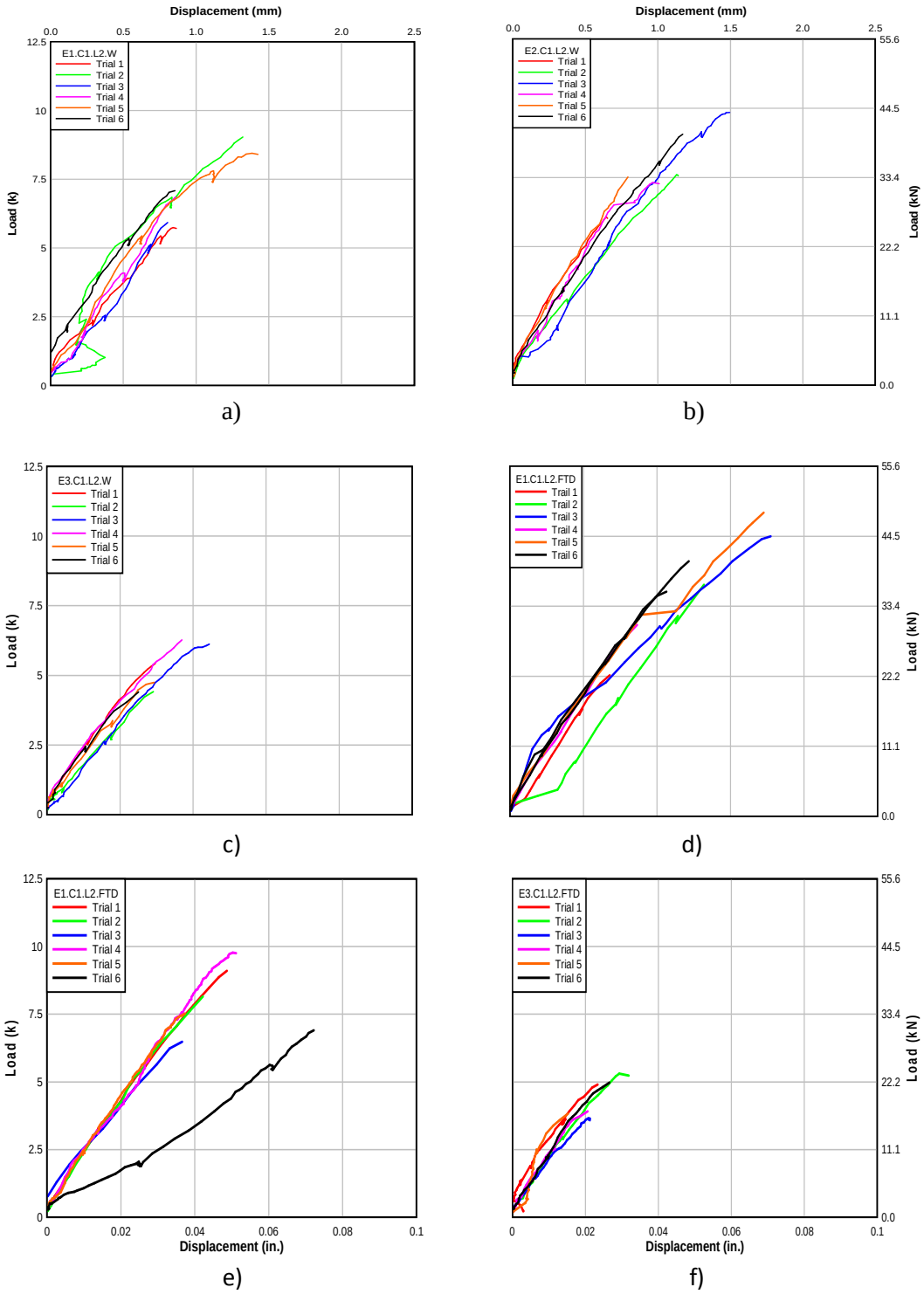

Fig. 8.10 – Load vs. displacement for moisture and freeze-thaw dry bond specimens

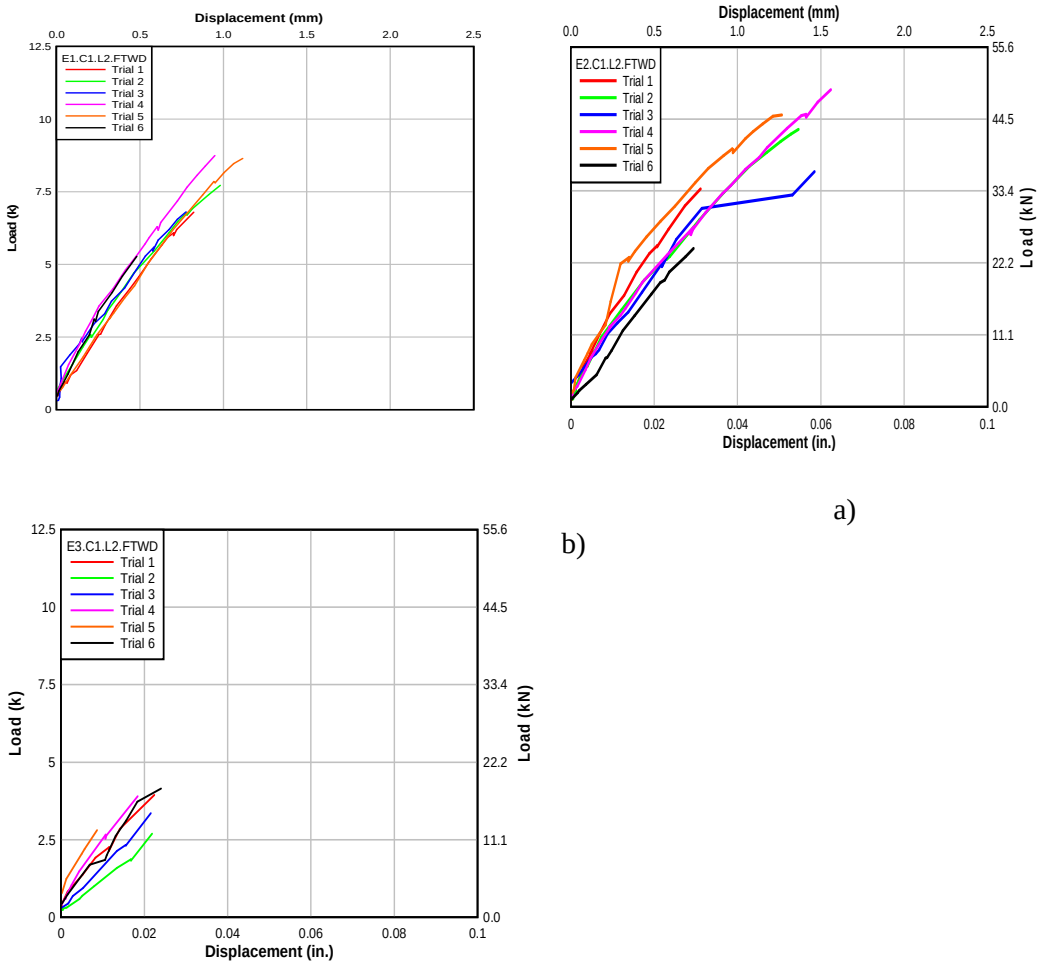

Fig. 8.11 – Load vs. displacement for freeze-thaw wet-dry bond specimens

9. RECOMMENDATIONS

9.1 NSM-CFRP Shear Strengthening

Based on the results of the full-scale test specimens, it is desirable to develop a design method for application of NSM-CFRP as transverse reinforcing. The traditional approach allows a designer to select a CFRP strip spacing, similar to stirrup spacing, to achieve the desired shear strength. To implement this approach an effective CFRP stress for design was determined. The effective CFRP stress, f_{fe}, for specimens from the literature review were found in *section 4.1*, and f_{fe} values for the specimens in this research were found in *section 7.2*. The effective stress can be calculated based on R2K or ACI predicted shear strength-transverse reinforcing interaction curves, but it was decided to use the R2K effective stress values because R2K predictions have been shown to have a better fit with experiments [Higgins, *et al.* 2004].

All the specimens from this research and from the literature review were considered, but only the specimens that used CFRP strips instead of bars, internal steel stirrups, and a flexural reinforcing ratio less than 3% were considered. The T-specimens from this research were not used because they fialed in flexure. Table 9.1 reports the specimens used and the corresponding effective CFRP stresses. The average effective CFRP stress from the experiments was 668 MPa (97 ksi). For simplicity, 670 MPa (95 ksi) was selected as the recommend value of f_{fe} to use for NSM-CFRP design.

Table 9.1 – Effective CFRP stress used for design

Specimen	f_{fe}	
	[MPa]	[ksi]
IT.7.18.6.S	682	99
IT.7.18.12.S	635	92
IT. 7.22.6.S	569	83
IT.5.22.12.S	834	121
IT.7.18.6.M	703	102
IT.7.22.6.FT	541	78
IT.7.22.6.FT-FTG	1434	208
IT.7.22.6.FTG	1041	151
Dias 07 2S-7LV	378	55
Dias 07 4S-7LV	333	48
Dias 08 2S-3LV	804	117
Dias 08 2S-5LV	719	104
Dias 08 2S-8LV	595	86
Dias 10 2S-4LV	558	81
Dias 10 2S-7LV	500	73
Dias 10 2S-10LV	417	61
Rounded Average	670	95

There are three possible design methods to choose from: R2K, AASHTO-MCFT, and ACI. It was determined that each design method should apply a strength reduction factor, ϕ, to the overall shear capacity and an NSM strength reduction factor, Ψ, to the CFRP effective stress. The goal of using these two reduction factors was to achieve a 1/10,000 probability of failure, or 1/10,000 chance that the actual member shear capacity will be below the design shear capacity. AASHTO and ACI already have ϕ factors of 0.9 and 0.75 respectively. It was determined that R2K should have the same ϕ factor as AASHTO because this factor represents accuracy in the design method, and R2K (similar to AASHTO) is more accurate than ACI. To calibrate the design approach, a graph of each of

the listed specimens was created with curves generated using R2K, AASHTO, and ACI. Bias for the design curves were not used in order to achieve the desired reliability for design without needing to correct for analysis bias individually.

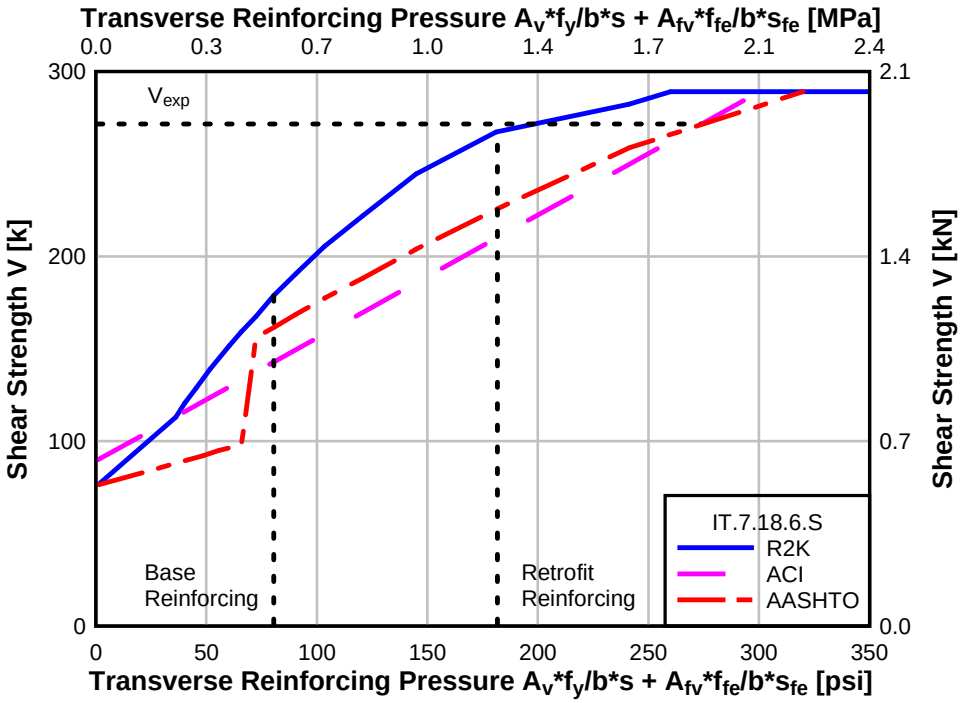

Fig. 9.1 – Example shear strength curves and retrofit capacity with average f_{fe}

The shear strength for each specimen can be determined by using these curves. The shear values for each design approach were multiplied by the appropriate strength reduction factor to provide design shear strength curves. Then a stress reduction factor, Ψ, was multiplied by the CFRP effective stress and the transverse reinforcing pressure was calculated. The value where this transverse reinforcing pressure intersects the corresponding design shear curve is the design shear strength. An example of this is shown in Figure 9.2

The design shear strength was determined for each of the specimens in Table 9.1 and then compared to the experimental shear strength. A ratio was defined for each specimen of $V_{exp}/\phi V_{design}$. When this ratio is less than one it represents failure. Therefore, statistics were performed to determine how many standard deviations the average ratio was removed from unity. This value, β, needs to be just above 3.5 to represent a 1/10,000 probability of failure. The values for the specimens and the statistics are shown in Table 9.2. Calibrating the ϕ and Ψ values for each design method was an iterative process. As mentioned before, the ϕ factors were kept as the recommended values for each method. Thus, a Ψ was chosen to establish the target β value for the group of specimens. The Ψ value was adjusted until β was above 3.5 for each method. From the iterations, the factors in Table 9.3 are suggested.

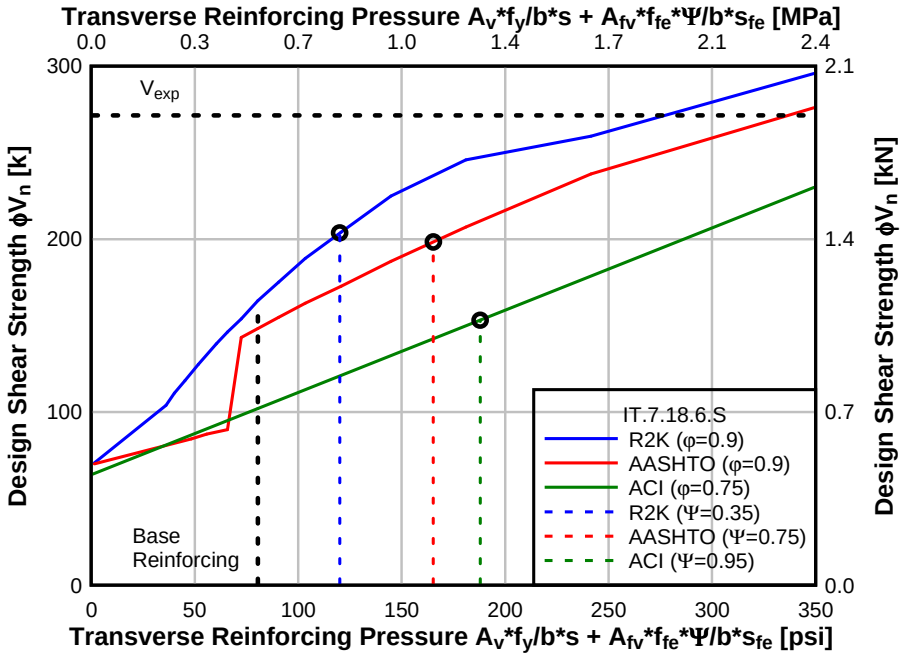

Fig. 9.2 – Example design shear curves and retrofit transverse reinforcing pressure

Table 9.2 – Design shears values and corresponding probability of failure

Specimen	V_{exp} [k]	ϕV_{R2K} [k]	$V_{exp}/\phi V_{R2K}$	ϕV_{AASHTO} [k]	$V_{exp}/\phi V_{AASHTO}$	ϕV_{ACI} [k]	$V_{exp}/\phi V_{ACI}$
IT.7.18.6.S	271.8	203.0	1.34	198.4	1.37	153.2	1.77
IT.7.18.12.S	229.7	184.0	1.25	174.1	1.32	127.5	1.80
IT. 7.22.6.S	262.0	181.0	1.45	185.0	1.42	142.2	1.84
IT.5.22.12.S	227.0	164.0	1.38	154.8	1.47	119.7	1.90
IT.7.18.6.M	262.5	194.0	1.35	192.6	1.36	148.7	1.77
IT.7.22.6.FT	252.9	187.0	1.35	188.7	1.34	145.2	1.74
IT.7.22.6.FT-FTG	303.8	184.1	1.65	197.7	1.54	152.1	2.00
IT.7.22.6.FTG	281.1	181.1	1.55	192.3	1.46	147.3	1.91
Dias 07 2S-7LV	36.9	26.5	1.39	31.2	1.18	23.2	1.59
Dias 07 4S-7LV	42.5	31.0	1.37	36.1	1.18	27.3	1.56
Dias 08 2S-3LV	42.6	27.5	1.55	29.9	1.42	20.0	2.13
Dias 08 2S-5LV	48.2	28.9	1.67	33.1	1.46	22.6	2.13
Dias 08 2S-8LV	53.4	31.1	1.71	36.8	1.45	26.5	2.01
Dias 10 2S-4LV	45.5	30.4	1.50	34.2	1.33	23.5	1.94
Dias 10 2S-7LV	50.5	32.3	1.56	37.6	1.34	26.9	1.88
Dias 10 2S-10LV	53.6	34.5	1.55	41.3	1.30	30.9	1.74
Mean			1.48		1.37		1.86
Stdev			0.14		0.10		0.17
Mean – 1.0			0.48		0.37		0.86
Beta			3.51		3.75		5.15

Table 9.3 – Suggested reduction factors for NSM-CFRP shear design

Method	Φ	Ψ
R2K	0.9	0.35
AASHTO	0.9	0.75
ACI	0.75	0.95

It is shown in Table 9.3 that R2K and AASHTO have larger NSM-CFRP effective stress reduction factors than ACI. This is because R2K and AASHTO provide more accurate predictions of shear strength and have smaller strength reduction factors. Thus, to achieve the same reliability, the Ψ factor must be smaller.

To design the NSM-CFRP shear reinforcing for a reinforced concrete girder with a known cross-section and material properties, the process consists of the following steps:

- Select design approach: R2K, AASHTO, or ACI
- Use appropriate ϕ and create design shear curve for section
- Choose a NSM-CFRP spacing
- Use appropriate Ψf_{fe} and calculate transverse reinforcing pressure
- Determine the design shear capacity by selecting the corresponding value from the design shear curve
- Check that design shear capacity is above the required shear demand

9.2 Example Shear Design

This section presents an example NSM-CFRP shear design for an existing bridge girder in an actual 1950's vintage RCDG bridge that follows the recommended design approach. The sample bridge girder is representative of the Springfield Bridge over the Willamette River and has the dimensions and properties listed in Table 9.4. It has hypothetically been determined that the girder needs to be strengthened in shear to handle a factored demand of 756 kN (170 kips) at a location 3.0 m (10 ft.) away from the support where the steel stirrup spacing is 381 mm (15 in.), and the moment demand is positive. This section is checked as an example, but an actual design would consider multiple sections including the location d_v away from the support where the shear demand is larger, and the stirrup spacing is smaller.

Table 9.4 – Example girder properties

Property	Metric	US
b_{eff}	221 cm	87 in
M/V.	6.0	6.0
b_w	33 cm	13 in
h	122 cm	48 in
cc	51 mm	2in
d	107 cm	42 in
F_y	276 MPa	40 ksi
F_{yv}	276 MPa	40 ksi
A_s	90.6 cm^2	14.04 in^2
A_v	2.6 cm^2	0.4 in^2
S_v	229	15
f_{fe}	670 MPa	95 ksi

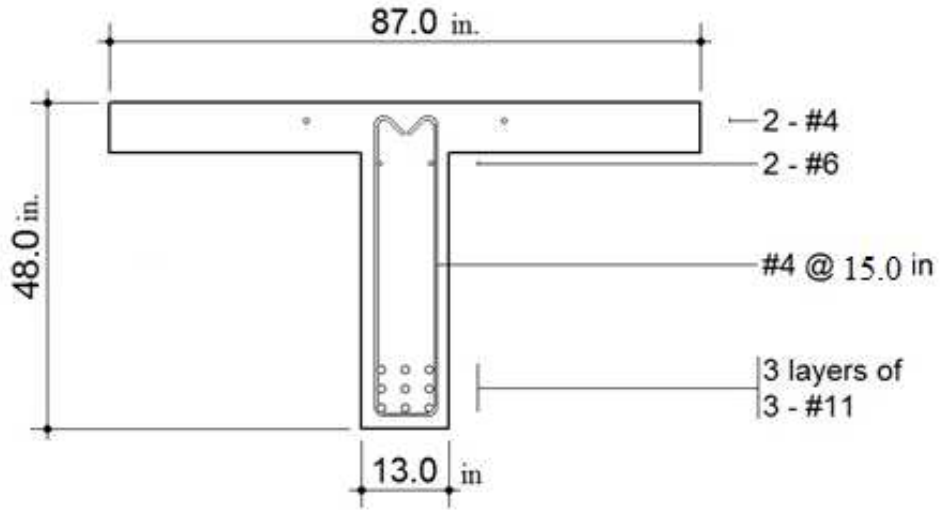

Fig. 9.3 – Cross-section of example girder 3.0 m (10 ft.) away from support

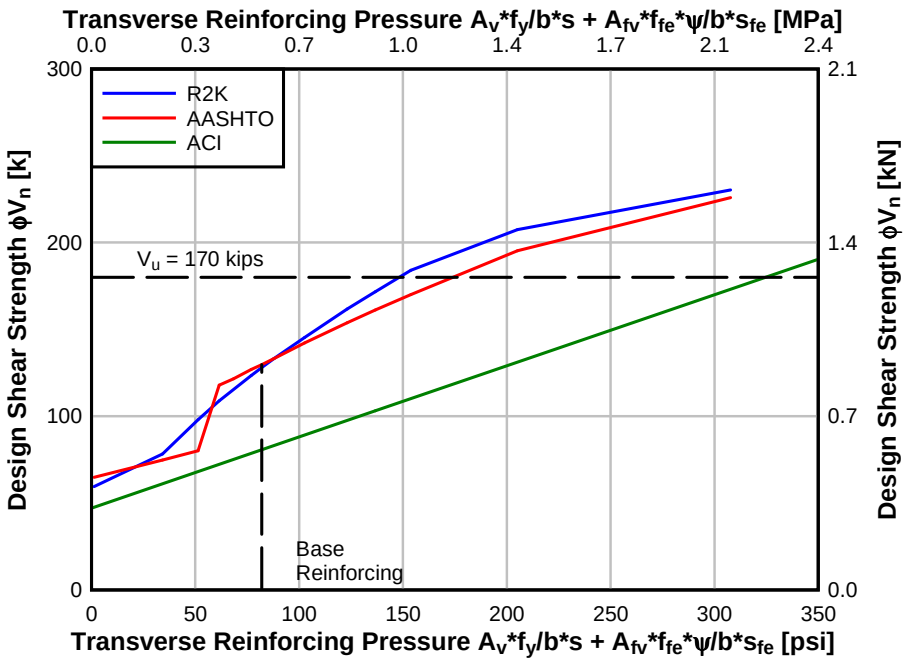

Fig. 9.4 – Design curves with base reinforcing and shear demand

The first step was to create design shear strength curves for the girder using the recommended shear strength reduction factors. Curves for all three design methods are demonstrated in Figure 9.4. Biases were not applied to these curves. The base transverse reinforcing pressure is determined from the internal stirrup spacing using the following equation:

$$Base = \frac{Av * fy}{b * s} = \frac{0.4in^2 * 40,000\,psi}{13in * 15in} = 82\,psi \qquad \text{Equation 9.1}$$

It is clear that the design strength with the current base reinforcing falls below the shear demand. The next step is to calculate a CFRP spacing that will provide a design shear

capacity above the demand. This was done by adding a CFRP contribution to the base reinforcing transverse pressure using Equation 9.2 and the recommended effective NSM-CFRP stress reduction factors.

$$CFRP = \frac{A_{fv} * f_{fe} * \psi}{b * s_f} \qquad \text{Equation 9.2}$$

$$Retro = Base + CFRP \qquad \text{Equation 9.3}$$

The design was completed by selecting the CFRP spacing and finding the corresponding design strength on the curve. The widest possible spacing that would achieve at least the factored shear demand was chosen. Table 9.5 shows the values in the calculations, and for comparison it lists the expected shear capacities (average expected shear capacity) for each method and NSM-CFRP spacing with no reduction factors applied. Figure 9.5 shows the shear curves with CFRP retrofitting values. AASHTO suggested a NSM-CFRP strip spacing of 178 mm (7.0 in.) is sufficient. R2K method suggested a more conservative spacing of 127 mm (5.0 in.). The ACI design method requires a spacing of 76 mm (3.0 in.); this spacing is in the realm of unrealistic and is due to the overly conservative nature of the ACI approach. This is particularly due to the calibration process used here that retained the strength reduction factored established for shear in ACI 318 (0.75) produced a much higher reliabiltiy (over 5) than the R2k or AASHTO-MCFT methods. It is recommended in this design to use the more conservative spacing suggested by AASHTO or R2K and therefore impliment a 127 mm (5.0 in.) NSM-CFRP spacing.

Table 9.5 – Caculated CFRP spacings and shear design capacities for example girder

Method	Retrofit Pressure (A_v*f_{fe}*Ψ/b*s)		CFRP spacing		ϕV_n		$V_{expected}$	
	[MPa]	[psi]	[mm]	[in]	[kN]	[kips]	[kN]	[kips]
R2K	0.92	134	127	5.0	770	170	1050	236
AASHTO	1.10	160	178	7.0	774	174	921	207
ACI	2.16	313	76	3.0	783	176	1072	241

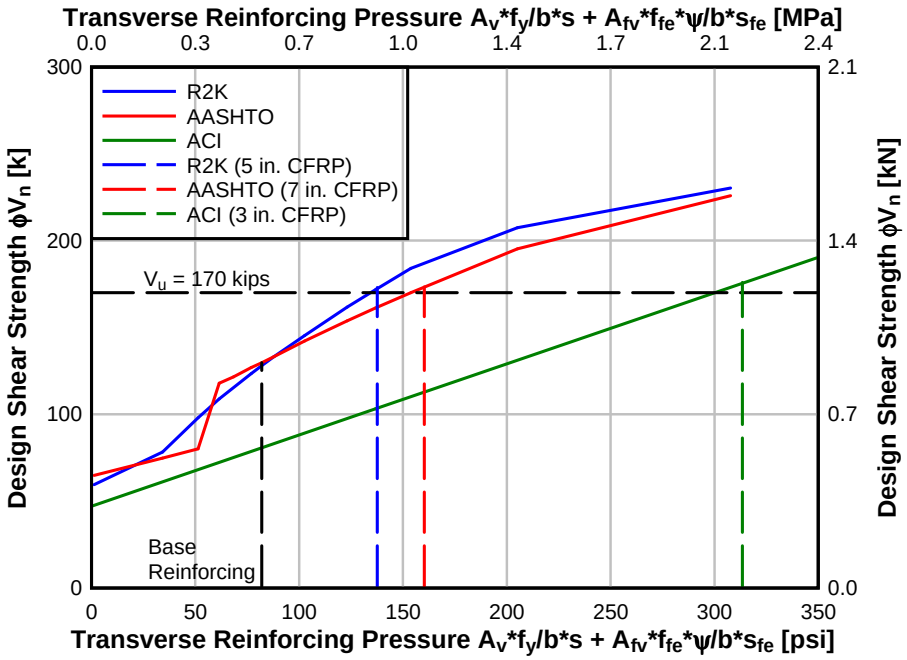

Fig. 9.5 – Example shear design curves with retrofit transverse pressures

9.3 Discussion

It would be expected that all three design methods should give similar results due to the calibrated reduction factors. One reason for the difference between R2K and AASHTO is that the factors were calibrated to a small population of specimens with specific M/V ratios

and amounts of flexural reinforcing. If more data were available, more precise design measures could be achieved over a wider range of input parameters.

Furthermore, the ACI method gave a NSM-CFRP spacing which was more conservative than the other two methods. This is partially because a ϕ factor of 0.75 was maintained for ACI in the reliability calibration and provided a higher reliability than the other two methods. If ϕ were changed to produce similar reliability levels with the other methods, then a wider NSM-CFRP spacing would be expected. Table 9.6 shows the ACI calibration values for a strength reduction factor ϕ of 0.95. This provides a reliability similar to that of the R2K and AASHTO-MCFT with β= 3.54. Figure 9.6 demonstrates the same design example with this ACI strength reduction factor. As expected, ACI now produces a NSM-CFRP spacing of 127 mm (5.0 in.) which is the same as R2K.

Table 9.6 – ACI design shear values with ϕ of 0.95.

Specimen	V_{exp} [k]	ϕV_{ACI} [k]	$V_{exp}/\phi V_{ACI}$
IT.7.18.6.S	271.8	194.1	1.40
IT.7.18.12.S	229.7	161.5	1.42
IT. 7.22.6.S	262.0	180.1	1.45
IT.5.22.12.S	227.0	151.6	1.50
IT.7.18.6.M	262.5	188.4	1.39
IT.7.22.6.FT	252.9	184.0	1.37
IT.7.22.6.FT-FTG	303.8	192.7	1.58
IT.7.22.6.FTG	281.1	186.6	1.51
Dias 07 2S-7LV	36.9	29.5	1.25
Dias 07 4S-7LV	42.5	34.6	1.23
Dias 08 2S-3LV	42.6	25.3	1.68
Dias 08 2S-5LV	48.2	28.6	1.68
Dias 08 2S-8LV	53.4	33.6	1.59
Dias 10 2S-4LV	45.5	29.8	1.53
Dias 10 2S-7LV	50.5	34.1	1.48
Dias 10 2S-10LV	53.6	39.1	1.37
Mean			1.47
Stdev			0.13
Mean – 1.0			0.47
Beta			3.54

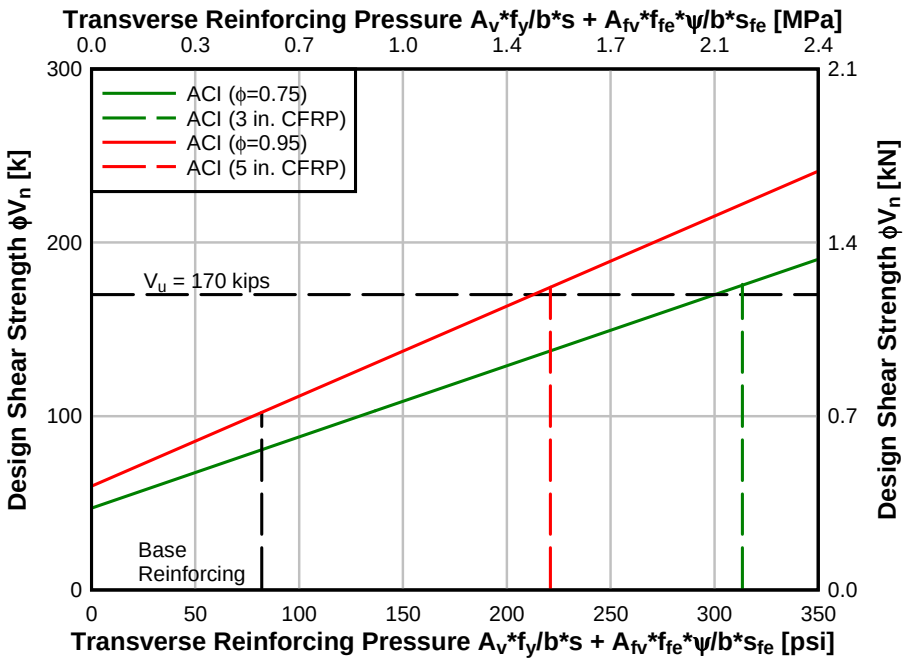

Fig. 9.6 – Example ACI shear design curves with different strength reduction factors

To complete a shear design, the flexural capacity also needs to be checked. Calculating the moment capacity determins a value of 2160 kN-m (1605 k-ft). Given the shear-moment ratio at the section considered, the corresponding shear at flexural capacity is 1188 kN (267 kips). To induce a flexural failure for the example girder and M/V ratio the transverse pressures and CFRP strip spacings for each design method would take a spacing tighter than 51 mm (2 in.). Spacings smaller than this are not realistic, and it can be seen in Figure 9.5 that the flexural capacity of 1188 kN (267 kips) falls above the design curves making a flexural failure for this design example unachievable. Table 9.7 reports the transverse pressures corresponding to a 51 mm (2 in.) NSM-CFRP spacing for each design method.

Table 9.7 – Expected NSM-CFRP spacing to induce flexural failure

Method	Retrofit Pressure for 51 mm (2 in.) spacing (A_v*f_{fe}*Ψ/b*s)	
	[MPa]	[psi]
R2K	1.45	210
AASHTO	2.45	356
ACI	2.96	429

It should be noted that the shear demand decreases away from the support; and consequently, a larger CFRP spacing could be used further along the shear span.

Another point is that specimens with lighter flexural reinforcing have R2K and AASHTO curves which flatten in the flexurally dominant region. A specimen with heavy flexural reinforcement has a steeper curve, and thus has larger reductions in shear strength for the same CFRP effective stress reduction factor (Ψ). As a result, it is not possible to have the same level of reliability for specimens with different amounts of flexural reinforcing with the present calibration and limited data. With more data, it would be possible to determine a sliding scale for Ψ based on whether the design shear strength falls in the flexurally dominate or shear dominate region of the curve.

9.3.1 Checking Reliability with R2K Model

This section looks at the reliability of the design example compared to the reliability of R2K values using statistics from the R2K models compared to experimental values. *Section 7.9* found the predicted shear capacity of the specimens in this research by adding a supplemental NSM-CFRP stirrup to the cross sections modeled with R2K. The values for the specimens used in this design recommendation are reported in Table 9.8. The average

bias from the experimental capacities for these models was 1.14 with a standard deviation of 0.16.

Table 9.8 – NSM-CFRP modeled in R2K compared to experimental values

Strengthened Specimen	V_{exp}		V_{R2K-R}		V_{exp} / V_{R2K-R}
	[kN]	[kips]	[kN]	[kips]	
2S-7LV	164	36.9	180	40.5	0.91
4S-7LV	189	42.5	205	46.2	0.92
2S-3LV	189	42.6	123	27.6	1.54
2S-5LV	214	48.2	154	34.7	1.39
2S-8LV	238	53.4	193	43.3	1.23
2S-4LV	202	45.5	194	43.6	1.04
2S-7LV	225	50.5	215	48.4	1.04
2S-10LV	239	53.6	239	53.7	1.00
T.6.18.6.S	1011	227.4	925	207.9	1.09
T.6.18.12.S	1043	234.5	826	185.6	1.26
IT.7.18.6.S	1209	271.8	1089	244.8	1.11
IT.7.18.12.S	1022	229.7	911	204.9	1.12
IT. 7.22.6.S	1165	262	1040	233.73	1.12
IT.5.22.12.S	1011	227.3	809	181.9	1.25
IT.7.18.6.M	1168	262.5	1064	239.1	1.10
IT.7.22.6.FT	1125	252.9	1029	231.4	1.09
Average:					1.14
Stdev:					0.16
Lower bound (3.5 σ)					0.58

A curve representing shear strength versus transverse pressure was plotted using R2K. The curve was then adjusted with the bias from the population of experiments to achieve an expected R2K curve. Then a lower bound curve was produced (3.5 standard deviations from the mean) to represent approximately 1/10,000 chance of failure. At the transverse pressure for the base specimen, a bias of 1.05 and standard deviation of 0.12 were applied based on work from Bentz [2000] because the base specimen does not have NSM-CFRP.

The lower bond curve has a horizontal portion because it is restricted to the lower bound of the base specimen. These curves are shown in Figure 9.7. At the transverse pressures, for spacings of 76 mm, 127 mm, and 178 mm (3 in., 5 in., and 7 in.), the shear demand of 170 kips is located above the lower R2K bound. This demonstrates that the chance of failure of a single girder is above 1/10,000 for the example girder and transverse pressures. The reason for this is because the calibrated reliability was based on CFRP effective stress instead of shear strength. However, a girder is part of a bridge system which has multiple girders acting together. If a hypothetical bridge with four girders is considered, then a truck load on the bridge would be shared over all four girders and would not fail any individual girder. Thus the system reliability will be better than a single girder and provide the desired reliability.

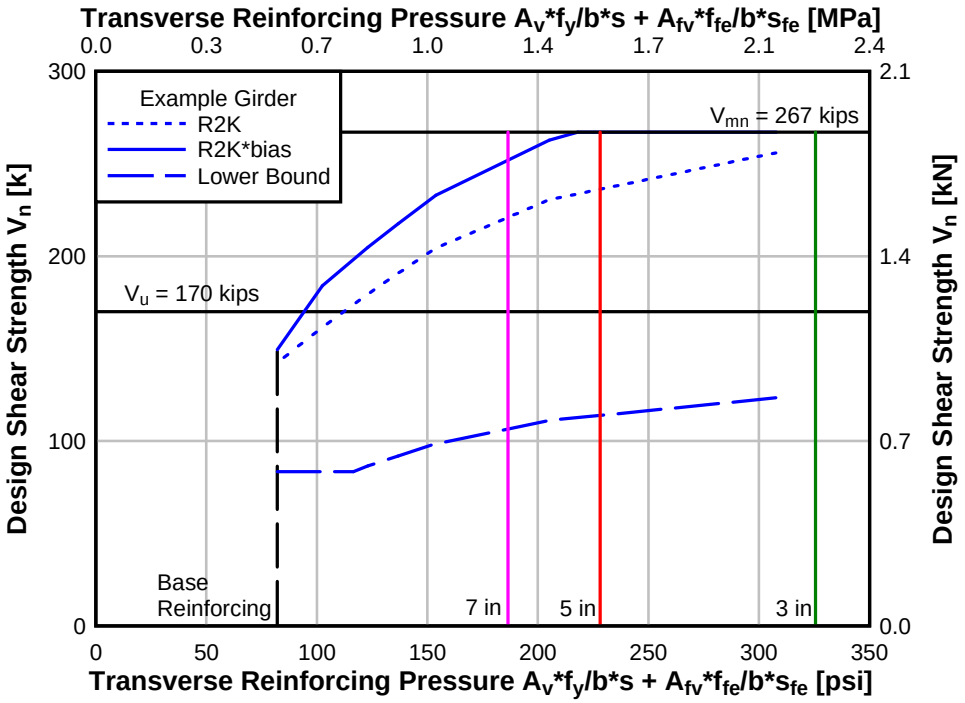

Fig. 9.7 – Example R2K curves with lower reliability bound

10. CONCLUSIONS

Eight full-scale specimens and 81 bond specimens were tested in this research to investigate NSM-CFRP for shear strengthening of large-size bridge girders. Based on the experimental results and analyses of these experiments, the following conclusions are made:

- Application of NSM-CFRP increased the shear strength of all full-scale specimens compared to the base capacities predicted from R2K and previous tests at Oregon State University.
- The primary failure mode for closely spaced NSM-CFRP consisted of the inner core of concrete cracking diagonally and the NSM reinforced outer shell of concrete peeling away from the inner core along the top and bottom of the diagonal crack.
- The T-oriented specimens failed in flexure and thus only a minimum value of shear contribution could be determined for the NSM-CFRP.
- Overall specimen stiffness measured by the applied shear versus the midspan displacement was not affected by application of NSM-CFRP as transverse reinforcing.
- Diagonal displacement sensors showed little to no increase in regional stiffness due to application of NSM-CFRP as transverse reinforcing.
- Moisture exposure did not lead to a significant decrease in shear capacity or stiffness compared to a similar control specimen.
- Freeze-thaw exposure did not produce a significant decrease in shear capacity or stiffness compared to a similar control specimen.

- Specimen IT.5.22.6.S initiated a flexural failure during testing. Half the CFRP strips were removed by saw-cutting to create specimen IT.5.22.12.S which failed in shear. The cumulative effects of saw-cutting, significant prior load history, and cracking on specimen IT.5.22.12.S are not fully known, and thus comparisons should be made with caution.
- Higher NSM-CFRP strains and shear panel deflections were measured in specimen IT.5.22.12.S when it had 152 mm (6 in.) CFRP spacing compared to specimen IT.7.22.6.S. The ratio of these strains is similar to the ratio of transverse strain predicted by Response-2000.
- The strains in the steel stirrups were reduced by the addition of NSM-CFRP as transverse reinforcing.
- ACI 318 provided a conservative prediction of the specimens unstrengthened base shear capacities compared to Response-2000.
- ACI 440 does not provide a design method specifically for NSM retrofitting, but adapting the present surface-bonded CFRP approach gave conservative predictions of shear capacity for the specimens considered.
- The approach by Nanni, *et al*. [2004] for determining NSM-CFRP shear capacity provided conservative values that were only slightly closer to the experimental shear capacities than ACI 440.
- An approach was developed to predict the shear capacity based on Response-2000 analysis of the specimens and those in the archival literature. The predictions using this method were conservative, but much closer than the ACI 440 or Nanni, *et al*. [2004] shear capacity design estimates.

- Effective CFRP stresses were calculated based on Response-2000 curves and experimental shear capacities. These stresses are much smaller than the tensile strength of the CFRP strips.
- Modeling the CFRP as a supplemental stirrup in Response-2000 provided reasonable estimates of the experimental shear capacities using an empirical average NSM-CFRP effective stress based on the experimental results.
- A design approach is presented for NSM-CFRP application using three design methods (R2K, AASHTO-MCFT, and ACI).
- Bond tests showed that epoxy type E2 was the strongest and that epoxy E3 was the weakest under the conditions considered in the test program.
- Environmental exposure showed no strength degradation in the E1 or E2 bond specimens.
- Freeze-thaw exposure caused strength reduction in the E3 bond specimens. Bond degradation of this adhesive may occur if used in NSM-CFRP applications for bridge girders subjected to many cycles of freezing and thawing.

10.1 Future Testing

Based on the results of this research, the following recommendations are made for future testing:

- Additional T-oriented specimens should be tested to determine the actual shear capacity increase due to NSM-CFRP retrofitting. These specimens should have less internal stirrups, more flexural reinforcing, and more compression steel to help force a shear failure.
- Additional IT-oriented specimens with light flexural reinforcing bars should be tested because only one was tested in this research. The specimen in this research had NSM-CFRP cut out to force a failure, thus the data may not be representative.
- More bond specimen testing could improve the level of confidence related to epoxy type, and allow other epoxies to be tested and compared.
- Tests on specimens subject to carbonization from long-term service life exposure would determine if NSM-CFRP is more or less effective in the carbonized concrete surface layer.
- Specimens subjected to salt water exposure could be tested to identify possible degradation for bridges in coastal environments.

11. REFERENCES

American Concrete Institute, 2008, "440.2R-08: Guide for the Design and Construction of Externally Bonded FRP Systems for Strengthening Concrete Structures," *ACI Manual of Concrete Practice*, Farmington Hills, Michigan.

American Concrete Institute, 2008, "318-08: Building Code Requirements for Structural Concrete and Commentary,: *ACI Manual of Concrete Practice*, Farmington Hills, Michigan.

ASTM D 3039/D 3039M-00, American Society of Testing and Materials, "Standard Test Method for Tensile Properties of Polymer Matrix Composite Materials," ASTM, West Conshohocken, PA, 2006.

ASTM C39/C39M-09a, 2009, "Standard test method for compressive strength of cylindrical concrete specimens," *ASTM International.*

ASTM C617-09a, 2009, "Standard practice for capping cylindrical concrete specimens," *ASTM International*.

ASTM E8/E8M-09a, 2009, "Standard test methods for tension testing of metallic materials," *ASTM International*.

Anwarul Islam A.K.M., 2009, "Effective Methods of using CFRP bars in Shear Strengthening of Concrete Girders," *Engineering Structures*, V. 31, No. 3, March, pp. 709-714.

Barros J.A.O., and Dias S.J.E., 2006, "Near Surface Mounted CFRP Laminates for Shear Strengthening of Concrete Beams," *Journal cement and concrete composites*, ISSN 0958-9465, 28:3 March, pp. 276-292.

Bianco V., Barros J.A.O., and Monti G., 2009, "Bond Model of NSM-FRP Strips in the Context of the Shear Strengthening of RC Beams," *Journal of Structural Engineering*, V. 135, No. 6, June, pp. 619-631.

Bentz E., 2000, "Sectional Analysis of Reinforced Concrete Members," PhD Thesis, University of Toronto.

Bianco V., Barros J.A.O., and Monti G., 2007, "A New Approach for Modeling the NSM Shear Strengthening Contribution in Reinforced Concrete Beams," FRPRCS-8, University of Patras, Greece, July.

Dawson M., 2008, "Scale Effects on Reinforced Concrete Beams Strengthened for Shear with Discrete Externally Bonded Carbon Fiber-Reinforced Polymer U-Wraps," Master Thesis, Oregon State University.

De Lorenzis L., and Nanni A., 2001, "Shear Strengthening of Reinforced Concrete Beams with near-Surface Mounted Fiber-Reinforced Polymer Rods," *ACI Structural Journal*, V. 98, No. 1, January-February, pp. 60-68.

De Lorenzis L., and Nanni A., 2002, "Bond Between Near-Surface Mounted FRP Rods and Concrete in Structural Strengthening," *ACI Structures Journal*, V. 99, No. 2, March-April, pp. 123-133.

Dias S.J.E., Bainco V., Barros J.A.O., and Monti G., 2007 "Low strength T-cross section RC beams shear-strengthened by NSM technique," FAELLA, C. [et al.], ed. – "Materiali ed approcci innovativi per il progetto in zona sismica e la mitigazione della vulnerabilità delle strutture : atti del Workshop…, Fisciano, Itália, 2007". [S.l.] : Polimetrica, ISBN 978-88-7699-065-6.

Dias S.J.E., and Barros J.A.O., 2008, "Shear Strengthening of T Cross Section Reinforced Concrete Beams by Near-Surface Mounted Technique," *Journal of Composites for Construction*, V. 12, No. 3, June.

Dias S.J.E., and Barros J.A.O., 2010, "Performance of reinforced concrete T beams strengthened in shear with NSM CFRP laminates," *Engineering Structures*, V. 32 pp. 373-384.

Grace N.F., 2004, "Concrete repair with CFRP." *Concrete. International*, V. 26, No. 5, May, pp. 45–52.

Green M.F., Bisby L.A., Beaudoin Y., and Labossiere P., 2000, "Effect of freeze-thaw cycles on the bond durability between FRP plate reinforcement and concrete," *Canadian Journal of Civil Engineering*, V 27, pp. 949-959.

Green M.F., Dent A.J.S., and Bisby L.A., 2003, "Effect of freeze-thaw cycling on the behaviour of reinforced concrete beams strengthened in flexure with fibre reinforced polymer sheets," *Canadian Journal of Civil Engineering*, V 30, pp. 1081-1088.

Hassan T., and Rizkalla S., 2003, "Investigation of Bond in Concrete Structures Strengthened with Near Surface Mounted Carbon Fiber Reinforced Polymer Strips," *Journal of Composites for Construction*, V. 7, No. 3, August, pp. 248-257.

Higgins C., Miller T., Rosowsky D.V., Yim S.C., Potisuk T., Daniels T.K., Nicholas B.S., Robelo M. J., et al., 2004, "SPR 350 Assessment Methodology for Diagonally Cracked Reinforced Concrete Deck Girder," Salem, Oregon: Oregon Department of Transportation.

Higgins C., Dawson M., Mitchell M., Sopal G., and Senturk A., 2008, "SPR 652 OTREC-RR-09-09, Environmental Durability of Reinforced Concrete Deck Girders Strengthened for Shear with Surface-Bonded Carbon Fiber-reinforced Polymer, Final Report," Salem, Oregon: Oregon Department of Transportation, May.

Howell D., 2009, “Shear Repair Methods for Conventionally Reinforced Concrete Girders and Deep Beams,” PhD Dissertation, Oregon State University.

Johnson B., 2011, “Design and Fatigue Performance of NSM-CFRP for Shear Strengthening of Reinforced Concrete Bridge Girders,” Master Thesis, Oregon State University.

Malvar L., Joshi N., Beran J., and Novinson T., 2003, “Environmental Effect on the Short-Term Bond of Carbon Fiber-Reinforced Polymer (CFRP) Composites” *Journal of Composites for Construction*, V. 7, No. 1, February.

Mitchell M., 2008, “Freeze-Thaw Durability of Reinforced Concrete Deck Girders Strengthened for Shear with Surface-Bonded Carbon Fiber-Reinforced Polymer,” Master Thesis, Oregon State University.

Myers, J. J., and Ekenel M., 2005, “Effect of Environmental Conditions on Bond Strength between CFRP Laminate and Concrete Substrate,” *ACI SP-230: 7th International Symposium on Fiber-Reinforced Polymer Reinforcement for Concrete Structures*, pp. 1571-1592.

Nanni A., Di Ludovico M, and Parretti R., 2004, “Shear Strengthening of a PC Bridge Girder with NSM CFRP Rectangular Bars,” *Advances in Structural Engineering*, V. 7, No. 4, August, pp. 297-309.

Rizzo A., and De Lorenzis L., 2009a, “Behavior and Capacity of RC beams strengthened in shear with NSM FRP reinforcement,” *Construction and Building Materials* 23, pp. 1555-1567.

Rizzo A., and De Lorenzis L., 2009b, “Modeling of Debonding Failure for RC Beams Strengthened in Shear with NSM FRP Reinforcement,” *Construction and Building Materials*, V. 23, pp. 1568-1577.

Sena Cruz J., and Barros J., 2004, “Modeling of Bond Between Near-surface Mounted CFRP Laminate Strips and Concrete,” *Computers and Structures*, V. 82, pp. 1513-1521.

Shield C., French C., and Milde E., 2005, “The Effect of Adhesive Type on the Bond of NSM Tape to Concrete,” *ACI SP230: 7th International Symposium on Fiber-Reinforced Polymer (FRP) Reinforcment for Concrete Structures*, American Concrete Institute, November, pp 355-372.

Turan O.T., Higgins C., and Rosowsky D.T., 2008, “Statistical Modeling of Coupled Shear-Moment Resistance for RC Bridge Girders,” *ASCE Journal of Bridge Engineering*, V. 13, No. 4, July/August.

Wight J., and MacGregor J., 2009, “Reinforced Concrete Mechanics and Design, Fifth Edition,” Pearson Prentice Hall, New Jersey.

Williams, and Higgins, 2008, “Fatigue of Diagonally Cracked RC Girders Repaired with CFRP,” *Journal of Bridge Engineering*, V. 3, No. 1, January, pp. 24-33.

12. APPENDICES

12.1 Appendix A – Definitions

Carbon Fiber Reinforcing Polymer (CFRP): A light-weight composite material made from carbon fibers and resin and formed into strips, rods, or sheets.

Near-Surface Mounted (NSM): A strengthening technique that consists of cutting rectangular grooves in the surface of the concrete and bonding reinforcing (see bar types below) in the grooves with an adhesive.

Externally Bonded Reinforcement (EBR): Strengthening method consisting of bonding reinforcing fabric to the surface of concrete with an adhesive. A common method is to wrap sheets of reinforcement in a U-shape around the outside of a girder.

CFRP bar: A piece of carbon reinforcing of *any* cross-section with uniaxial orientation.

CFRP strip or tape: A rectangular cross-section reinforcing bar with uniaxial orientation.

CFRP rod: A *round* cross-section reinforcing bar with uniaxial orientation.

CFRP sheet: Woven reinforcing used as external concrete reinforcing.

12.2 Appendix B – Beam Specimen Crack Maps

The crack maps below show the cracked condition of the east side of the specimens after precracking and after failure. The CFRP strips are shown on the failure crack maps in red. The location of the CFRP strain gages is also shown. The dominate failure crack for each specimen is highlighted in blue. Specimen IT.7.22.6.S has an additional crack highlighted in green. This is the dominate failure crack on the west side of the beam; it is highlighted to demonstrate the difference that can occur between the two sides.

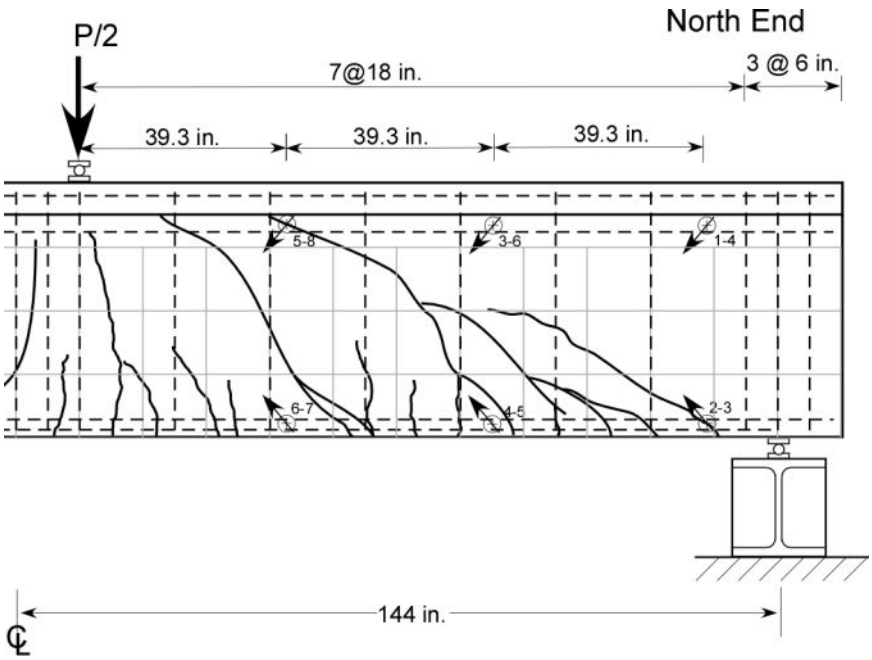

Fig. 12.1 – Specimen T.6.18.6.S crack map (baseline test)

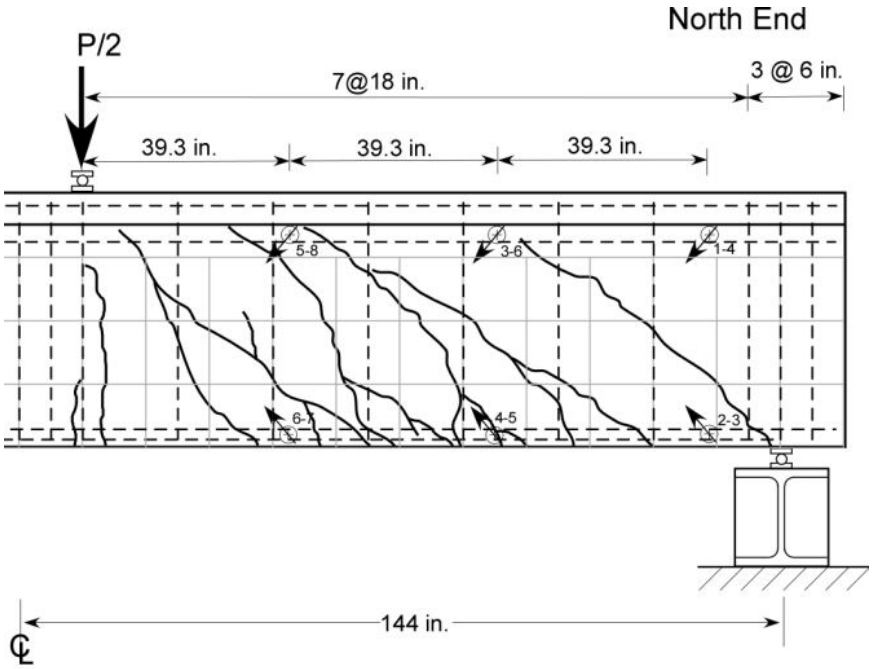

Fig. 12.2 – Specimen T.6.18.12.S crack map (baseline test)

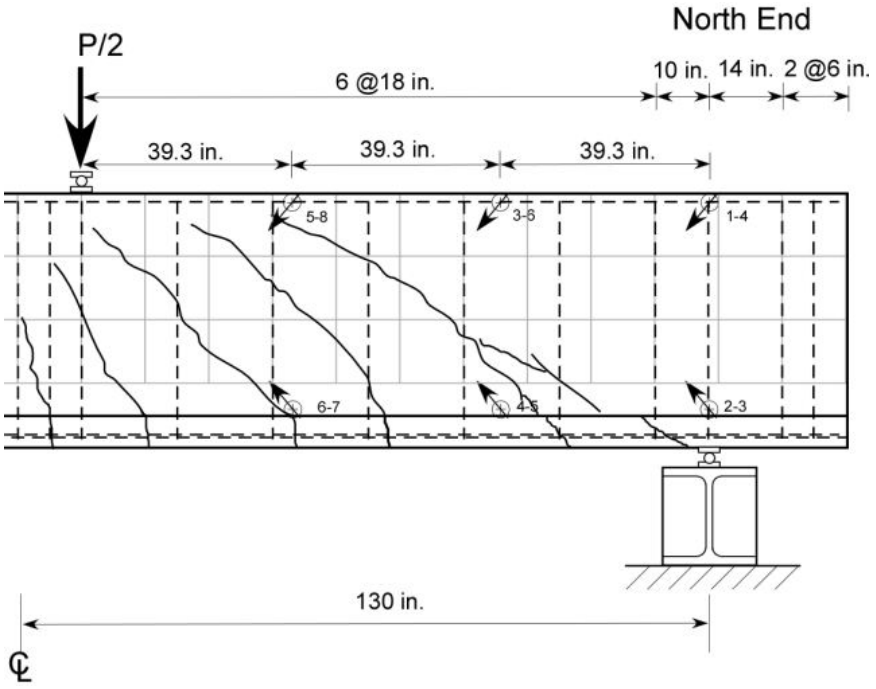

Fig. 12.3 – Specimen IT.7.18.6.S crack map (baseline test)

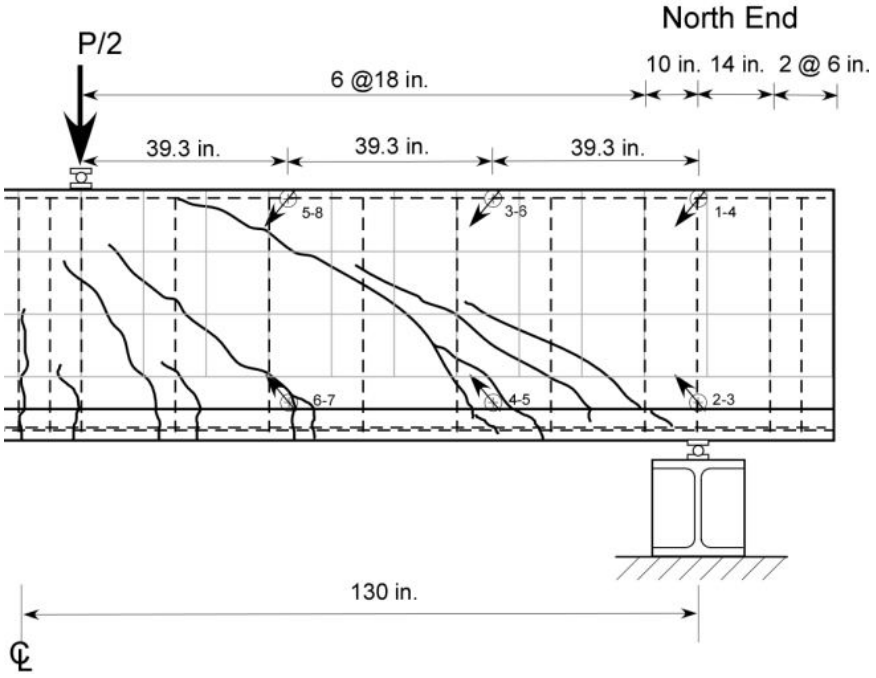

Fig. 12.4 – Specimen IT.7.18.12.S crack map (baseline test)

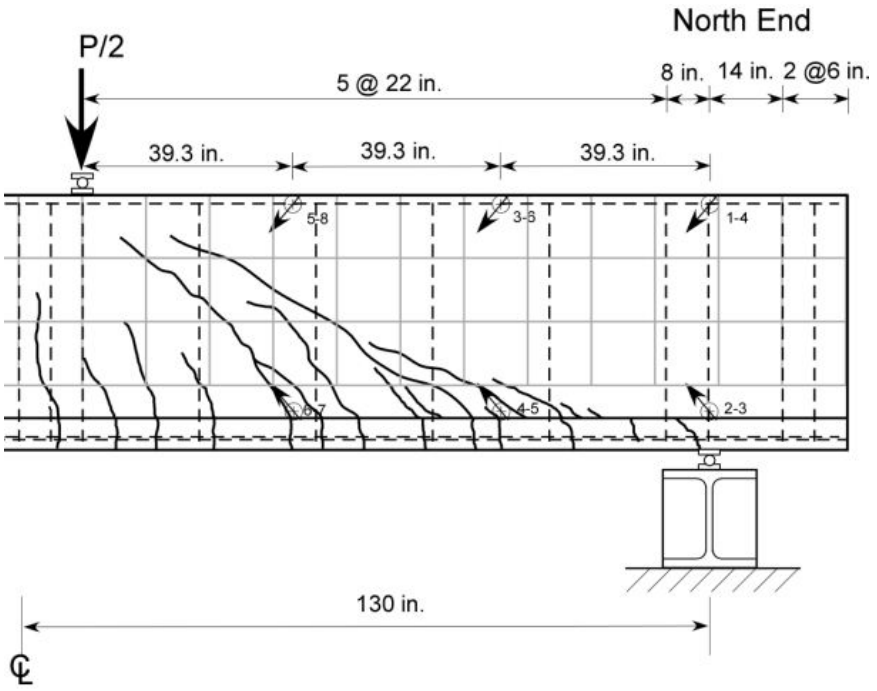

Fig. 12.5 – Specimen IT.7.22.6.S crack map (baseline test)

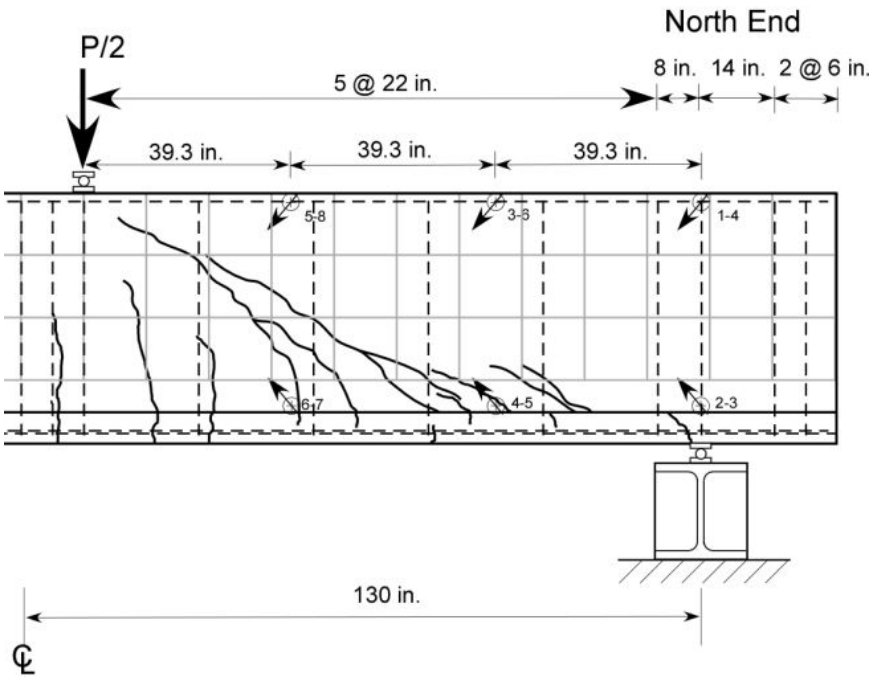

Fig. 12.6 – Specimen IT.5.22.12.S crack map (baseline test)

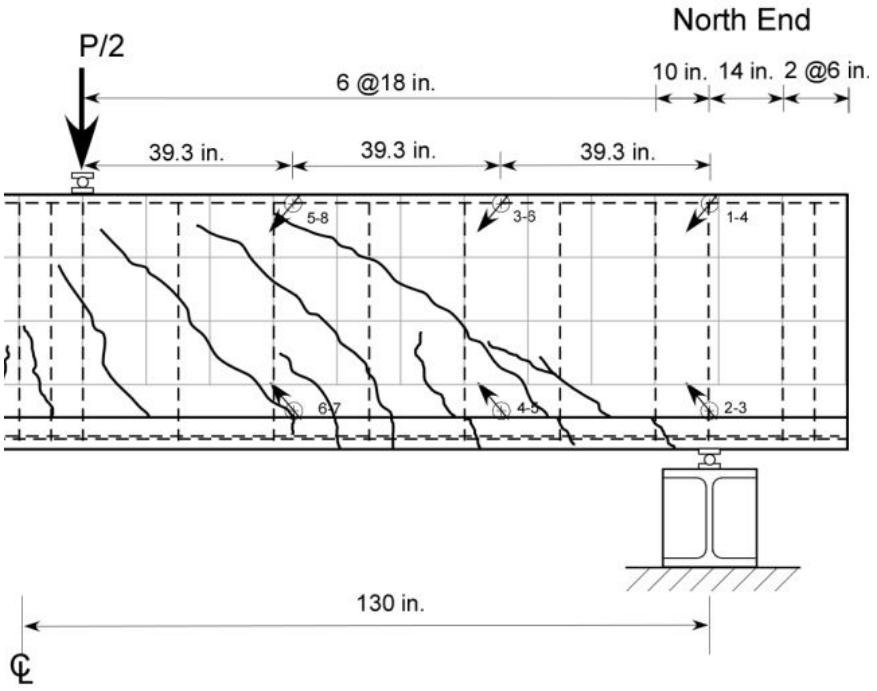

Fig. 12.7 – Specimen IT.7.18.6.M crack map (baseline test)

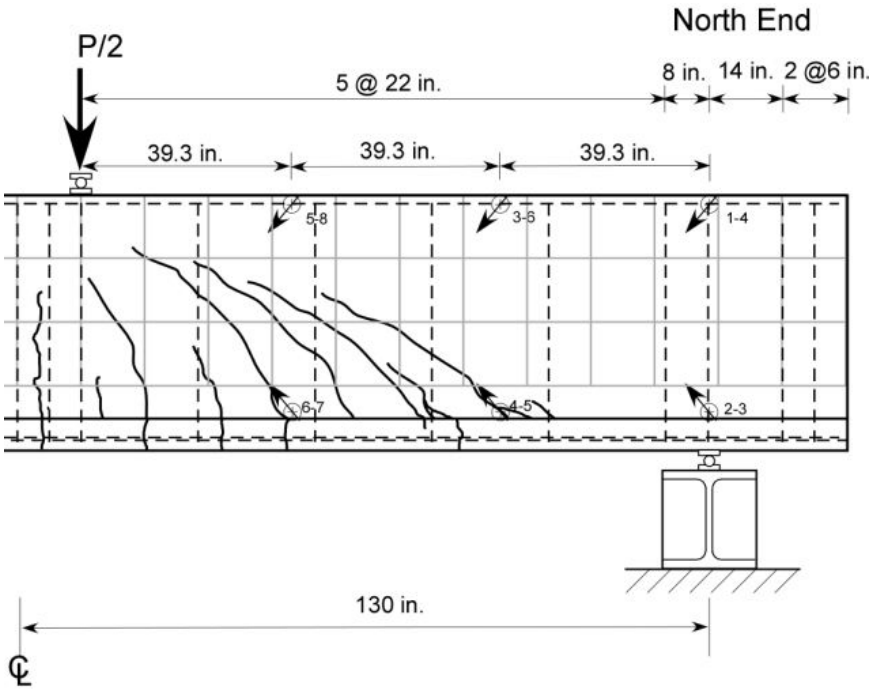

Fig. 12.8 – Specimen IT.7.22.6.FT crack map (baseline test)

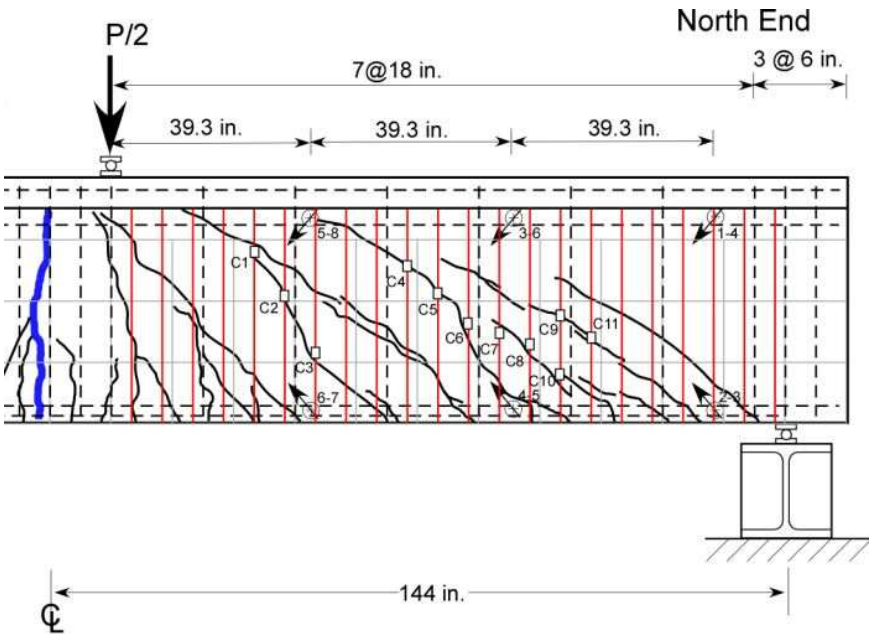

Fig. 12.9 – Specimen T.6.18.6.S crack map (failure test)

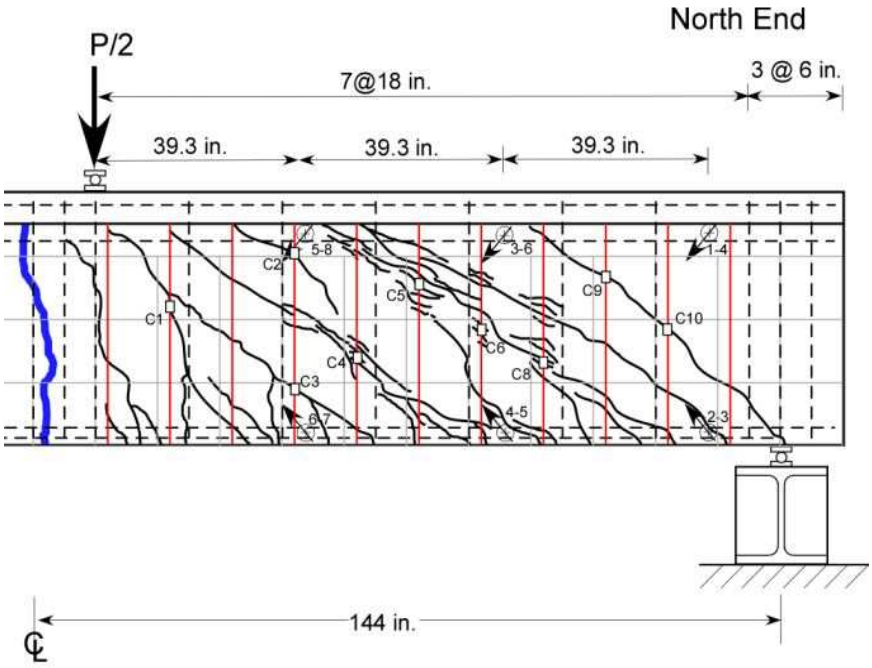

Fig. 12.10 – Specimen T.6.18.12.S crack map (failure test)

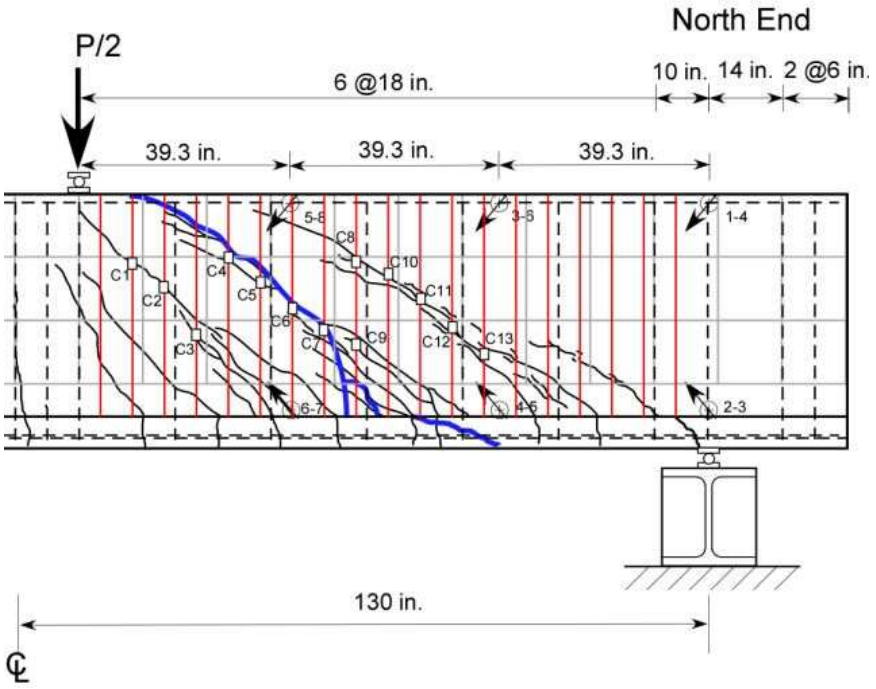

Fig. 12.11 – Specimen IT.7.18.6.S crack map (failure test)

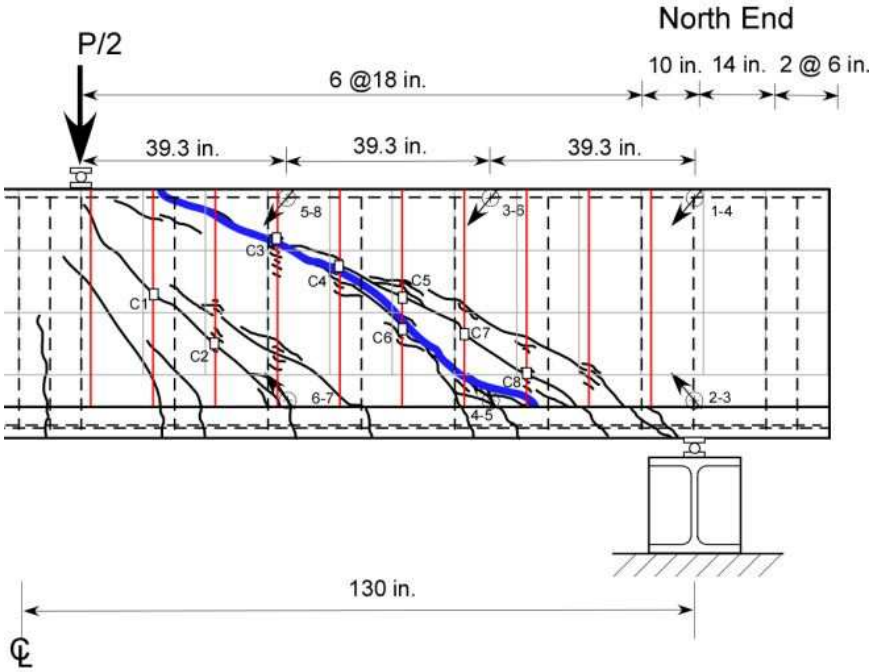

Fig. 12.12 – Specimen IT.7.18.12.S crack map (failure test)

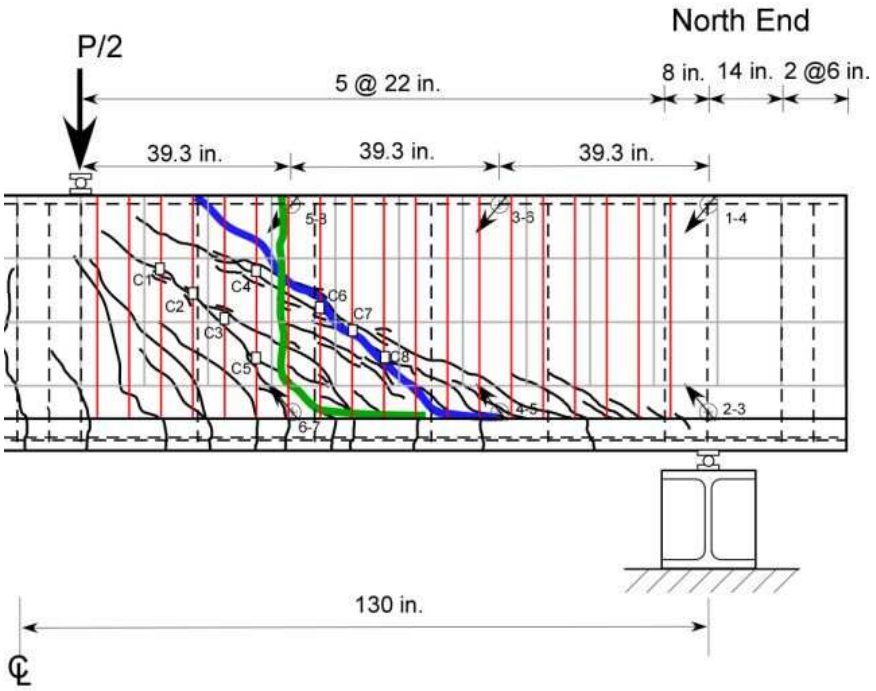

Fig. 12.13 – Specimen IT.7.22.6.S crack map (failure test)

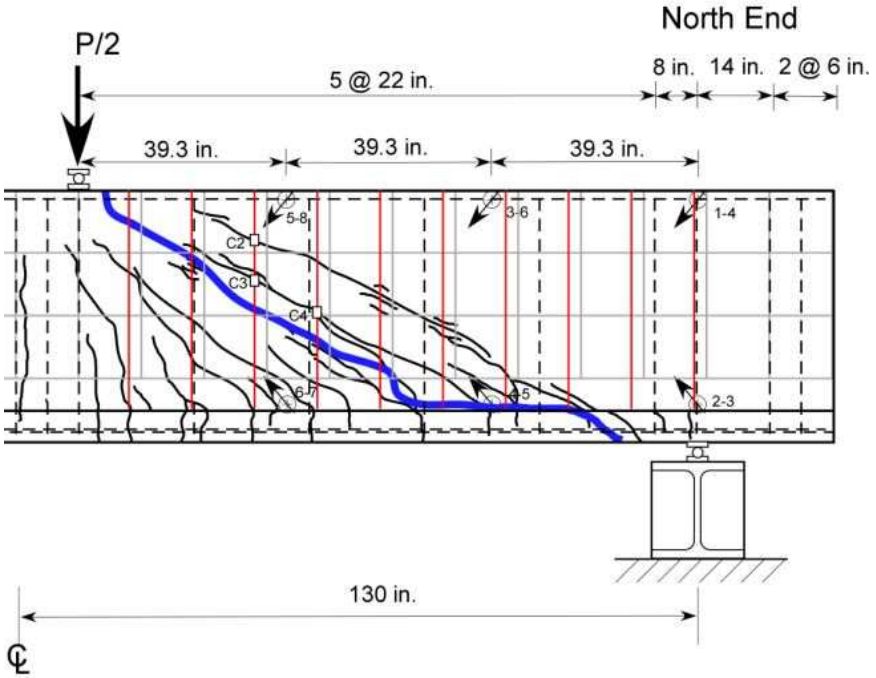

Fig. 12.14 – Specimen IT.5.22.12.S crack map (failure test)

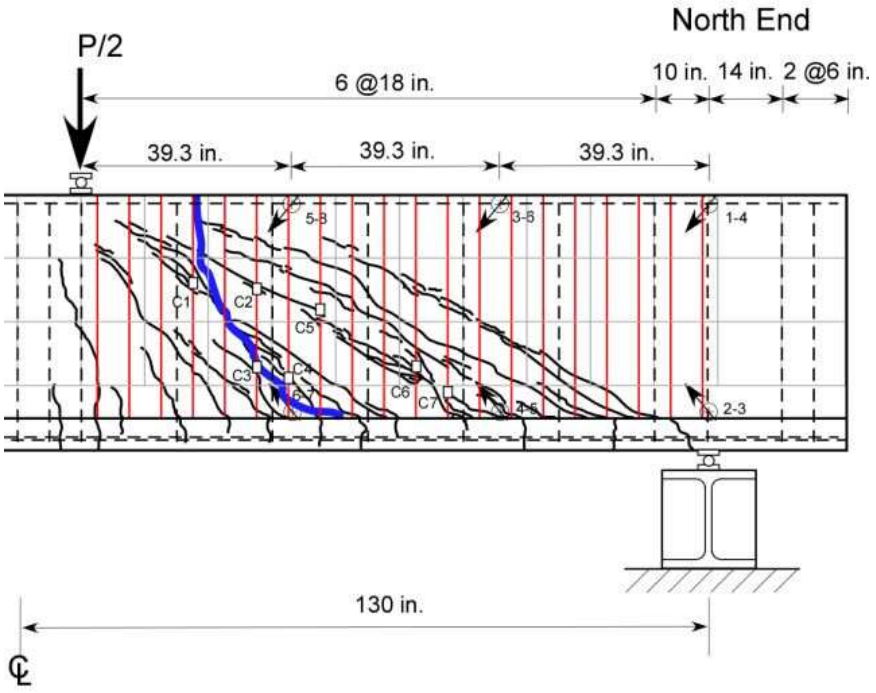

Fig. 12.15 – Specimen IT.7.18.6.M crack map (failure test)

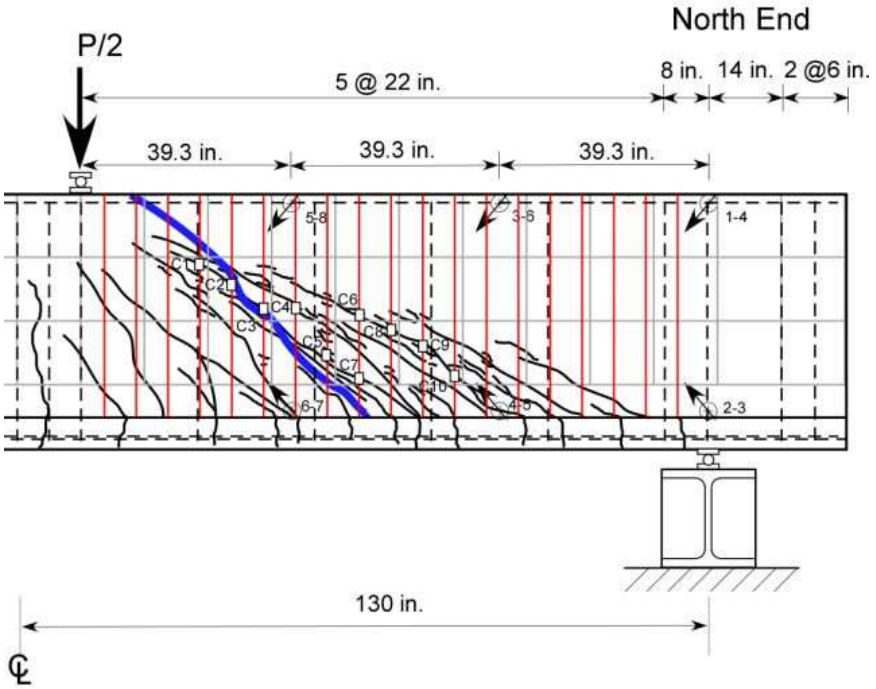

Fig. 12.16 – Specimen IT.7.18.6.FT crack map (failure test)

12.3 Appendix C – Beam Specimen Experimental Data

Appendix C describes the location of the sensors used during beam specimen testing. The instrumenting process is described in *Section 4.* Data from each instrument was collected at a rate of 4 Hz and plots of selected data are shown in this appendix.

12.3.1 Flexural Strain Gage Locations

Strain gages were attached to the flexural reinforcing bars at midspan. Three gages were placed on the IT-specimens and four on the T-specimens. The location and labeling of these sensors are shown below in Figure 12.17.

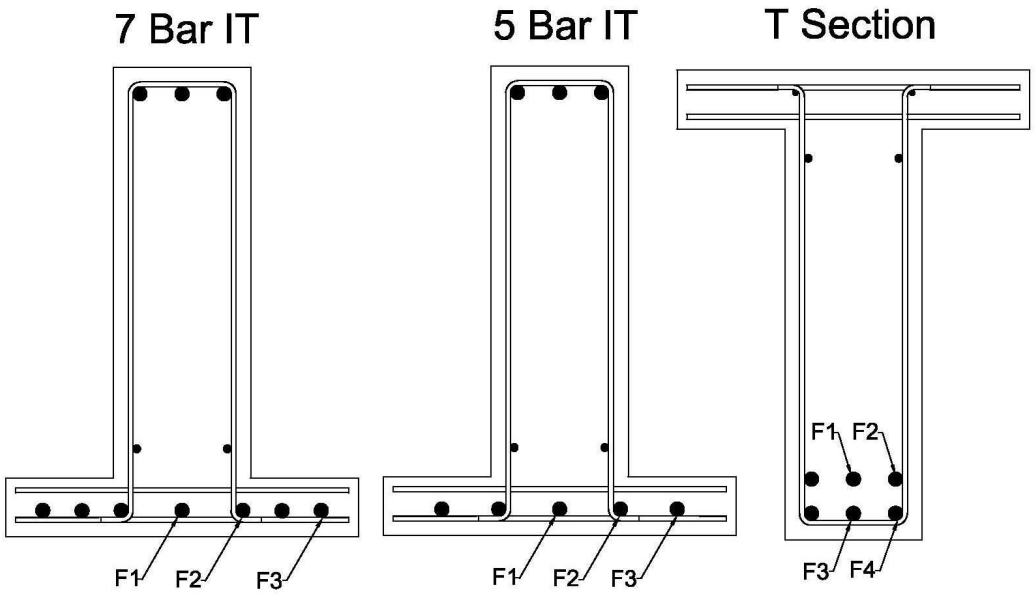

Fig. 12.17 – Flexural strain gage labeling and location

12.3.2 Stirrup Strain Gage Locations

Strain gages were attached at mid-height to the internal steel stirrups in the shear span on the north end of each specimen. Only the west leg of each stirrup was instrumented. These gages were labeled incrementally with "S1" being the closest to midspan.

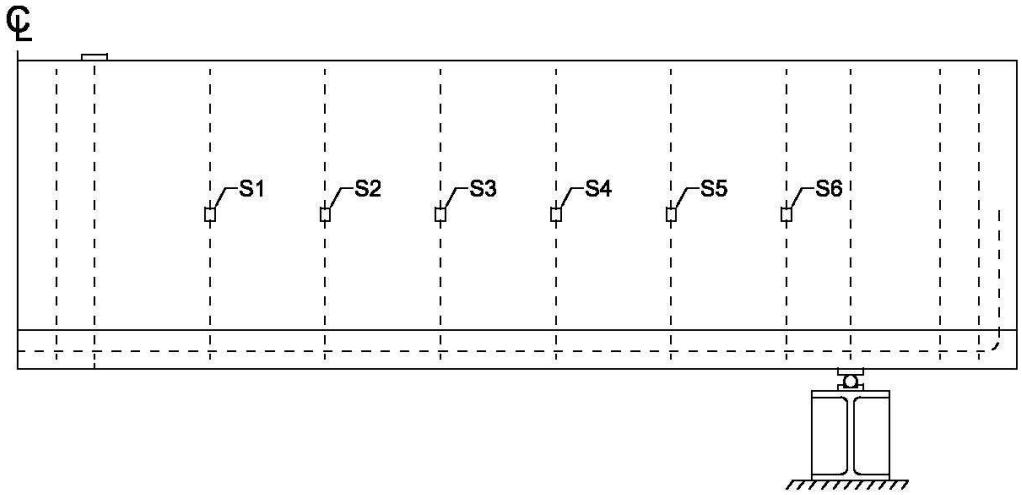

Fig. 12.18 – Stirrup strain gage labeling and location

12.3.3 CFRP Strain Gage Locations

Strain gages were attached to CFRP strips during retrofitting. They were located on dominate cracks after precracking. The gages were labeled incrementally with one being closest to midspan. The locations of the gages are shown in *Appendix A* on the retrofit crack maps.

12.3.4 Midspan Displacements

A 127 mm (5 in.) string potentiometer was placed on both the east and sest sides of each specimen to measure midspan displacement. This was done by attaching the sensor's string to a small steel rod that was epoxied into a hole at midspan near the bottom of each specimen. The actual midspan displacement was calculated by taking the average of these

two midspan displacements and subtracting the average support displacements. Removing the support displacement leaves only the vertical displacement produced by the specimen's bending.

12.3.5 Support Displacements

Four displacement sensors were used to measure the displacement of the specimen at the support locations. A small square of aluminum was glued to the beam directly above the support on the NE, NW, SE, and SW corners. A displacement sensor pushed on this piece of aluminum measured the vertical displacement. Not all researchers account for support displacement, but it is clearly a large enough factor to consider. The data in the plots below shows that support displacements frequently surpass 0.25 mm (0.1 in.), which is a significant at around 10% of the overall displacement measured.

In some tests a support sensor slipped off of the piece of aluminum or was bumped during testing. When this occurred the bad data was removed and an estimate was made by assuming the support displacement was a ratio of the other sensor on the same end of the specimen. An example of this is shown below in Figure 12.19 with the SE sensor.

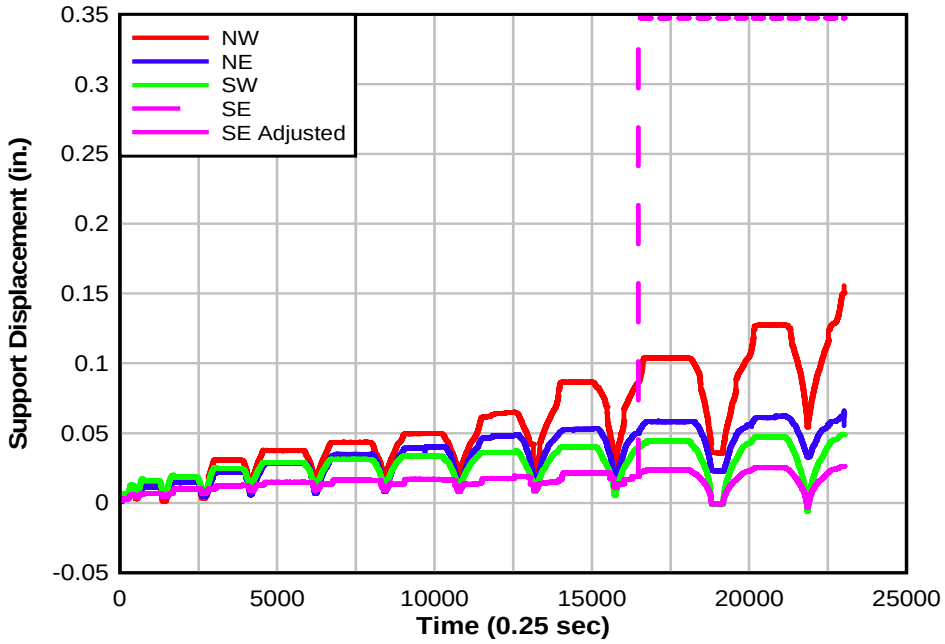

Fig. 12.19 – Specimen IT.7.18.6.M support displacements vs. time (failure test)

12.3.6 Diagonal Displacements

Six 51 mm (2 in.) string potentiometers were used to measure the diagonal displacement over three regions of each specimen. The sensors were anchored to the beam with a threaded rod, and a brass wire attached the sensor's string to a second anchor point. The sensors were named for the two anchor points they were connected to. For example, sensor "3-5" was located at anchor point 3 and connected to anchor point 5. The diagonal sensor locations are shown below in Figure 12.20.

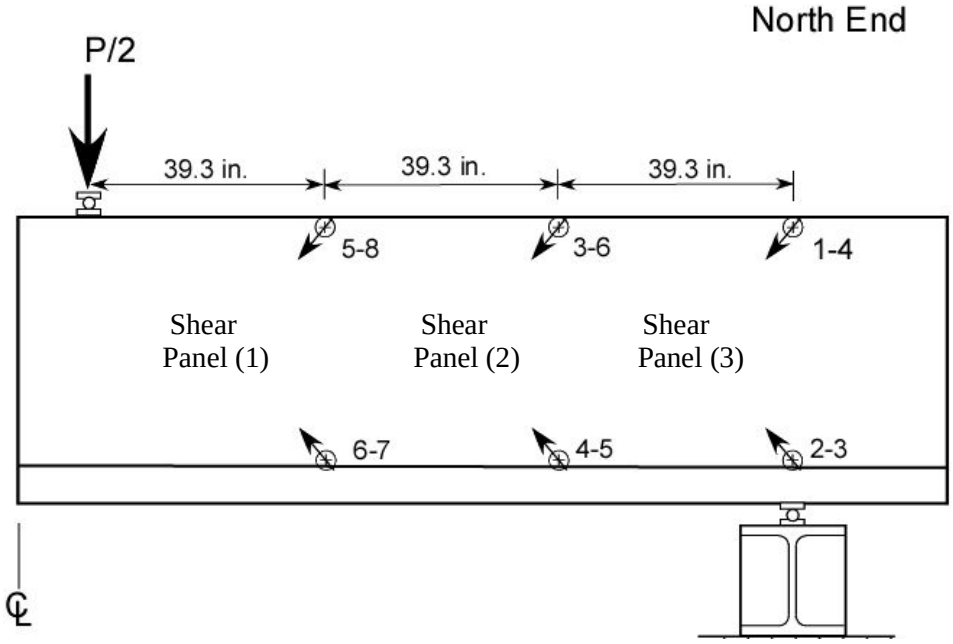

Fig. 12.20 – Diagonal sensor location and labeling

12.3.7 Graphs of Data

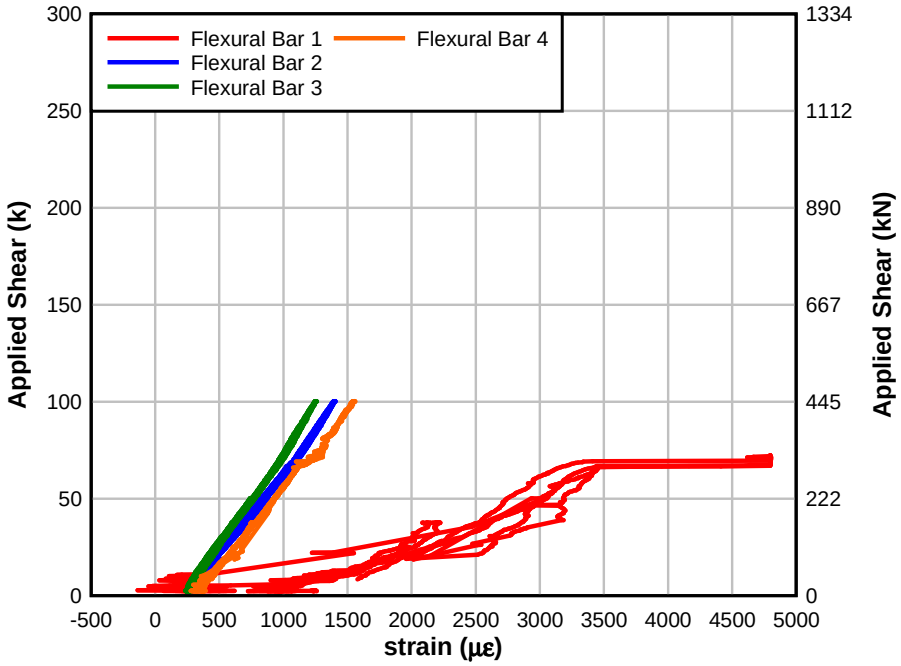

Fig. 12.21 – Specimen T.6.18.6.S applied shear vs. flexural bar strain (baseline test)

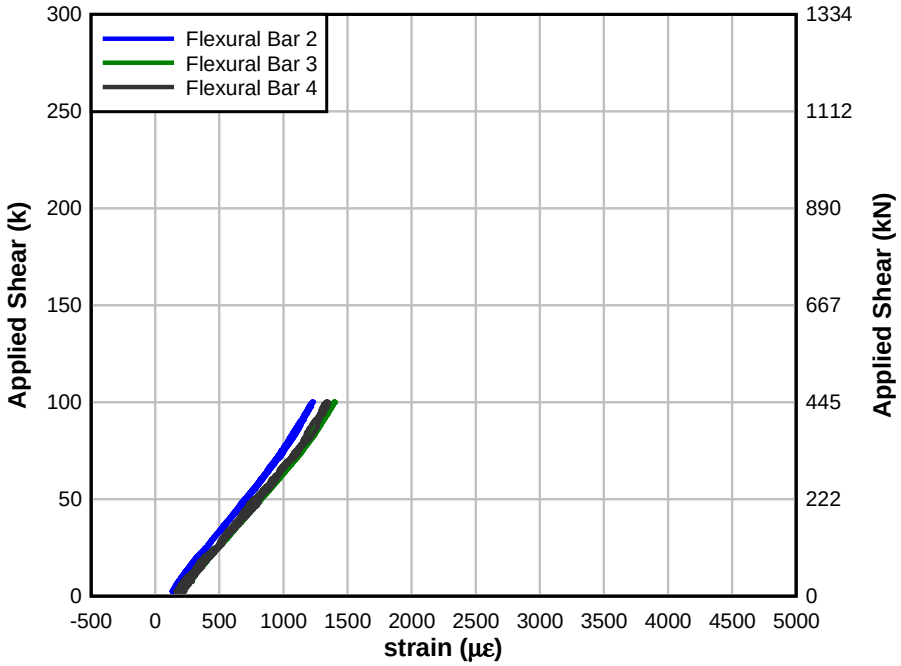

Fig. 12.22 – Specimen T.6.18.12.S applied shear vs. flexural bar strain (baseline test)

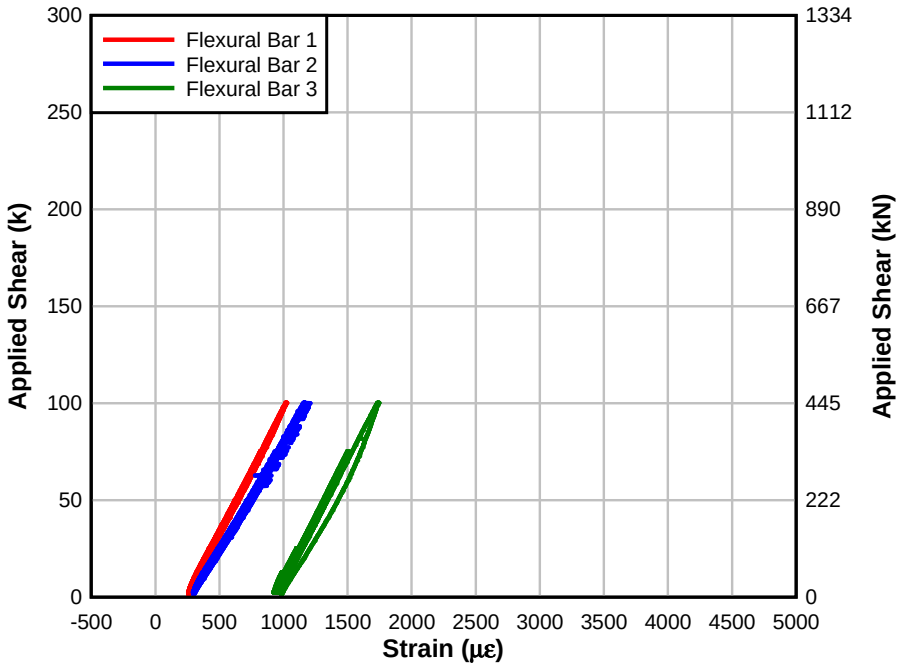

Fig. 12.23 – Specimen IT.7.18.6.S applied shear vs. flexural bar strain (baseline test)

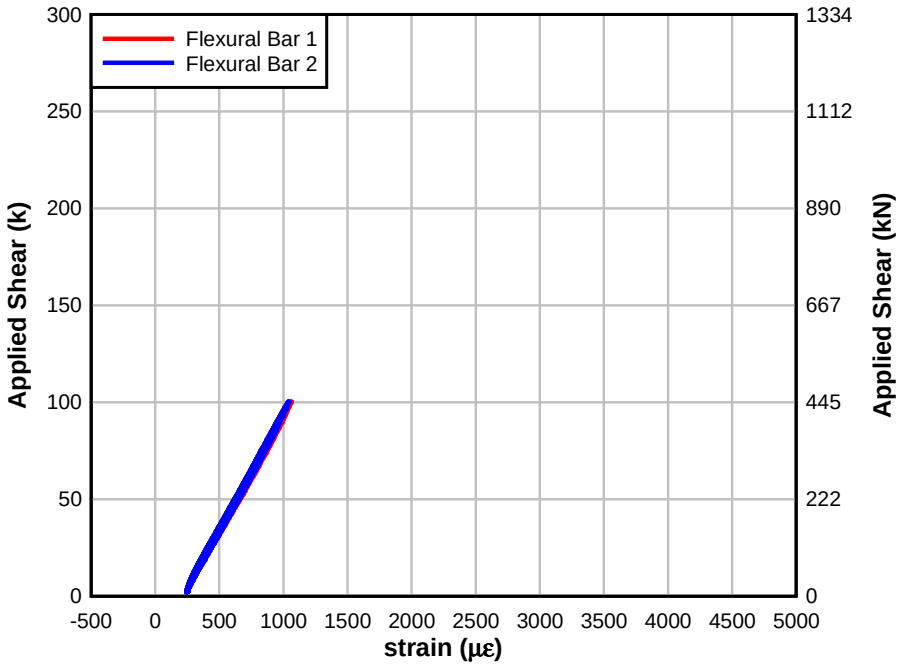

Fig. 12.24 – Specimen IT.7.18.12.S applied shear vs. flexural bar strain (baseline test)

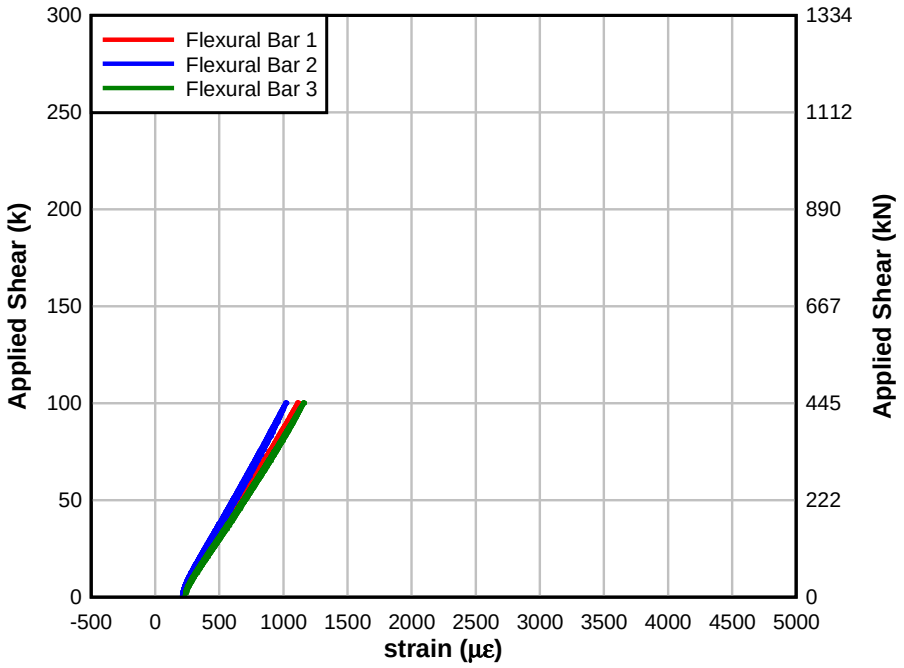

Fig. 12.25 – Specimen IT.7.22.6.S applied shear vs. flexural bar strain (baseline test)

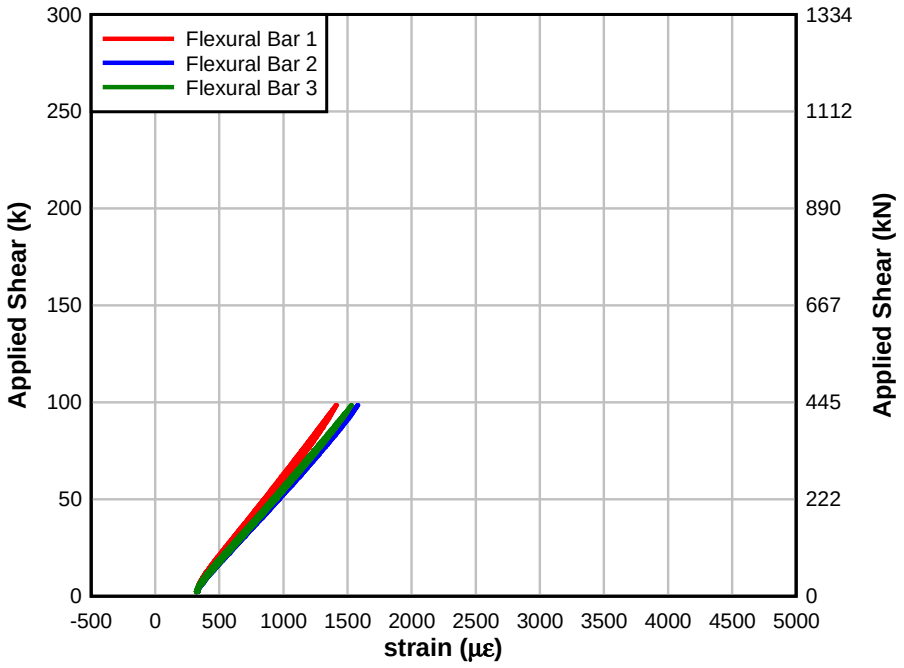

Fig. 12.26 – Specimen IT.5.22.12.S applied shear vs. flexural bar strain (baseline test)

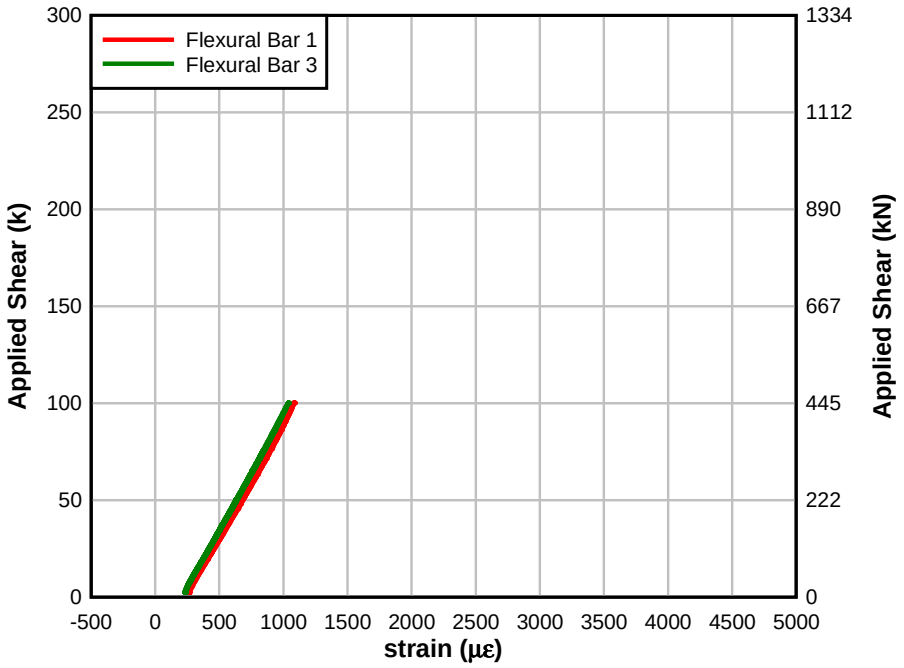

Fig. 12.27 – Specimen IT.7.18.6.M applied shear vs. flexural bar strain (baseline test)

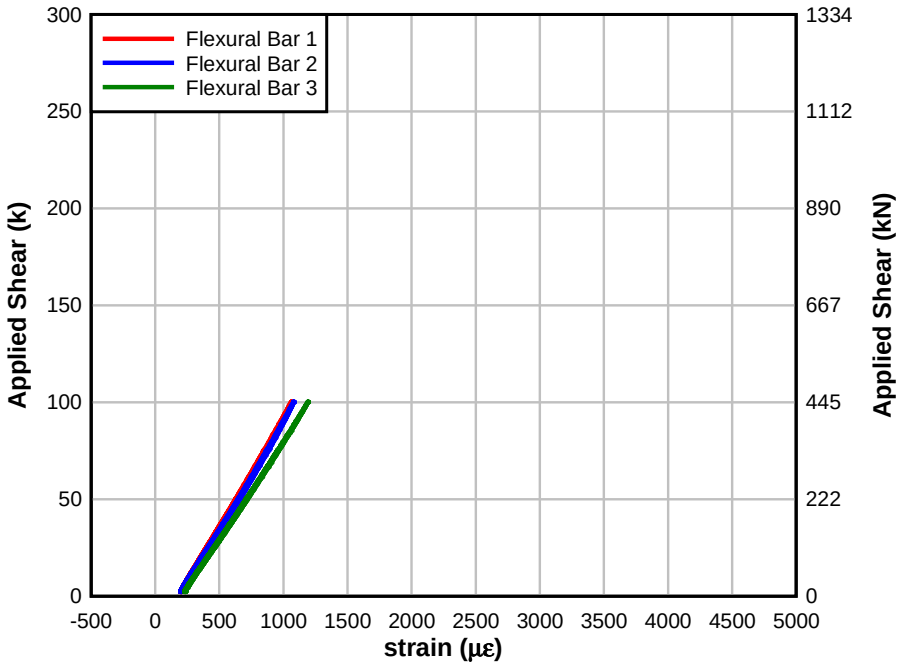

Fig. 12.28 – Specimen IT.7.22.6.FT applied shear vs. flexural bar strain (baseline test)

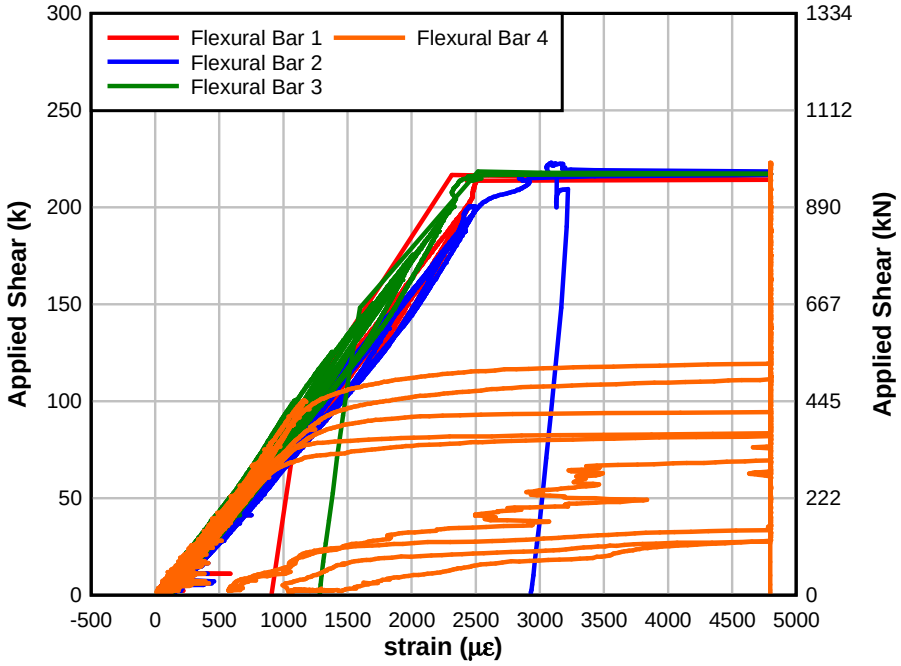

Fig. 12.29 – Specimen T.6.18.6.S applied shear vs. flexural bar strain (failure test)

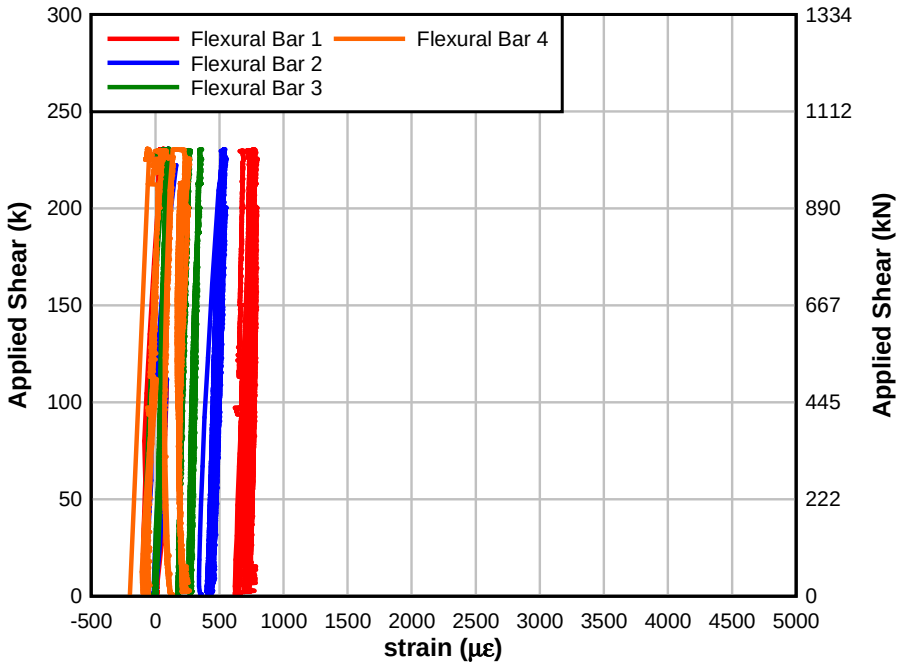

Fig. 12.30 – Specimen T.6.18.12.S applied shear vs. flexural bar strain (failure test)

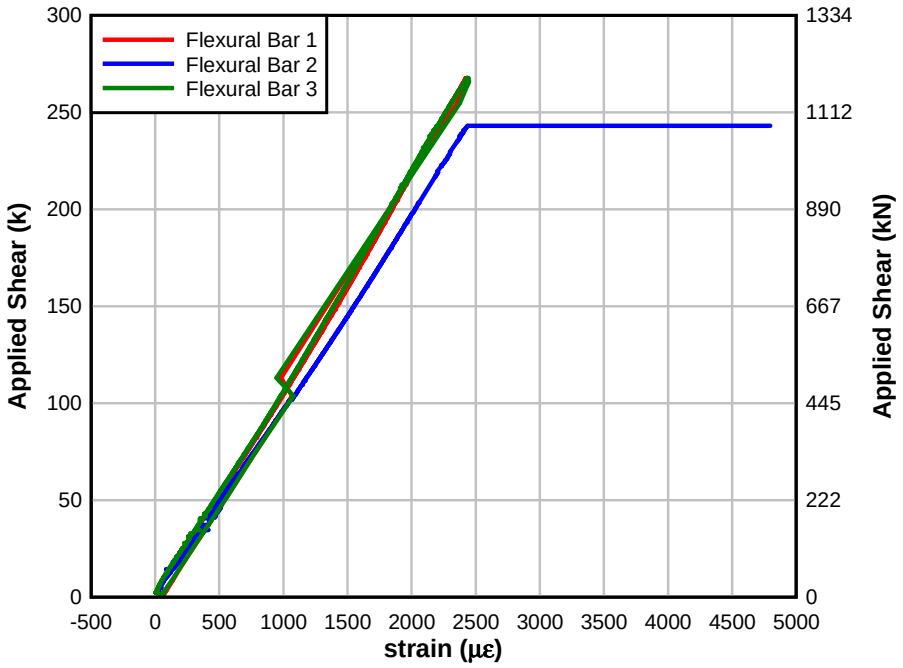

Fig. 12.31 – Specimen IT.7.18.6.S applied shear vs. flexural bar strain (failure test)

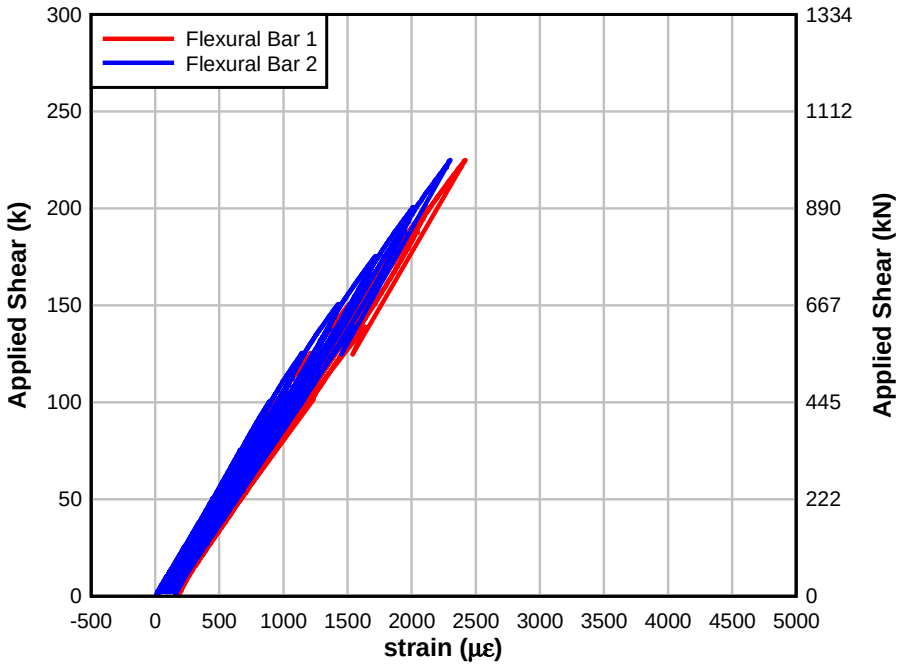

Fig. 12.32 – Specimen IT.7.18.12.S applied shear vs. flexural bar strain (failure test)

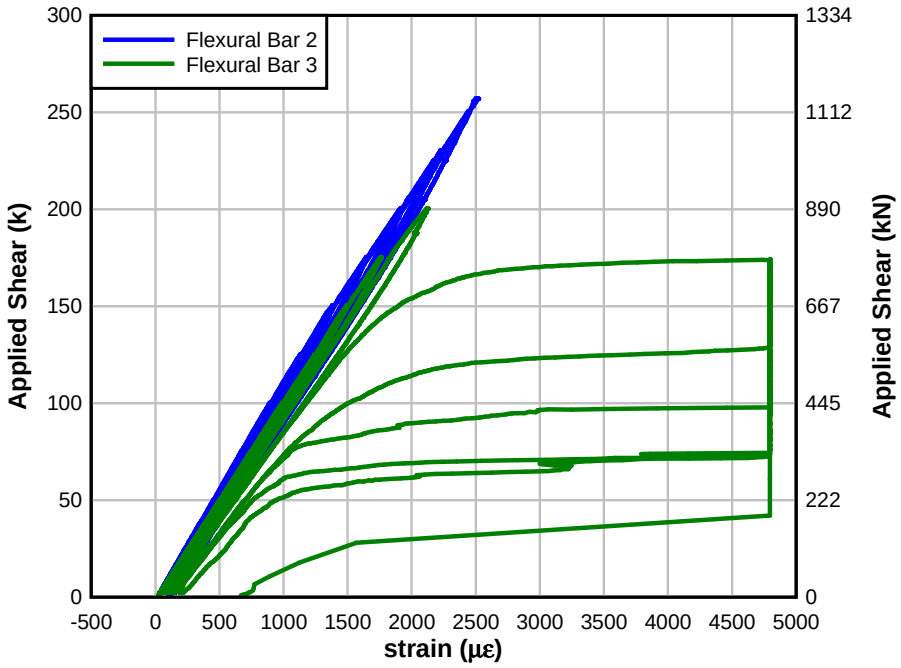

Fig. 12.33 – Specimen IT.7.22.6.S applied shear vs. flexural bar strain (failure test)

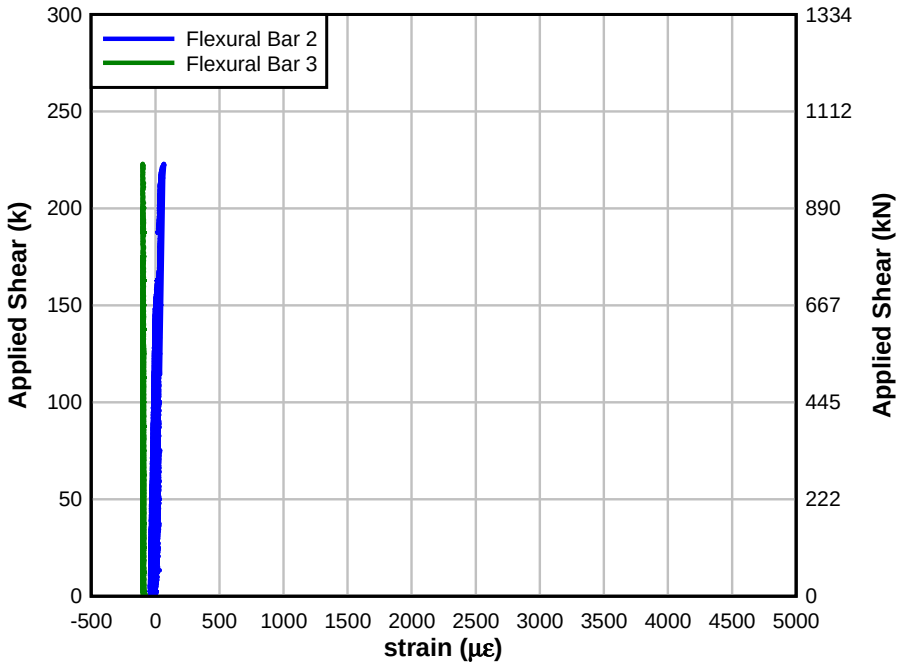

Fig. 12.34 – Specimen IT.5.22.12.S applied shear vs. flexural bar strain (failure test)

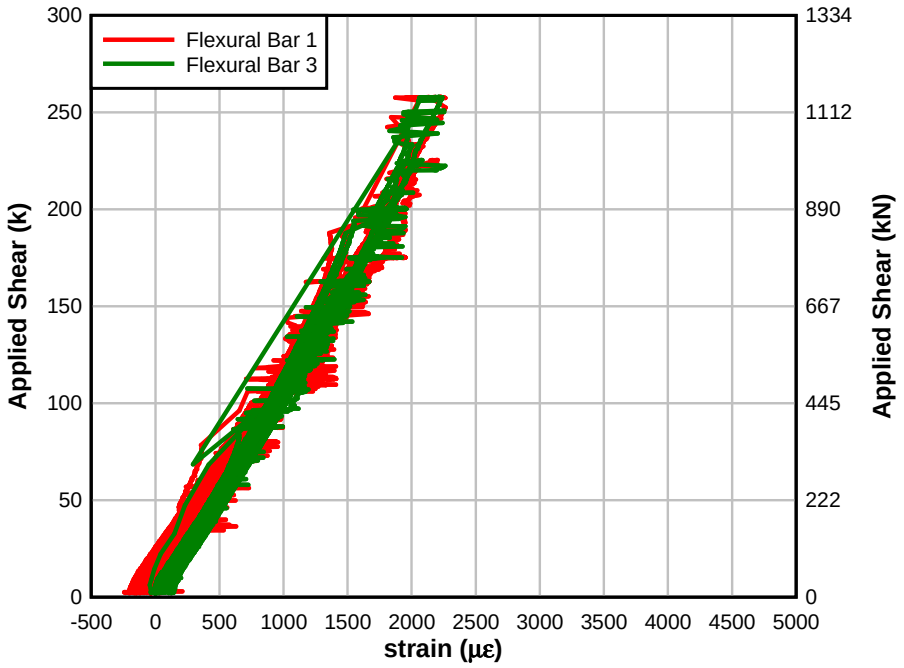

Fig. 12.35 – Specimen IT.7.18.6.M applied shear vs. flexural bar strain (failure test)

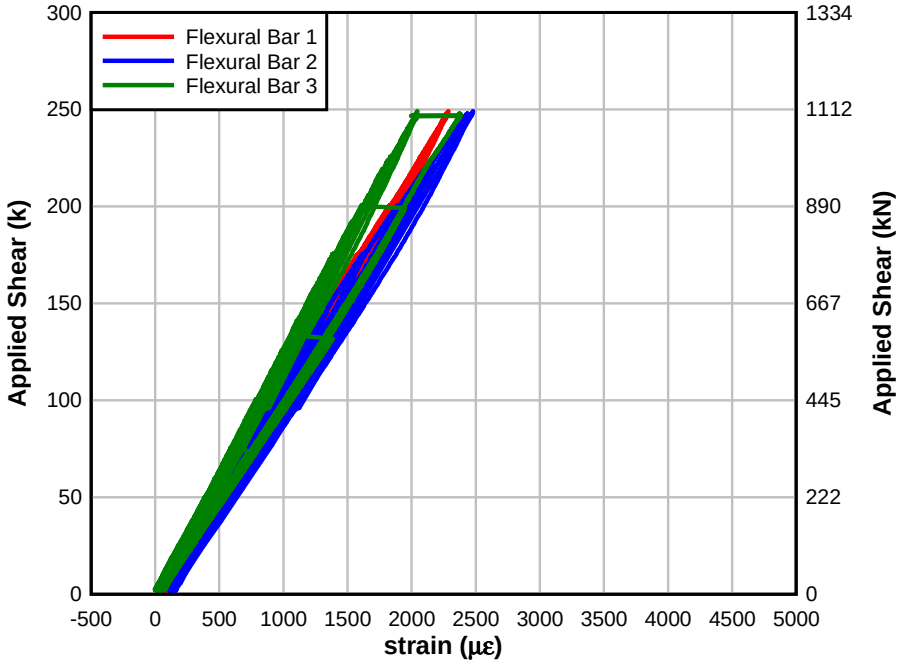

Fig. 12.36 – Specimen IT.7.22.6.FT applied shear vs. flexural bar strain (failure test)

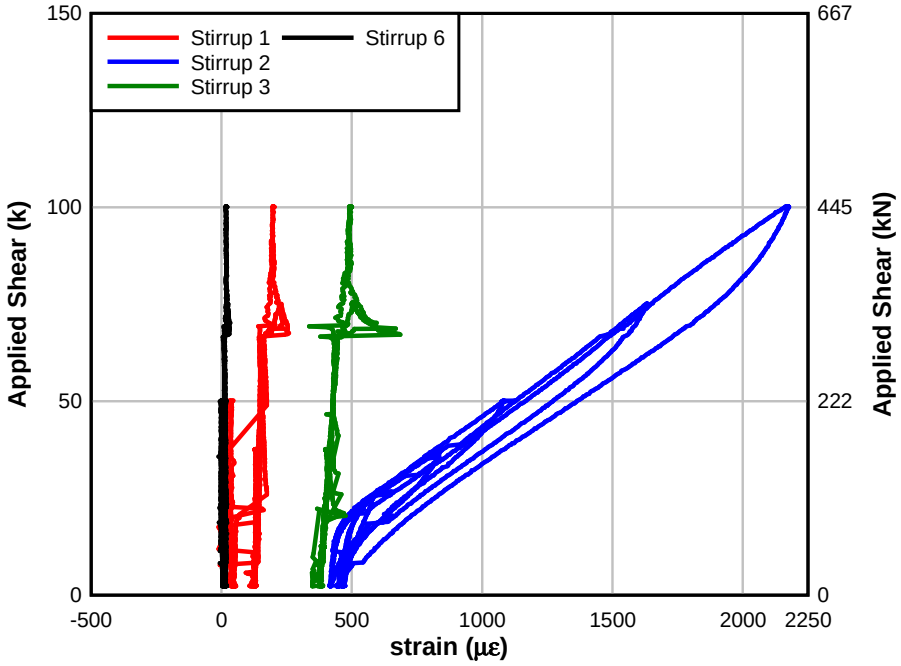

Fig. 12.37 – Specimen T.6.18.6.S applied shear vs. stirrup strain (baseline test)

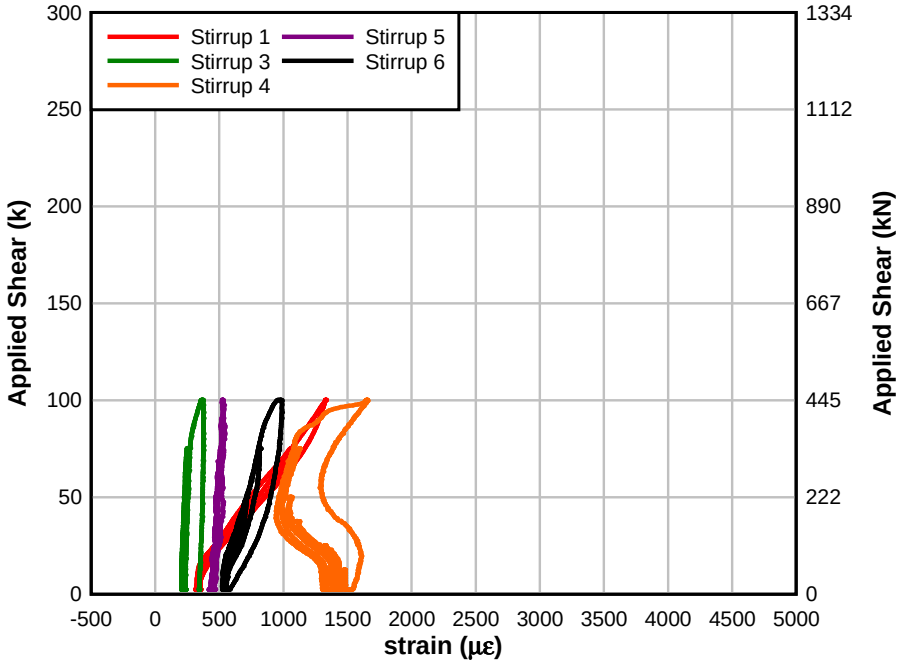

Fig. 12.38 – Specimen T.6.18.12.S applied shear vs. stirrup strain (baseline test)

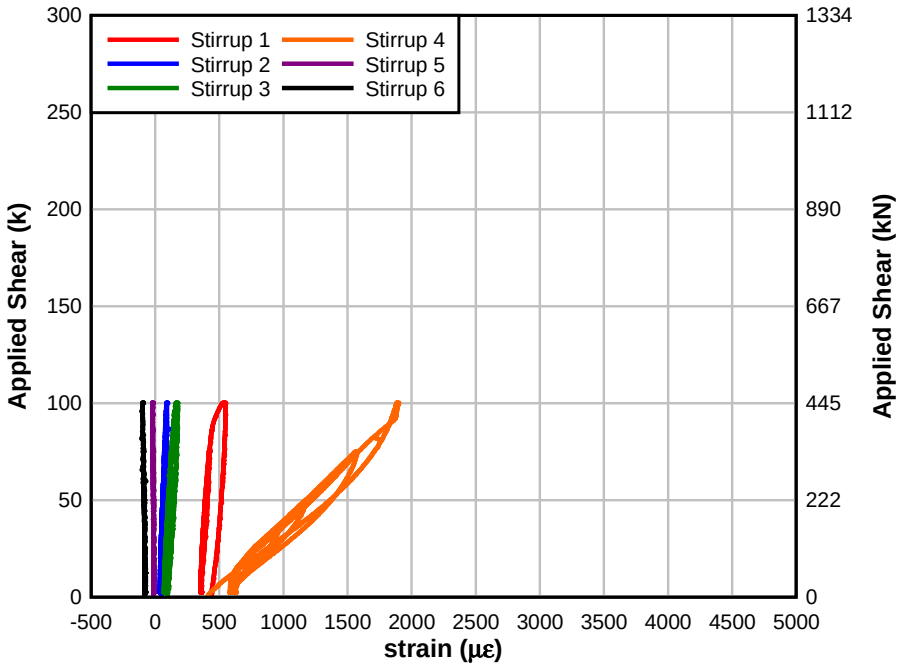

Fig. 12.39 – Specimen IT.7.18.6.S applied shear vs. stirrup strain (baseline test)

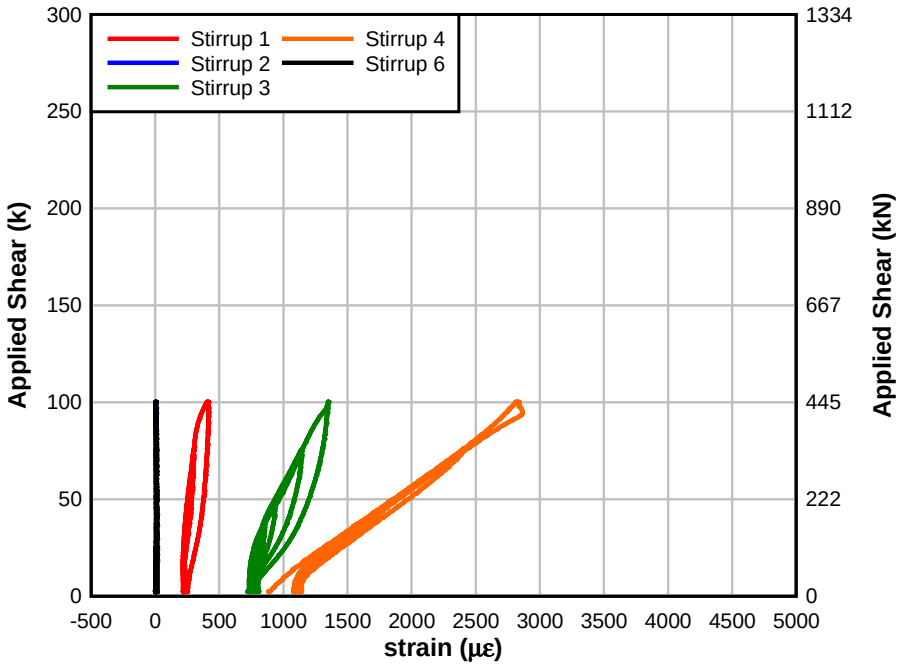

Fig. 12.40 – Specimen IT.7.18.12.S applied shear vs. stirrup strain (baseline test)

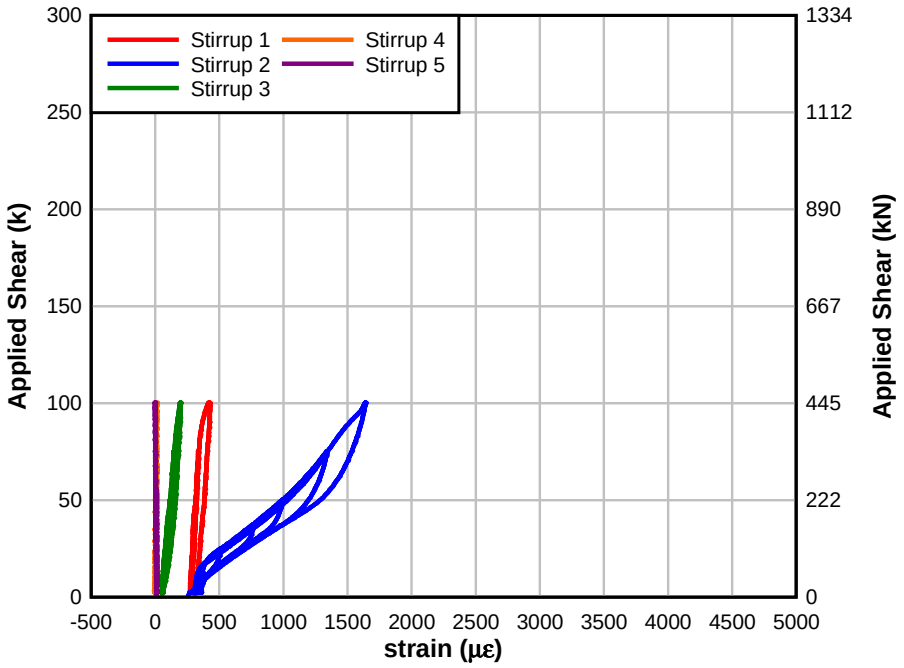

Fig. 12.41 – Specimen IT.7.22.6.S applied shear vs. stirrup strain (baseline test)

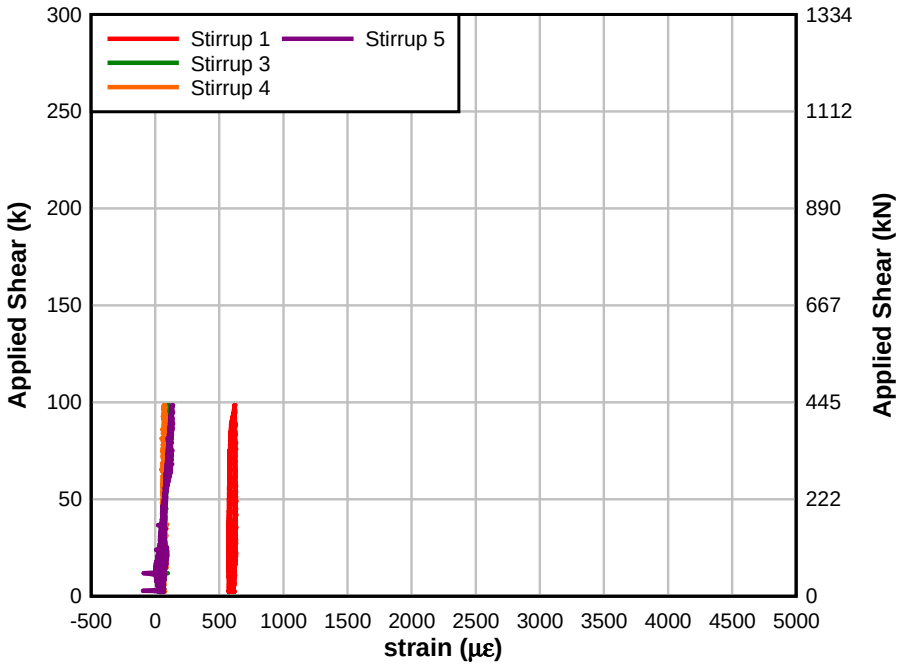

Fig. 12.42 – Specimen IT.5.22.12.S applied shear vs. stirrup strain (baseline test)

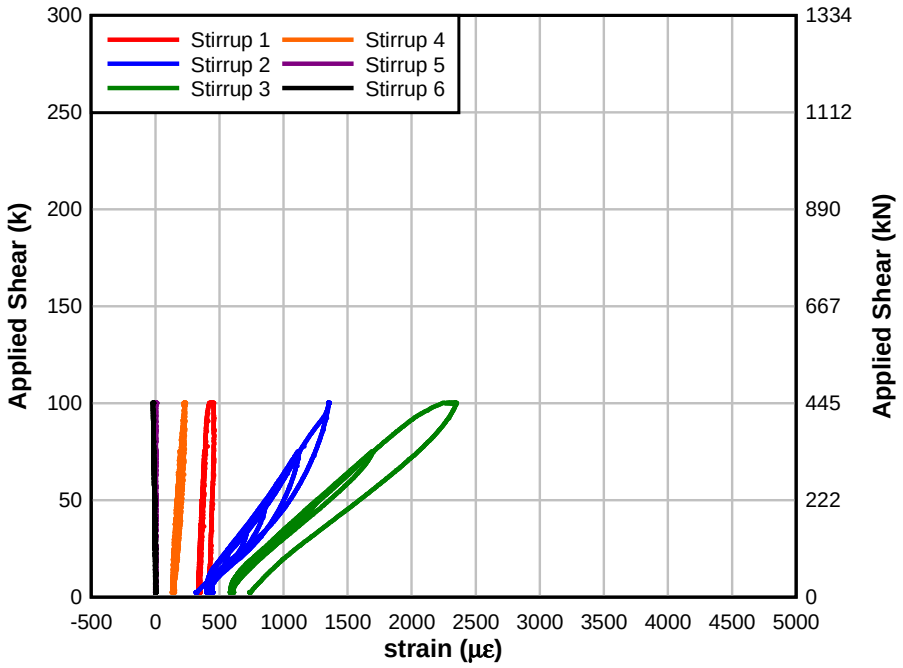

Fig. 12.43 – Specimen IT.7.18.6.M applied shear vs. stirrup strain (baseline test)

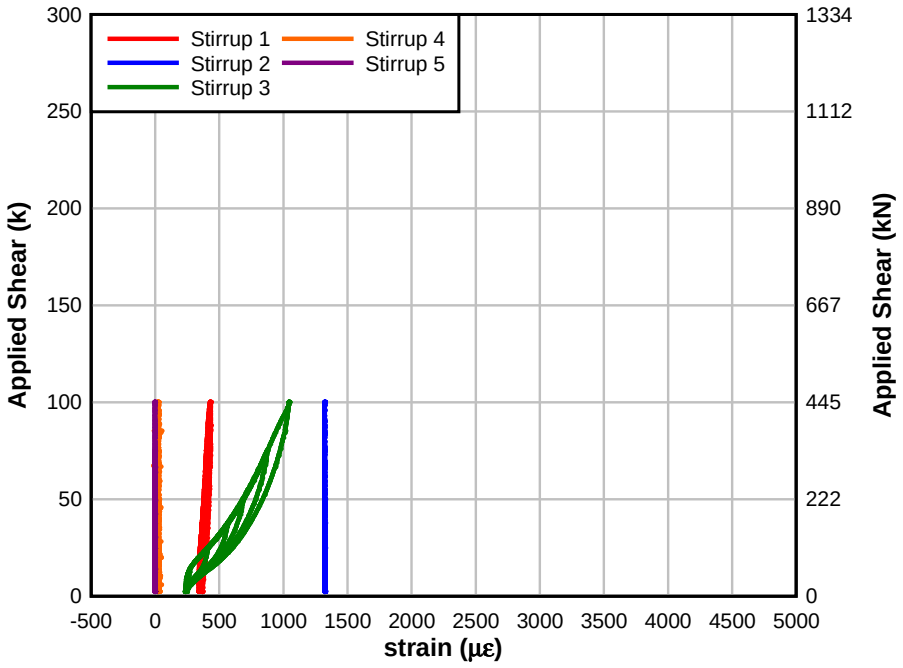

Fig. 12.44 – Specimen IT.7.18.6.FT applied shear vs. stirrup strain (baseline test)

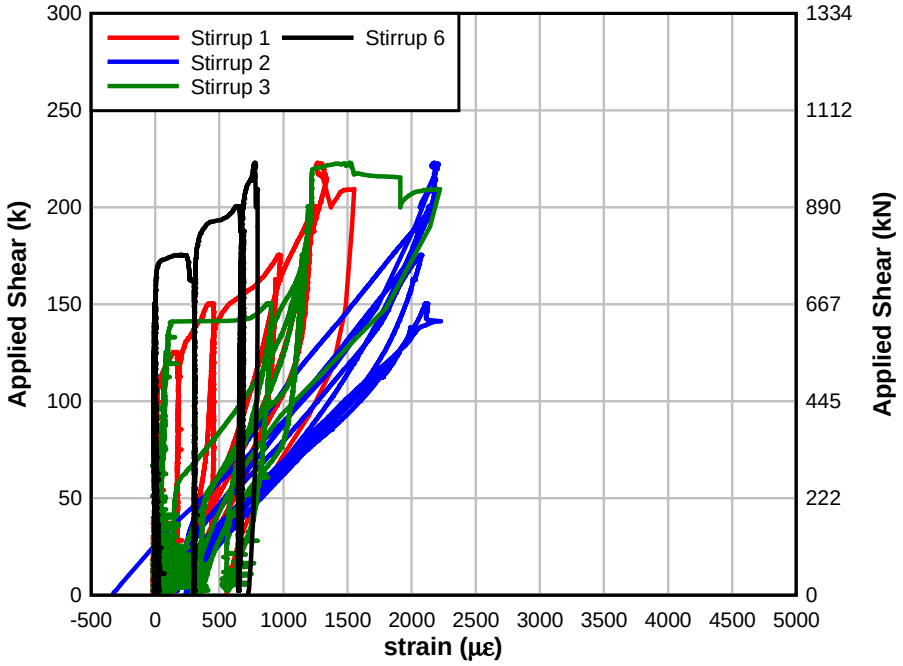

Fig. 12.45 – Specimen T.6.18.6.S applied shear vs. stirrup strain (failure test)

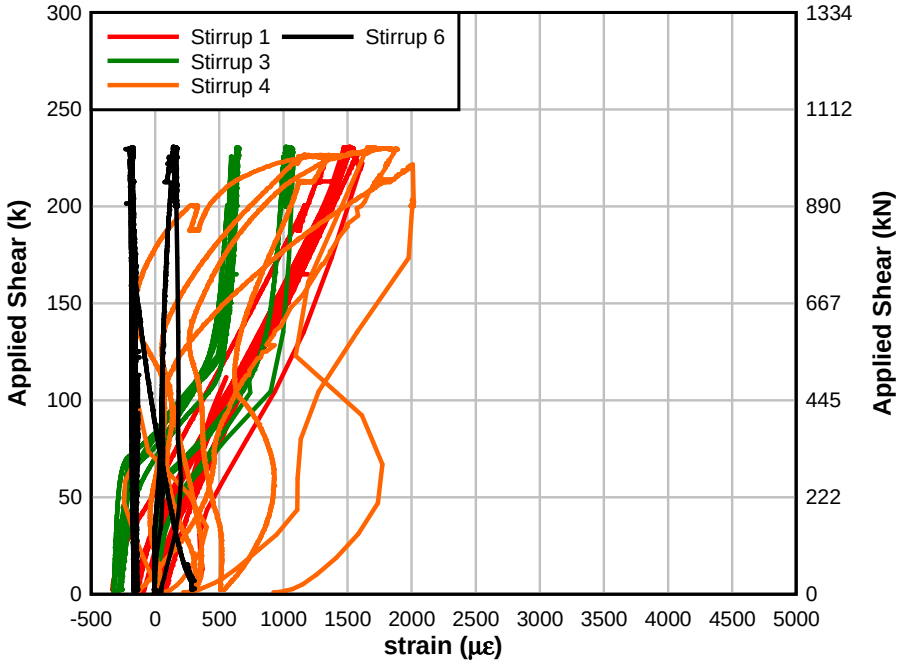

Fig. 12.46 – Specimen T.6.18.12.S applied shear vs. stirrup strain (failure test)

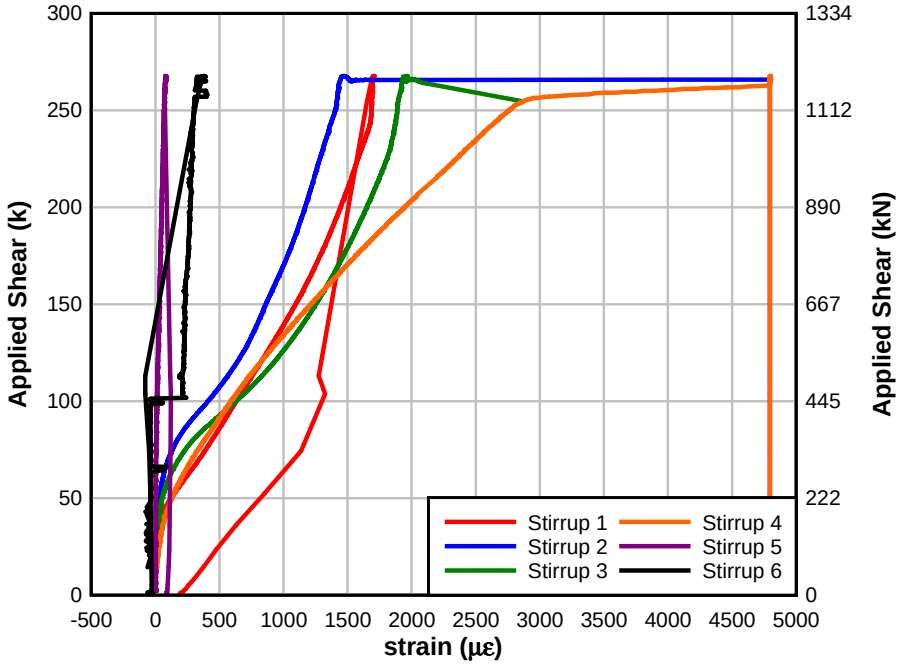

Fig. 12.47 – Specimen IT.7.18.6.S applied shear vs. stirrup strain (failure test)

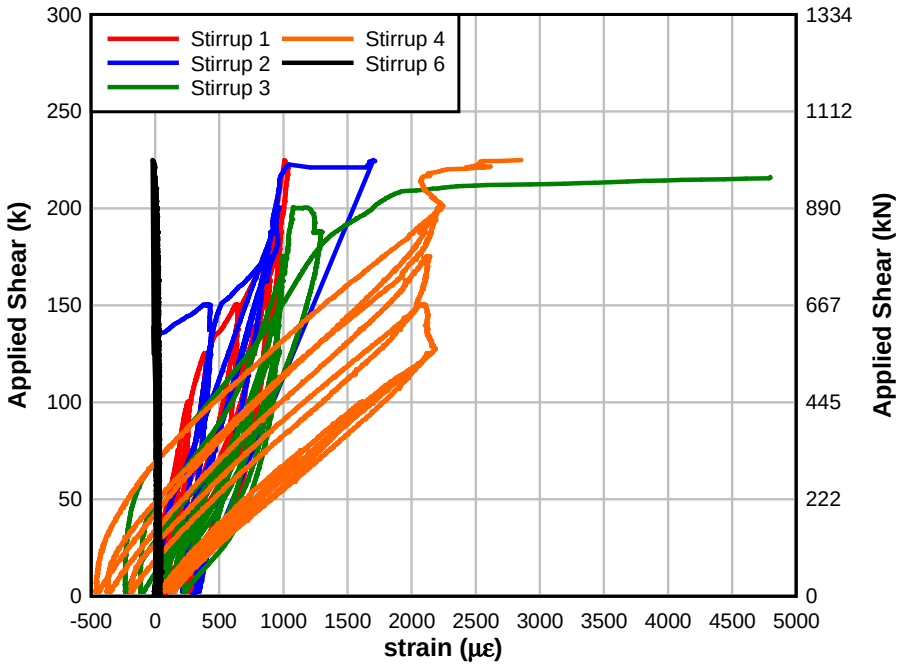

Fig. 12.48 – Specimen IT.7.18.12.S applied shear vs. stirrup strain (failure test)

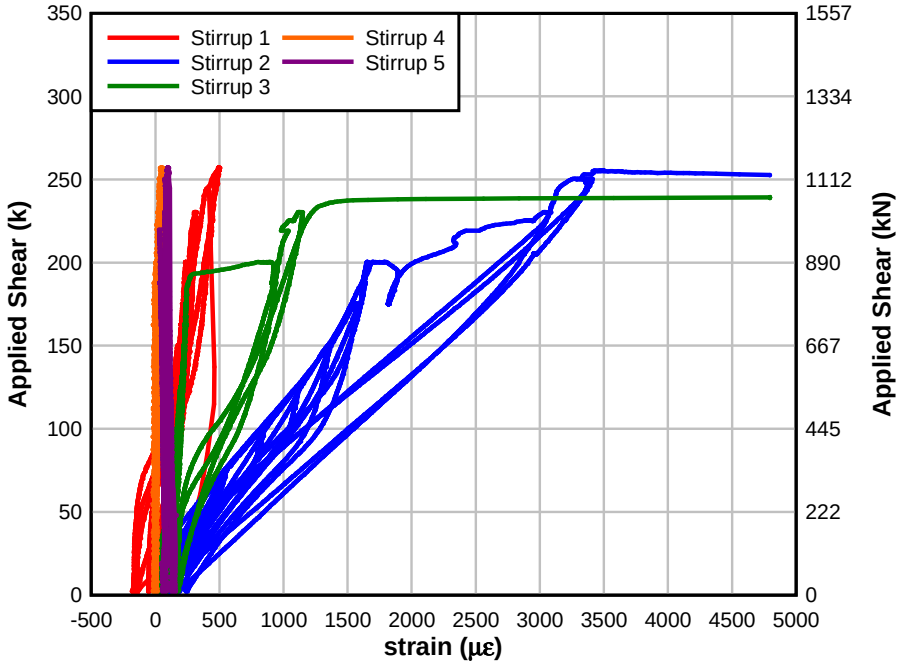

Fig. 12.49 – Specimen IT.7.22.6.S applied shear vs. stirrup strain (failure test)

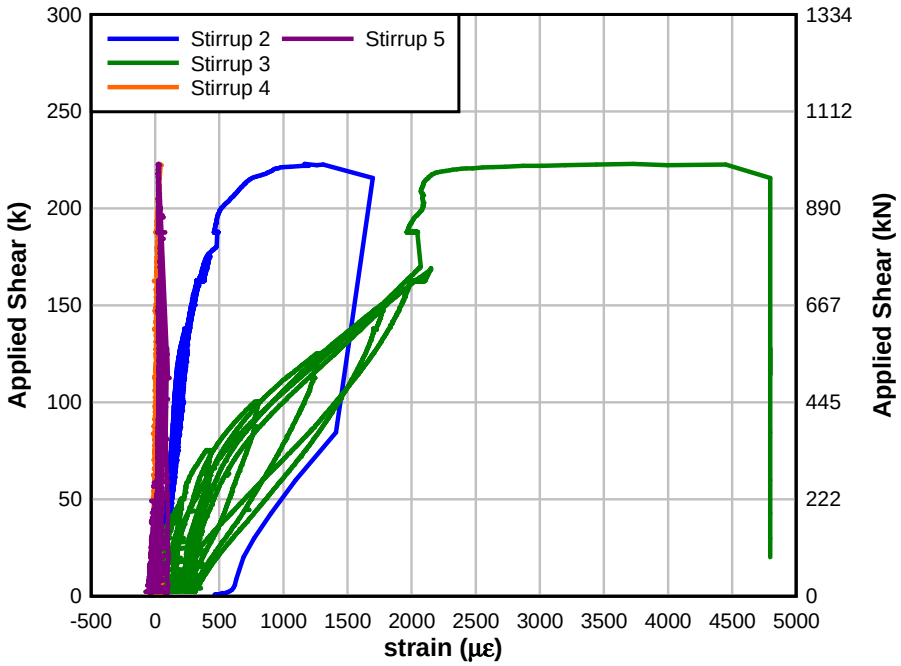

Fig. 12.50 – Specimen IT.5.22.12.S applied shear vs. stirrup strain (failure test)

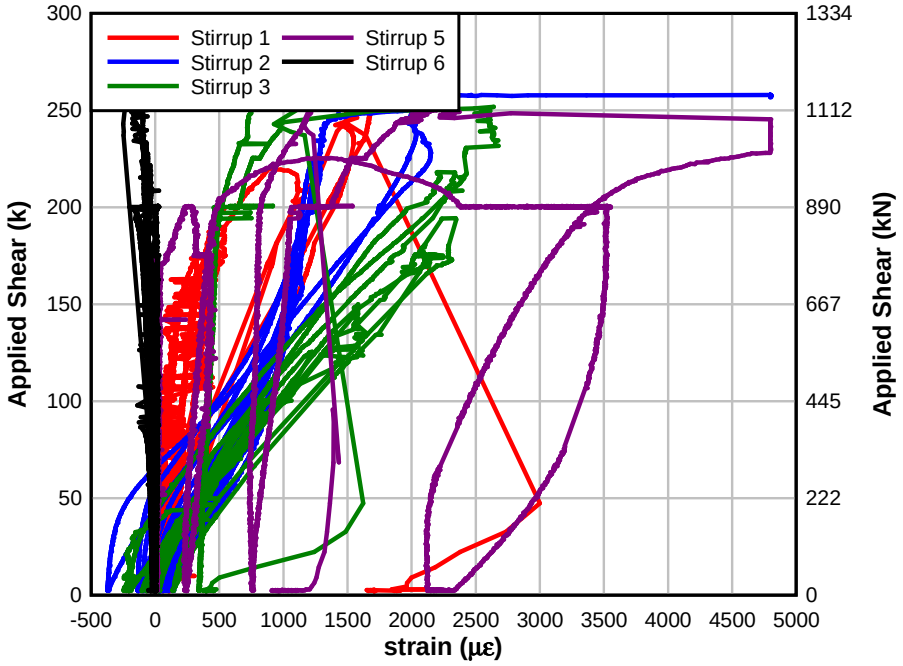

Fig. 12.51 – Specimen IT.7.18.6.M applied shear vs. stirrup strain (failure test)

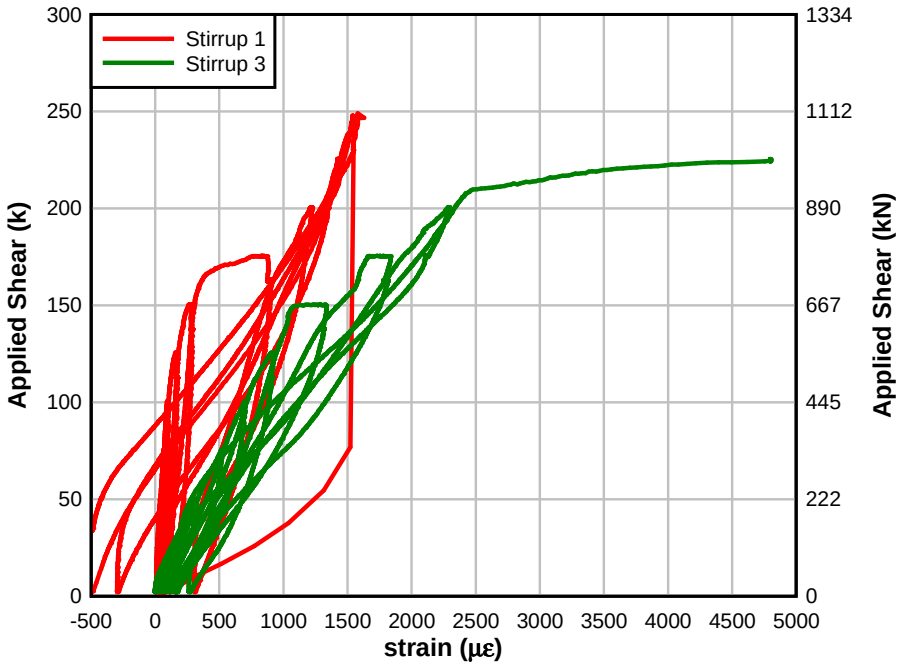

Fig. 12.52 – Specimen IT.7.22.6.FT applied shear vs. stirrup strain (failure test)

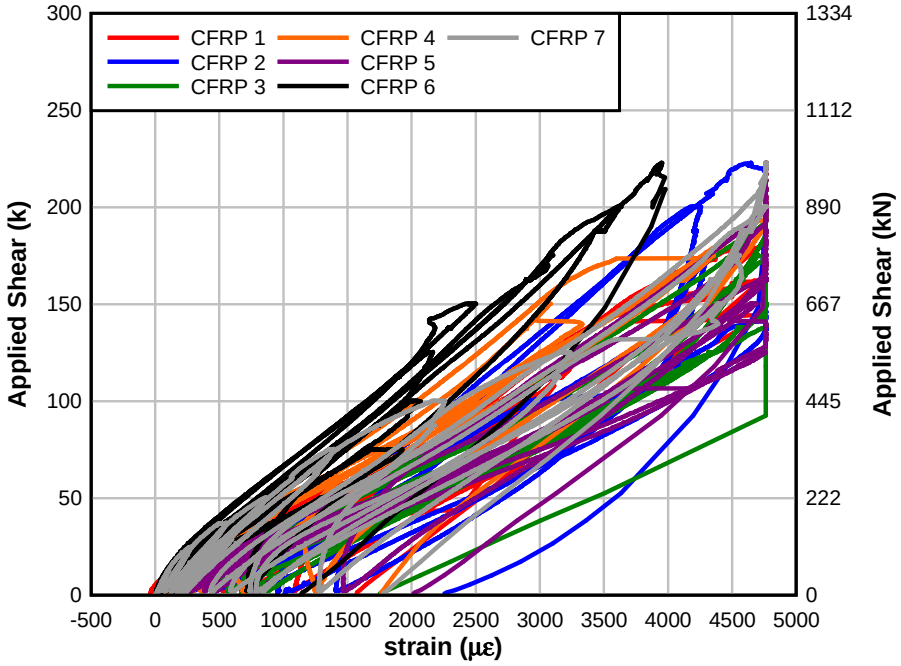

Fig. 12.53 – Specimen T.6.18.6.S applied shear vs. CFRP strain (failure test)

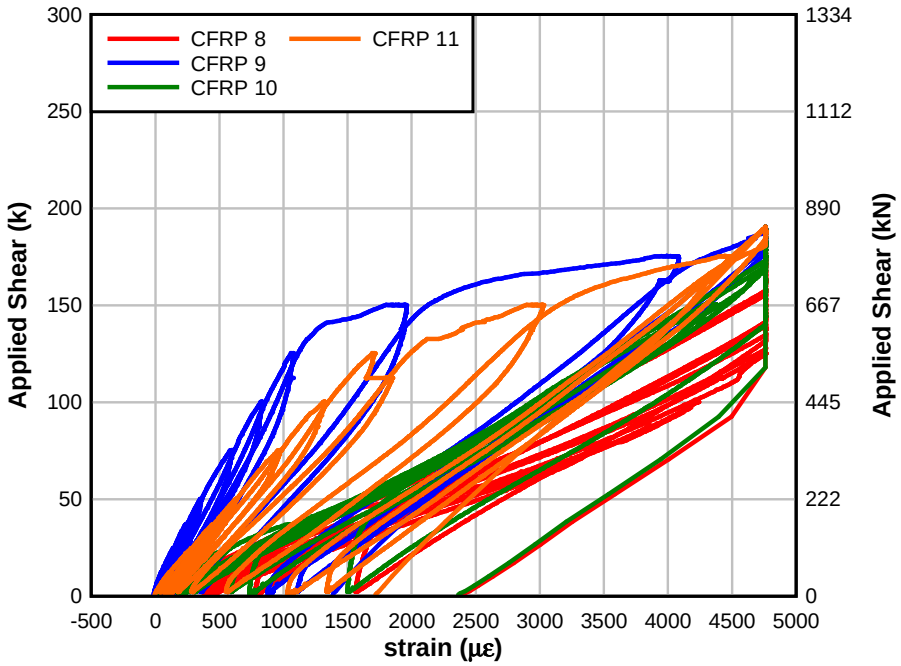

Fig. 12.54 – Specimen T.6.18.6.S applied shear vs. CFRP strain (failure test)

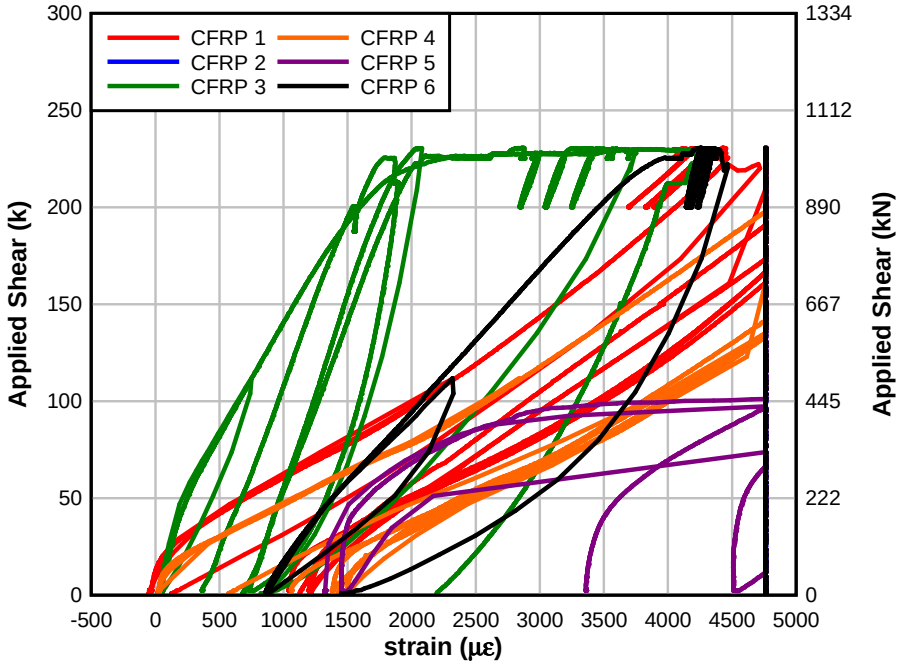

Fig. 12.55 – Specimen T.6.18.12.S applied shear vs. CFRP strain (failure test)

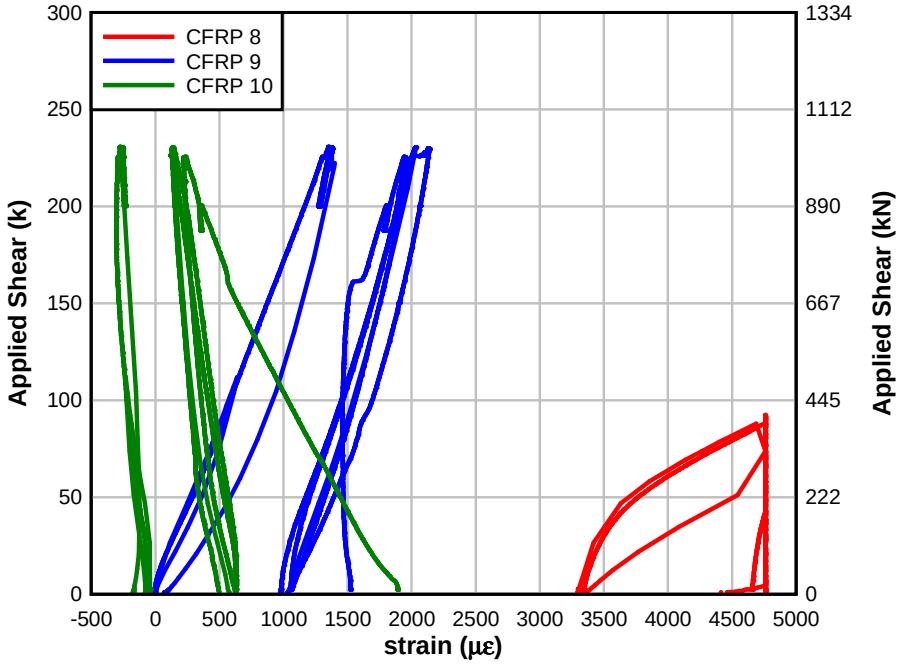

Fig. 12.56 – Specimen T.6.18.12.S applied shear vs. CFRP strain (failure test)

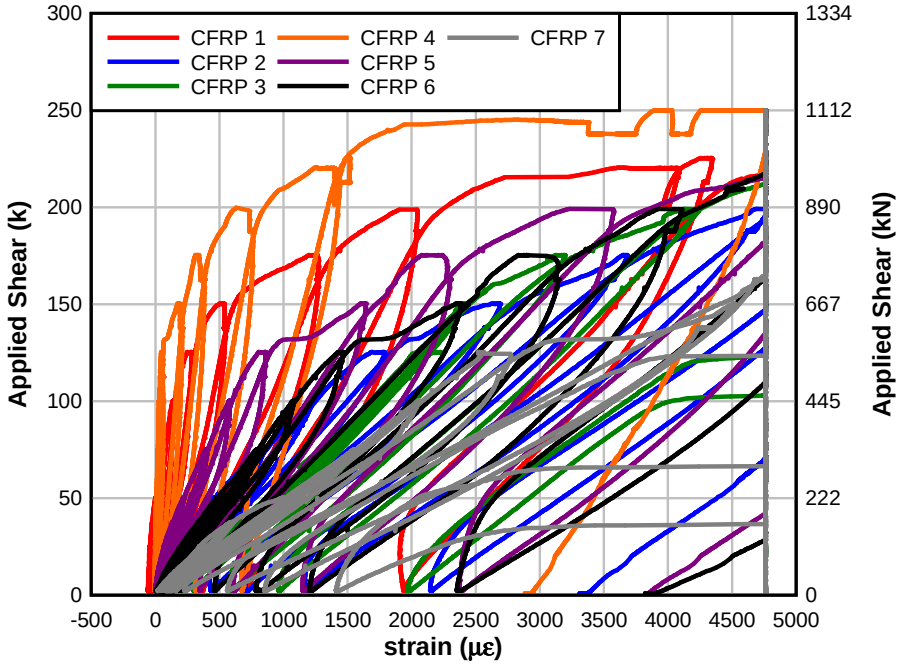

Fig. 12.57 – Specimen IT.7.18.6.S applied shear vs. CFRP strain (tested to 500K)

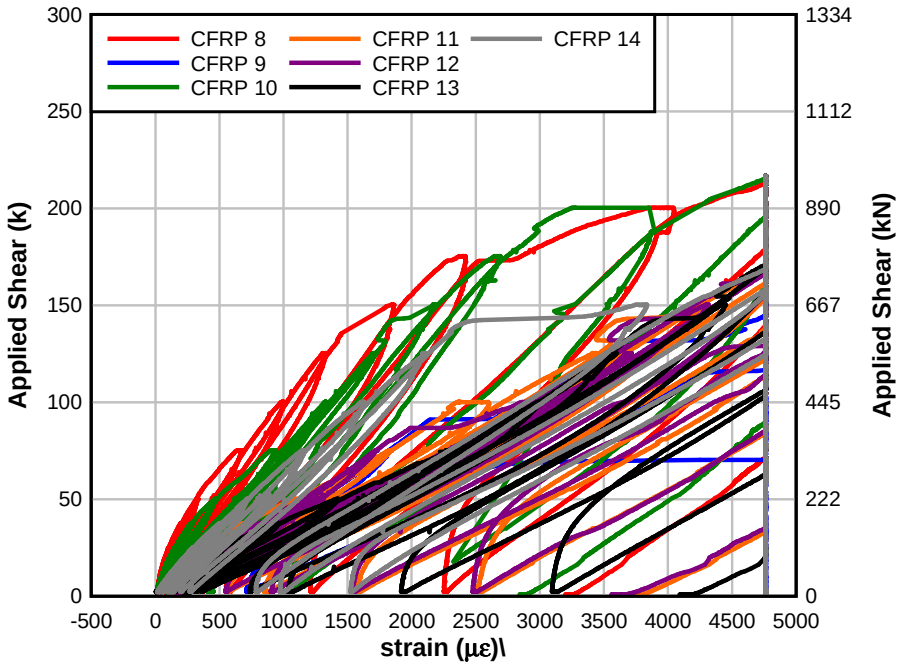

Fig. 12.58 – Specimen IT.7.18.6.S applied shear vs. CFRP strain (tested to 500K)

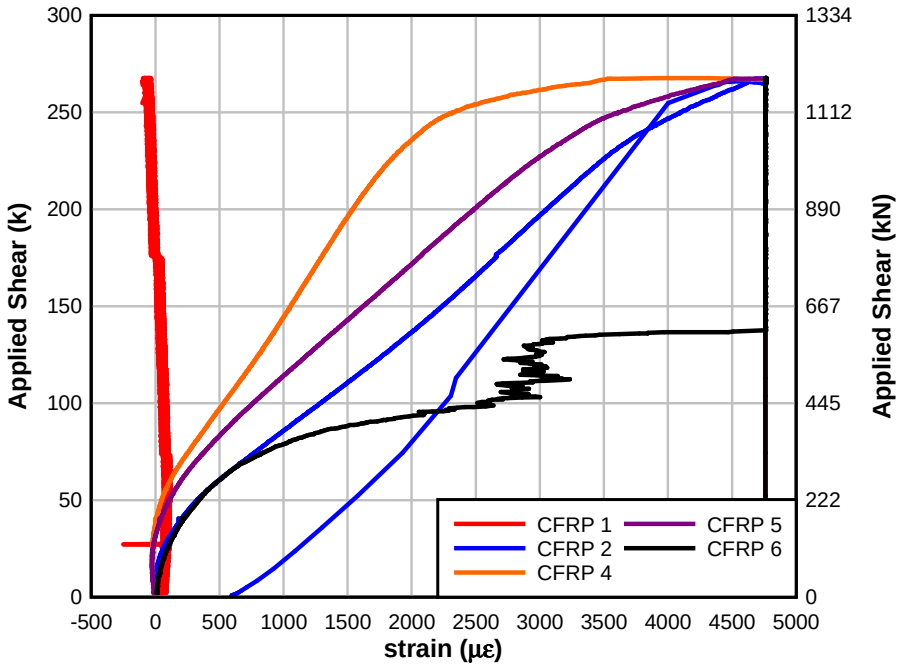

Fig. 12.59 – Specimen IT.7.18.6.S applied shear vs. CFRP strain (failure test)

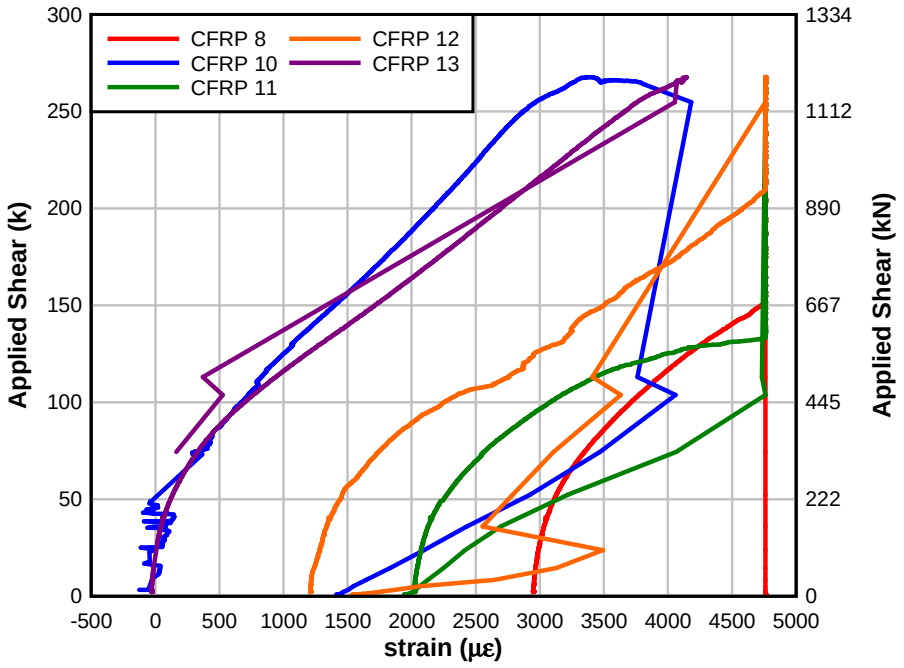

Fig. 12.60 – Specimen IT.7.18.6.S applied shear vs. CFRP strain (failure test)

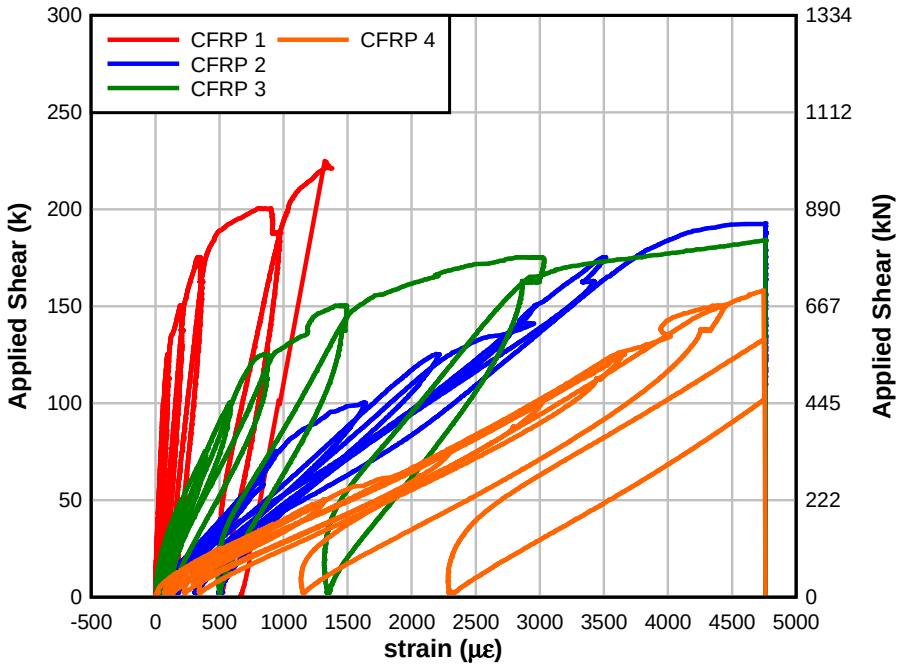

Fig. 12.61 – Specimen IT.7.18.12.S applied shear vs. CFRP strain (failure test)

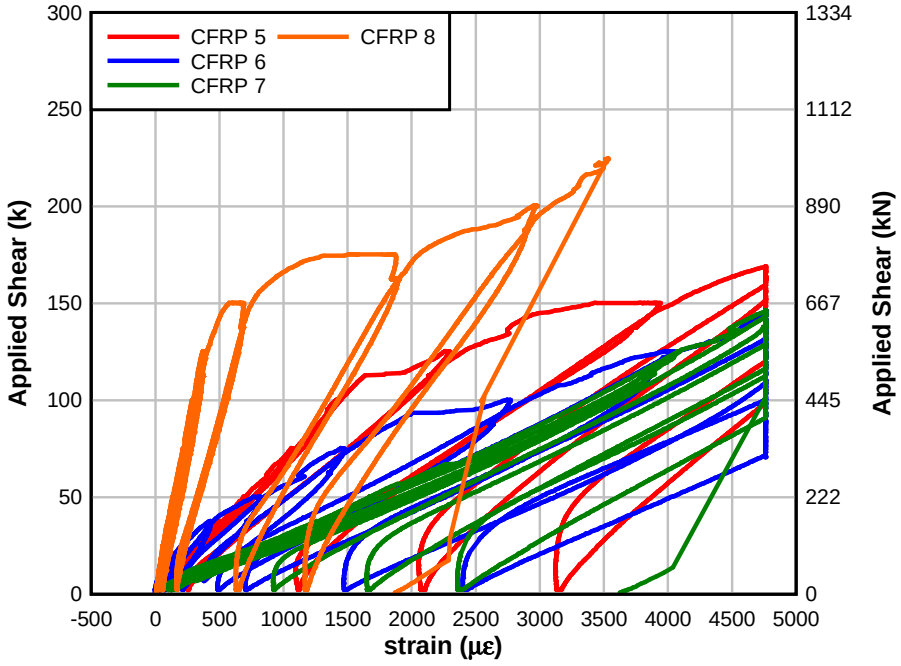

Fig. 12.62 – Specimen IT.7.18.12.S applied shear vs. CFRP strain (failure test)

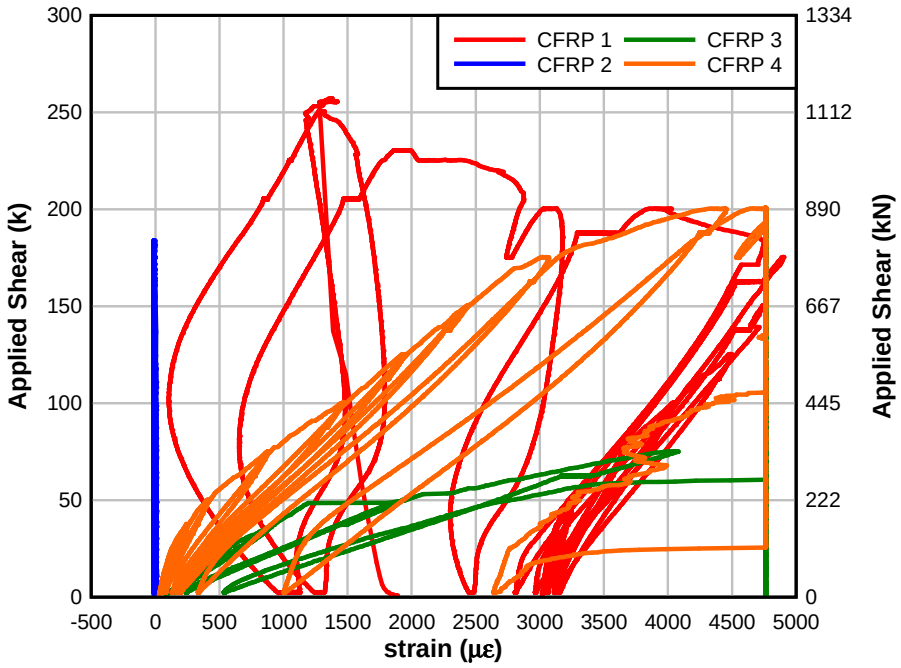

Fig. 12.63 – Specimen IT.7.22.6.S applied shear vs. CFRP strain (failure test)

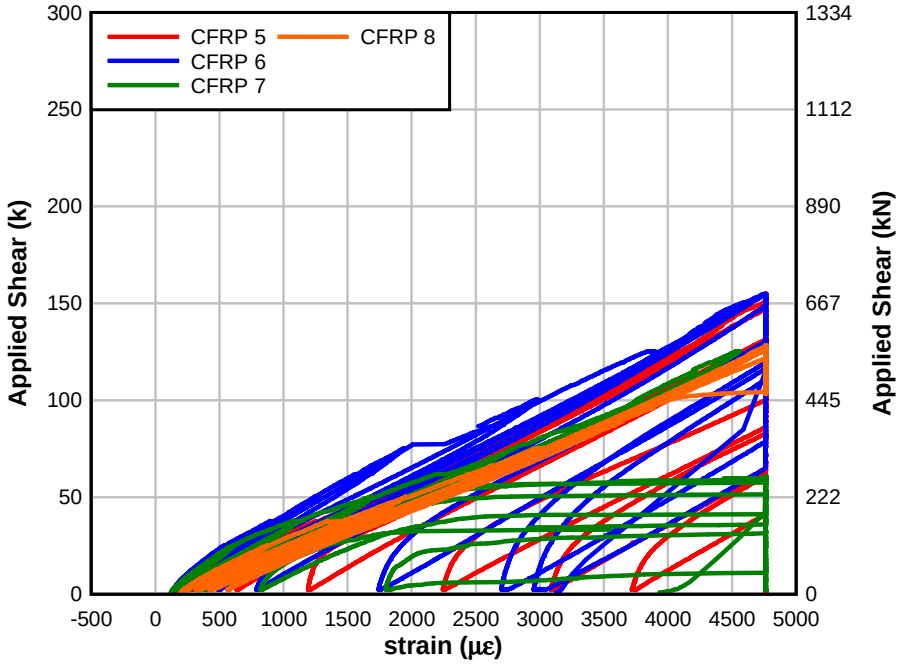

Fig. 12.64 – Specimen IT.7.22.6.S applied shear vs. CFRP strain (failure test)

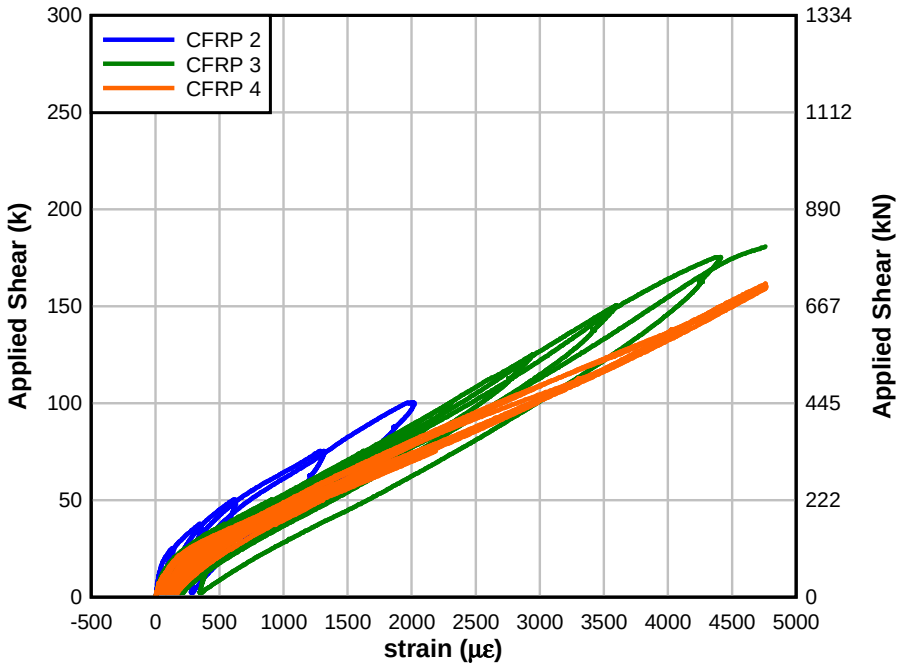

Fig. 12.65 – Specimen IT.5.22.12.S applied shear vs. CFRP strain (failure test)

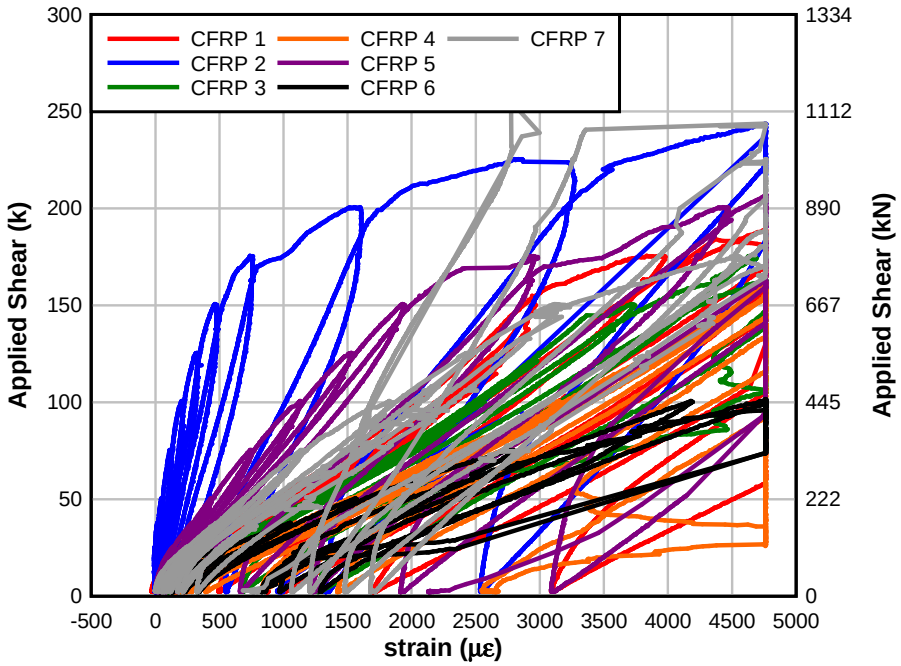

Fig. 12.66 – Specimen IT.7.18.6.M applied shear vs. CFRP strain (failure test)

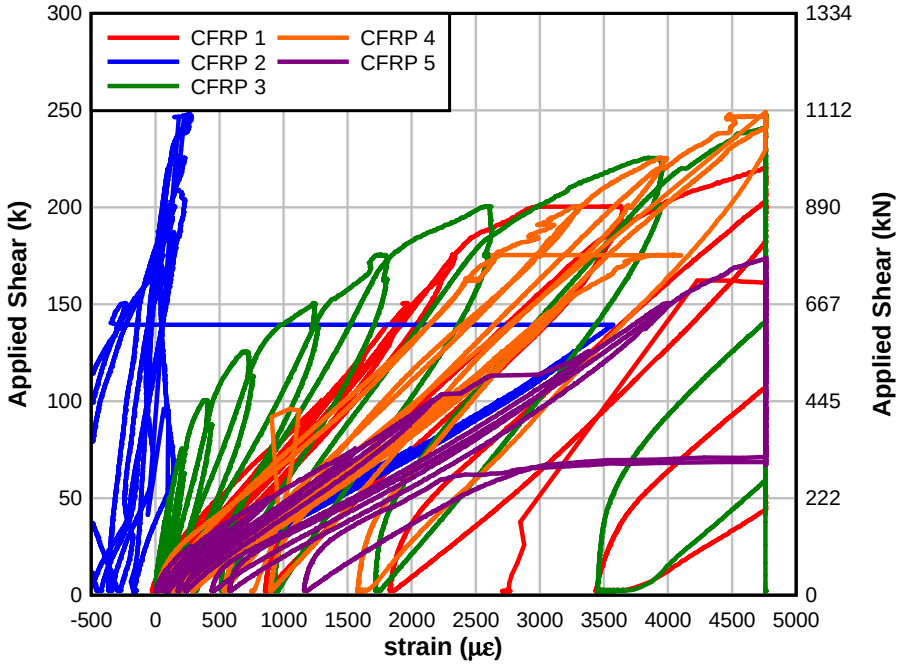

Fig. 12.67 – Specimen IT.7.22.6.FT applied shear vs. CFRP strain (failure test)

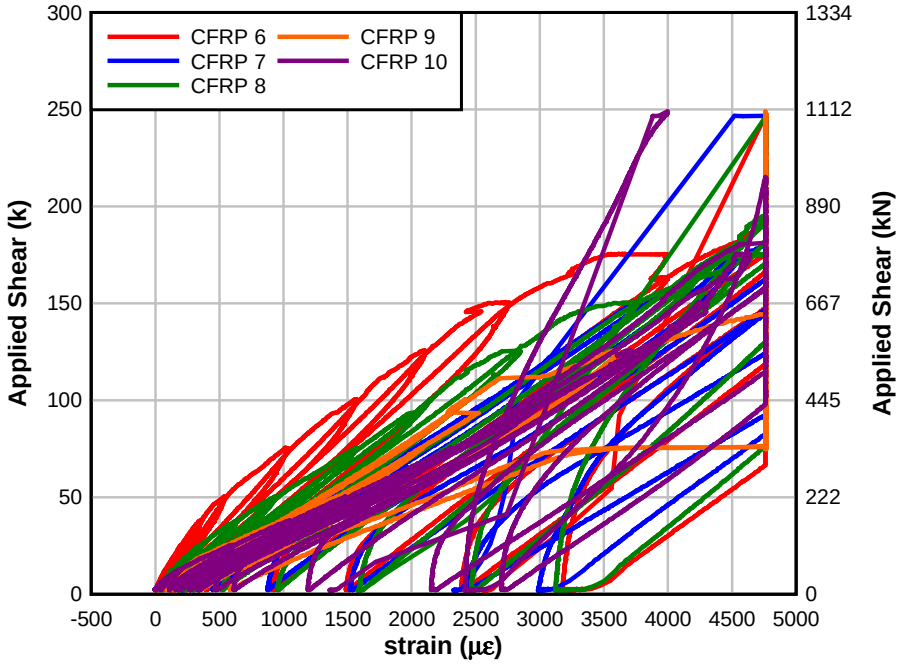

Fig. 12.68 – Specimen IT.7.22.6.FT applied shear vs. CFRP strain (failure test)

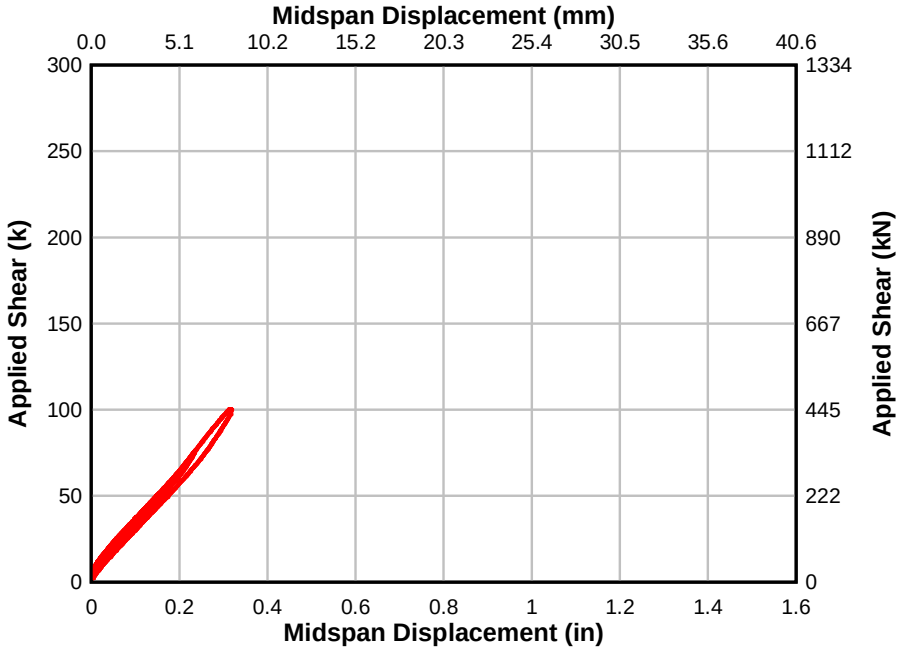

Fig. 12.69 – Specimen T.6.18.6.S applied shear vs. midspan disp. (baseline test)

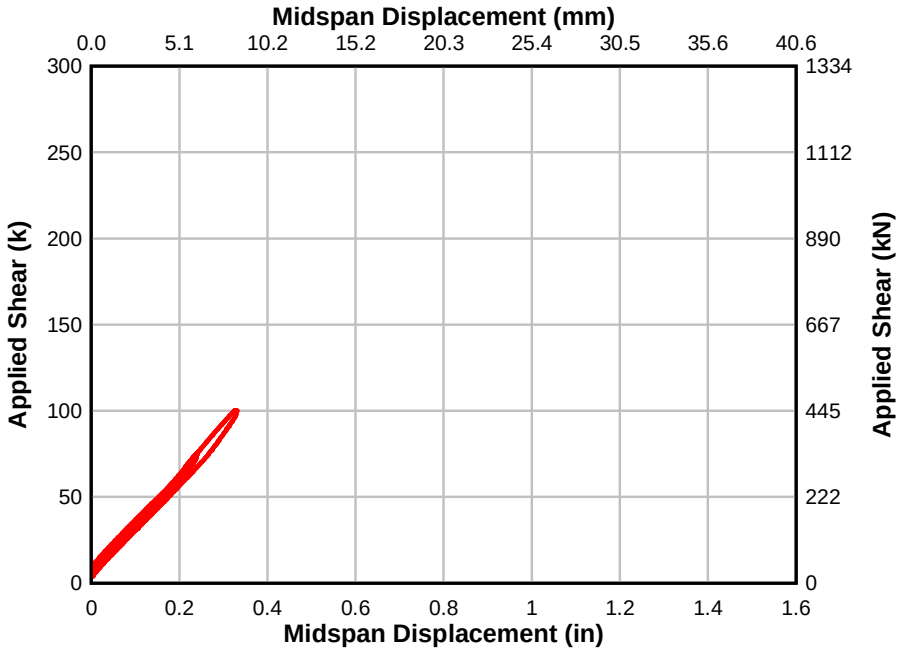

Fig. 12.70 - Specimen T.6.18.12.S applied shear vs. midspan disp. (baseline test)

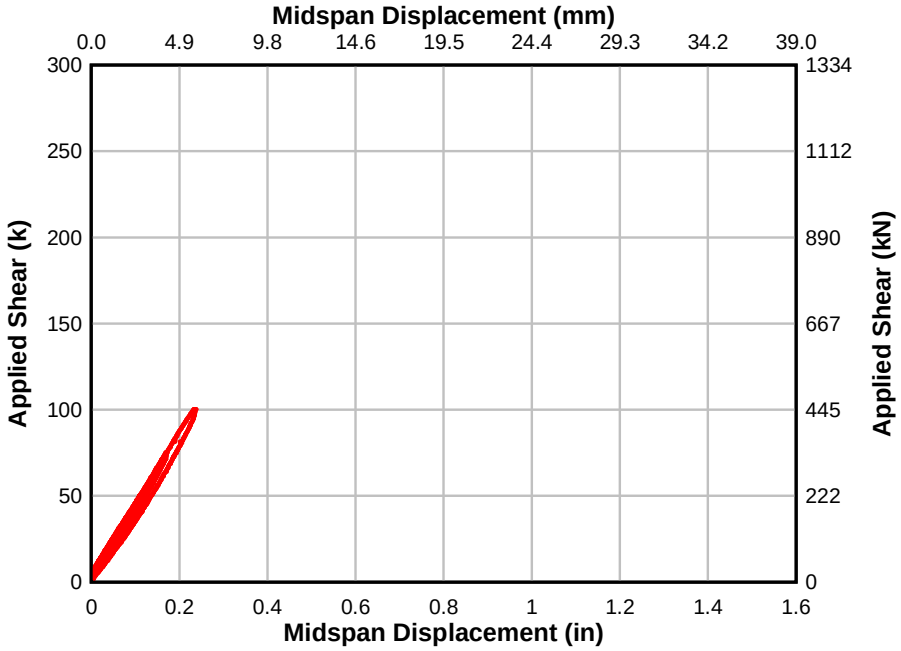

Fig. 12.71 - Specimen IT.7.18.6.S applied shear vs. midspan disp. (baseline test)

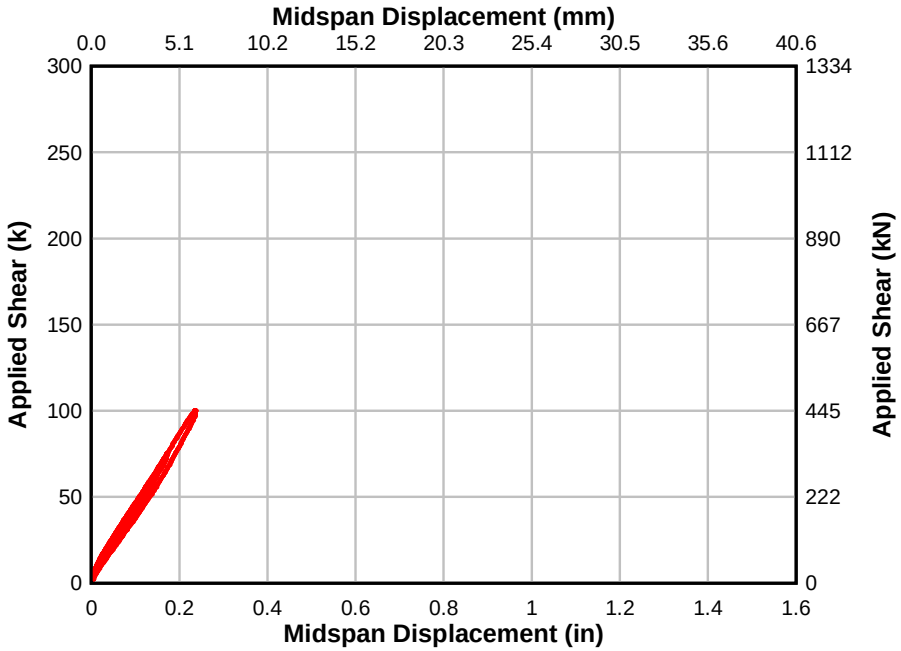

Fig. 12.72 - Specimen IT.7.18.12.S applied shear vs. midspan disp. (baseline test)

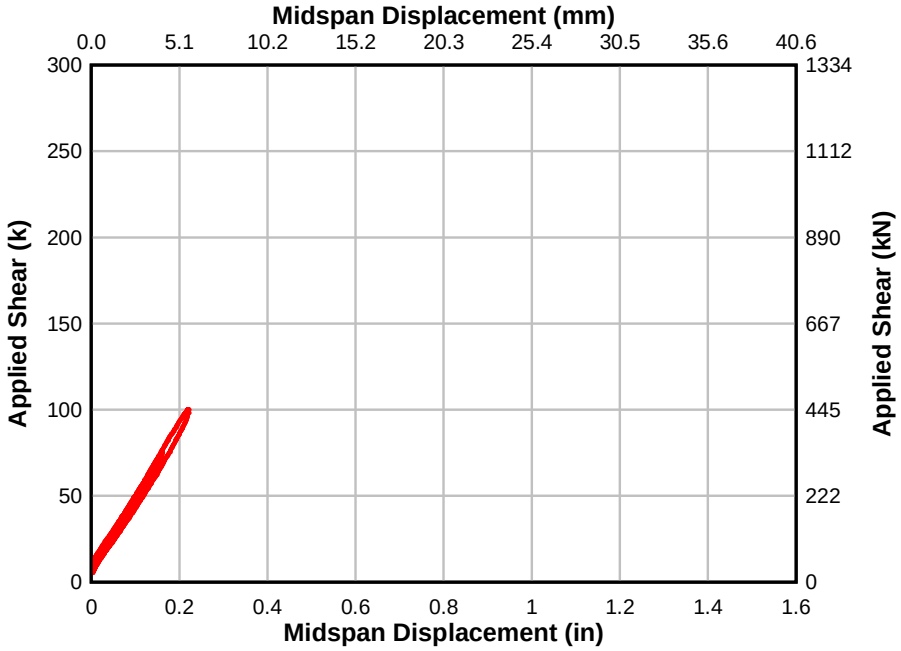

Fig. 12.73 - Specimen IT.7.22.6.S applied shear vs. midspan disp. (baseline test)

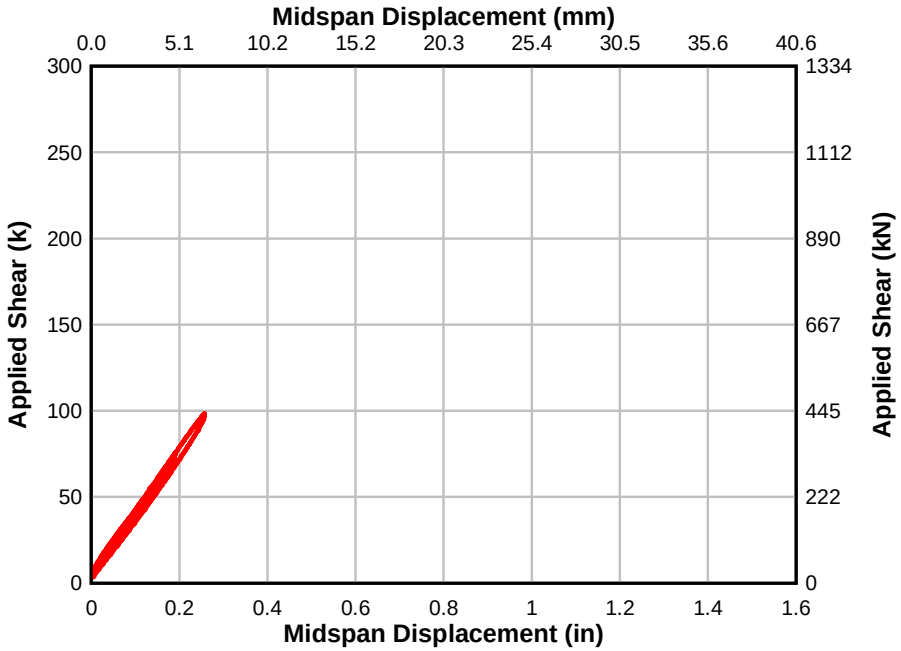

Fig. 12.74 - Specimen IT.5.22.12.S applied shear vs. midspan disp. (baseline test)

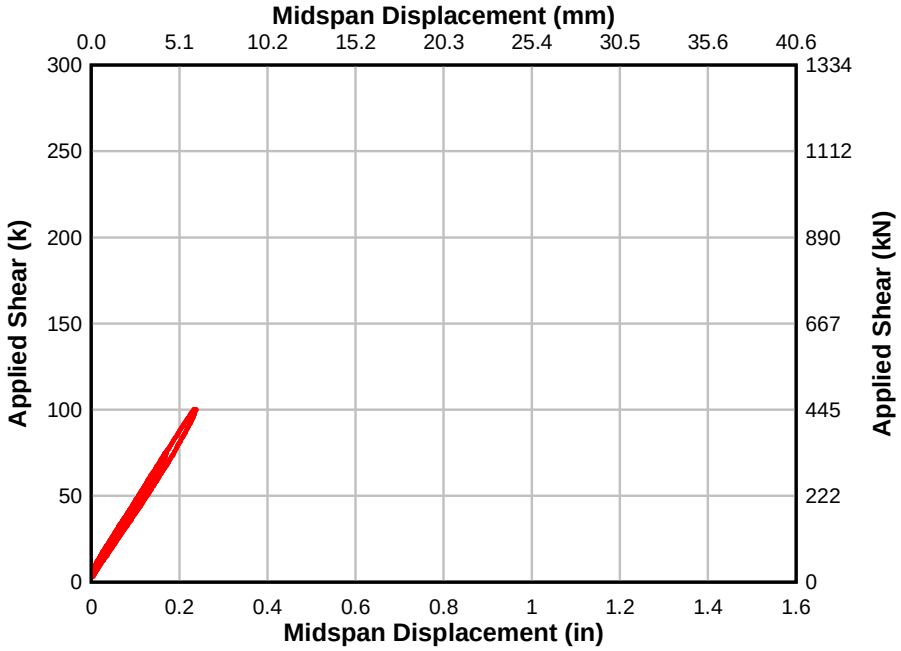

Fig. 12.75 - Specimen IT.7.18.6.M applied shear vs. midspan disp. (baseline test)

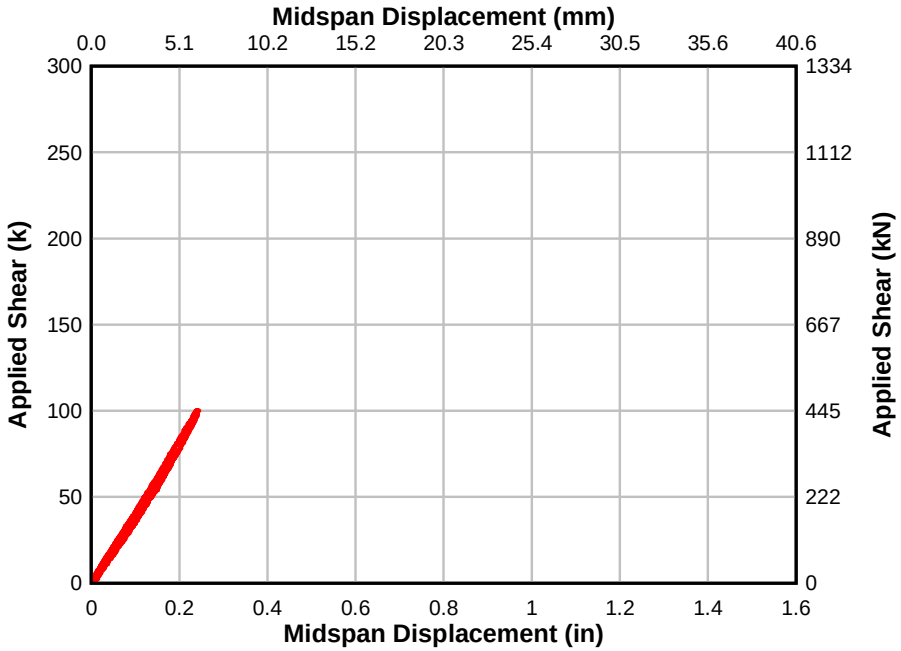

Fig. 12.76 - Specimen IT.7.22.6.FT applied shear vs. midspan disp. (baseline test)

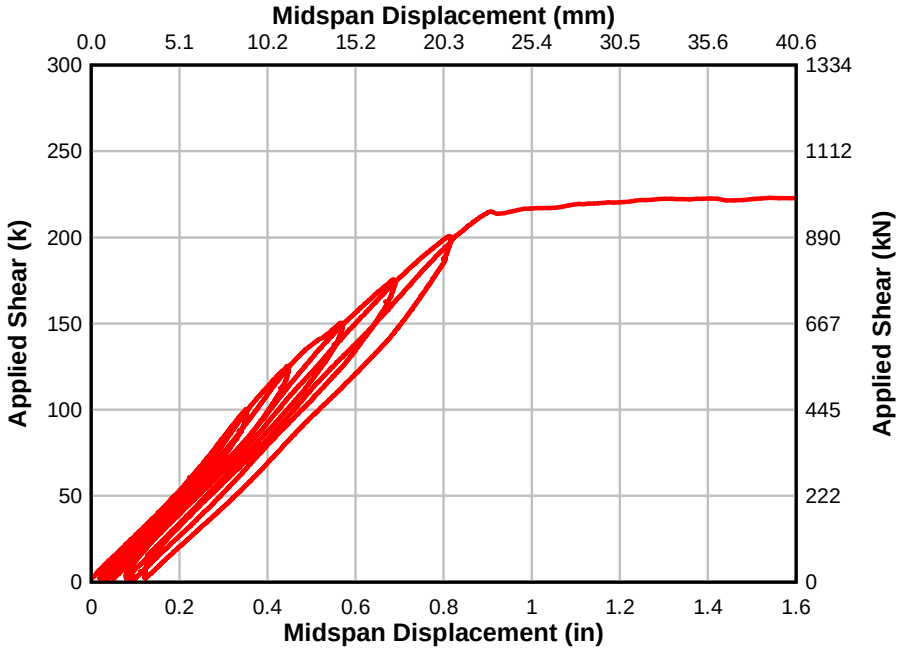

Fig. 12.77 - Specimen T.6.18.6.S applied shear vs. midspan disp. (failure test)

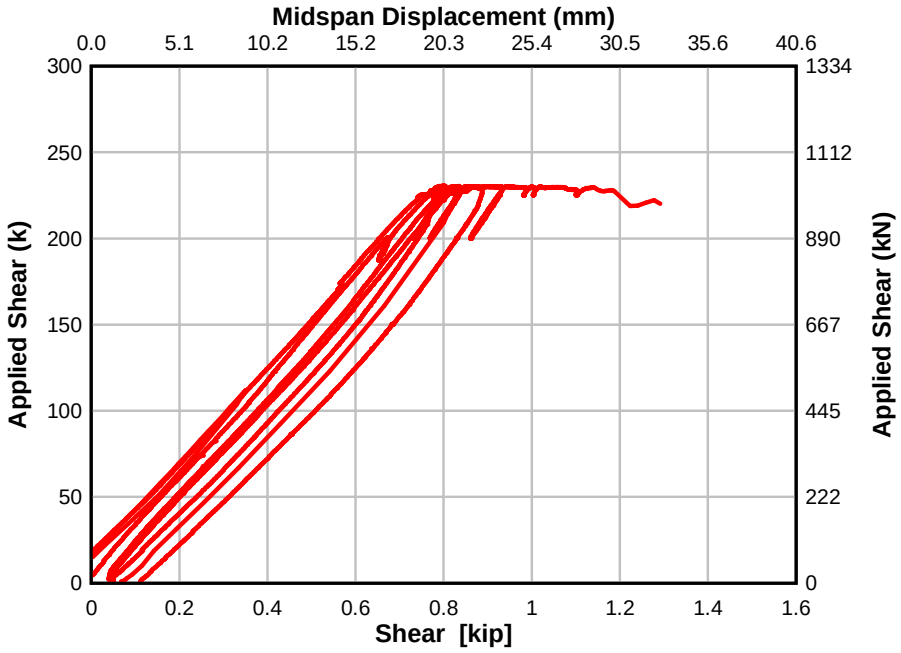

Fig. 12.78 - Specimen T.6.18.12.S applied shear vs. midspan disp. (failure test)

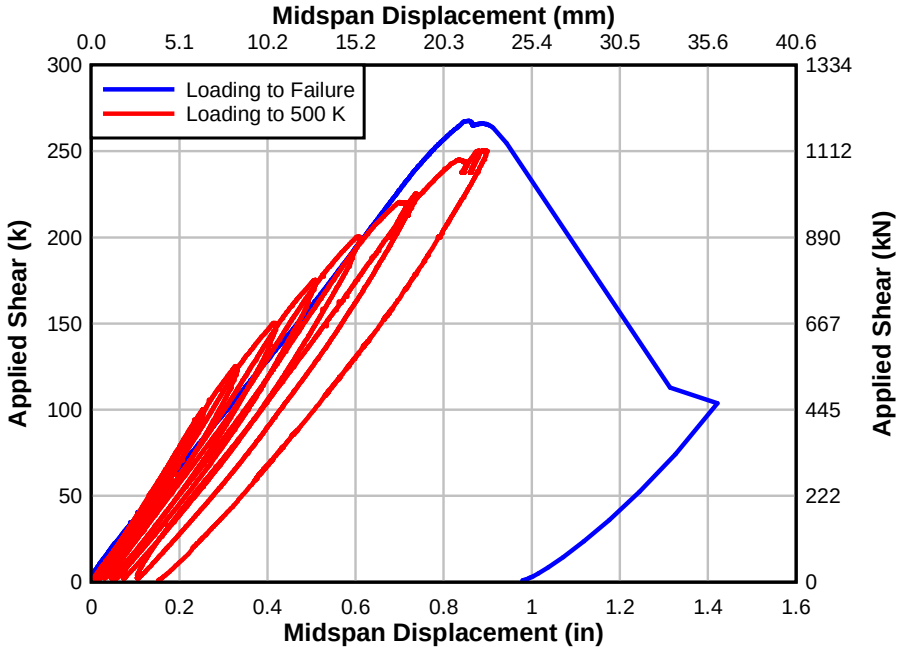

Fig. 12.79 - Specimen IT.7.18.6.S applied shear vs. midspan disp. (failure test)

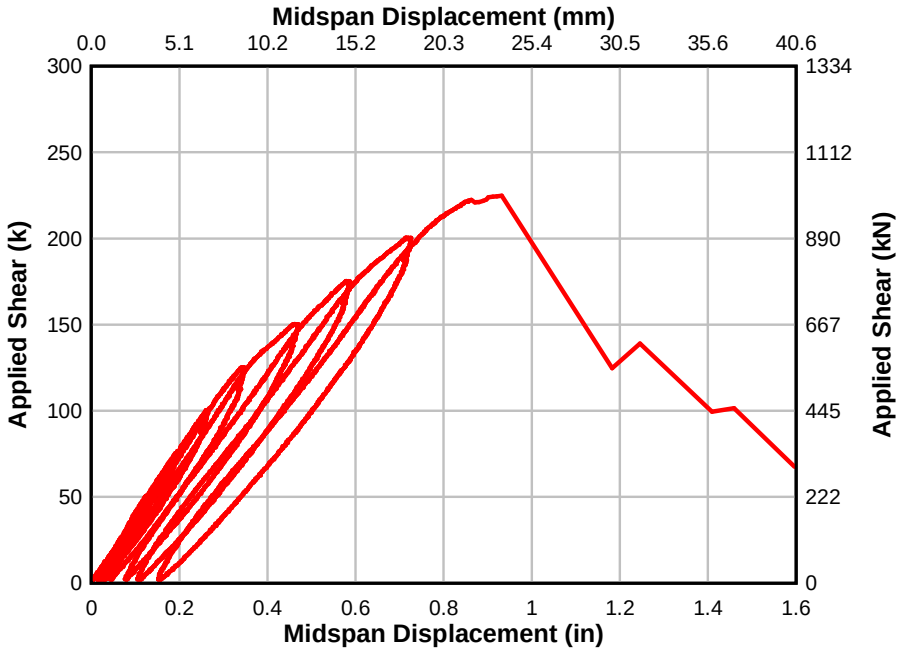

Fig. 12.80 Specimen IT.7.18.12.S applied shear vs. midspan disp. (failure test)

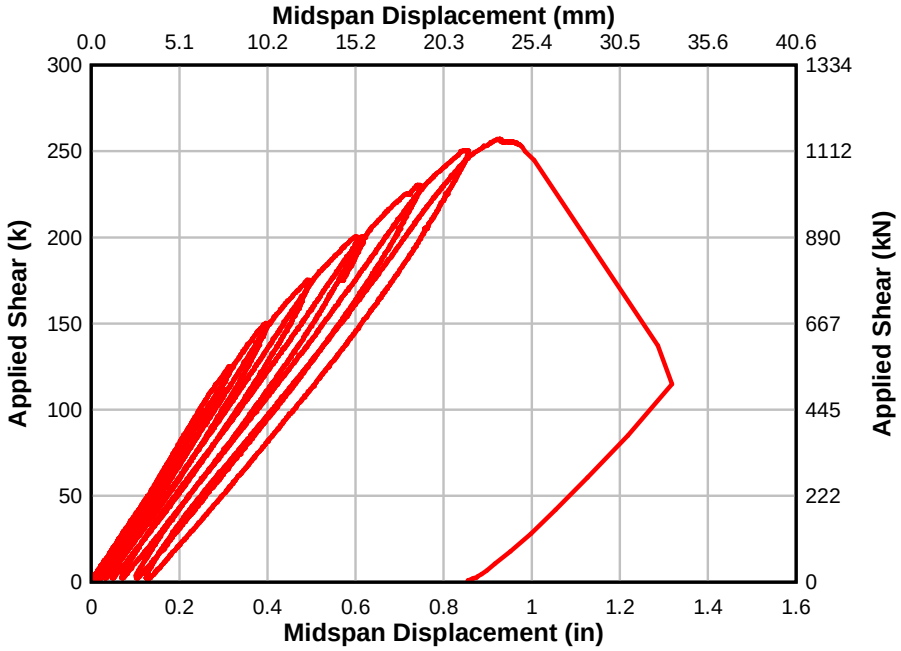

Fig. 12.81 - Specimen IT.7.22.6.S applied shear vs. midspan disp. (failure test)

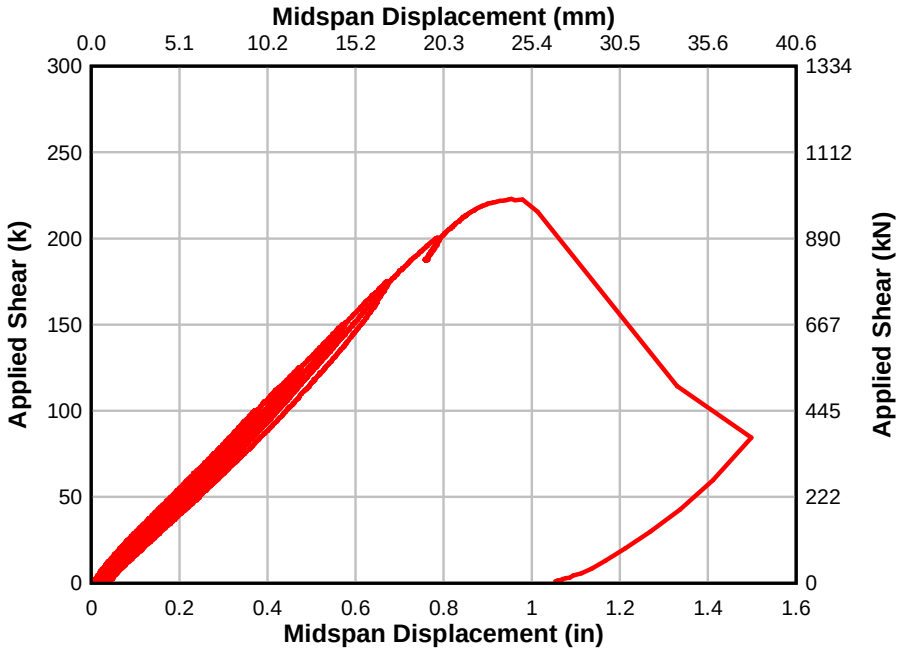

Fig. 12.82 - Specimen IT.5.22.12.S applied shear vs. midspan disp. (failure test)

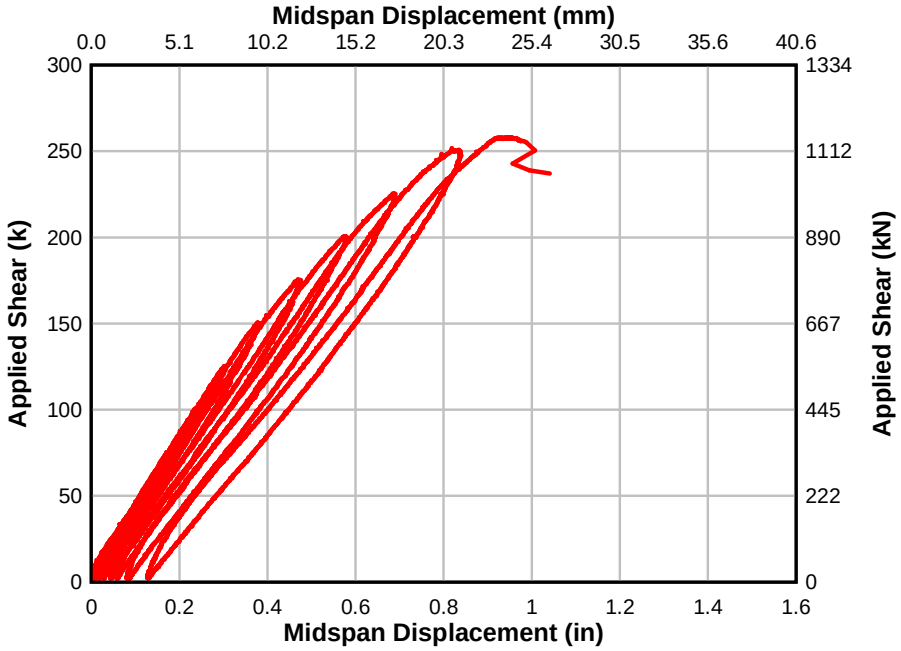

Fig. 12.83 - Specimen IT.7.18.6.M applied shear vs. midspan disp. (failure test)

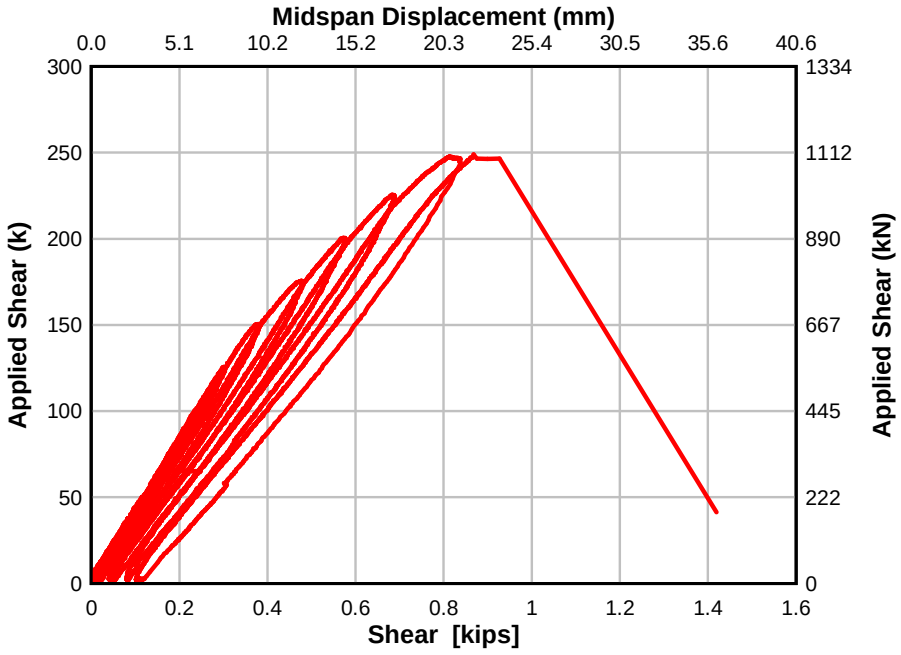

Fig. 12.84 - Specimen IT.7.22.6.FT applied shear vs. midspan disp. (failure test)

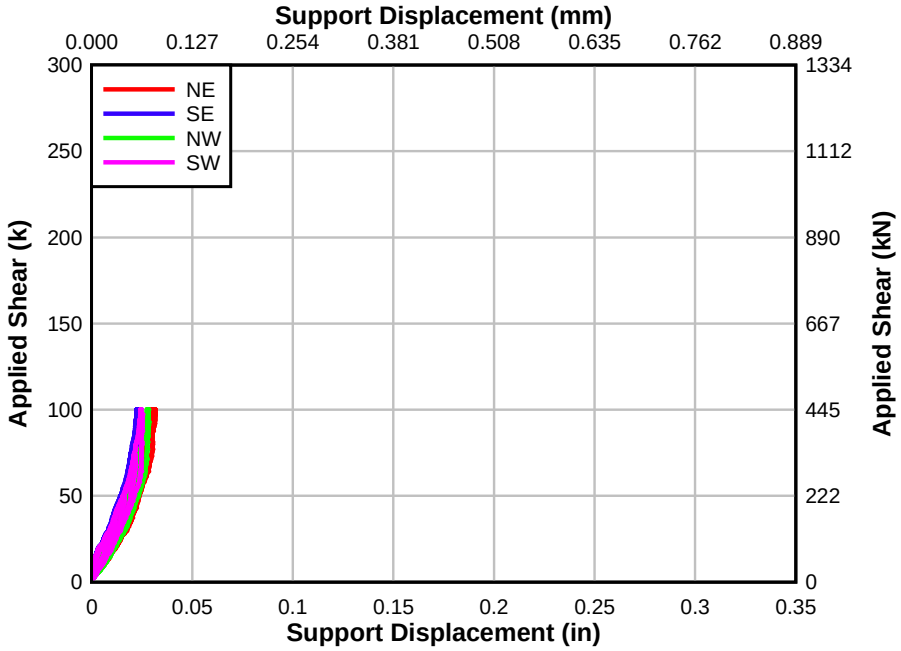

Fig. 12.85 - Specimen T.6.18.6.S applied shear vs. support disp. (baseline test)

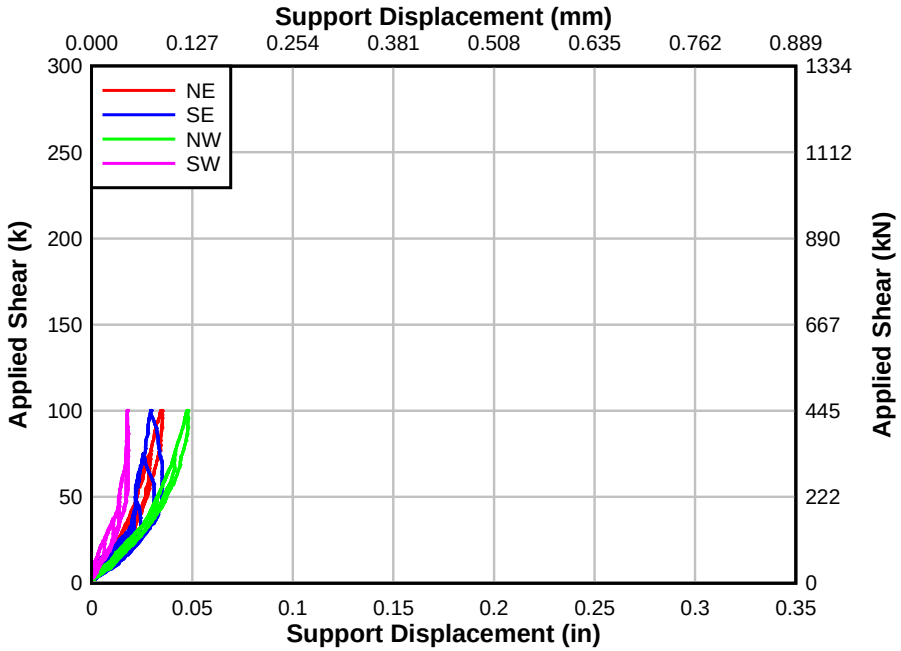

Fig. 12.86 – Specimen T.6.18.12.S applied shear vs. support disp. (baseline test)

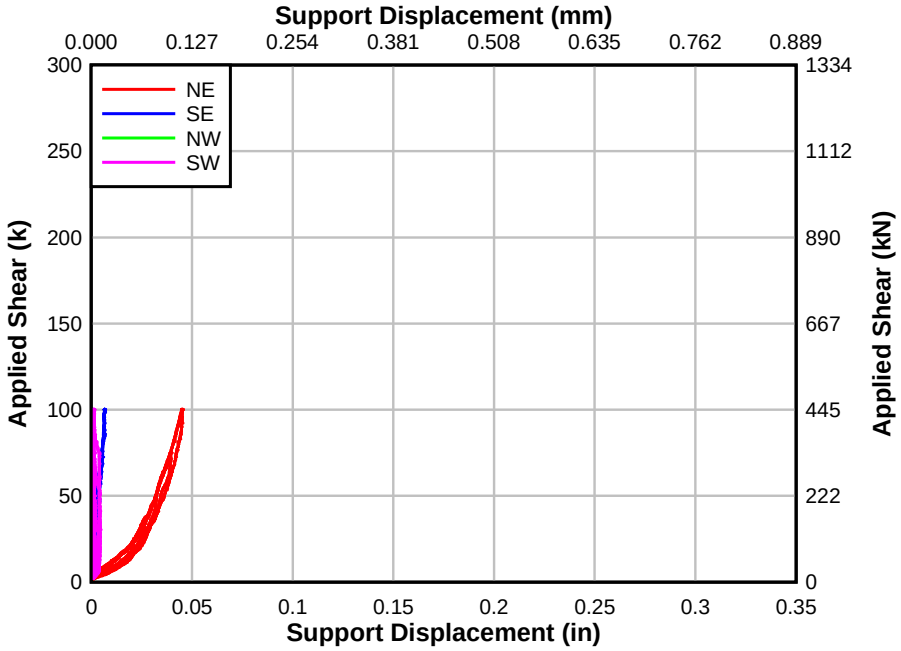

Fig. 12.87 – Specimen IT.7.18.6.S applied shear vs. support disp. (baseline test)

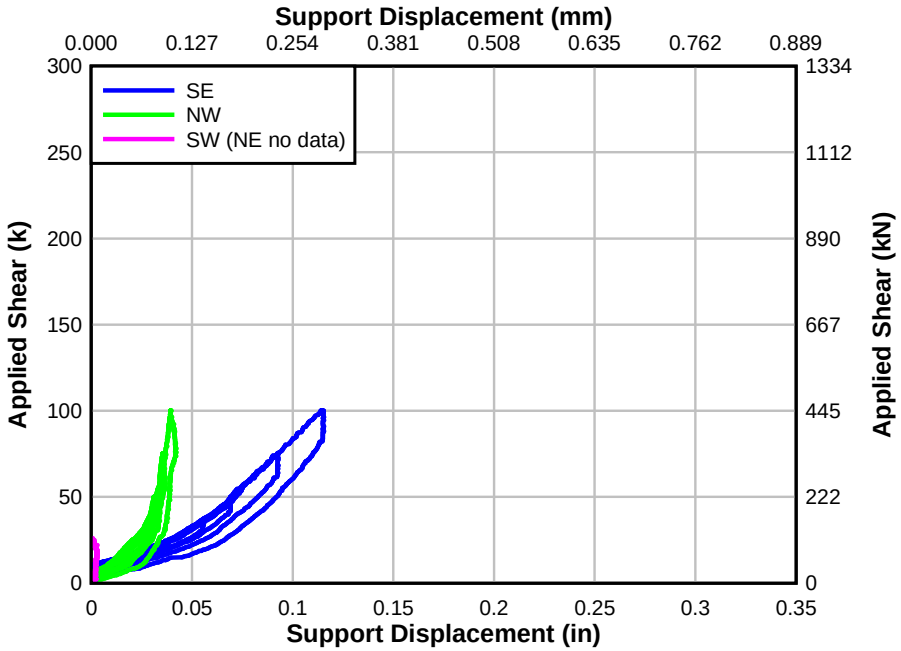

Fig. 12.88 – Specimen IT.7.18.12.S applied shear vs. support disp. (baseline test)

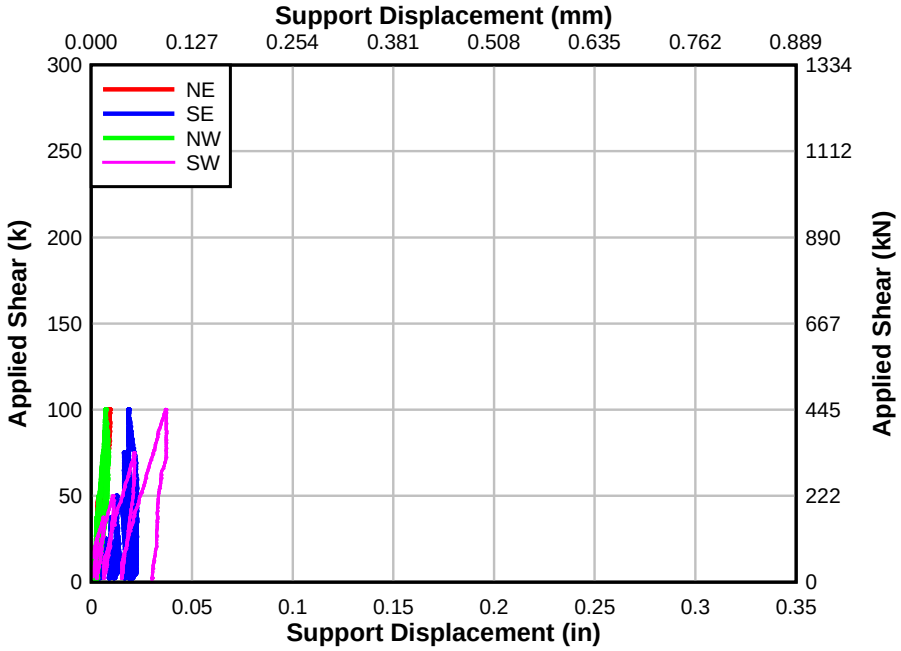

Fig. 12.89 – Specimen IT.7.22.6.S applied shear vs. support disp. (baseline test)

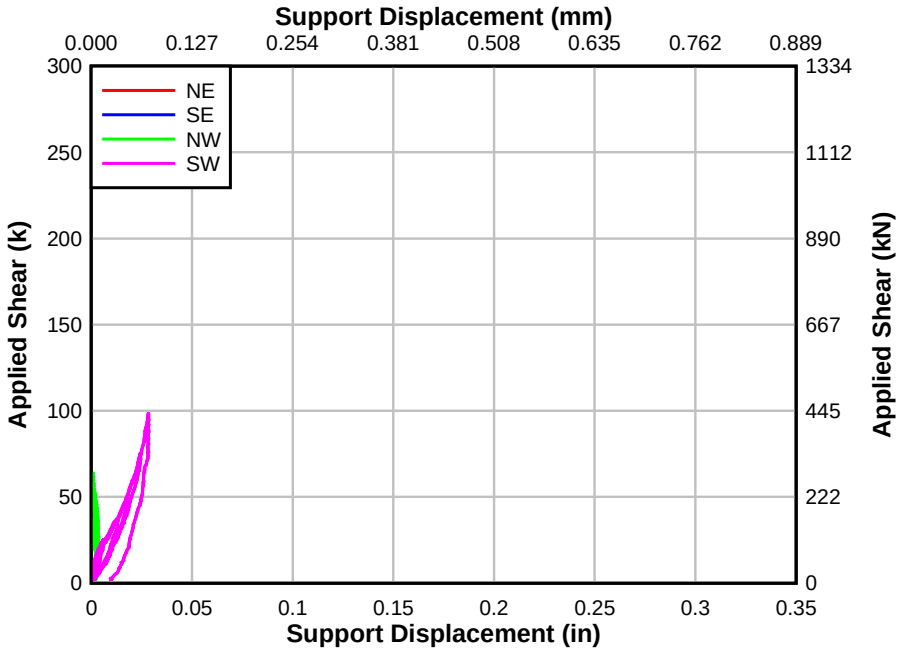

Fig. 12.90 – Specimen IT.5.22.12.S applied shear vs. support disp. (baseline test)

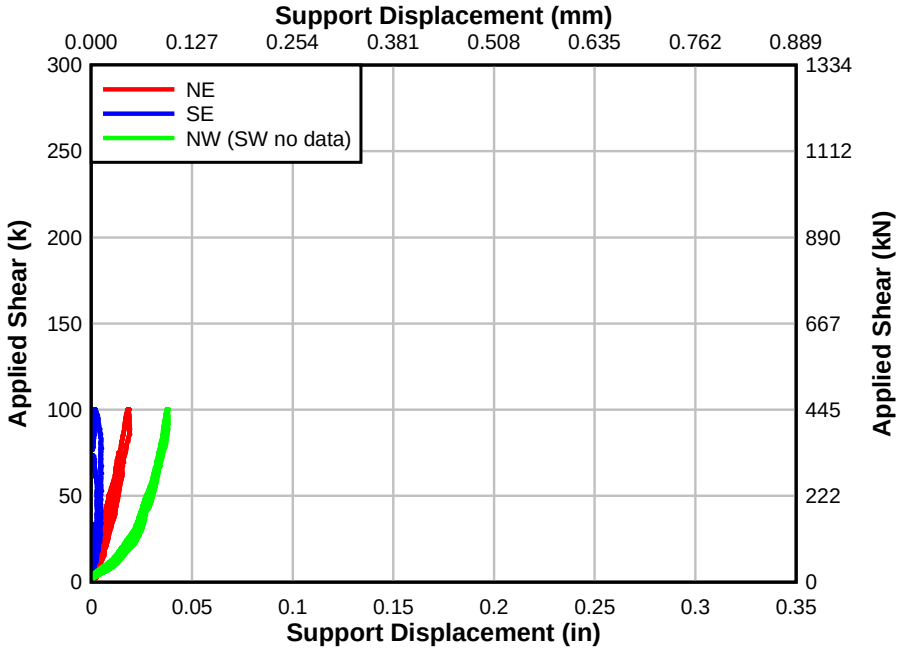

Fig. 12.91 – Specimen IT.7.18.6.M applied shear vs. support disp. (baseline test)

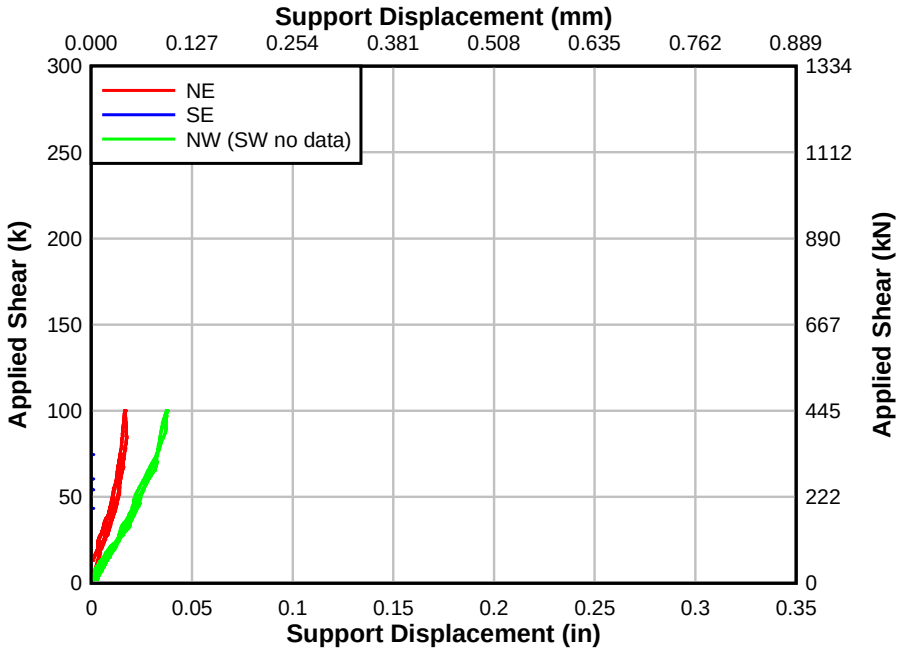

Fig. 12.92 – Specimen IT.7.22.6.FT applied shear vs. support disp. (baseline test)

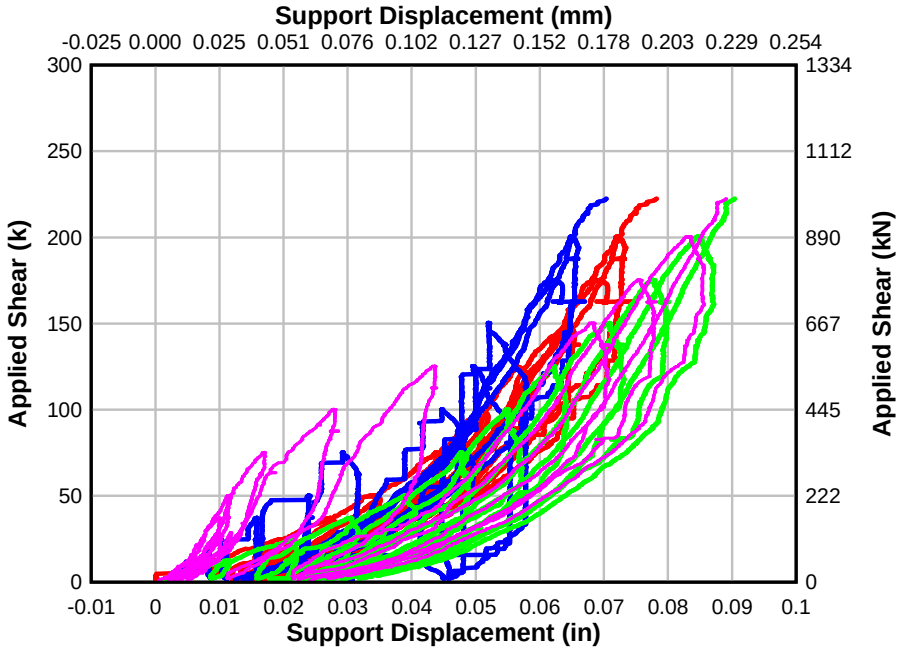

Fig. 12.93 – Specimen T.6.18.6.S applied shear vs. support disp. (failure test)

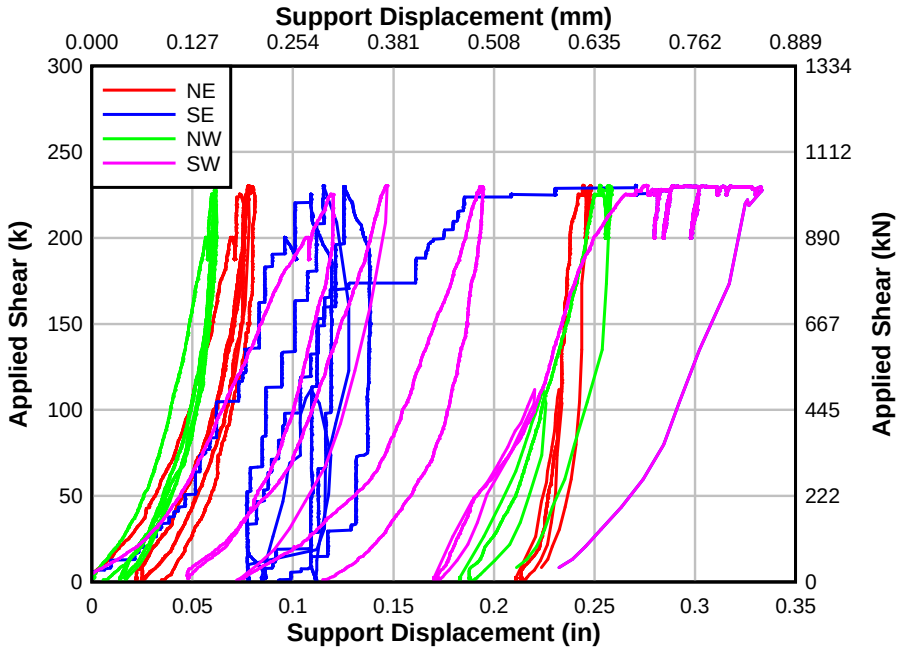

Fig. 12.94 – Specimen T.6.18.12.S applied shear vs. support disp. (failure test)

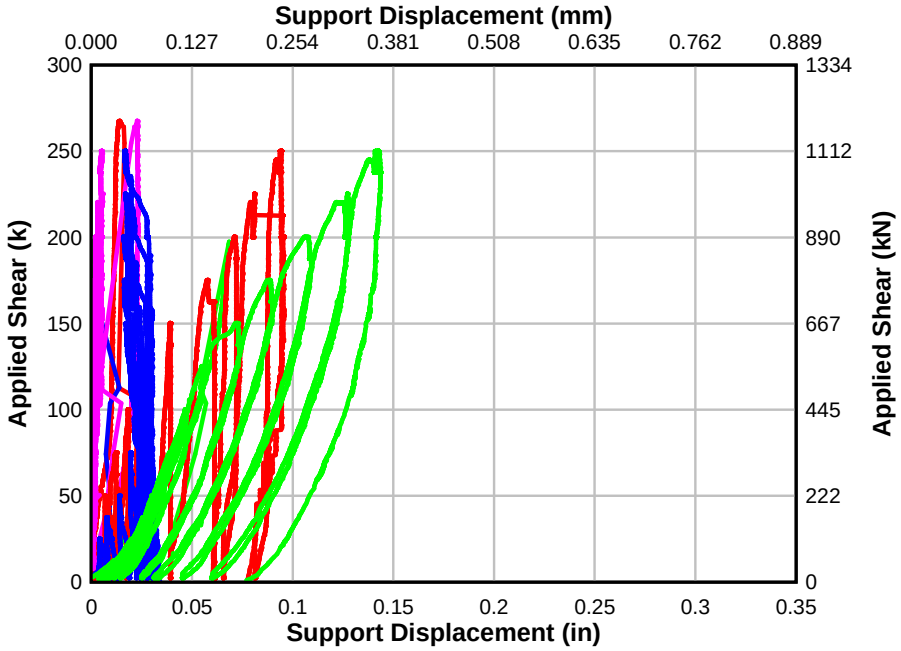

Fig. 12.95 – Specimen IT.7.18.6.S applied shear vs. support disp. (failure test)

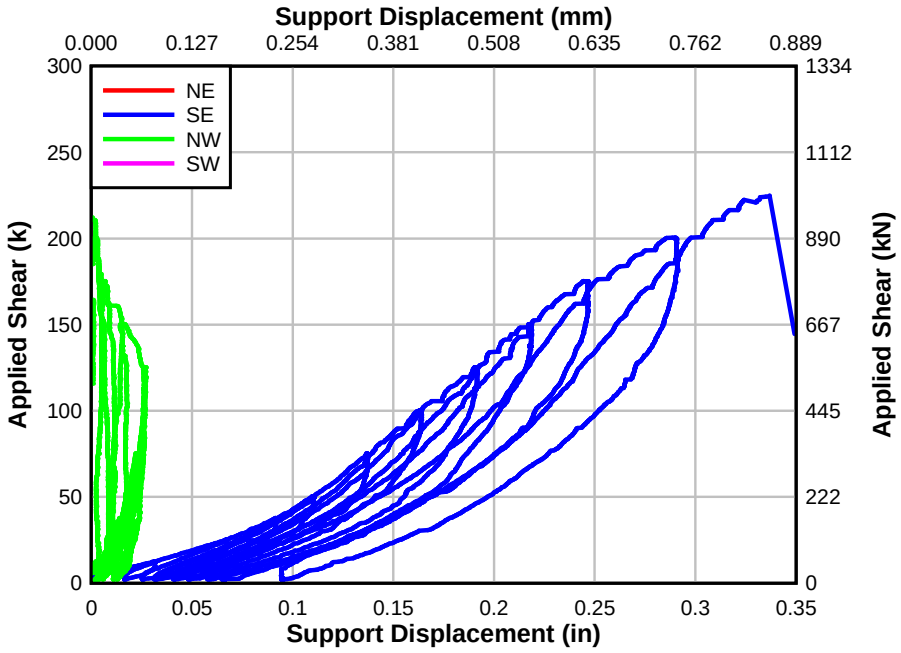

Fig. 12.96 – Specimen IT.7.18.12.S applied shear vs. support disp. (failure test)

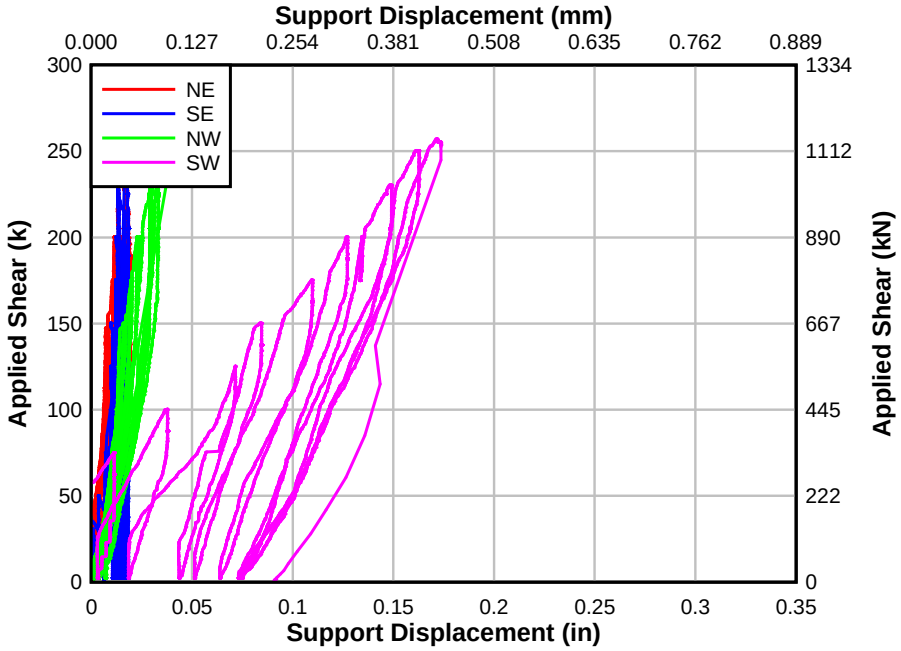

Fig. 12.97 – Specimen IT.7.22.6.S applied shear vs. support disp. (failure test)

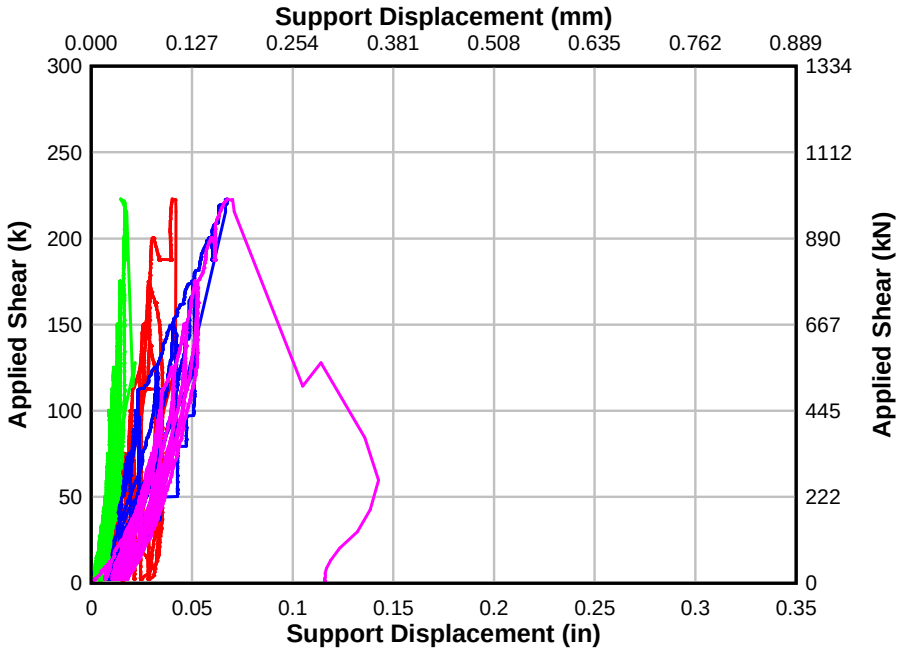

Fig. 12.98 – Specimen IT.5.22.12.S applied shear vs. support disp. (failure test)

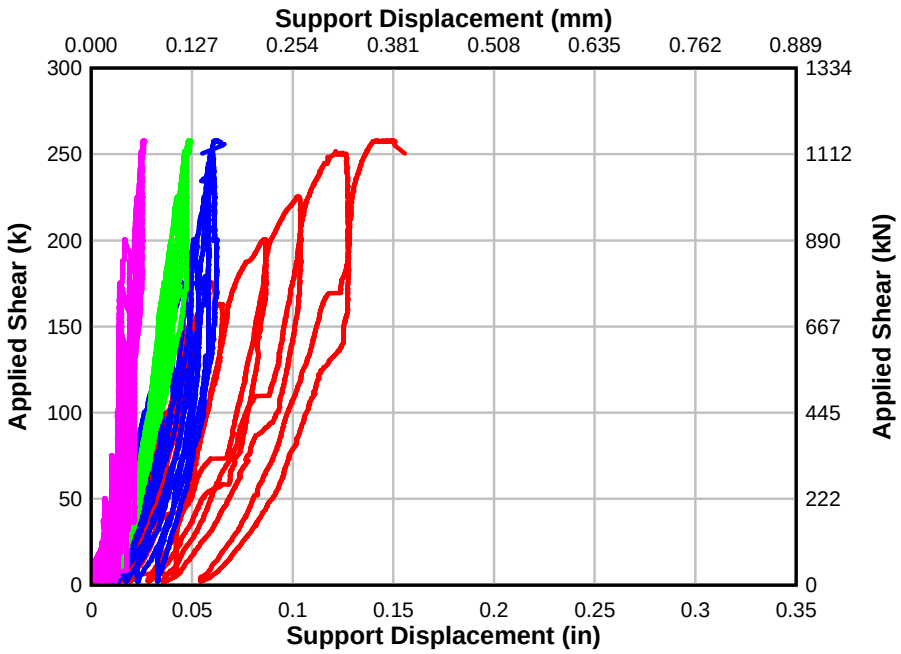

Fig. 12.99 – Specimen IT.7.18.6.M applied shear vs. support disp. (failure test)

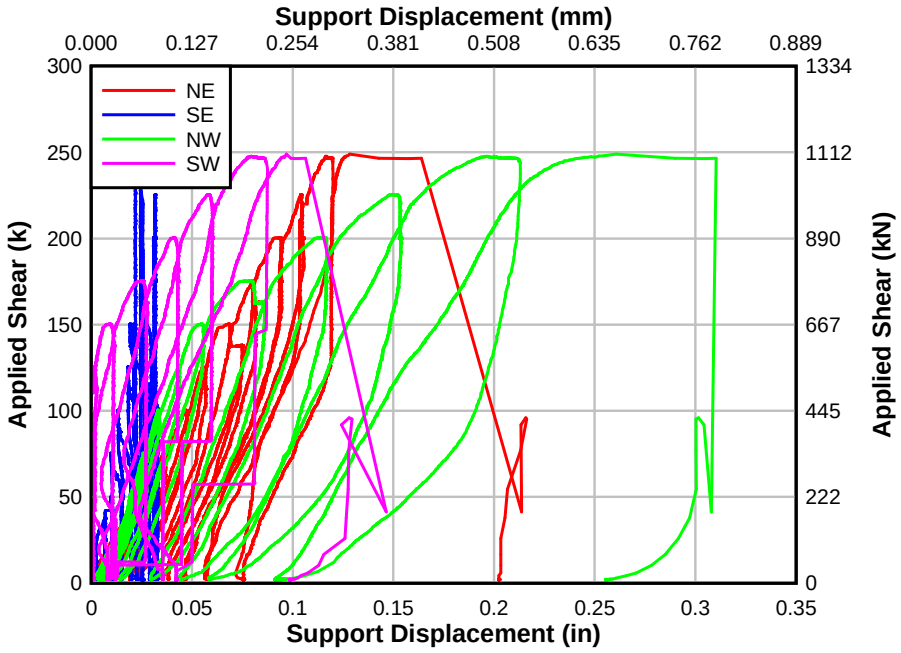

Fig. 12.100 – Specimen IT.7.22.6.FT applied shear vs. support disp. (failure test)

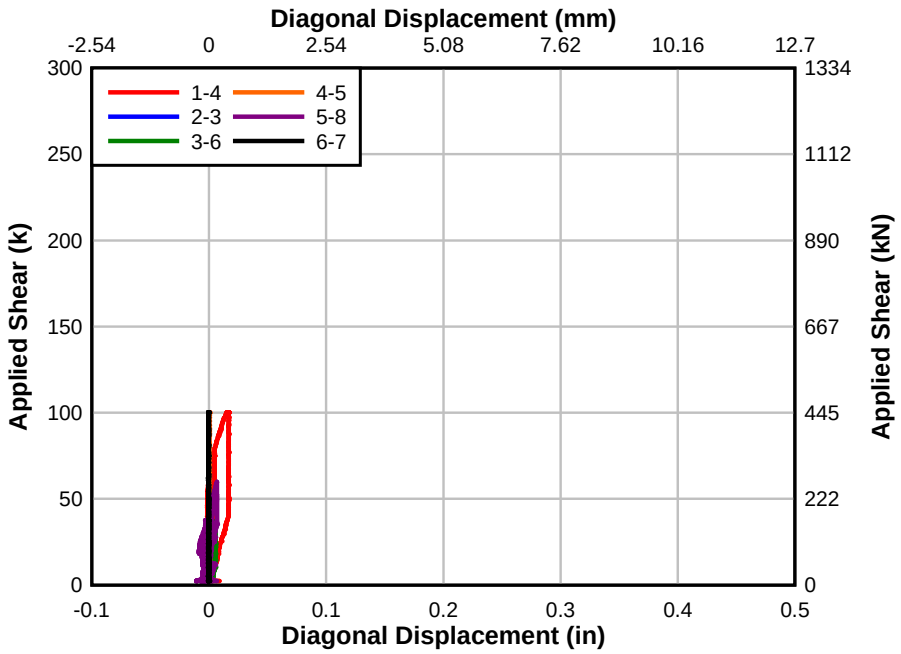

Fig. 12.101 - Specimen T.6.18.6.S applied shear vs. diagonal disp. (baseline test)

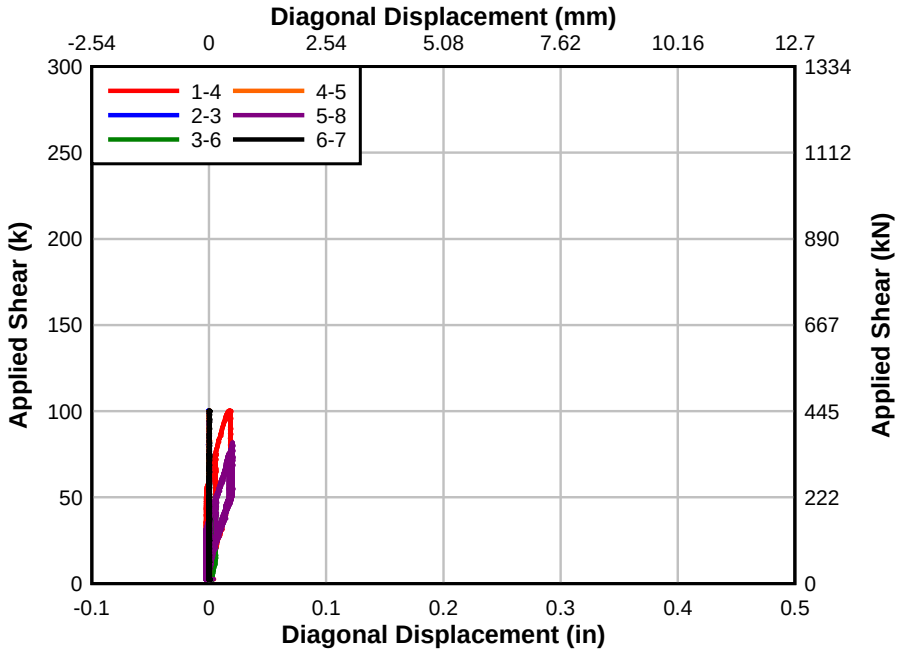

Fig. 12.102 - Specimen T.6.18.12.S applied shear vs. diagonal disp. (baseline test)

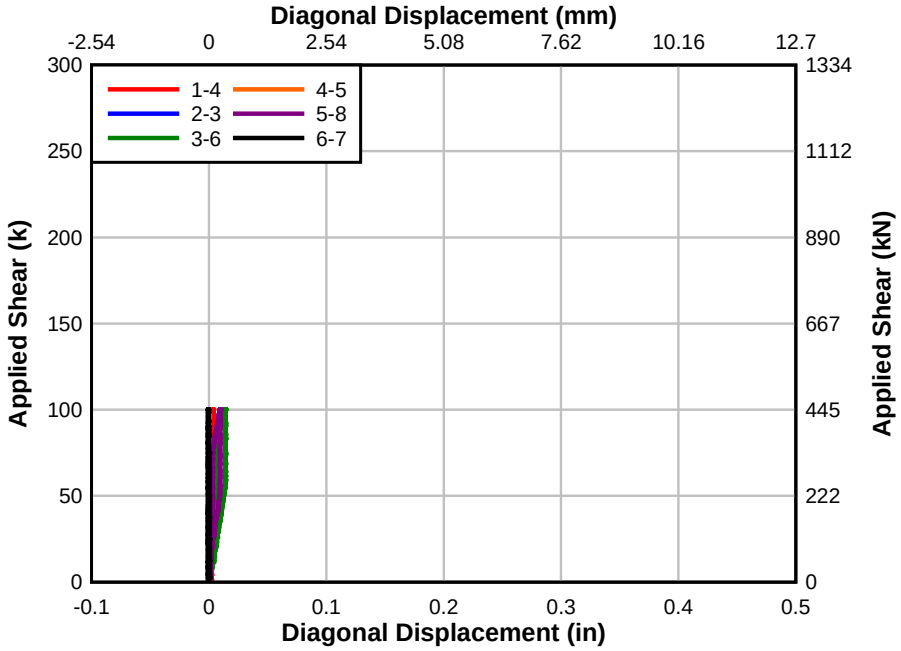

Fig. 12.103 - Specimen IT.7.18.6.S applied shear vs. diagonal disp. (baseline test)

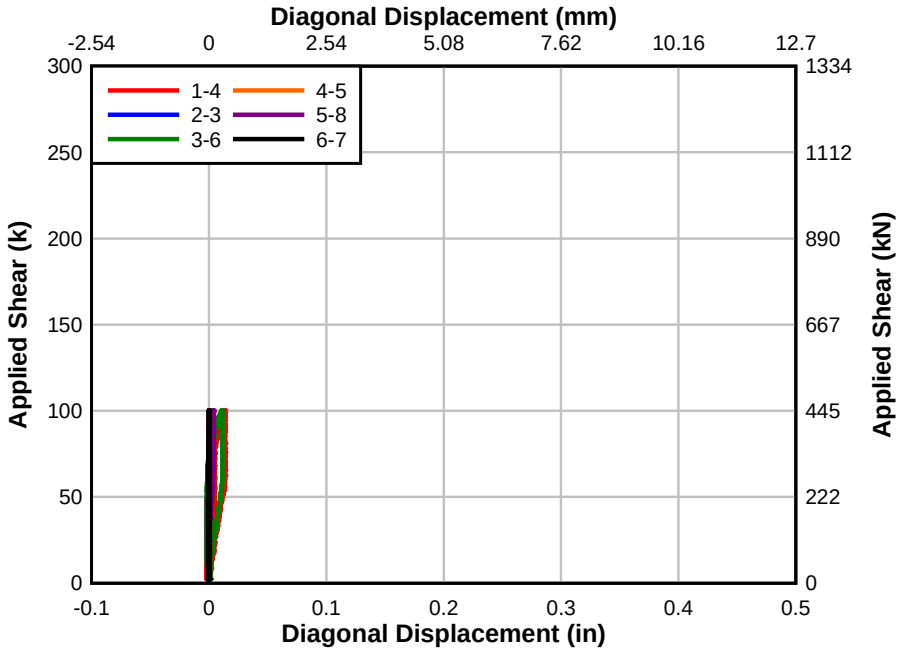

Fig. 12.104 - Specimen IT.7.18.12.S applied shear vs. diagonal disp. (baseline test)

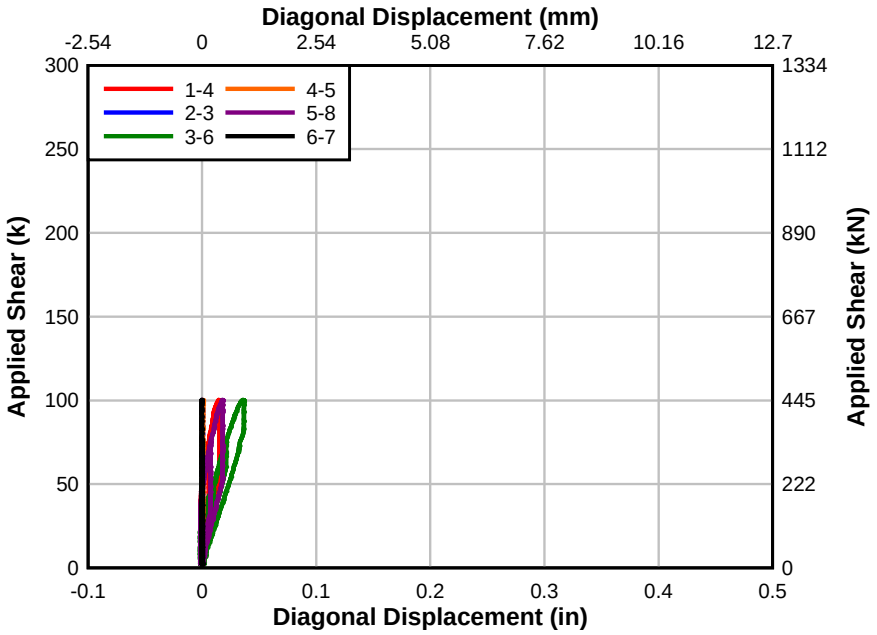

Fig. 12.105 - Specimen IT.7.22.6.S applied shear vs. diagonal disp. (baseline test)

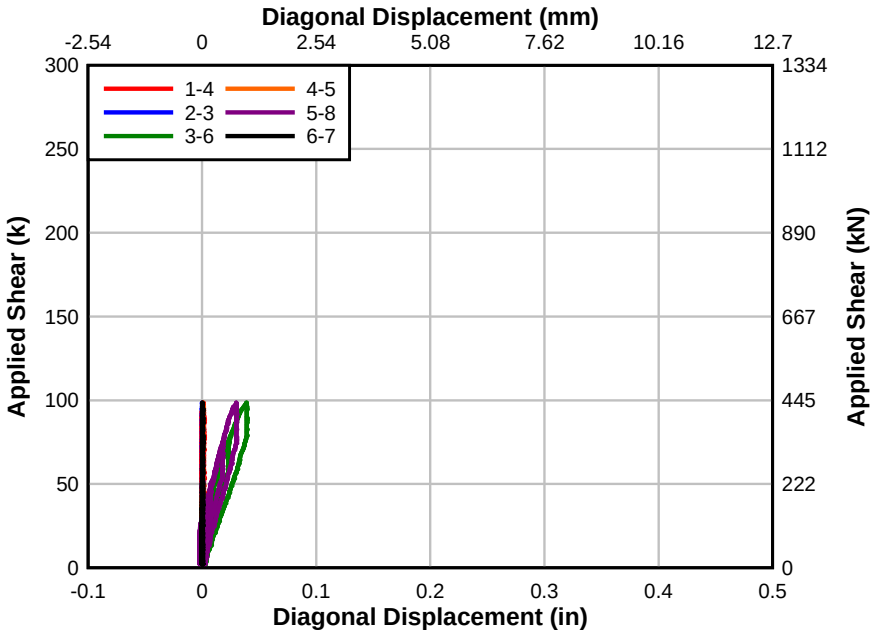

Fig. 12.106 Specimen IT.5.22.12.S applied shear vs. diagonal disp. (baseline test)

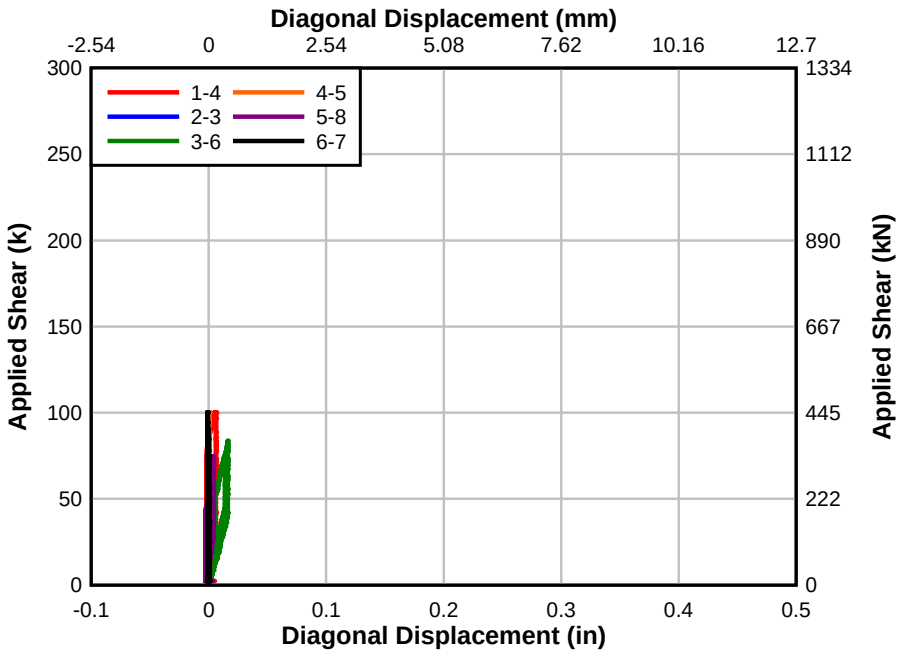

Fig. 12.107 - Specimen IT.7.18.6.M applied shear vs. diagonal disp. (baseline test)

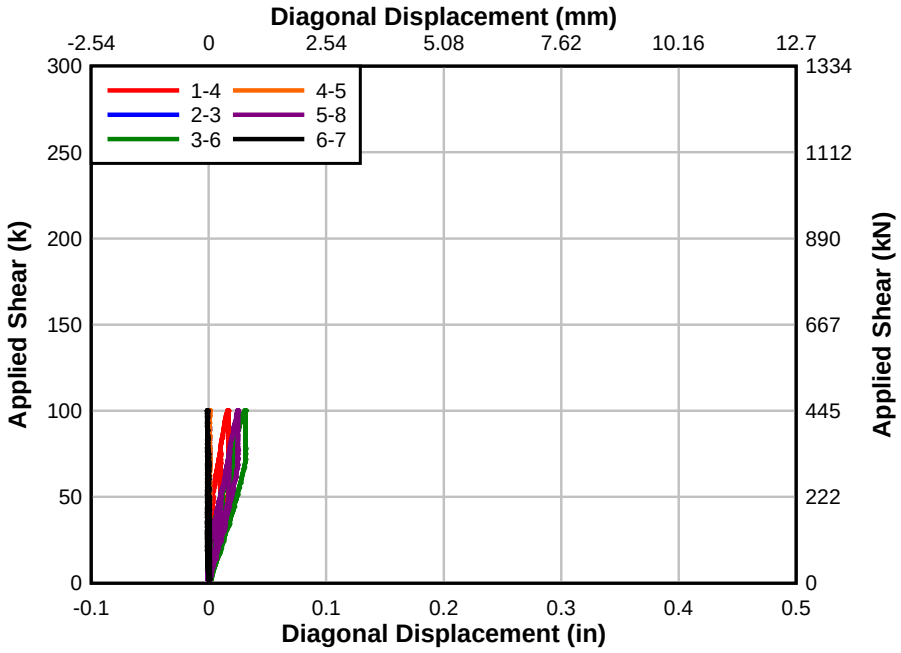

Fig. 12.108 - Specimen IT.7.22.6.FT applied shear vs. diagonal disp. (baseline test)

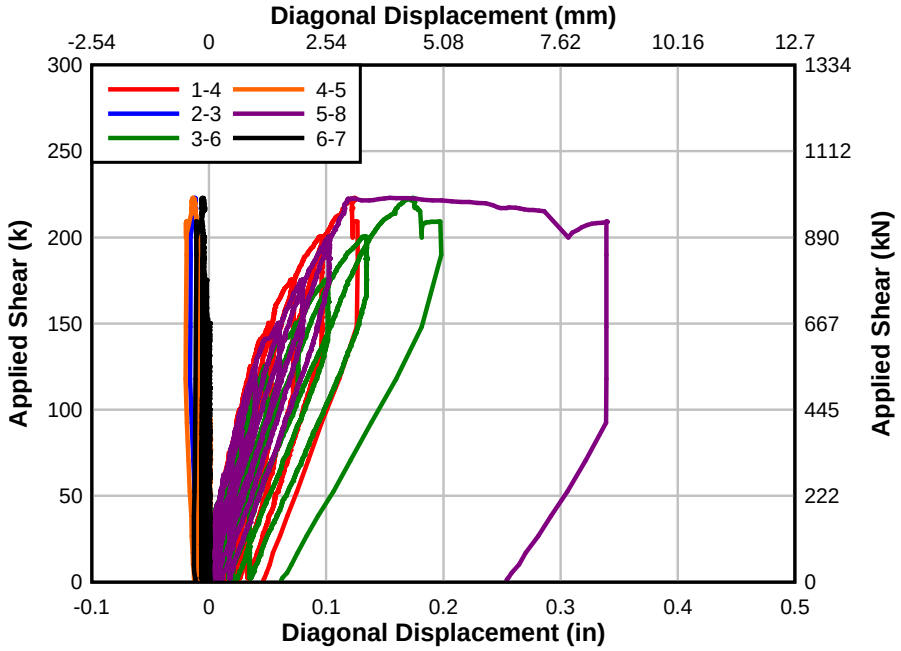

Fig. 12.109 - Specimen T.6.18.6.S applied shear vs. diagonal disp. (failure test)

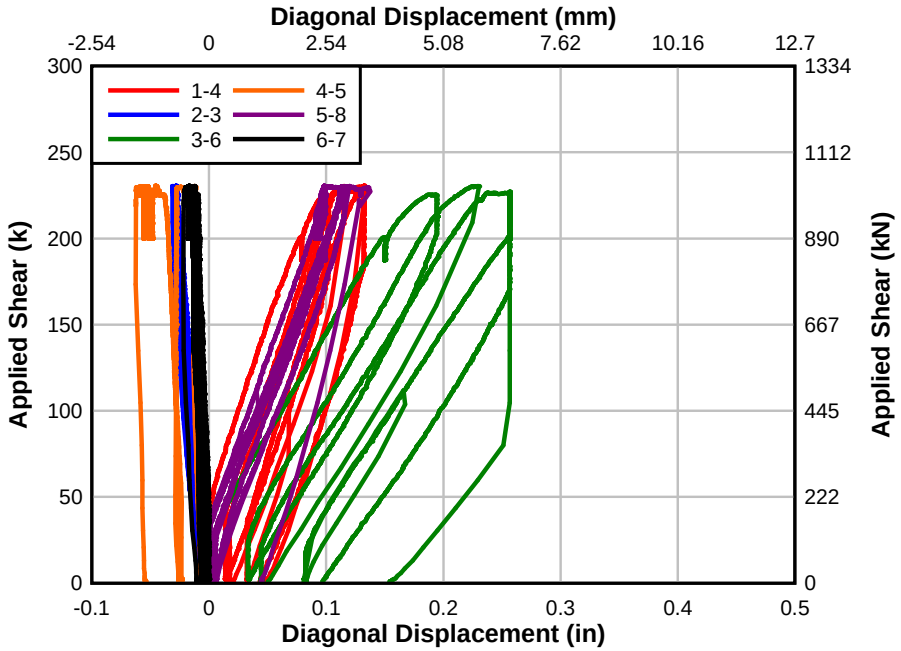

Fig. 12.110 – Specimen T.6.18.12.S applied shear vs. diagonal disp. (failure test)

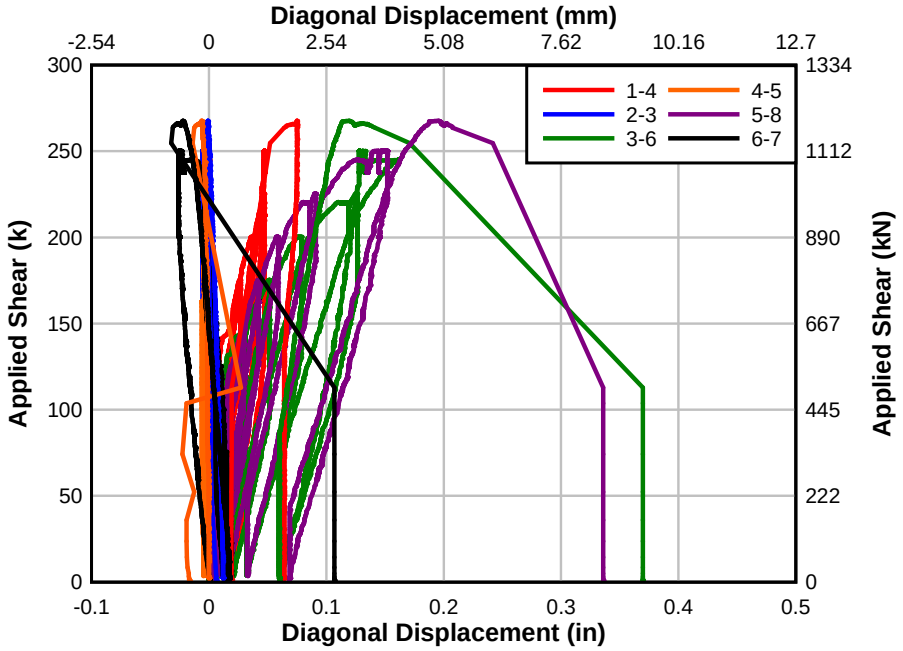

Fig. 12.111 – Specimen IT.7.18.6.S applied shear vs. diagonal disp. (failure test)

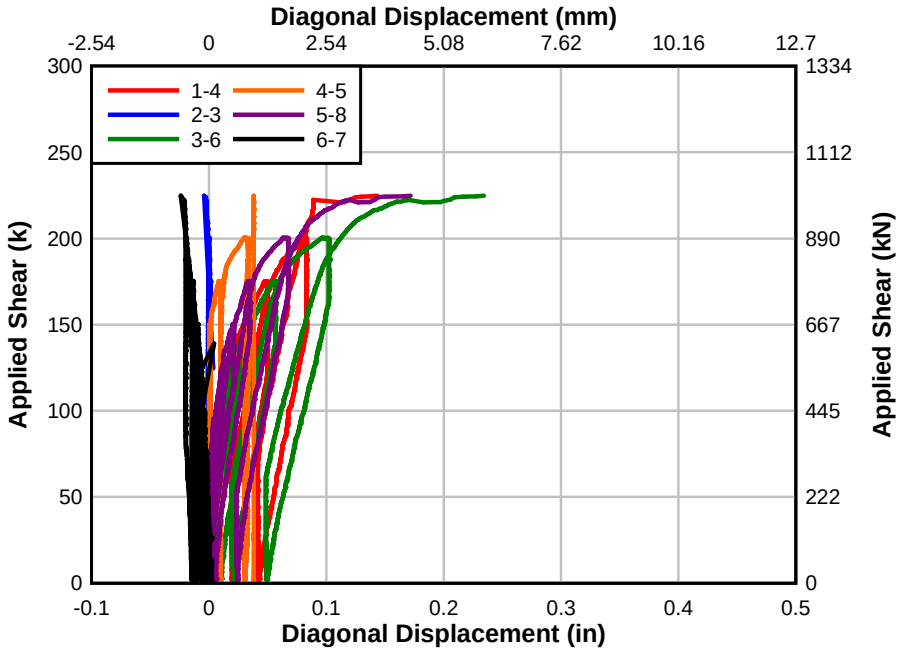

Fig. 12.112 – Specimen IT.7.18.12.S applied shear vs. diagonal disp. (failure test)

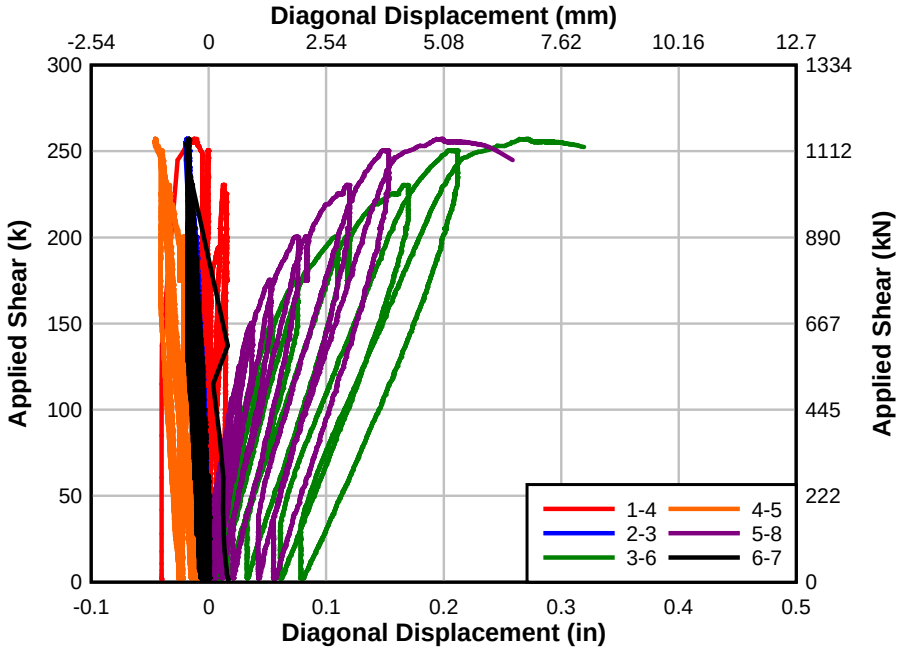

Fig. 12.113 – Specimen IT.7.22.6.S applied shear vs. diagonal disp. (failure test)

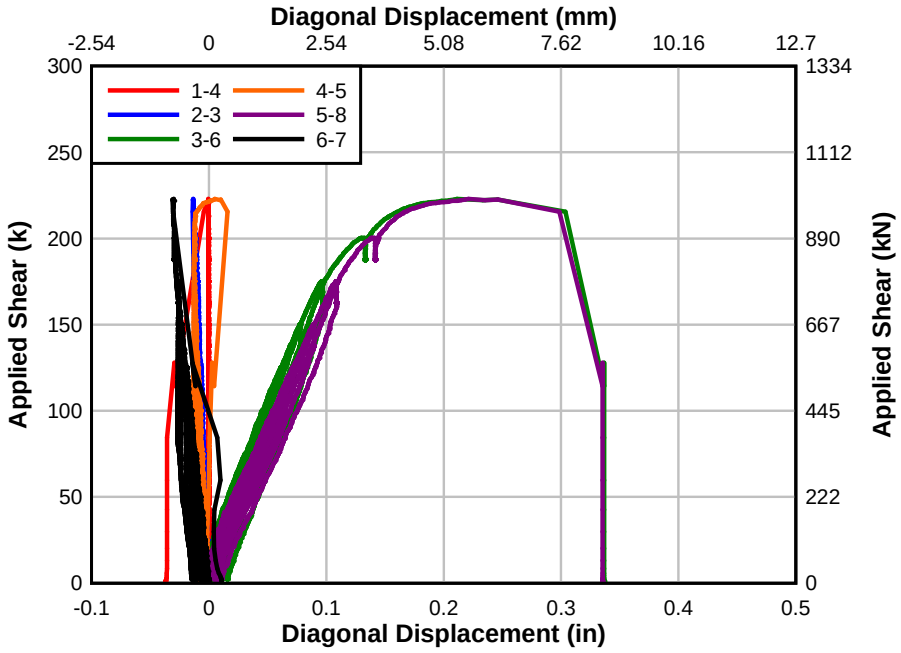

Fig. 12.114 – Specimen IT.5.22.12.S applied shear vs. diagonal disp. (failure test)

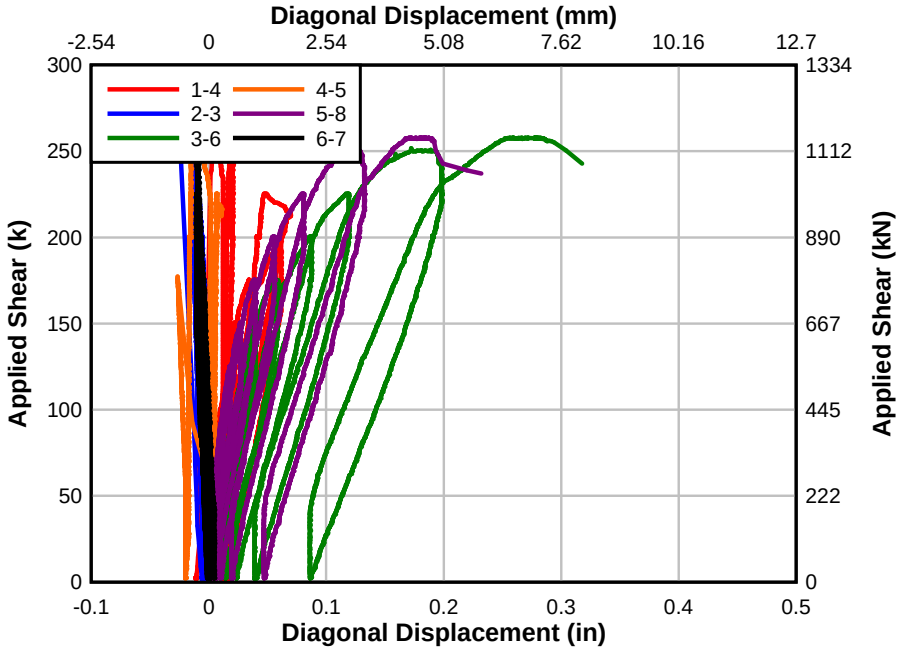

Fig. 12.115 – Specimen IT.7.18.6.M applied shear vs. diagonal disp. (failure test)

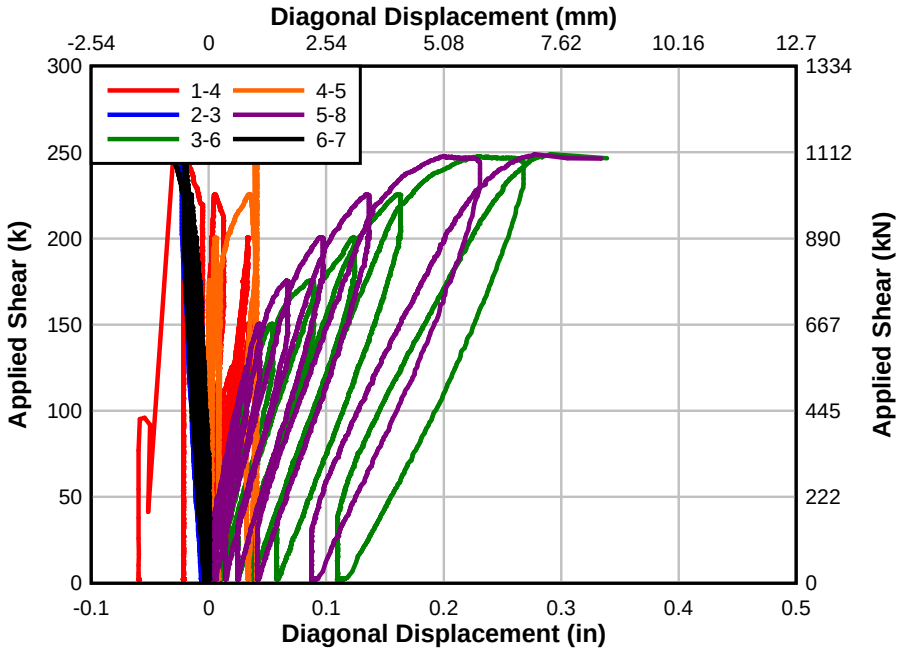

Fig. 12.116 – Specimen IT.7.22.6.FT applied shear vs. diagonal disp. (failure test)

12.4 Literature Review Specimens

This research created models in R2K of specimens from experiments in the literature review. The values used in this paper are reported below in Table 12.1. Figures 12.117 to 12.122 are the resulting shear curves for each specimen used from the literature.

Table 12.1 - Specimen properties from literature

Specimen	f'_c	f_y	f_{yv}	f_{yfrp}	A_s	A_v	A_{frp}	s_v	s_f	M/V @dv	CFRP type
	MPa [ksi]	MPa [ksi]	MPa [ksi]	MPa [ksi]	mm^2 [in^2]	mm^2 [in^2]	mm^2 [in^2]	mm [in]	mm [in]		
BS90-7A	31.0 [4500]	427 [62.0]	345 [50]	1875 [272]	1290 [2]	142 [0.22]	142 [0.22]	356 [14]	178 [7]	2.42	bar
2S-7LV	18.6 [2698]	699 [101*]	538 [78]	2951 [428]	1813 [2.81]	57 [0.088]	28 [0.043]	300 [11.8]	114 [4.5]	2.26	strip
4S-7LV	18.6 [2698]	699 [101*]	538 [78]	2951 [428]	1813 [2.81]	57 [0.088]	28 [0.043]	180 [7.1]	114 [4.5]	2.26	strip
2S-3LV	31.1 [4511]	445 [64.5]	533 [77.3]	2951 [428]	1877 [2.91]	57 [0.088]	28 [0.043]	300 [11.8]	267 [10.5]	1.9	strip
2S-5LV	31.1 [4511]	445 [64.5]	533 [77.3]	2951 [428]	1877 [2.91]	57 [0.088]	28 [0.043]	300 [11.8]	160 [6.3]	1.9	strip
2S-8LV	31.1 [4511]	445 [64.5]	533 [77.3]	2951 [428]	1877 [2.91]	57 [0.088]	28 [0.043]	300 [11.8]	99 [3.9]	1.9	strip
NB90-73-a	29.3 [4250]	545 [79.0]	655 [95]	2213 [321]	1523 [2.36]	57 [0.088]	103 [0.16]	160 [6.3]	74 [2.9]	1.41	bar
NB90-73-b	29.3 [4250]	545 [79.0]	655 [95]	2213 [321]	1523 [2.36]	57 [0.088]	103 [0.16]	160 [6.3]	74 [2.9]	1.41	bar
NB90-45-b	29.3 [4250]	545 [79.0]	655 [95]	2213 [321]	1523 [2.36]	57 [0.088]	103 [0.16]	160 [6.3]	46 [1.8]	1.41	bar
NS90-73-a	29.3 [4250]	545 [79.0]	655 [95]	2213 [321]	1523 [2.36]	57 [0.088]	103 [0.16]	160 [6.3]	74 [2.9]	1.41	strip
B.IT.NC.NS	23.0 [3338]	468 [67.9]	343 [49.8]	2068 [300]	6039 [9.36]	258 [0.4]	65 [0.1]	457 [18]	749 [29.5]	6.56	strip
2S-4LV	39.7 [5758]	724 [105]	542 [78.6]	2744 [398]	1819 [2.82]	57 [0.088]	28 [0.043]	300 [11.8]	180 [7.1]	1.91	strip
2S-7LV	39.7 [5758]	724 [105]	542 [78.6]	2744 [398]	1819 [2.82]	57 [0.088]	28 [0.043]	300 [11.8]	114 [4.5]	1.91	strip
2S-10LV	39.7 [5758]	724 [105]	542 [78.6]	2744 [398]	1819 [2.82]	57 [0.088]	28 [0.043]	300 [11.8]	81 [3.2]	1.91	strip

*Value is a weighted average of different strength reinforcing in the specimen

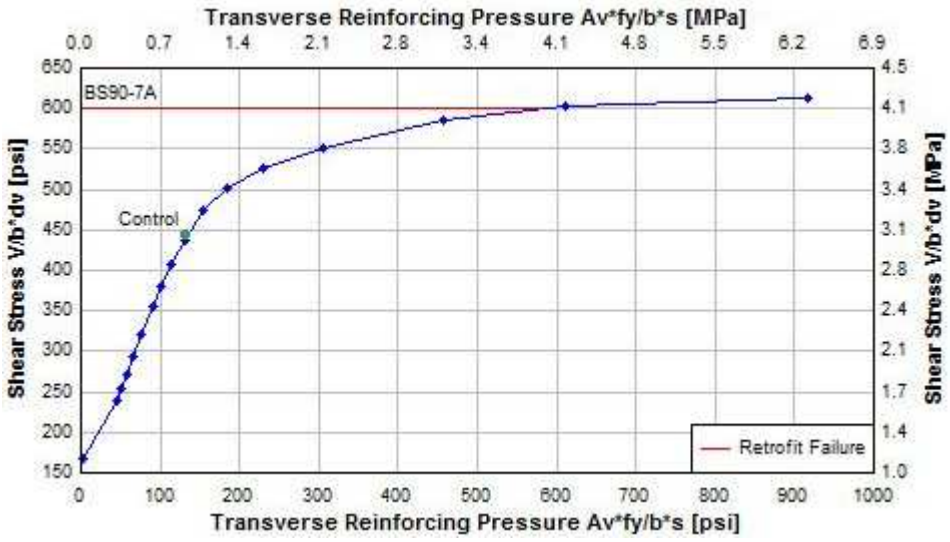

Fig. 12.117 – Shear curve for [De Lorenzis, 2001]

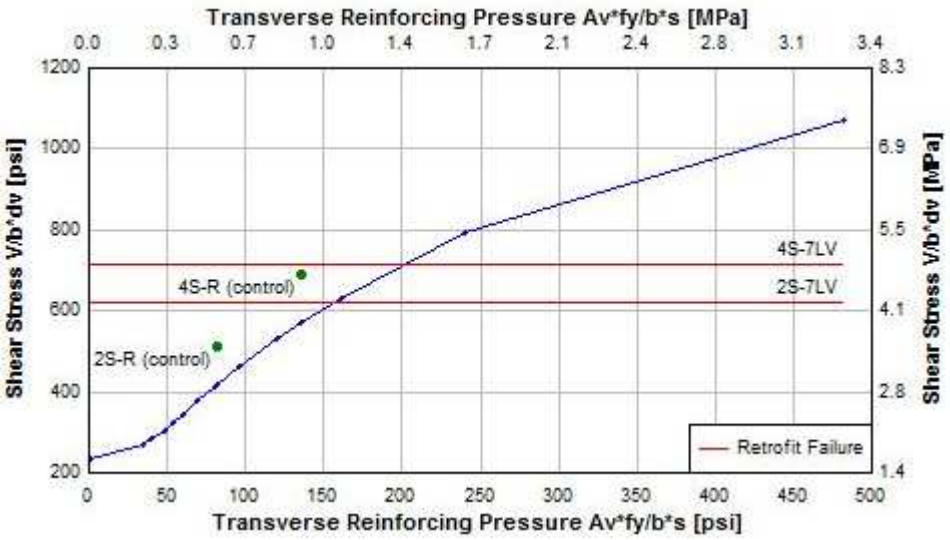

Fig. 12.118 – Shear curve for [Dias, 2007]

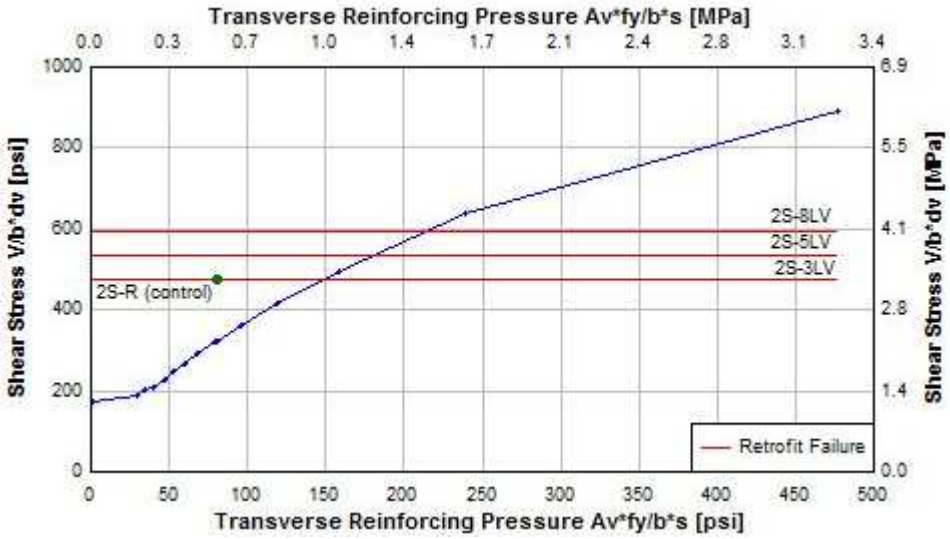

Fig. 12.119 – Shear curve for [Dias, 2008]

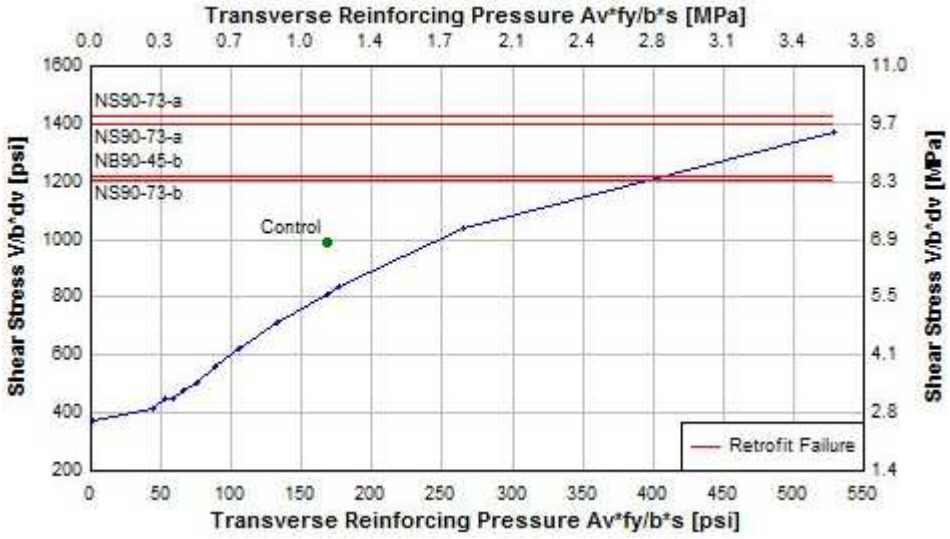

Fig. 12.120 – Shear curve for [Rizzo, 2009]

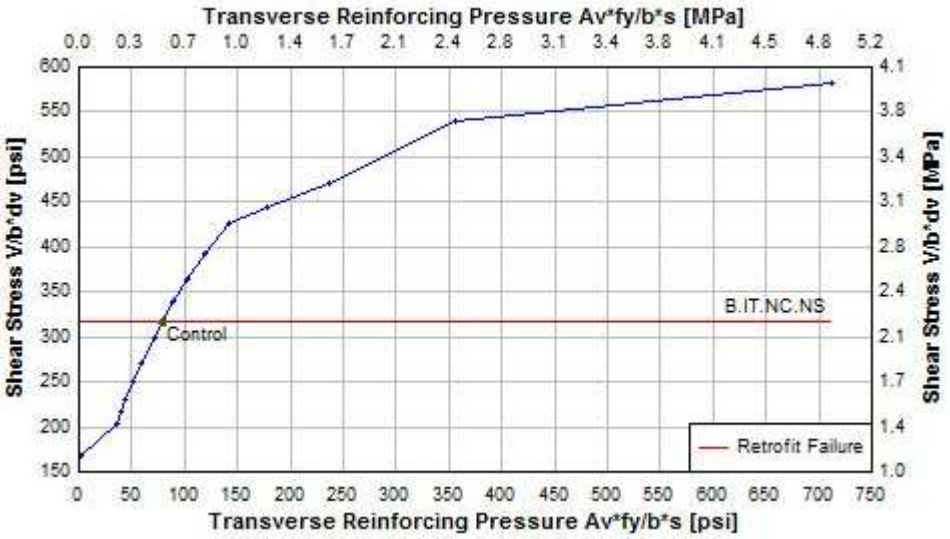

Fig. 12.121 – Shear curve for [Howell, 2009]

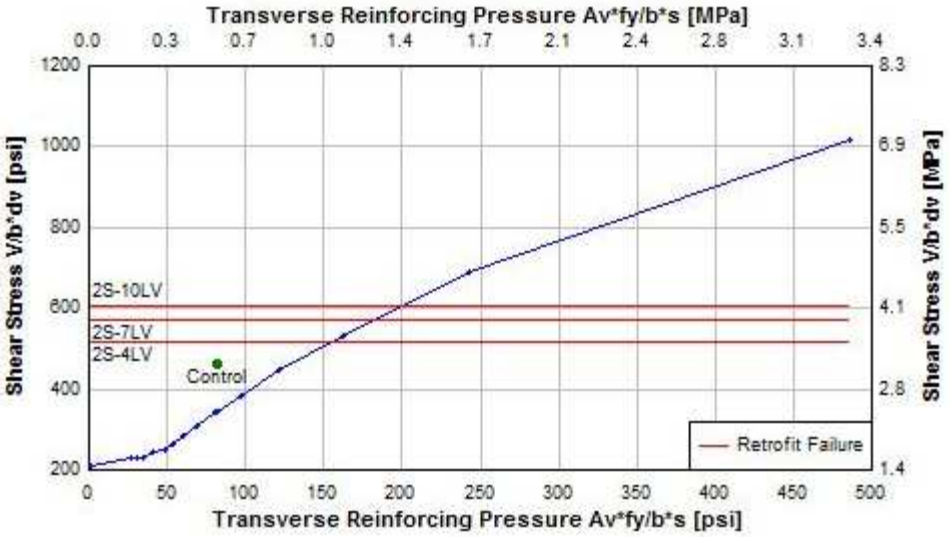

Fig. 12.122 – Shear curve for [Dias, 2010]